Remerciements

Cette thèse représente trois années importantes de ma vie. Ce fut une période d'échanges, de doutes et d'avancées. De nombreuses personnes ont contribué d'une manière ou d'une autre, à ce projet et son bon déroulement, je le leur dois. A travers cette page j'espère leur signifier toute ma gratitude.

Je tiens à remercier en premier lieu mes encadrents Bijan Mohammadi et Carole Sinfort qui m'ont accordé leur confiance en me proposant ce sujet et qui ont accepté de guider ce travail. Je les remercie pour leurs apports et leur contribution importante dans ces travaux de recherches. Ils m'ont poussé et m'ont offert de précieux conseils dans toutes les phases du travail tout en me laissant un grand espace de liberté pour conduire mes recherches. De plus ils ont démontré une patience réellement extraordinaire pendant mon processus d'apprentissage et pour ma gestion du temps. Ils ont su composer avec mes défauts d'organisation. Leurs "boosts" de motivations durant les phases difficiles du travail etaient très appréciables. Pour tout ceci je leur exprime toute ma sincère reconnaissance.

Je remercie messieurs Yves Brunet et Denis Flick d'avoir accepté d'être rapporteur de ce mémoire, surtout dans des délais aussi brefs. Je remercie également les autres membres du jury : Michel Cuer et Bernard Boniccelli.

Je profite de cette page pour remercier l'ensemble des membres du Cemagref et plus particulièrement tous les membres de l'UMR ITAP. L'équipe Pulvérisation du Cemagref est le berceau de ces recherches. Merci donc à tous ceux qui y participent, qui m'ont accueilli et qui ont collaboré à mon travail, notamment Bernadette Ruelle qui a pris la responsabilité de l'équipe ainsi qu'Ariane Vallet et ses conseils en mécanique des fluides. Une pensée pour tous ceux avec qui j'ai partagé des moments agréables au labo ou en dehors. Merci à tous pour votre gentillesse, ces mois passés à travailler à vos cotés ont vraiment été très bénéfiques et enrichisants sur le plan professionnel et personnel.

Bien sûr tout ce travail n'aurait pu être effectué sans l'appui moral de tous mes amis et les nombreux bon moments passés ensemble. Plus généralement, merci à tous ceux qui ont su éviter une connexion trop prolongée de mes neurones.

Magalie, Nico et Yvan, mes collegues de bureau, collocataire du une pièce, pour avoir crée une ambiance de travail agreable tout en supportant mes sauts d'humeurs surtout lors de la redaction du manuscrit.

Je souhaite bonne chance à Nico à qui je passe "le temoin" sur la poursuite de ces travaux de recherche.

Cette ambiance bonne enfant se retrouvait naturellement dans les repas du midi et la pause

café qui s'en suivait. La célèbre équipe de volley du Cemagref, avec laquelle j'ai souvent perdu. Ainsi que tous les autres thésards de les nouveaux arrivants que je n'ai fait que croiser. J'espère que nos routes se recroiserons prochainement (qui sait... ?).

Enfin mes amis Nantais et le reste du contingent. Lisou, David, Moïse, Magic qui nous a rejoint un peu tard, Tof qui est parti un peu tôt, la canourgue en général... les Jules-pompom, David Krisprolls, Matisse, Laureda et compagnie pour toutes les bonnes soirées passées ensemble... Tous les ouzbeks Nantais même si je les ai peu vu durant ces années. Je n'oublie pas bien sûr et les grands moments 'festifs' passés ensemble.

Mes pensées vont finalement à ma famille tout particulièrement. Durant ces trois années ma famille a été très importante et malgré l'éloignement elle a toujours été présente avec moi. Merci à papa, maman et à ma soeur pour toute l'affection et l'aide que vous m'avez donné, pour leur soutien et encouragement mais surtout de m'avoir donné le plus beau des heritages, une Education. Enfin un clin d'oeil à mon arrière grand mère et à ma grand mère, qui ne sont plus là, pour l'amour qu'elles ont transmis à mes parents et qui me l'on rendu.

Table des matières

Introduction Générale

Problématique générale et contexte

Contexte Général

L'augmentation de la population mondiale engendre des besoins croissants et nécessite par conséquent des rendements agricoles élevés. La "Révolution Verte", qui a mis les technologies les plus avancées (engrais, pesticides, machinerie agricole ...) à la disposition de l'agriculture pour répondre à cette demande, n'a fait qu'accélerer la dégradation de l'environnement en accentuant les pollutions de l'air, de l'eau et du sol.

La prise de conscience de cette nuisance a conduit au développement du concept d'éco-agriculture (sustainable agriculture) qui s'attache à protéger les ressources naturelles de façon durable. [1]. Cette notion "d'activité écologiquement viable" a ainsi engendré l'apparition de l'agriculture dite "de précision" qui adopte les nouvelles technologies pour essayer de maîtriser les rejets polluants dans la nature [2].

Dans ce contexte actuel de protection de l'environnement, la maîtrise des pulvérisations agricoles de produits phytosanitaires est essentielle. En effet, l'agriculture moderne utilise de nombreux produits chimiques de synthèse en environnement extérieur dans le but d'améliorer les rendements. Tout au long de leur cycle végétatif, les plantes cultivées sont menacées par les attaques d'insectes, les maladies et la prolifération de mauvaises herbes. Si elles ne sont pas enrayées dès que les parasites sont en mesure de nuire, ces menaces peuvent conduire à des résultats dommageables, voire catastrophiques quant aux rendements des cultures et à la qualité des récoltes. C'est pourquoi, les traitements phytosanitaires sont indispensables afin d'obtenir des cultures dans un état sanitaire correct.

Cependant ces traitements peuvent conduire à des effets très préjudiciables. Cette pression sociale vis-à-vis des problèmes de protection de l'environnement fait ressortir une demande d'évaluation scientifique. Au-delà des problèmes de contamination d'eau et des résidus dans les aliments, l'exposition par voie aérienne des populations qui résident autour de surfaces agricoles traitées doit être estimée.

Utilisation des pesticides dans l'agriculture

D'après les données de l'UIPP[1] près de 75 000 tonnes de produits phytosanitaires ont été vendues en 2003 sur le marché français, ce qui place la France comme premier consommateur européen.

La pulvérisation de pesticide dans les vignes est un exemple d'activité nécessitant un apport technologique certain tant elle est néfaste pour l'environnement. En France, les vignes

[1] Union des Industries de la Protection des Plantes

consomment près de la moitié de la totalité de matières actives (par rapport au nombre de molécules) et 20% du volume avec seulement 4% de la Surface Agricole Utile (SAU) [3].

De plus, des essais sur un pulvérisateur à jet assisté par air (air-blast sprayer), couramment utilisé pour ce type de culture, ont montré des pertes s'échelonnant entre 64% et 94% au printemps et entre 44% et 67% en été, par rapport à la quantité totale de pesticide pulvérisée [4]. [5] attribue cette mauvaise efficacité aux méthodes de pulvérisation, à la volatilisation des produits, au ruissellement sur les feuilles et à la dérive des jets.

Ainsi, les viticulteurs sont soumis à une pression grandissante pour réduire l'usage de ces produits et limiter les pertes et la pollution environnementale engendrée [6].

Le transfert des pesticides vers l'environnement

La dynamique du transport et du mouvement des produits phytosanitaires, peut être décrite en deux étapes [7] :

- pendant la pulvérisation (dérive et dépôts hors cible)
- après l'application

Durant l'application, les produits phytosanitaires peuvent être perdus au sol ou dans l'air, à cause d'une mauvaise orientation des trajectoires de gouttes ou de leur transport par le vent. Les substances sont transportées et transformées dans l'atmosphère puis peuvent se déposer sur des zones très éloignées des sources d'émissions. Par rapport à la pollution des eaux, la pollution de l'air reste encore mal connue.

La volonté de réduire les volumes d'application et la tolérance d'éventuels voisinages à l'égard de certaines molécules ont fait de la dérive une des préoccupations les plus importantes pour les communautés scientifiques et techniques, et plus particulièrement au Cemagref. Les procédés pour garantir une inertie suffisante des gouttes afin qu'elles impactent leur cible, les dispositifs pour minimiser l'effet des variables climatiques ainsi que l'utilisation de zones tampon pour limiter l'impact de la dérive sont les axes de travail les plus fréquents décrits par la littérature [3].

On peut identifier différents processus qui entrent en jeu et agissent simultanément ou successivement et dont l'importance relative dépend notamment des conditions de rejet. La dérive dépend essentiellement :

- des caractéristiques de la source d'émission
- des conditions météorologiques
- de la topographie et des conditions orographiques

Dans le cas de la vigne et des autres cultures à port érigé, il faut également prendre en compte l'orientation des jets[2] et l'effet d'écran de la végétation.

La modélisation

L'approche de la dispersion des pesticides fait nécessairement appel à des outils de modélisation pour analyser les stratégies de réduction d'impacts. En effet, la simulation numérique de tels écoulements semble indispensable tant les essais en champ sont difficiles ([3],[8]). Il est par ailleurs souvent impossible de rendre compte en laboratoire de l'ensemble des phénomènes qui interviennent dans l'évolution d'un polluant. Les modèles permettent de tester et donc de développer des modèles physiques via des expériences numériques. Ces expériences permettent,

[2]En viticulture, les jets sont souvent orientés de manière à traiter deux rangs - ou plus - de chaque côté, en un seul passage.

dans certains cas, de simuler une partie de la complexité de l'atmosphère. Il est donc important de fournir des outils numériques pour prévoir les transports sur de longues distances.

Les modèles de dispersion sont, par définition, des implémentations numériques de modèles physiques qui décrivent l'évolution de polluants atmosphériques. Cette modélisation comprend plusieurs composantes, à savoir les modélisations du "terme source", de la "propagation" de cette source dans l'environnement et l'effet sur les "cibles". En ce qui concerne le second point, la nature turbulente des écoulements atmosphériques proches du sol rend la prédiction des mouvements des polluants dans l'air assez complexe et nécessite l'emploi de logiciels spécifiques. La maîtrise de ces outils fait appel à de nombreuses compétences et reste souvent réservée aux spécialistes.

En effet, bien que certains de ces modèles se montrent assez performants dans l'analyse, ils sont d'un point de vue pratique lourds d'utilisation. Ils nécessitent donc des temps de calcul importants et des calculateurs puissants pour être utilisés correctement. La raideur des équations (grande dispersion des temps caractéristiques), les fortes hétérogénéités, les nombreux couplages, induisent des coûts importants dans les schémas numériques. Ces limitations numériques dues aux coûts des calculs impliquent une adaptation de l'utilisation de ces outils en fonction de la complexité des enjeux à traiter.

Une deuxième limitation réside dans les données d'entrée des modèles. L'évaluation par des experts de ces données ([9, 10] cités par [11]) révèle de fortes incertitudes, souvent de l'ordre de 50% ou 100%. Ces incertitudes peuvent toucher l'ensemble des données (masses de polluants injectées -conditions initiales, conditions aux limites, inventaire des émissions-, données de sol -topographie, orographie-, processus de pertes -dépôts-, réactions chimiques -constantes de réaction- et les caractéristiques du transport -champs météorologiques). Par exemple, pour fonctionner correctement, les modèles de dispersion nécessitent des données climatiques de bonne qualité. Or dans le cas de la dispersion des pesticides, celles-ci sont le plus souvent mesurées dans des stations météorologiques situées sur des surfaces standards et qui sont plus ou moins éloignées des parcelles cultivées. La représentativité de ces stations climatiques et des données qu'elles fournissent sont fortement liées à leur emplacement et leur environnement et peut donc être mise en question.

Une autre grande limitation relève de la formulation des modèles. La modélisation physique n'est pas en mesure de décrire les phénomènes atmosphériques complexes avec une extrême précision et un certain nombre d'hypothèses doivent donc être admises dans la physique des modèles. Ces simplifications peuvent être spécifiques aux applications pour lesquelles ces modèles sont dédiés, ou motivées par d'autres raisons : réduire le temps de calcul ou éviter l'usage de paramètres qui sont difficilement mesurables dans la réalité. La connaissance des potentialités de ces modèles sous leur forme "simplifiée" en les appliquant dans d'autres situations peut être une étape utile et nécessaire pour pouvoir les évaluer. Cela sert à préciser les limites de leurs hypothèses et les possibilités d'application.

Certaines simplifications, appelées paramétrisations, permettent une représentation approchée de processus physiques essentiels. Différentes paramétrisations physiques peuvent raisonnablement permettre d'estimer une même quantité et il peut être difficile de les départager. On peut ainsi constater que le nombre et la disparité des outils modélisant la dispersion atmosphérique disponibles sont très importants, en relation avec le nombre de fluctuations dans les formulations et de problématiques concernées. De plus, ces modèles de dispersion connaissent un développement incessant. C'est pourquoi, il est très aléatoire de faire un choix définitif parmi le nombre conséquent de codes mis à la disposition des utilisateurs.

Toutes ces limitations ont pour conséquence que le choix d'approximations numériques (maî-

trise des coûts de calcul), le choix, voire la correction de données et la composition d'un modèle sur la base des paramétrisations existantes sont déterminants quant à la qualité du modèle. Une grande liberté est ainsi laissée au modélisateur. L'expérience du modélisateur peut lui permettre d'effectuer les bons choix dans le but d'approcher au mieux les observations. On parle généralement d'ajustement des modèles (ou de "tuning" en anglais).

En prévision, ces ajustements sont centraux puisqu'ils déterminent les performances du modèle (scores de prévision). Sur une période courte, les meilleurs ajustements peuvent donner de très bons résultats mais seront peu robustes. A l'inverse, des ajustements pour de longues périodes sont plus robustes mais moins efficaces. Ces ajustements font partie intégrante de la démarche de prévision.

La pratique de l'ajustement de modèle soulève plusieurs difficultés. Il est possible que les optimisations du modélisateur ne soient pas conformes à la physique. Par exemple, un choix de paramétrisation peut permettre de compenser une erreur faite sur un champ d'entrée. La validité du modèle pose alors question. La formulation du modèle n'est pas assurée d'être la meilleure d'un point du vue physique et les données choisies ne sont pas nécessairement les plus proches de la réalité.

Pour résumer, le choix doit donc se porter sur un modèle capable d'estimer, par rapport à la complexité des données et au niveau de précision demandé par l'analyse, les concentrations de polluants le plus précisèment possible. Il dépend bien entendu aussi des compétences techniques des personnes désirant entreprendre la simulation ainsi que des renseignements disponibles, des détails et de la précision des bases de données.

Les trois principales sources d'incertitude précédemment listées sont les approximations numériques, la formulation du modèle et les données d'entrée. Il convient donc de considérer les phénomènes observés dans les sorties de modèle à la lumière des ces incertitudes. Dans ces conditions, les concentrations simulées par les modèles ne peuvent être qu'incertaines, dans des limites à préciser.

Enjeux et objectifs du projet de thèse

Ce projet de recherche concerne l'étude des phénomènes de dérive et vise plus particulièrement à caractériser les flux aériens issus de la parcelle au cours de l'application des pesticides. Le but est de prédire leur devenir et par conséquent leur répartition dans l'environnement.

Les remarques préliminaires ont déterminé les orientations des travaux de recherches. Le recours à un logiciel de CFD s'avère long, fastidieux à utiliser et pas nécessairement adapté : le développement d'un modèle plus spécifique constitue une solution péferable. Ainsi on a décidé de se tourner vers le développement d'un modèle dédié, caractéristique des problèmes posés au Cemagref.

On part du constat suivant : proposer une solution fine et précise concernant le problème de la dispersion atmosphérique des pesticides, étant donné la complexité du problème et la rareté des données disponibles, semble vain.

La vocation de ce travail de thèse est donc la création et le développement d'un outil simplifié d'évaluation déterministe, majorant les pertes. Cet outil de simulation est basé sur un modèle numérique à faible coût de calcul, capable de traiter l'influence du vent et celle de la topographie sur les caractéristiques dynamiques du transport aérien, ainsi que sur la concentration des produits à des échelles pluri-parcellaires.

Dans l'optique de gestion des risques qui a justifié l'exploration de ce thème de recherche, l'objectif de ce travail est double : d'une part, il faut **quantifier les émissions** vers l'atmosphère

pendant les applications et d'autre part, il faut **prévoir leur dispersion** géographique (et temporelle).

La finalité est de prévoir les éventuelles zones d'influence par une cartographie de la répartition des polluants. Cela permettrait alors d'appréhender les résolutions à prendre pour éviter les conséquences néfastes. Le développement de la modélisation physique, c'est-à-dire de l'explication et la description mathématique des phénomènes physiques, n'est pas la préoccupation principale de cette thèse. L'accent est essentiellement mis sur la réalisation d'un modèle opérationnel utilisant au maximum les connaissances déjà disponibles.

Desription des travaux

Méthode et approche générale

L'indication déterminante pour la modélisation de la dispersion aérienne est la taille du domaine de calcul. Selon l'échelle considérée, certains détails du domaine ou processus peuvent être négligés ou modélisés plus ou moins finement. L'utilisation d'un modèle à complexité réduite a été retenue. Elle prend en compte les différentes échelles de manière couplée mais indépendante. Elle est basée sur la définition de fonctions analytiques dont la forme est fixée a priori. Les résultats capitalisés dans les précédentes études fournissent les moyens de formaliser et de paramétrer ces fonctions analytiques.

On choisit de travailler aux niveaux des échelles dimensionnant un bassin versant, c'est à dire quelques dizaines de kilomètres. Comme cela a déjà été évoqué auparavant, ce choix implique des contraintes fortes sur les modèles mathématiques envisagés pour la simulation car la complexité est un enjeu majeur. Il est en effet illusoire de s'orienter vers des modèles permettant une prédiction fine aux échelles inférieures au mètre. Cependant, on constate que pour une prédiction efficace, les effets à petites échelles doivent tout de même être pris en compte par une première phase de modélisation.

Evidemment, la complexité des procédés utilisés dans la modélisation découle essentiellement de la complexité des scénarios considérés. Et selon le degré de complexité pris en compte, le modèle est plus ou moins gourmand en temps de calcul. Il existe, par conséquent, un certain compromis à trouver entre rapidité de calcul et précision. C'est l'une des principales difficultés de la simulation numérique. Dans cette thèse, l'accent sera clairement mis sur la rapidité de calcul. Le but principal étant une complexité réduite, la simplicité des structures de données requises est également essentielle. Enfin, pour modéliser au mieux le comportement du polluant et de l'écoulement porteur, il est nécessaire de réduire au maximum le nombre de paramètres de calage difficilement quantifiables.

Hypothèses

Il est important de définir le système auquel on s'intéresse dans le cadre de ce travail. Il s'agit de la couche d'air particulière qu'on appelle couche limite atmosphérique (CLA) et qui sera présentée plus en détail dans la section 2.1.

Certains polluants ont un comportement plus facile à modéliser que d'autres car ils suivent l'écoulement fluide sans l'influencer (comportement de scalaire passif). C'est ce type de polluant qui est considéré tout au long de cette étude.

Plan et Organisation des Chapitres

La première partie de ce document (I) concerne une présentation des bases nécessaires à la compréhension de la thèse. L'interprétation complète de la présence des pesticides dans l'air requiert une bonne connaissance des processus impliqués. Elle va permettre d'identifier les principaux phénomènes, les hypothèses et de caractériser différentes variables. Parrallèlement à la physique, elle introduit certaines modélisations (paramétrisations physiques et données) sur laquelle reposent les simulations des parties suivantes.

Pour réaliser les objectifs présentés, différents types de modèles ont été développés. Les 3 parties suivantes décrivent l'architecture du système de simulation complet modélisant la dispersion aérienne. Le système joue le rôle d'une plateforme multi-modèles et chaque partie correspond à un niveau du système global :

- le 1er niveau (II) correspond à l'étude d'un écoulement au sein de la végétation. La mise au point de ce modèle va permettre d'identifier une représentation des rangs de vigne d'une parcelle par leur effet sur le devenir des jets de pulvérisation pendant l'application.
- le 2ème niveau (III) a pour fonction de déterminer les distributions de concentation locales pour des temps courts grâce à la théorie des jets turbulents. Elle permet d'estimer les émissions de la parcelle traitée. Ces émissions vont caractériser le terme source du le niveau suivant.
- le dernier niveau de la plateforme (IV) concerne la dispersion à une échelle méso.

A chaque étape, une première partie synthétise l'état de l'art et répertorie certaines techniques disponibles. Le type d'outil idéal n'existe pas et il faut donc trouver, celui qui est le mieux adapté pour répondre à la problématique posée. Ces revues rapides de l'existant permettent d'autre part de faire le point sur les difficultés soulevés et sur les verrous scientifiques, ainsi que d'envisager d'autres types de modélisation pour améliorer la plateforme de simulation. Elles ont également le rôle, de justifier et d'expliciter les choix effectués (paramétrisations, simplifications,...) dans les modélisations utilisés dans cette thèse. Les parties scientifiques qui forment l'essentiel du manuscrit ont été rédigées en anglais. l'accessiblité du document au plus grand nombre. Chaque partie est présentée par une courte introduction française afin d'insister sur les motivations et l'organisation générale du document.

Première partie

THEORY : Background

Cette partie a pout but de détailler les phénomènes liés à notre problématique et dont la connaissance est nécessaire à l'élaboration d'un modèle de dispersion atmosphérique. Le terme dispersion atmosphérique désigne dans ce rapport, le phénomène physique c'est à dire les mécanismes de mélange d'une substance dans l'air de l'atmosphère. Elle caractérise le devenir, dans le temps et dans l'espace d'un ensemble de particules (panache d'aérosols, de gaz, de poussières...) rejetées dans l'atmosphère et la façon dont ce nuage est transporté et dilué (effets de turbulence, gravité,...). Les deux phénomènes principaux régissant l'évolution du nuage dans l'atmosphère sont le déplacement du nuage (advection) et la dilution (diffusion) du nuage.

Cette première partie a pour objet de rappeler les phénomènes physiques intervenant dans la couche limite atmosphérique et de présenter les concepts ainsi que les outils qui vont servir de base à leur modélisation. Il s'agit donc de préciser et d'expliquer les paramètres à prendre en compte dans la démarche de modélisation, afin de l'éclairer et d'y porter un regard critique (logique et cohérence de la démarche).

Dans ce dessein, on décrit les équations et les hypothèses sur lesquelles sont basées la majorité des modèles. A partir de ces équations on pourra dériver des solutions analytiques pour des problèmes idéalisés et par conséquent simplifiés, notamment les modèles classiques de dispersion gaussiens ou plus tard les modèles de jets turbulents. Ce cheminement va permettre d'exposer et de mettre en perspective les différentes approximations sous-jacentes. Ainsi on va développer les hypothèses simpilifactrices utilisées pour obtenir des solutions sous forme close, sur lequelles repose l'approche présentée dans cette thèse.

Remarques sur les motivations de cette partie

Dans le cadre de cette thèse, on a choisit de travailler à 2 échelles caractéristiques distinctes : l'échelle du paysage (bassin versant de quelques dizaines de km) et une échelle plus locale, à savoir l'échelle d'un couvert (échelle d'un rang de vigne). Que ce soit à l'échelle locale ou à plus grande échelle, les principes théoriques utilisés et le point de départ des différents modèles reposent sur les équations fondamentales de la mécanique des fluides. Cependant, les traitements sont différents suivant l'échelle d'observation des processus.

On a décidé de présenter ces résultats classiques, car dans la bibliographie existante, les équations et les hypothèses associées sont souvent données, mais plus rarement les détails complets de la méthode employée pour y parvenir. Par ailleurs cette étape, détaillant les phénomènes liés à la dispersion atmosphérique, permet de s'appuyer sur des bases solides, pour l'élaboration d'un modèle de dispersion atmosphérique et de mettre en relief les insuffisances de la théorie.

Plan

Dans un premier temps, les notions nécessaires à la compréhension de la dispersion atmosphérique seront introduites. On commence par énumérer les différents processus impliqués lors de la dispersion d'un polluant dans (1.1). On s'attache alors a montrer comment ces phénomènes peuvent être modélisés et quelle est leur traduction en termes mathématiques.

En partant de la notion fondamentale de conservation de la masse, traduite mathématiquement, on liste la suite d'approximations successives effectuées pour décrire les écoulements atmosphériques (1.2).

On rappelle aussi quelques notions sur les problèmes liés à la turbulence (1.3). En effet, en raison du caractère turbulent de toutes les variables présentes, les équations nécessitent un traitement spécifique. On utilise donc des méthodes statistiques (décomposition de Reynolds)

basées sur une description des propriétés moyennes de l'écoulement. Ces traitements statistiques entraînant des problèmes de fermeture, on utilisera la théorie élémentaire du gradient-diffusion.

Ensuite, à partir des équations générales décrivant la dispersion d'un scalaire passif dans un écoulement quelconque, on va émettre les hypothèses supplémentaires concernant notre champ d'application (écoulements atmosphériques) qui vont nous permettre d'arriver aux équations d'advection diffusion (1.4.1). Ces équations "finales", de la couche limite atmosphérique correspondent à la dynamique de ce que l'on veut modéliser et servent de base à la plupart des modèles de dispersion.

Pour finir on présente la dérivation d'une solution analytique particulière de cette équation qui est à la base des modèles de dispersion à panache gaussien. Ce modèle classique est le modèle de dispersion atmosphérique le plus répandu. Sa dérivation nous permet d'exposer un exemple simple de solution analytique.

Les limites principales de ce type de modèle sont qu'il ne tient pas compte de la topographie et ne peut être utilisé avec des champs de vent non uniforme pour la dispersion des polluants. Le calcul de la distribution horizontale et verticale de la turbulence se déduit des différents tableaux de paramétrisation existants qui sont basés sur des mesures expérimentales. Il est alors possible de simuler facilement pour une source ponctuelle définie, le panache des émissions pour une classe de stabilité et un vent donné. Ces solutions analytiques simples seront adaptées dans le cadre du modèle numérique réduit de dispersion (partie IV) développé dans cette thèse.

Dans le chapitre 2, on présente les bases de la structure et de la stratification de la couche limite atmosphérique, ce qui permet de spécifier les échelles qui nous intéressent pour cette étude. Les transferts turbulents dans l'atmosphère sont souvent de types convectifs et sont donc influencés par la stabilité de l'atmosphère qui est présentée dans 2.2.

Mots clés : *Mécaniques des fluides, Dispersion scalaire, ADE, modèles de dispersions gaussien, CLA, stabilité atmosphérique*

Keywords : *Fluid mechanics, Transport mixing, ADE, gaussian dispersion model, ABL, atmospheric stability*

Chapitre 1

Transport Theory

Before going on to discuss the more specific scenarios of relevance to this study, it is worth discussing the basics of pollution dispersal. The transport of pollutant occurs in a large variety of environmental, agricultural and industrial processes. Accurate prediction of the transport of these pollutants is crucial to the effective management of these processes. The transport of these pollutants can be adequately described by the advective-diffusion equation (ADE).

The most popular technique is the Gaussian Plume Method which assumes that the pollutant spreads in such a manner that the pollutant maintains a Gaussian distribution across the plume. It will be also presented.

1.1 Dispersion Process Overview

Dispersion of pollutants in the atmosphere is governed by dominant mechanisms categorized into two broad groups : **transport** and **transformation** (see figure 1.1). The second group, refers to those processes that change a substance of interest into another substance.

1.1.1 Transport Processes Description

Any contaminant released into the atmosphere is transported by a variety of processes that can be classified generically as either advection or molecular and eddy diffusion (often referred to as turbulent dispersion). **Advection** is simply the transport of the pollution by the mean flow in the atmosphere.

The diffusion process in turbulent flow is made up of two contributions : one of molecular scale, due to the *random thermal agitation* of the molecules, and another of much larger scale, due to *random turbulent bulk* motion within the fluid. These two mechanisms differ in two key ways.

First, the resultant motions are on entirely different scales ; the typical span of turbulent movement is many orders of magnitude larger than the *mean free path length* of the diffusing particles. Molecular diffusion is rarely of significance in comparison with eddy diffusion, in atmospheric flows.

Second, due to the macroscopic size of the parcels of air involved in any single turbulent movement, there is a continuity constraint. As such a parcel moves, it displaces another, and at the same time leaves a vacant region that must be filled. This lads to the characterization of turbulent flow by a group of random, closed-loop motions commonly referred to as *atmospheric whirls*, called *turbulent eddies*.

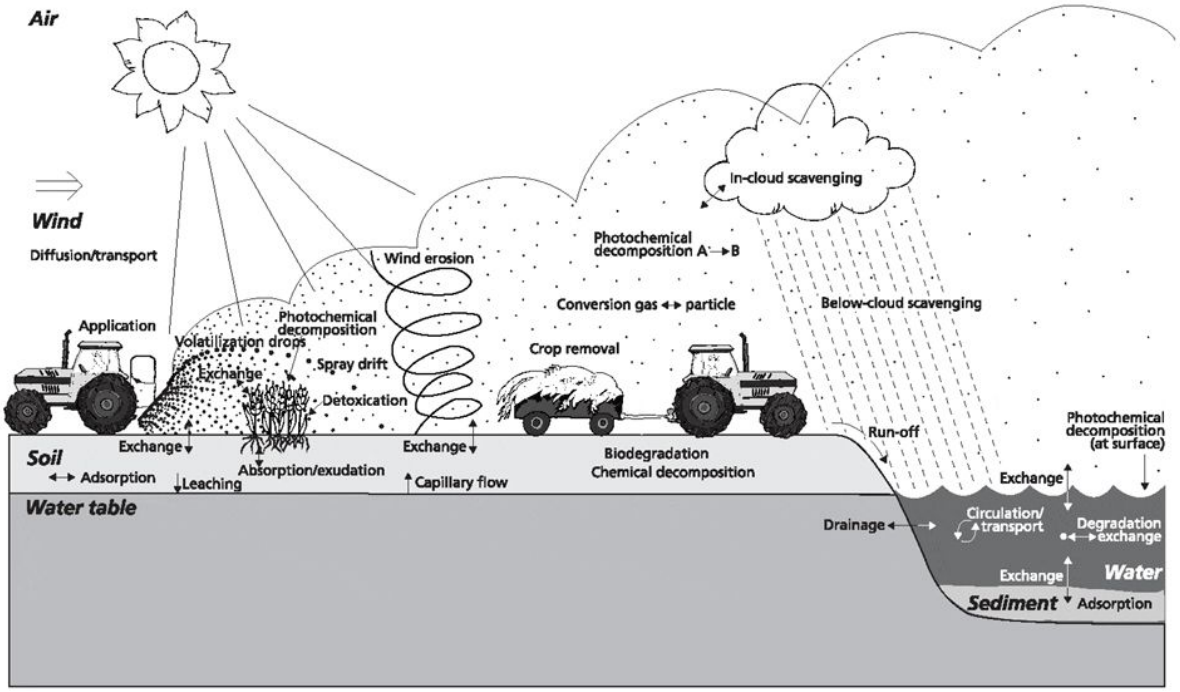

FIG. 1.1 – Processes for pesticides dispersion in the environment (from [12]).

1.1.2 Molecular diffusion

Molecular diffusion is the spreading as a result of the random motion of gas molecules in the air. It is a redistribution of mass (or energy) by Brownian motion and tends towards uniformity in mass (or energy). *Brownian motion* is thermal energy and results in random molecular collisions. There is motion in all directions, but there is a tendency for the mass (or energy) to move from areas of high concentration to areas of low concentration. *Passive diffusion* refers to mixing processes that occur due to random motions and that have no direct feedback on the dynamics of the fluid motion[1]. *Active diffusion* relates to mixing processes that have a direct feedback on the equations of motion due to changes in the density of the carrier fluid.

1.1.3 Turbulent diffusion

Atmospheric movements are almost always turbulent. Wind speed, wind direction, temperature, pressure, humidity and concentration of atmospheric constituents show a spatial and temporal variability. It causes e.g. diffusion of a plume perpendicular to the wind direction or exchange between the air and the surface.

Turbulence is a random, unresolved and unpredictable motion of the air. The motion of a fluid is usually separated into the mean part and turbulent ones. Turbulence is a key feature of many environmental flows. Compared with the other scales of meteorological motions,

[1]Trace species in the atmosphere (i.e. excluding water) have very small concentrations, and do not affect the solution of the equations for the wind fields. This provides an important simplification for air quality models because it allows the mass continuity equations for trace species to be solved independently of the continuity equations for air. Thus, wind fields generated by meteorological models can simply be read as inputs (passive transport) [13].

turbulence is on the small end of scale. The nature of turbulent diffusion is not as clear cut and fundamental as molecular diffusion is : it involves a parameterization of processes that can't be solved directly (see 1.3.2). The strengths and weaknesses of the approach, need to be kept in mind when dealing with turbulent diffusivities.

There are two other considerations to be recognized in turbulent diffusion characterizations. First, there is an implicit averaging time assumed, which is associated with the "mean flow" definition. Secondly, not all fluctuations from the mean flow are random. The thermal eddies of a convective boundary layer transport mass from the surface to the top of the convective boundary layer in an organized manner. This convective eddy transport could be thought of as advection, but since it occurs in less than 1 hour and cannot be simulated deterministically, it is typically viewed as a component of eddy diffusion.

There are two different mechanisms that generate turbulence :

– **mechanical turbulence** and
– **thermal turbulence**.

It is important to differentiate between these two types of turbulence because they are associated with eddies of different sizes and lifetime, which influence diffusion and surface exchange in a different fashion.

Deviations due to *mechanical turbulence* are generated by friction drag exerted on the wind by the surface, and flow through and around obstacles. This friction is caused by the roughness of the surface. As a result the wind speed increases with height. A rough surface like a forest generates more turbulence than a smooth surface like water. Essential for this form of turbulence is that it is generated by the wind. Mechanical turbulence is characterised by small eddies, with a relatively short lifetime especially near the surface.

Turbulent fluctuations can be enhanced or suppressed thermally by buoyancy forces arising from relative differences in temperature in air layers. *Thermal turbulence* is caused by heating of the air near the surface due to solar radiation. This air is somewhat warmer than the surrounding air, has consequently a lower density, and is lifted up. Colder air is taking its place. Due to these air movements larger, so called 'convective', eddies are generated. They have relatively long lifetimes and cause diffusion due to upward and downward air movements that can last up to $10 - 20$ minutes.

1.1.4 Cascade Energy Process

Eddies cover a wide range of spatial scales, and are responsible for the dissipation of energy in the flow. This energy dissipation can be represented as a cascade of energy conversion from the larger eddies to the smaller ones, where the large eddies extract energy from the main advective flow. These eddies are unstable and smaller eddies extract energy from them. This process continues as smaller and smaller eddies feed off the larger ones, until finally the eddies are so small that the viscosity of the fluid forces the conversion of the eddy energy into heat.

1.1.5 Plume dispersion and Eddies

Turbulent eddies displace parcels of air within a puff of contaminant, mixing polluted air with clean air. This mixing by bulk displacement eventually causes polluted air to occupy larger volumes at lower concentrations. However, not all eddies influence the dispersion of a contaminant in the same way.

Small eddies displace material on short distances, and contribute less to the dispersion of the pollutant, except perhaps at the edges of the puff, where mixing with clean air may cause some notable redistribution of material ("entrainment") (see figure 1.2).

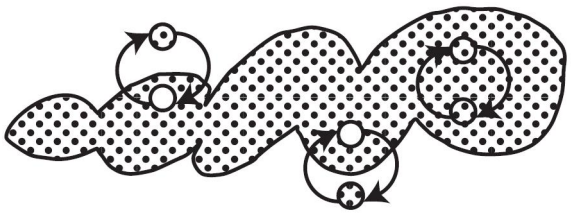

FIG. 1.2 – Schematic illustration of mixing of a plume by exchange of air parcels between the plume and the air outside the plume.

Conversely, eddies that are much larger than plume do not cause diffusion of the plume, but lead to a displacement of the whole plume. In fact, they tend to displace the entire mass of pollutant as a whole, a process known as '*meandering*' and thus contributes little to the internal mixing of the puff (figure 1.3). When the plume becomes wider, larger eddies also play a role in the diffusion.

Eddies that have spatial scales comparable to the size of the puff or plume are the most efficient in causing rapid mixing.

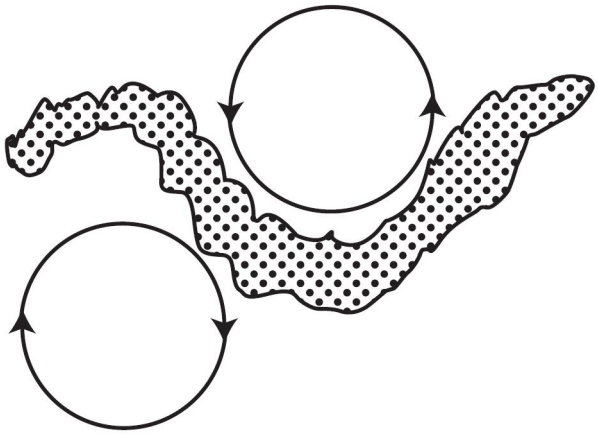

FIG. 1.3 – Effect of large eddies on the shape of a plume.

1.1.6 Terminology

When reading the Atmospheric Dispersion Modelling literature, one can easily become confused by different usage of the terms 'diffusion' and 'dispersion'. 'Diffusion' is often used without mentioning whether it is meant to include both molecular and eddy diffusion. To further complicate matters, some texts use the term 'dispersion' to refer to the combined effects of eddy diffusion and advection, whereas other texts use the term 'dispersion' in the sense of 'turbulent dispersion' but without the qualifier 'turbulent'.

For the sake of clarity in this discussion, the term 'diffusion' encompasses the combined effects of molecular and eddy diffusion. But, in atmospheric flows, the contribution of molecular

diffusion is several orders of magnitude less than that due to turbulent diffusion, and can usually be neglected.

When discussing about pollutant dispersion *entrainment* is often mentionned (see for example 5.2.2). This represents the mixing in ambient fluid into the plume which leads to the dilution of the pollution. In this part, the word 'plume' will be used to designate a continuous release of pollutant from a point source, while the word 'puff' will be used about an instantaneous released quantity of pollutant.

1.2 General governing Transport equation

The immediate destination is to lay out the governing equations that we will be using as the starting point for developing a framework to understand the statistics of atmospheric turbulence and dispersion. Specifically, this will lead up to the Atmospheric Dispersion Equation (ADE).

The starting point is really rather basic : it starts with the the mass conservation concept. It is assuming that mass conservation can be written quite simply as

$$c(\mathbf{x}, t) = P(c) + J(\mathbf{x}, t) \tag{1.1}$$

where the space- and time-varying property of interest (c) is affected by some physical redistribution processes (the operator P) and some biogeochemical source/sink/transformation process (J).

1.2.1 The continuum approach in Fluid Physics.

First, let us recall the basic approach of Fluid Physics where fluid phases are made up of a lot of molecules. For engineering practical purposes, it is not really necessary to deal with such complexity. This is more the realm of Statistical Physics which rests on a more fundamental description level.

The approach considers the fluid as a continuum and treats the real medium like a fictitious one within which any fluid property is averaged over a well chosen volume. From this averaging procedure, we define a fluid particle as a given set of elementary molecules enclosed in a particular delimited volume. The characteristic size of this averaging volume is obviously greater than the intermolecular distance, but should be small enough to lead to some meaningful averaged quantities. The physical fluid properties are then averaged over this set of molecules, and assigned to the centroïd of the fluid particle.

The concept of fluid particle makes it possible to derive local and integral forms of classical transport equations in the framework of Continuous Mechanics. Each spatial point within the real fluid domain is characterized by some averaged (macroscopic) fluid properties (e.g. viscosity, density, diffusivity,...) reflecting microscopic transport phenomena.

1.2.2 Integral Form of Conservation Law

Consider some extensive[2] property. Now define τ, which is stuff per volume of this property :

$$\Psi = \int_{\mathcal{R}} \tau \mathrm{d}\mathcal{R} \tag{1.2}$$

[2]Depends on the size or extent of the system and is the sum of its parts (mass, concentration, energy,...).

Here $\mathcal{R}(t)$ denotes a Lagrangian volume. The goal is to know how Ψ changes with time, that is :

$$\frac{\mathrm{d}\Psi}{\mathrm{d}t} = \frac{\mathrm{d}}{\mathrm{d}t}\int_{\mathcal{R}} \tau \mathrm{d}\mathcal{R} \tag{1.3}$$

Consider an Eulerian box, a fixed, non-deforming volume of fluid. At time t, let the Lagrangian volume $\mathcal{R}(t)$ coincide with the Eulerian volume R . In this case, since it is fixed to a control volume (doesn't vary as a function of time), the time derivative on the RHS in equation (1.3) can be taken inside :

$$\frac{\mathrm{d}\Psi}{\mathrm{d}t} = \frac{\mathrm{d}}{\mathrm{d}t}\int_{R} \tau \mathrm{d}R = \int_{R} \frac{\partial \tau}{\partial t}\mathrm{d}R \tag{1.4}$$

But this only gives the local change in Ψ. To take into account the motion of the fluid through the control volume the notion of flux must be considered.

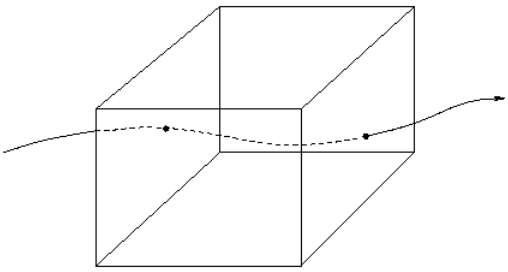

FIG. 1.4 – Eulerian Viewpoint.

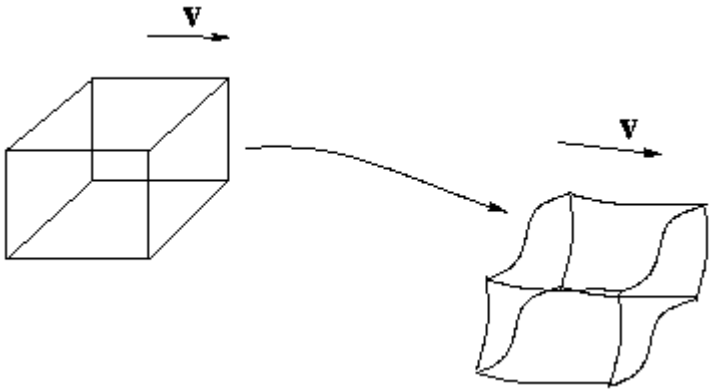

FIG. 1.5 – Lagrangean Viewpoint.

Flux and conservation

A *flux* is defined to be the amount of some quantity moving across a given surface per unit of time[3]. Very often, a flux can be derived from a *flux density*, which is a vector field so that the corresponding flux across a surface S is

$$\Phi = \int_S \phi \cdot \mathbf{n}\, \mathrm{d}S \tag{1.5}$$

where $\mathbf{n}$ is the unit normal to the surface.

Conservation (or Balance) law

In the conservation principle, the *Reynold's transport theorem* is the basis of both the fluid flow and solute transport equations. In an arbitary region R with surface $\partial R = S$, the total

[3] This ignores quantities like magnetic flux.

change in τ with respect to time must equal the local rate of change of τ within the region plus the flux out of the region. So, a conservation law is an equation of the form :

$$\frac{\mathrm{d}\Psi}{\mathrm{d}t} = \frac{\mathrm{d}}{\mathrm{d}t}\int_R \tau \mathrm{d}R = \int_R \frac{\partial \tau}{\partial t}\mathrm{d}R + \int_S \phi \cdot \mathbf{n} \mathrm{d}S - \int_R q \mathrm{d}R, \tag{1.6}$$

with the interpretation that τ is a density of something, so that the $\Psi = \int_R \tau \mathrm{d}R$ is the amount of this something inside R, the surface integral is the flux across the boundary of R, and $\int_R q \mathrm{d}R$ is a *source term*.

For example, τ could be ordinary mass density, in which case the source term is usually zero. Or τ could be a concentration of some chemical, in which case q would represent the result of a chemical reaction involving the chemical (creating or destroying it). In the latter case, the flux density might arise from a combination of movement of a macroscopic medium (e.g. fluid) and molecular diffusion of the chemical within the fluid.

Provided that the functions involved are sufficiently smooth ($\mathcal{C}^1$ is usually enough), the general conservation law can be rewritten as (**divergence or Gauss' theoreme**)

$$\frac{\mathrm{d}\Psi}{\mathrm{d}t} = \int_R \frac{\partial \tau}{\partial t}\mathrm{d}R + \int_R \nabla \cdot \phi \mathrm{d}R - \int_R q \mathrm{d}R \tag{1.7}$$

Differential Form of Conservation Law
If this is assumed to hold for *every* region R, we can apply the *Raymond-Dubois theorem*[4] to conclude that

$$\frac{\partial \tau}{\partial t} + \nabla \cdot \phi = q. \tag{1.8}$$

For example, in a continuum with mass density ρ and velocity $\mathbf{v}$, the mass flux is ρv and $q = 0$, so we get the law of mass conservation :

$$\frac{\partial \rho}{\partial t} + \nabla \cdot (\rho \mathbf{v}) = 0. \tag{1.9}$$

1.2.3 Derivation of the solute transport equation

The equation of mass conservation expresses a budget for the addition and removal of mass from a defined region of fluid. Conservation of mass requires that the time rate of change of mass within the control volume equals the rate at which mass enters the control volume plus the rate at which mass is gained or lost within the control volume due to sources and sinks.

Within the control volume there is a distribution of some species defined by the concentration field, $c(x, y, z)$. The total mass within the control volume is

$$M = \int_R c \mathrm{d}R. \tag{1.10}$$

M can change over time due to sources and sinks located within the volume, or due to fluxes of mass across the control volume boundaries.

In this case the flux under consideration is the net flux of mass out of the control volume, $\phi = c\mathbf{U}_c$, due to advection. In a fluid system there are two forms of mass flux, advection and diffusion (two types of velocity).

[4] If f is locally integrable and $\int_R f \mathrm{d}V = 0$ for every region R, then $f = 0$ *almost everywhere*.

Molecular diffusion

It is necessary to distinguish between two types of velocity : the velocity of the conserved substance, $\mathbf{U}_c$, and the ambient velocity $\mathbf{U}$. In the case of fluid flow, these are identical, whereas they differ for solute transport, as a solute may spread more rapidly than a fluid carrying it, due to such processes as diffusion, or more slowly if solute retardation occurs. The general conservation equation is rearranged :

$$\frac{\partial c}{\partial t} + \nabla \cdot (c\mathbf{U}) + \nabla \cdot [c\,(\mathbf{U}_c - \mathbf{U})] = q \tag{1.11}$$

The two types of velocity mentioned here are entirely generic and applicable to any kind of conserved property travelling within a medium.

Now the $c\,(\mathbf{U}_c - \mathbf{U})$ term should be considered. This represents the mixing of solute transport throught the fluid by diffusion. The following form of *Fick's Law* is employed , based on dimensionless concentration c :

$$c\,(\mathbf{U}_c - \mathbf{U}) = -\mathbf{D} \cdot \nabla c \tag{1.12}$$

where $\mathbf{D}$ is the molmecular diffusion tensor.

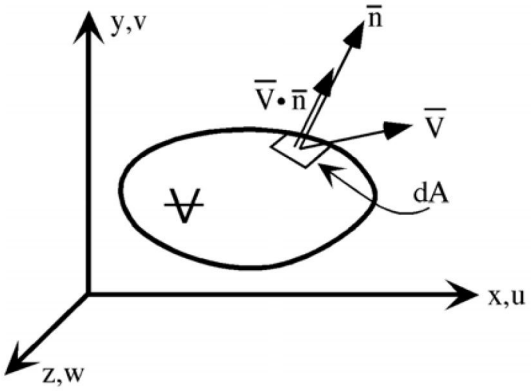

FIG. 1.6 – A control volume.

The mass conservation equation becomes :

$$\frac{\partial c}{\partial t} + \nabla \cdot (\mathbf{U}c) - \nabla \cdot (\mathbf{D} \cdot \nabla c) = q \tag{1.13}$$

$$\frac{\partial c}{\partial t} = -\nabla \cdot (\mathbf{U}c - \mathbf{D} \cdot \nabla c) + q \tag{1.14}$$

1.2.4 Divergence and mixing Ratio

Equation (1.13) can be written in the advective form :

$$\frac{\partial c}{\partial t} + \mathbf{U} \cdot \nabla c - \nabla \cdot (\mathbf{D} \cdot \nabla c) - q = -c \cdot \nabla \mathbf{U} \tag{1.15}$$

where the right hand side of Equation (1.15) would be zero if divergence and convergence of air masses were considered negligible.

A dimensionless quantity called the mixing ratio of the trace species can also be defined as :

$$\chi \equiv \frac{c}{\rho} \tag{1.16}$$

Using equation (1.16) and rearranging provides :

$$\frac{\partial \chi}{\partial t} + \mathbf{U} \cdot \nabla \chi = -\frac{\chi}{\rho}\left(\frac{\partial \rho}{\partial t} + \nabla \cdot (\mathbf{U}\rho)\right) \tag{1.17}$$

The continuity equation can be solved in terms of number density using either the flux form or in the advective form using mixing ratio, whichever is most convenient. It may be easier to avoid instability and to ensure mass conservation with number density in the flux form. It is simpler to treat divergence and vertical transport in the advective form because the mixing ratio is not affected by changes in pressure or temperature.

1.3 Turbulence

Instantaneous values at particular points in space are difficult to measure and visualise when considering three-dimensional turbulent flows. So for a source in a turbulent flow, there is prospect of success only for a theory of concentration statistics and the governing equations are often averaged over time.

In fact, the problem is that we cannot know, measure or solve all of the fluid motions. In order to completely describe the motion of the fluid, we need to take into account movement on scales ranging from the molecular (order $10^{-8}m$) to catchement area (order $10^{6}m$), for all of these motions that can contribute to changes in pesticides concentration. We are talking about 10^{14} orders of magnitude. However, it is possible to describe the molecular diffusion without knowing the individual motions of individual molecules : there are fundamental statistical mechanical laws that can be derived to describe the behavior in a statistical sense.

1.3.1 Turbulence approach and Time averaging

The various forms of the advection equation discussed above represent the instantaneous continuity equation. To get insight in the turbulent transport processes within the flow, the *Reynolds-averaged transport equation* describing the mixing of a passive dispersed phase are used. Starting point for the derivation of the governing equations of a turbulent flow is the *Reynolds decomposition* of the flow variables, which divides an instantaneous variable into a mean deterministic part and a turbulent stochastic part (see figure 1.3.1). The first one is the large scale of fluid motion and the other represents some small scale. It implies that there is some kind of conceptual **scale separation** and presupposes that the small scale processes are both stationary and random. Temporal averages require that the time scales of interest be short compared with scales at which average properties of the flow change appreciably.

$$\mathbf{U} = \overline{\mathbf{U}} + \mathbf{U}' \tag{1.18}$$

where

$$\overline{\mathbf{U}} = \frac{1}{T}\int_T \mathbf{U} \mathrm{d}t \tag{1.19}$$

which, naturally, requires that

$$\int_T \mathbf{U}' \mathrm{d}t = 0 \tag{1.20}$$

Here primed coordinates refer to the turbulent fluctuations of terms about their mean values.

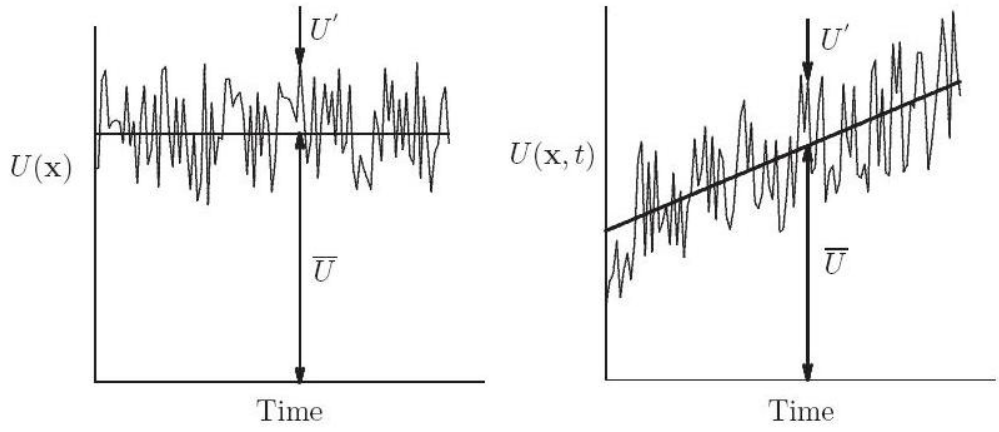

FIG. 1.7 – Instantaneous velocity in a turbulent flow with time-average for statistically steady flow (left), and ensemble-average for unsteady flow (right).

Now the same thing could be argued about the concentration c[5], i.e., there is some smoothly varying, mean concentration distribution coupled with some randomly varying component :

$$c = \overline{c} + c', \tag{1.21}$$

$$\overline{c} = \tfrac{1}{T}\textstyle\int_T c \mathrm{d}t, \text{ and} \tag{1.22}$$

$$\int_T c' \mathrm{d}t = 0 \tag{1.23}$$

and the mean flux can be written as :

$$\mathbf{U}c = \left(\overline{\mathbf{U}} + \mathbf{U}'\right)\left(\overline{c} + c'\right) \tag{1.24}$$

$$= \overline{\mathbf{U}}\ \overline{c} + \mathbf{U}'\overline{c} + \overline{\mathbf{U}}c' + \mathbf{U}'c' \tag{1.25}$$

$$\overline{\mathbf{U}c} = \overline{\mathbf{U}}\overline{c} + \tfrac{\overline{c}}{T}\textstyle\int_T \mathbf{U}' \mathrm{d}t + \tfrac{\overline{\mathbf{U}}}{T}\int_T c' \mathrm{d}t + \tfrac{1}{T}\int_T \mathbf{U}'c' \mathrm{d}t \tag{1.26}$$

$$= \overline{\mathbf{U}}\overline{c} + \overline{\mathbf{U}'c'} \tag{1.27}$$

and

$$\frac{\partial c}{\partial t} = \frac{\partial}{\partial t}(\overline{c} + c') \tag{1.28}$$

$$= \tfrac{\partial \overline{c}}{\partial t} + \tfrac{\partial}{\partial t}\left(\tfrac{1}{T}\textstyle\int_T c' \mathrm{d}t\right) \tag{1.29}$$

$$= \tfrac{\partial \overline{c}}{\partial t} \tag{1.30}$$

[5] a time average concentration is appropriate for continuous sources, for which the mean concentration field is steady, $\frac{\partial c}{\partial t} = 0$. In the case of an unsteady source, c will be an ensemble mean concentration.

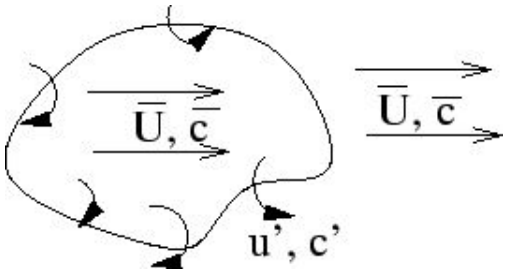

The order of integration and differentiation in continuous systems can be reversed (this is not always th case, see example the canopy flow in 3.2.4), and the mean distributions are time invariant. The integrals of the fluctuating components are by definition zero, except the integral $\overline{\mathbf{U}'c'}$. This is because there is likely to be a non-zero correlation between velocity and concentration fluctuations, since the former likely causes the latter. In fact, it is the *cross-correlation function* between velocity and concentration and will in general, not be zero. Therefore the equation (1.12)can be rewritten into the mean form :

$$\frac{\partial \overline{c}}{\partial t} = -\nabla \cdot \left(\overline{\mathbf{U}}\ \overline{c} + \overline{\mathbf{U}'c'} \right) + \nabla \cdot D \cdot \nabla \overline{c} + \overline{q} \tag{1.31}$$

where the first term on the right hand side is the 'macroscopic' *advective flux divergence*, and the second term is the *divergence of the* ***Reynolds Flux***. The 'overbar' refers to time averaging[6] as we have defined it for the velocity and concentration earlier. As a side note, if the stuff we were dealing with was momentum, then the equivalent term would be '***Reynolds Stress***'. This term $\nabla \cdot \left(\overline{\mathbf{U}'c'} \right)$ in right-hand side of the equation represents dispersion caused by both small and large scale turbulent processes, or eddies.

The balance equations alone do not provide complete systems ; they need appropriate constitutive relations for 'closure'. Turbulent dispersion introduces additional unknowns into the continuity equation. **Closure theory** is the large body of work which attempts to 'close' equation by finding various theoretical or observational relations in turbulence to solve for the additional unknowns.

1.3.2 The closure problem

The term $\overline{\mathbf{U}'c'}$, as it concerns an extra unknown variable (Reynolds flux or shear stress), an extra relation is needed to solve this equation analytically. This is called a closure-problem. The *K-theory* (or *mixing length theory*) which is a substitution method for averages $\overline{\mathbf{U}'c'}$ of turbulent fluctuations is recalled. This is the simplest closure approximation.

First-order Closure assumption : K-theory

An usual engineering practice is to model the turbulent transport term using the *eddy diffusivity* concept, also known as the *gradient approximation*. This model is motivated from the *Kinetic Theory of Gases*, where the mass flux is found to be proportional to the gradient of the mass fraction and the molecular diffusivity **D** is found to be proportional to the mean molecular speed and the mean free path between molecular collisions (see also (1.12), *Fick's Law*).

[6]The ensemble averaging operator, denoted with an overbar, fulfils the so called Reynolds conditions.

Gradient transport models are derived from the continuity equation with the turbulent fluxes of material assumed to be uniquely linearly to mean gradients concentration of c, with K being the constant of proportionality.

In a randomly moving fluid, there is a characteristic space scale of displacement, which can be called l'_{turb}. This may be the mean vertical motion of a fluid parcel caused by breaking internal waves, or the horizontal movement caused by eddies sweeping by. This random displacement, coupled with a large scale mean gradient in concentration results in an apparent concentration fluctuation c'. Thus, by making an analogy between the random turbulent motions of 'fluid particles' and the random molecular motion in a fluid, the turbulent transport term is written as

$$c' = -Bl'_{turb}\nabla \cdot \overline{c} \tag{1.32}$$

$$\overline{\mathbf{U}'c'} = -\overline{\mathbf{U}'Bl'_{turb}\nabla \cdot \overline{c}} = -\overline{\mathbf{U}'Bl'_{turb}}\ \overline{\nabla \cdot \overline{c}} \tag{1.33}$$

$$= -\mathbf{D_T}\overline{\nabla \cdot \overline{c}} \tag{1.34}$$

with the eddy tutbulent diffusivity $\mathbf{D_T}$ given by

$$\mathbf{D_T} = \overline{\mathbf{U}'Bl'_{turb}} \tag{1.35}$$

By a trial-and-error procedure and comparison with experimental data, the constant B is found to be around 0.1, but this depends on how l'_{turb} is defined.

The causes of random concentration fluctuations are separating into two components : one due to the large scale distribution of c (thus a concentration dependent part) and one due to the fluid motion (and hence not related to c, $\mathbf{D_T}$). Thus :

$$\frac{\partial \overline{c}}{\partial t} = -\nabla \cdot \left(\overline{\mathbf{U}}\ \overline{c}\right) + \nabla \cdot \left[\left(\mathbf{D_T} + D\right)\nabla \cdot \overline{c}\right] + \overline{q} \tag{1.36}$$

The $\mathbf{D_T}$ term is with the molecular diffusion term since they are functionally similar in form. $\mathbf{D_T}$ may be a function of space and hence should be kept inside the derivative in the R.H.S. of equation (1.36). The eddy diffusivity concept is usually much better for an *inert scalar* than for a *reacting scalar*. For high Reynolds numbers $D << \mathbf{D_T}$, which suggests that the molecular diffusion may be neglected. Now, the turbulent diffusivity will be denoted by the symbol $\mathbf{K}$ (rather than $\mathbf{D_T}$) to conform to the standard notation in atmospheric pollution.

To illustrate this, consider a wind flow of $5ms^{-1}$ with a typical turbulence intensity of 10%, so that $U' = 0.5m/s$. In the atmospheric boundary layer, the lengthscale is proportional to the height above the ground . Let us take that $l'_{turb} \approx 500m$. Then $\mathbf{K} \approx 25m^2s^{-1}$. At standard temperature and pressure, the molecular diffusivity of air is $\approx 2.2\times10^{-5}m^2s^{-1}$. Molecular action is always present at the smallest (e.g. *Kolmogorov*) scales, but these contribute very little to the overall diffusion of the scalar. In other words, the dispersion is a function of the large scales only and the turbulent diffusivity suffices. $\mathbf{K}$ is a property of the fluid flow (not of the fluid, and not of the pollutant studying). It is often called the turbulent diffusivity coefficient since it appears in the equation like a diffusivity term.

Applications and Limitations

K-theory is typically used in dispersion models, where the emphasis is often on atmospheric chemistry and regional transport. An important consideration is that gradient transport models

of diffusion have implicit time and space scales. The mean wind components represent averages over some time scale and space scale. Velocity fluctuations with time and space scales less than those implicit in the mean wind components are considered turbulence. Therefore, they are implicitly included in the proportionality constant **K**. However, the rate of diffusion of a plume depends on the plume size (see 1.1.5).

This limits the applicability of K-theory models of diffusion to instances where the size of the plume is greater than the size of the dominant turbulent eddies so that all of the turbulence implicit in K is taking part in the diffusion. The vertical diffusion of point sources can be modeled using K-theory for sources near the ground, where the turbulent eddies are sure to have scales less than the thickness of the plume. However, K-theory can be used to model elevated releases only when the vertical extent is spread out over several hundred meters.

There is a lot of criticism behind the use of the gradient approximation for modelling turbulent transport and indeed sometimes equation 1.34 fails to predict the correct magnitude of $\overline{U'c'}$. Nevertheless, the eddy diffusivity concept remains a very useful approximation for providing a tractable closure. In fact, this is not so unreasonable for undisturbed flows. In the surface layer for example, one relationship between the vertical fluxes and vertical gradients of windspeed, temperature and humidity are consistent with an eddy diffusivity and is given by :

$$K_z = k_v u_* z/\phi(z/L) \tag{1.37}$$

where $k_v \approx 0,4$ is the Von Karman constant, z is height above ground, u_* is the friction velocity, L an appropriate length scale and ϕ is some unknown "universal function".

1.4 The Atmospheric Dispersion Equation

The traditional approach to model contaminant transport is by using of the *Advection Dispersion Equation* (**ADE**). The ADE of air pollution in the atmosphere is essentially a statement of conservation of the suspended material. Solutions to the ADE in a macroscopically homogeneous system give a plume that spreads by a *Fickian* dispersive process.

Consider first a neutral plume in a neutral Planetary Boundery Layer (see 2) (i.e. temperature θ constant, no *buoyancy forces*). The plume is advected by the wind and dispersed by the turbulence. The dispersion of a non-reactive species whose instantaneous concentration is c is considered. It is assumed too that this additive is released passively (isokinetically), or that we are only calculating its spread in regions far enough from any catastrophic injection point that its motion can be considered driven uniquely by regular atmospheric flow.

A plume model assumes also that conditions are horizontally homogeneous (everywhere the same) and steady state. As shown in figures 1.8 and 1.10, plume models attempt to capture some essence of what is seen, but they make no claim to depict reality. Plume models are useful for quick estimates, so long as the wind direction is relatively steady, the wind speed is greater than $1ms^{-1}$, and the distances downwind from the release are on the order of $20km$ or less.

1.4.1 Derivation of the ADE

As already said, generally in atmospheric flow, transport by molecular diffusion can be neglected relative to convection ($0 \sim D << \mathbf{K} = \mathbf{D_T}$) then the *Peclet number*[7] is $P_e >> 1$. The

[7] A Peclet number is a dimensionless number that defines the ratio of transport by advection to the rate of transport by molecular diffusion

FIG. 1.8 – Industrial Air Pollution Plume : diffusion of smoke from a tall stack during afternoon.

continuity equation under *Boussinesq approximation* (density is treated as constant in time except where multiplied by gravity (ie except as it affects buoyancy)) tell us $\nabla \cdot \mathbf{U} = 0$, hence, in advection form the conservation equation, for large P_e and away from any source, becomes

$$\boxed{\frac{\partial \overline{c}}{\partial t} + \overline{\mathbf{U}} \cdot \nabla \overline{c} = \nabla \cdot (\mathbf{K} \nabla \cdot \overline{c}) + \overline{q}} \tag{1.38}$$

The possibility that the eddy diffusivity should be a tensor, viz.,

$$\overline{u_i' c'} = -K_{ij} \frac{\partial \overline{c}}{\partial x_j} \tag{1.39}$$

$$\tag{1.40}$$

where $\mathbf{K} = (K_{ij})$ is the *eddy difFusivity*, a function of location and time, has been examined in wind tunnel simulations of flow near ground ([14],[15],[16]), but the off-diagonal components of

K were found to be negligible. So we write :

$$\overline{u'c'} = -K_x \frac{\partial \overline{c}}{\partial x} \tag{1.41}$$

$$\overline{v'c'} = -K_y \frac{\partial \overline{c}}{\partial y} \tag{1.42}$$

$$\overline{w'c'} = -K_z \frac{\partial \overline{c}}{\partial z} \tag{1.43}$$

where the K's are scalar eddy diffusivities ($[m^2 s^{-1}]$) which could be different for different directions of motion ($K_x \neq K_y \neq K_z$). The eddy diffusivity is allowed to be a function of the direction $K_i = K_i(x, y, z)$. This is usually the case in atmospheric turbulence : the velocity fluctuations are not really equal in the three directions. Note that we have by assumption ruled out the possibility that a mean gradient along direction i could drive a mean flux along a different direction j.Hence the eddy viscosity is strictly speaking a (diagonal) tensor.

Turbulent eddy diffusivities in the atmosphere

Unfortunately, the turbulent diffusivities K_x, K_y and K_z are unknown in most flows, and in the atmospheric boundary layer, K_z is not constant, but increases with height above the ground. In addition, K_y and K_z increase with distance from the source, because the turbulent diffusion is affected by different scales of turbulence in the atmosphere as the plume grows. Typically in the atmosphere $K_y > K_z$, which explains why the cross-section of a plume often takes An elliptic shape.

The above parameterisations for the alongwind flux $\overline{u'c'}$ and the crosswind flux $\overline{v'c'}$ are rather poor, and it is troublesome to determine the appropriate diffusivity, because the horizontal components of the wind contain variations out to very long timescales. Vertical motion, however, is restricted to short timescales (due to presence of the ground), so the K-model for the vertical flux is often good.

If the turbulence is uniform and external to the plume then it may be assumed that the turbulent diffusivity, **K**, is a constant. Now K_x, K_y, K_z are set constant (spatially uniform diffusivity) [8]. Under these restrictions, our flow field is a homogeneous field of turbulence. In reality there can be no such thing as homogeneous turbulence, particularly in the region of a barrier such as the ground (adjacent to which the length scale for motion normal to the wall vanishes). The conservation equation becomes :

$$\frac{\partial \overline{c}}{\partial t} + \overline{\mathbf{U}} \cdot \nabla \overline{c} = = \mathbf{K} \nabla^2 \cdot \overline{c} = \mathbf{K} \cdot \Delta \overline{c} + \overline{q} \tag{1.44}$$

In reality, the exchange coefficients K_{x_j}, are never constant in time or space. However, if they are assumed to be constant, then the turbulent diffusion process have the form of pure "Fickian diffusion", although in fact they represent turbulent convection. This simplification leads to the Gaussian Plume Model.

$$\frac{D\overline{c}}{Dt} = \frac{\partial \overline{c}}{\partial t} + \overline{\mathbf{U}} \nabla \cdot \overline{c} = \mathbf{K} \nabla^2 \overline{c} + \overline{q} \tag{1.45}$$

[8] these 'constants' are atmospheric statistics that are invariant in space over (i) some interval in time, the averaging interval ; or (ii), if ensemble averages are used, across the ensemble.

This is often called the advection-diffusion equation.

Often this equation is simplified by ignoring the advective terms. If the spatial variation of the density and the advection of the resolvable flow velocities are ignored, the K-Diffusion model is written in the following simplified form (also ignoring the source term) :

$$\frac{\partial \overline{c}}{\partial t} = K_x \frac{\partial^2 \overline{c}}{\partial x^2} + K_y \frac{\partial^2 \overline{c}}{\partial y^2} + K_z \frac{\partial^2 \overline{c}}{\partial z^2} \tag{1.46}$$

The solution of this equation for a release at the surface ($z = 0$) is given through a Fourier transform analysis as shown in the section B.1 (see also B.2 and B.3). In this case the exact solution to the equation takes the form of a Gaussian distribution with :

$$\overline{c} \propto \exp\left(-\frac{x^2}{2\sigma_x^2} - \frac{y^2}{2\sigma_y^2} - \frac{z^2}{2\sigma_z^2}\right) \tag{1.47}$$

1.4.2 Analytical solutions for the ADE

Analytical solutions are of fundamental importance in describing and understanding physical phenomena. Analytical solutions (as opposed to numerical ones) explicitly take into account all parameters of a problem, so that their influence can be reliably investigated and it is easy to obtain the asymptotic behavior of the solution, which is usually difficult to generate through numerical calculations.

There are numerous available known analytical solutions for general initial and boundary conditions to the linear advective diffusion equation with uniform flow and constant coefficients (see, for example [17], [18]). Among these specific solutions, the best-known is the so-called Gaussian solution. In fact, the models based on it (so-called Gaussian models) use empirical parameters of dispersion in order to force the Gaussian solution to represent the actual concentration field. Moreover numerical solutions are expansive and cannot be easily "interpreted" as this simple model.

Nevertheless practical problems generally involve non uniform velocity fields and variable diffusion coefficients. Unfortunately, no general exact solution is known for the complete form of the three-dimensional ADE describing the atmospheric transport and dispersion of air pollution (equation (1.48)).

$$\frac{\partial \overline{c}}{\partial t} + \overline{u}\frac{\partial \overline{c}}{\partial x} + \overline{v}\frac{\partial \overline{c}}{\partial y} + \overline{w}\frac{\partial \overline{c}}{\partial z} = \frac{\partial}{\partial x}\left(K_x \frac{\partial \overline{c}}{\partial x}\right) + \frac{\partial}{\partial y}\left(K_y \frac{\partial \overline{c}}{\partial y}\right) + \frac{\partial}{\partial z}\left(K_z \frac{\partial \overline{c}}{\partial z}\right) + \overline{q} \tag{1.48}$$

But in a few specialized cases, there exists few analytical solutions to the ADE with variable coefficients.

Analytical solutions to this equation for the case of dispersion of passive pollutants in a turbulent flow were first obtained in the 1920's by Roberts (1923) and Richardson (1926). [19] presented a bi-dimensional solution for ground-level sources only, in cases where both the wind speed and vertical diffusion coefficients follow power laws as a function of height.

[20] obtained a solution to the transient problems considering the velocity u, constant and taking K_z as a function of height and of the friction velocity employing Legendre polynomials.

[21] presented an analytical solution to the two dimensional problem for a source on the ground, considering power type profiles for the wind and diffusion coefficients, and also the pollutant absorption effect by soil.

[22], [23] and [24] provided analytical solutions to the one dimensional advective diffusion equation with arbitrary time dependant diffusion and velocity coefficients.

In [25], analytical solutions are provided for the one-, two- and three- dimensional ADE with spatially variable velocity and diffusion coefficients. By assuming that the velocity is proportional to distance and the diffusion coefficient is proportional to the square of the velocity, there is a simple transformation which reduces the spatial variable equation into a constant coefficient problem.

[26] provided analytical solutions to the one dimensional ADE with the diffusion coefficient as an asymptotic function of distance.

In [27] work, a closed form solution of the three-dimensional ADE in a Cartesian coordinate system is obtained by applying rules, based on the Lie symmetries, to manipulate the exponential of the differential operators that appear in its formal solution.

[28] provided analytical solutions for radial flow in two and three dimensions to the ADE with the diffusion coefficient proportional to some power of the Péclet number.

[29] derived analytical solutions to the two dimensional ADE with constant, linear, asymptotic and exponentially time dependant diffusion coefficients.

[30] solved a three dimensional problem for a continuous source on ground level, considering that wind velocity and the diffusivities have power type profiles.

[31] presented a mathematical model for atmospheric dispersion in low winds with eddy diffusivities as linear functions of downwind distance (see also [32]).

[33] reported the state-of-art of the ADMM (Advection Diffusion Multilayer Model, subdividing the ABL in different layers) model, with solutions of the one and two-dimensional, steady state and time dependent ADE obtained by Laplace transform application.

In [34], operational models that use solutions of the advection-diffusion equation based on more realistic assumptions than that of homogeneous wind and eddy diffusivity coefficients are presented. In particular a new parameterization for a model using a solution that accepts wind and eddy diffusivity profiles described by power functions of height is introduced. A short review of the analytical solutions of the following two-dimensional ADE is also provided.

$$\overline{u}\frac{\partial \overline{c}}{\partial x} = \frac{\partial}{\partial z}\left(K_z \frac{\partial C}{\partial z}\right) + \overline{q} \tag{1.49}$$

Many of these analytical solutions are restricted to problems with specific boundary conditions and have limited practical relevance or are complicated to evaluate.

1.5 The Diffusion Equation and the Gaussian Dispersion Model

1.5.1 Presentation of the classic Gaussian Dispersion Model

Because of the highly random nature of the motion of the turbulent eddies, it is obvious that the concentration of a dispersing plume is also in general a random variable, about which one can only make probabilistic predictions [35]. Hence, attempts to describe concentration distributions have been restricted to considering ensemble average concentrations, which show much more reguIar behaviour and can be more easily described mathematically [36] (see 1.9).

Indeed, it has been shown experimentally that in a field of homogeneous turbulence, ensemble average concentrations can be approximated by a Gaussian distribution [35]. No rigo-

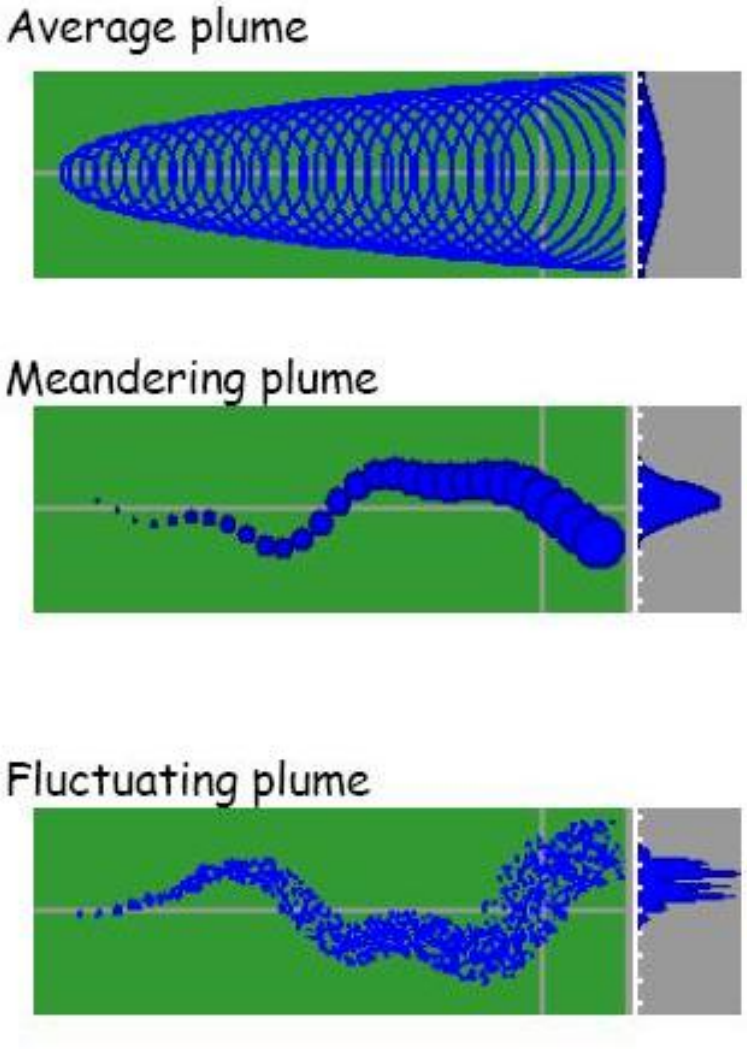

FIG. 1.9 – The figure shows that the shape of the plume depends of the averaging time chosen. A time averaged plume envelope (ideal plume) is shown at the top and a snapshot of an instantaneous plume boundary profile at the bottom. Relative concentration are plotting on the right (from [37]).

rous theoretical justification for the observed Gaussian distribution seems to exist ; Csanady sumarizes some of the more convincing arguments, but concedes that "··· the question why a Gaussian distribution is observed in experiments is not yet satisfactorily answered···". Few investigations into this question have been undertaken in the recent literature. Nonetheless, common practice is to assume a Gaussian distribution for averaged concentration distributions, and this is the basis of the Gaussian puff model and its variants.

Gaussian models are usually used in the case of gas dispersion and atmospheric pollution ([38], [39], [40]). With adaptations, this kind of modelling can be used for particle diffusion where the wind direction is considered as the centre line of the smoke cloud. On the perpendicular direction of the wind, the distribution has a Gaussian shape with a linear increase of the amplitude while moving downwind from the emission source. That leads to a high concentration of particles close to the source witch decreases continuously while going further. This model being a conservative model means that the integer of equal length sections of the cloud in wind

direction contains the same amount of particles. The increasing rate of the cloud is linked to dispersion coefficients (K_x, K_y, K_z) that depend on air stability and surface roughness (see 2.2 and 2.4). Gaussian models are well known to be robust for dispersion applications, even if they are considered as rather statistical and of low theoritical interest by the scientific community.

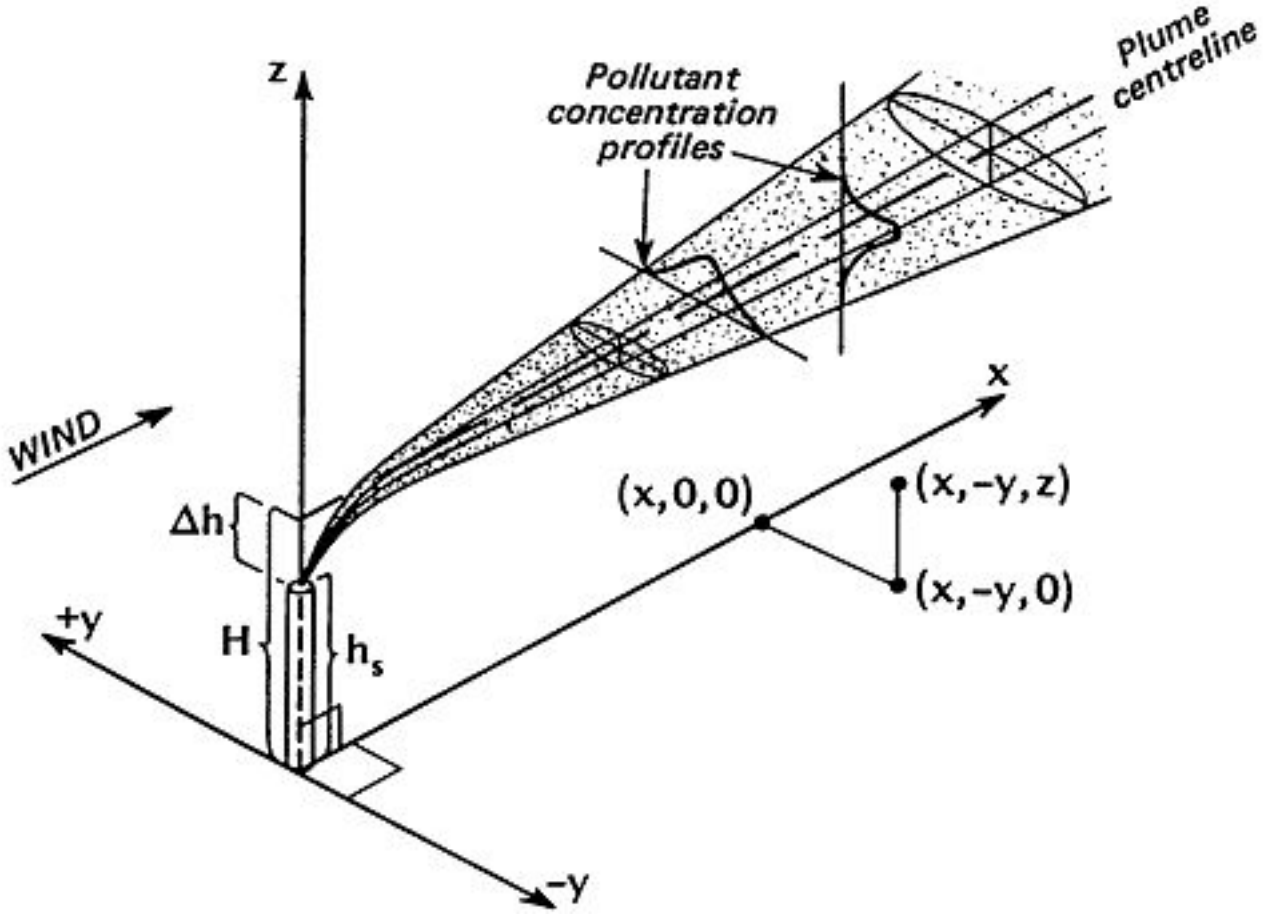

FIG. 1.10 – Gaussian Plume Model

The remainder of the conservation equations are neglected, thus the Gaussian Plume Model is a major simplification of the fundamental physics of an atmospheric flow. Steady-state meteorological conditions are assumed, and hence it assumes that the plume has a straight centre-line, pointing in the wind direction. Therefore, it cannot represent recirculation of the pollutant since complex wind conditions are not allowed. Mass is conserved, there are no material losses due to chemical reaction or from deposition.

This paragraph presents the Gaussian Plume Dispersion model for a pollutant release from a ground source. This is accomplished by a *K-diffusion* equation given by equation :

$$\frac{\partial c}{\partial t} = K_{c_x}\frac{\partial^2 c}{\partial x^2} + K_{c_y}\frac{\partial^2 c}{\partial y^2} + K_{c_z}\frac{\partial^2 c}{\partial z^2}, \tag{1.50}$$

where $c(x, y, , z, t)$ is the ensemble-average concentration ($[kgm^{-3}]$), M is the mass of contaminant released $t = 0$ ($[kg]$), x, y, z are the coordinates relative to the centre of mass of the plume ($[m]$),

The usual practice is to adopt a coordinate system where the x-axis is along the direction

of the mean wind, U, the y-axis is in the cross-wind direction, i.e. perpendicular to the x-axis and horizontal, and the z-axis is vertical. The following conditions are added :

– initial conditions :

$$c(x, y, z, 0) = 0, \text{ for } x \neq 0, y \neq 0, z \neq 0 \tag{1.51}$$

– boundary conditions : Pollutant concentration tends to zero at large distances from the source $c \to 0$ as $|x|, |y|, z \to +\infty$

$$c(\pm\infty) \longrightarrow 0; \nabla c(\pm\infty, t) \longrightarrow 0 \tag{1.52}$$

– continuity :

$$\int_{-\infty}^{+\infty} \int_{-\infty}^{+\infty} \int_{-\infty}^{+\infty} c(x, y, z, t) \mathrm{d}x\mathrm{d}y\mathrm{d}z = M \tag{1.53}$$

where M is the mass of the release $[kg]$.

Using forward and reverse three-dimensional Fourier transform an analytical solution is given by (see chapter B) :

$$c(\mathbf{x}, t) = \frac{M}{(2\pi)^{3/2} \sigma_x \sigma_y \sigma_z} \exp\left[-\left(\frac{x^2}{2\sigma_x^2} + \frac{y^2}{2\sigma_y^2} + \frac{z^2}{2\sigma_z^2}\right)\right] \tag{1.54}$$

This is the Gaussian Plume equation for a ground-level pollutant release. σ_x, σ_y, and σ_z represent the standard deviations (the spread of the plume and also known as the dispersion coefficients $[m]$) of the Gaussian distribution in the x, y and z directions. They increase downstream, i.e. $\sigma_x = \sigma_x(x)$, $\sigma_y = \sigma_y(x)$ and $\sigma_z = \sigma_z(x)$. These functions determine the nature of the result and have to be estimated empirically. They are also often given in the following form :

$$\sigma_x = \sqrt{2K_{x_c} t}, \ \sigma_y = \sqrt{2K_{y_c} t}, \ \sigma_z = \sqrt{2K_{z_c} t} \tag{1.55}$$

Simplifications due to Symmetry

In practical atmospheric dispersion of pollutant clouds, the wind has to be taken into account. As the magnitude of the vertical velocity component is smaller than that of the horizontal, advection in the vertical direction is neglected in comparison to that in the horizontal direction. This assumption is valid except for particulate pollutants (with appreciable settling velocities) under low wind speed conditions. Owing to the restriction of this analysis to horizontally-uniform flows [9], $\overline{w} = 0$ and $\overline{u} = \overline{u(z)}$. By choice of axes [10] we can set $\overline{v} = 0$.

Figure 1.11 illutrates the relative diffusion coordianate system, and the qualitative difference between puff and plume diffusion. The moving coordinate system for puff diffusion is advected with the mean wind, as indicated by the arrow. In general, the three dispersion coefficients are distinct, and the puff contours will be ellipsoidal in shape, rather than spherical.

[9] but note that the concentration statistics will in general not be horizontally uniform.

[10] Here we assume dispersion on the local scale ; for longer range dispersion, in which case the plume occupies a deeper region of the height-axis, it will not be possible to eliminate $\overline{v}$ by choice of the orientation of the y-axis because the mean wind direction in general varies with height.

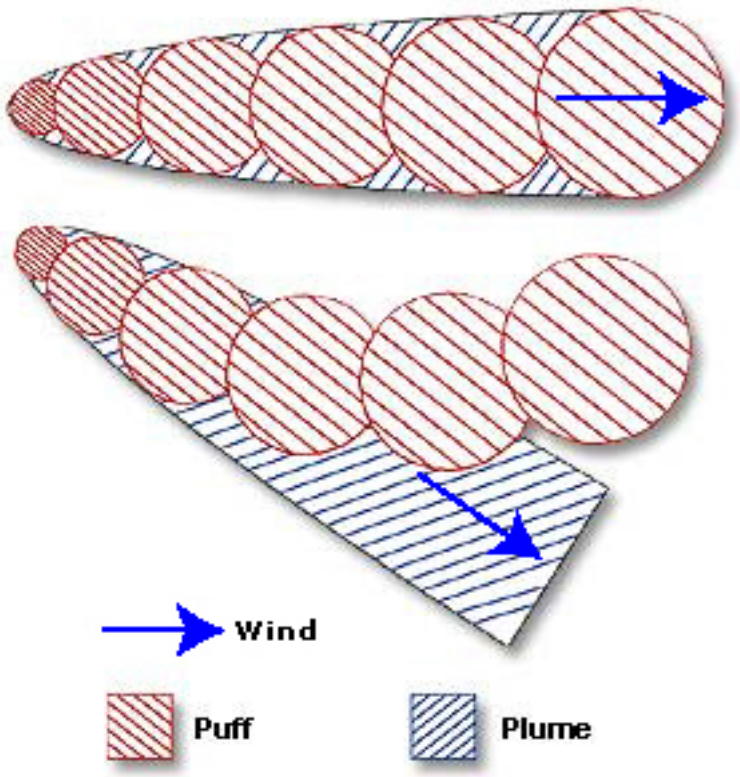

FIG. 1.11 – Gaussian Puff vs Gaussian Plume : A comparison between Gaussian puff (top) and plume (bottom) diffusion, showing concentration contour surfaces.

Slender or thin plume approximation

It is assumed that

$$\left|\overline{u}\frac{\partial \overline{c}}{\partial x}\right| >> \left|\frac{\partial \overline{u'c'}}{\partial x}\right| \tag{1.56}$$

(neglect of divergence of streamwise mass flux carried by turbulent flow ; there are some problems for which in some regions this may be in seriously in error).

A consequence of that would be, that the alongwind flux is just $\overline{uc}$, i.e. alongwind transport occurs entirely by the mean wind, so in the model, the total alongwind mass flux $M_f[kgs^{-1}]$ is

$$M_f = \int_{-\infty}^{y=\infty} \int_{z_0=0}^{z=\infty} \overline{uc}\mathrm{d}y\mathrm{d}z \tag{1.57}$$

So, to ensure the conservation of mass, such models must satisfy this integral, where the integration is taken over the $y-z$ plane, perpendicular to the plume axis. The underlying equation is linear so superposition of solutions is possible.

1.6 Problem Limitation

Most operational models predict the ensemble mean transport and diffusion for the conditions specified. However, atmospheric releases are individual realizations from imperfectly defined ensembles. The within-ensemble variance of certain processes can be quite large. For

instance, the first-order approximation of the lateral concentration profile of a plume is the often-assumed Gaussian shape. Inspection of tracer plumes reveals fluctuations superimposed on this Gaussian shape of the order of a factor of two. These fluctuations are not addressed or characterized in most operational transport and diffusion models [37].

In practice most of the estimates of dispersion from continuous point sources are based on the Gaussian approach. A basic assumption for the application of this approach is that the plume is dispersed by homogeneous turbulence. However, due to the presence of the ground, turbulence is usually not homogeneous in the vertical direction. Moreover, the input parameters of the Gaussian plume model are often related to simple turbulence typing schemes or stability classes.

The time dependence of $c(x, y, z, t)$ in equation (B.44) is contained in the dispersion coefficients, which are functions of time and meteorological characteristics of the flow. One of the major challenge when creating a Gaussian model of atmospheric dispersion is to correctly define the dispersion parameters [41]. However, growth of the dispersion coefficients are found to depend on complex statistical properties of the turbulent flow. These parameters are usually difficult to assess, and require research-grade turbulence measurements ([42]).

In the absence of such measurements, it is general practice to use semi-empirical parametrizations (see E.1). These are formed by observing the behaviour of dispersing plumes or puffs under a broad range of conditions, and generally express the dispersion coefficients as functions of downwind distance from the source and atmospheric stability. To use such parameterizations, one must first characterize the atmospheric stability, preferably by a simple scheme based on inexpensive and easily obtained measurements.

The problem with such stability classes is that each covers a broad range of stability conditions ; they are also very site-specific and biased towards neutral stability when unstable or convective conditions actually exist. In addition, the influence of these factors on the calculated ground-level concentration is considerable.

Wind data to drive the Gaussian plume model can come from a single point measurement of wind speed and direction and is assumed to apply for the entire domain. This is only a useful approximation over flat and homogeneous terrain and during long lasting stationary conditions.

So, deriving the Gaussian dispersion equation requires the assumption of constant conditions for the entire plume travel distance from the emission source point to the downwind ground-level receptor. Yet it cannot be said with any reasonable certainty that the wind-speed at the plume centreline and the atmospheric stability class are known exactly or that they are constant for the entire plume travel distance. Whether such homogeneity actually occurs is a matter of pure chance, particularly for large distances. Also, determining the exact wind-speed and atmospheric stability class at the plume centreline height requires (a) the prediction of the exact plume rise and (b) the exact relation between wind-speed and altitude ... neither of which are achievable.

Steady state solutions are often obtained with the time-dependent equation ($\partial c/\partial t \neq 0$), but with all meteorological and other parameters kept constant. One then calculates forward in time until the steady state is reached for the concentration. Steady state model by the nature of the inherent assumption of the time constancy of the parameters can be applied only for shorter distances and for shorter travel time.

However, as far as regulatory applications are concerned, Gaussian approach seems to be the best. [43], has noted that the Gaussian formula, properly used, is peerless as a practical diffusion-modelling tool. It is mathematically simple and flexible and moreover it is accord with much through not all-working theory.

In short, the Gaussian models assume an ideal steady-state of constant meteorological conditions over long distances, idealised plume geometry, uniform flat terrain, complete conservation of mass, and exact Gaussian distribution. Such ideal conditions rarely occur. This formula is widely used in practical prediction problems since it is relatively simple . This can be controversial though, since the results have implications for planning applications and risk assessments.

The different advantages are summarized by the following list :

- wide acceptance
- relative simplicity
- effective in spite of many inherent assumptions when used properly
- requires minimal input data and without detailed input data other more realistic models only marginally improve predictions

Chapitre 2

Basic Meteorology

This Chapter combines a general introduction to basic meteorology and a description of the atmosphere. The goal of this part is a description of the main features that occur in our domain of interest within the atmosphere and drive the pollutant transport.

The atmosphere can be divided into various regions where different length scales and different driving mechanisms are important (see figure 2.1). The choice of appropriate length scales is important in obtaining a phenomenological description of the turbulent processes through dimensional analysis (2.1.6). The first section (2.1) provides the basic properties of the atmospheric boundary layer.

One of the important themes of this thesis is the degree of mixing (level of turbulence) in the atmosphere (see 2.1.5 and 2.1.6). This quantity provides the basis for answering the 'how much' questions. One way to deal with this turbulence is to consider the "stability concept". In the section 2.2, a range of stabilities typically encountered are associated with the differing levels of turbulence.

Another aspect is the major effect that the mean wind (speed and direction) has on the movement and dispersion of pollutant. This is obviously the most important meteorological parameter that controls the spreading of pollutants. The wind speed and direction provides the basis for addressing "where" the plume goes and "when" the plume arrives. Wind can be crudely regarded as the manifestation of a fluid, the air, moving across a rough surface, the earth. The movement is almost exclusively caused by the non-uniform heating of the atmosphere by solar radiation which drives convective flows of air above the surface. So, the last section 2.4 presents the main features of the wind within the ABL.

2.1 Atmospheric Boundary Layer Description

2.1.1 Introduction

Many of the cases of interest in *ATD* (*Atmospheric Transport Diffusion*) occur in the *troposphere*, the portion of the atmosphere up to $15km$ above the ground. However, there are cases when transport and diffusion within the upper atmosphere are important (e.g., protecting air traffic from volcanic ash, tracking the path of materials from major explosions, or tracking the dispersion of materials originally constrained within the lower atmosphere but which slowly leak into the layers of air aloft). This part mainly discusses atmospheric processes near the surface, which is the domain of this study.

Meteorologists distinguish the layer reaching from the earth's surface up to altitudes of about one kilometer, from the free atmosphere above ([44]). The *atmospheric boundary layer* (ABL), also known as the *planetary boundary layer* (PBL) or peplosphere, is used to characterize this lowest part of the atmosphere. Its behavior is directly influenced by its contact with the Earth's surface, and is therefore often in a highly turbulent state. The movement of the air is retarded and physical quantities such as flow velocity, temperature, moisture etc., display rapid fluctuations (turbulence) and vertical mixing is strong. Most emissions, transports and transformation of pollutants takes place within the ABL. Its wind and turbulence fields are therefore important for understanding nature and mechanisms behind the dispersion of pollutants. The part of meteorology studying the small scale effects in the ABL is called micrometeorology or boundary layer meteorology.

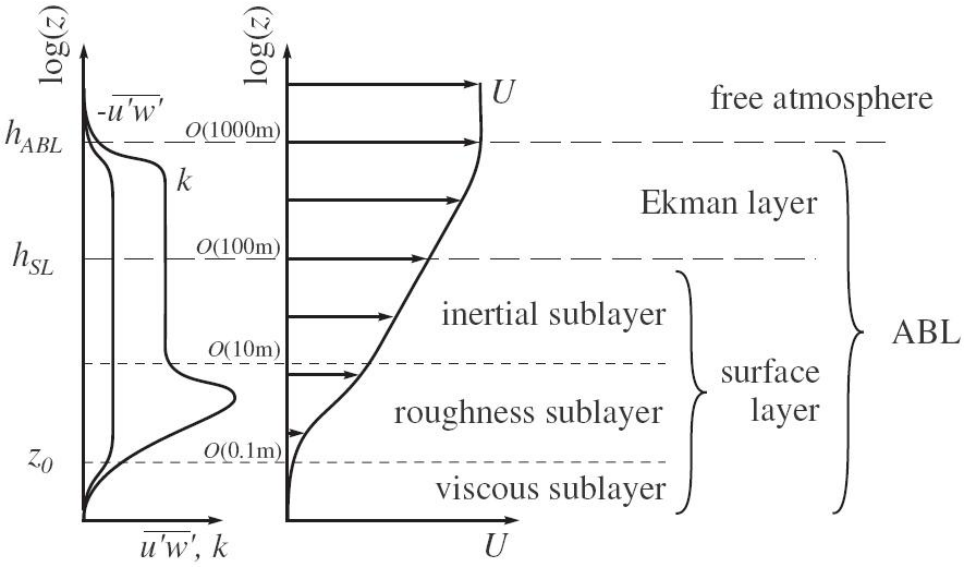

FIG. 2.1 – The structure of the atmospheric boundary layer [45]. Schematic overview over different layers in atmospheric flow with typical profiles for mean wind $\overline{u}$, reynolds-stress $-\overline{u'w'}$ and turbulent kinetic energy k (from [46]).

2.1.2 The Structure of the Atmosphere

Approaching the earth from outer space one would first enter the stratosphere, which extends approximately $60km$ aloft, then, at about $15km$ height, one would reach the denser troposphere. According to dominant processes and typical flow lengthscales, the lower atmosphere may be decomposed in several layers : surface layer, Ekman Layer and free atmosphere. A schematic overview of different layers in atmospheric flow is given in figure 2.1.

2.1.3 The surface layer

The Planetary 'Surface Layer' (PSL) refers to the lowest part of the ABL previously defined (10% of the whole ABL depth $\sim 100m$) [45]. It is the more turbulent part of the ABL. It is characterized by approximately constant vertical fluxes of heat and momentum between the Earth's surface and the ABL above it. The surface layer defines also the region where surface effects dominate and coriolis effects become less important.

The **surface layer** could be considered in several parts :

– The upper part, the *inertial sublayer*, is a region where effective height is the only length scale in adiabatic conditions, where profiles obey *semi-logarithmic laws* or their diabatic extensions, and where the mean flow can be described one-dimensionally using *surface-layer similarity theory* ([47]).

– The lower part is the region close to and within the canopy itself, where the mean flow is three-dimensional because it is mechanically and thermally influenced by nearby canopy elements. This region is called the *roughness sublayer*, but the terms '*transition layer*' and '*interracial layer*' are also used.
The roughness sublayer extends from the ground up to $2-5$ canopy heigths. Significant spatial variations in the properties of the flow and departures from behaviour predicted from surface layer theories are observed. Turbulence here is generated by both wake production in the low pressure region behind roughness elements and by shear production [14]. Destruction of turbulence through viscous dissipation is especially important close to the ground. The important length scales in the roughness sublayer include the roughness length z_0 representing the drag induced by the roughness elements, as well as lengths defining the geometry and spacing of the roughness elements.

Since flows at high Reynolds number are considered (see 2.1.6), direct effects of viscosity are small except in the thin viscous sublayer in the very proximity of bottom roughness elements. Above the viscous sublayer, the viscosity is negligible and the turbulent flow field is characterised by the evolution of internal boundary layers that develop around each roughness element. At a larger distance, the flow does not feel anymore every particular surface element, but behaves, as if the surface was a homogeneous rough boundary.

2.1.4 ABL Depth

The ABL depth varies broadly (about $100-3000m$), depending on meteorological conditions. At a given wind speed, e.g. $8m.s^{-1}$, and so at a given rate of the turbulence production, a ABL in wintertime Arctic could be as shallow as $50m$, a nocturnal ABL in mid-latitudes could be typically $300m$ in thickness, and a tropical ABL in the trade-wind zone could grow to its full theoretical depth of $2000m$. The depth of the ABL is therefore governed by the energy and scales of the turbulent eddies which can vary in size from a few tens of meters at night to one to three kilometres during warm sunny afternoons.

The depth and character (its mean vertical structure) of the ABL is governed by exchange, via turbulent fluxes, of heat, moisture, shear-stress, all three originating from the air masses contact with the earth's surface. The vertical extent of these fluxes depend on the nature of the surface and therefore on the type of surface (forest, open land, urban, lake, ocean, etc), time of day as well as on the history of the air. Others main external factors determine these quantities : the free atmosphere wind speed ; the surface heat (more exactly buoyancy) balance ; the free atmosphere density stratification ; the free atmosphere vertical wind shear or baroclinicity...

2.1.5 ABL Turbulence

The factor that distinguishes the ABL from the rest of the atmosphere is its turbulent nature. Turbulence is more efficient at mixing pollutants than is the generally laminar-like flow of the 'free atmosphere' above it. The main sources of energy that generates turbulence are 'friction' or 'drag' of the air with the ground (wind shear arising from the no-slip condition at

the surface, mechanical turbulence), the shear layer between the top of the boundary layer and the free stream, and heat (thermal convection) [44]. Friction results in so-called shear-stress induced turbulence while heat (given off at day time or taken from the ground at night time) generates vertical motion in the air through buoyant forces- warm air rises, cold air descends.

Although above the ABL turbulence is usually small, there can be turbulent patches due to other processes, e.g. gravity wave breaking. Above the surface layer, turbulence gradually dissipates losing its kinetic energy to friction as well as converting the kinetic to potential energy in a density stratified flow. The balance between the rate of the turbulent kinetic energy production and its dissipation determines the planetary boundary layer depth. In its average state, the atmosphere has a large amount of energy in long wavelengths and decreasing energy as scales become smaller. *Kinetic energy spectrum* decreases toward the smallest scale processes and the atmosphere is essentially a weakly stratified fluid, exhibiting quasi-horizontal flow.

2.1.6 General characteristics of the ABL

In fluid dynamics, few adimensional numbers are used to classify different flow regimes. These numbers are interpreted as a relationship between different mechanical forces that are involved in physical processes.

One of the major factors affecting atmospheric dispersion is the level of turbulence. The **Reynolds number** R_e is interpreted as a relationship between inertial and viscous forces. A flow is condidered as turbulent when R_e is higher than a critical value Re_{crit}. For typical velocities of $\mathcal{U}_{wind} \approx 10m.s^{-1}$ (on the order of 0.1 to $10ms^{-1}$), lengthscales of about the thickness of the ABL $\mathcal{L}_{ABL} \approx 1000m$ and a kinematic viscosity of about the order of $\nu_{air} \approx 10^{-5}m^2s^{-1}$, the Reynolds number of atmospheric flows is arround

$$Re_{atmo} = \frac{|(\mathbf{u}\cdot\nabla)\,\mathbf{u}|}{|\nu_{air}\Delta\mathbf{u}|} \approx \frac{\mathcal{U}_{wind}\mathcal{L}_{ABL}}{\nu_{air}} \approx 10^9 >> 2500 \approx Re_{crit} \tag{2.1}$$

Such are the Reynolds numbers associated with the ABL, that it could be expected to be highly turbulent at all times.

The Richardson number R_i is used in stratified shear flows to described the influence of temperature on turbulence production or dissipation [46]. It is calculated using temperature gradients $\partial T/\partial z$ and velocity gradients $\partial U/\partial z$. β is the expansion coefficient.

$$R_i = \beta\frac{\frac{\partial T}{\partial z}}{\left(\frac{\partial U}{\partial z}\right)^2} \tag{2.2}$$

Flows with Richardson numbers of about zero ($-0.01 < Ri < 0.01$) are considered to be quasi-neutrally stratified, hence the effect of temperature gradients on the turbulence production and dissipation is negligible.

2.2 The ABL & Stability

2.2.1 Vertical temperature gradient

Thermal effects can enhance or diminish the turbulence (see also D.2). In the atmosphere the pressure decreases with height. Consider a parcel of air as it rises, due to mechanical turbulence

caused by the surface roughness. Due to the pressure decrease this air parcel will expand. Some energy is needed for this expansion and this will be taken from the air parcel itself, so that the air cools down and consequently gets a higher density. The rate at which the temperature of such a parcel would drop is known as the Adiabatic Lapse Rate (ALR).

This ideal is rarely encountered and the Environmental Lapse Rate (ELR) which is the gradient of the temperature profile is actually what occurs. The relative magnitudes of the ALR and ELR determine the type of atmosphere at any place or time.

Ideally one would expect a temperature gradient of $-0.01°Cm^{-1}$ in the atmosphere. But over longer time periods other processes than expansion/compression, like solar radiation, cooling due to long wave radiation from the air ('radiative cooling'), condensation of water vapour to clouds or evaporation of clouds may lead to vertical temperature gradients in the real atmosphere that deviate from the theoretical gradient.

2.2.2 Stable atmosphere

Stable Conditions are often encountered over land in a cloudless atmosphere during night time, when the air close to the surface is cooled down because it looses its energy by radiation.

Under these conditions, the ELR is less negative than the ALR and a mechanically displaced air packet will find itself relatively either colder, if displaced upwards, or warmer, if displaced downwards, and will thus tend to move back towards its initial position.

In such a situation the vertical movements, e.g. generated by mechanical turbulence are suppressed. Thus, a stable atmosphere is less prone to mechanical turbulence which is effectively damped out by the thermal effects.

2.2.3 Neutral atmosphere

Neutral Conditions occur when the ALR and ELR are equal and are symptomatic of the day-night, night-day transitions or heavily overcast skies (cloudy and windy). In these cases the heating effects of the sun are absent and the insulating effect of the cloud cover tends to damp any temperature stratification. An air parcel under these conditions will move with any turbulent mixing but will not oppose or supplement the motion due to imbalances in buoyancy forces.

The temperature gradient is $-0.01°Cm^{-1}$ and mechanical turbulence dominates. In Western Europe the atmosphere is much more frequently neutral or nearly neutral than stable or unstable.

2.2.4 Unstable atmosphere

Unstable Conditions occur when the ELR is more negative than the ALR. Such a condition is called a strong lapse rate and leads to an unstable boundary layer. The vertical movements generated by e.g. mechanical turbulence are stimulated, thermal turbulence is important, and mixing up to larger heights occurs. Unstable conditions occur typically in a cloudless atmosphere during still, hot summer days when the earth's surface is warmed up by radiation which then emits radiation which heats the air above.

2.2.5 Temperature inversion

An extreme case is where the temperature in the real atmosphere increases with height, ELR is positive, and it is said it is an ('*temperature inversion*'). Vertical movements are then suppressed so much that there is almost no exchange across the inversion and the wind speed at either side of the inversion can differ much.

2.3 Effect of stability on plume dispersion

Atmospheric stability has an important effect on dispersion. and is illustrated by figure 2.2.

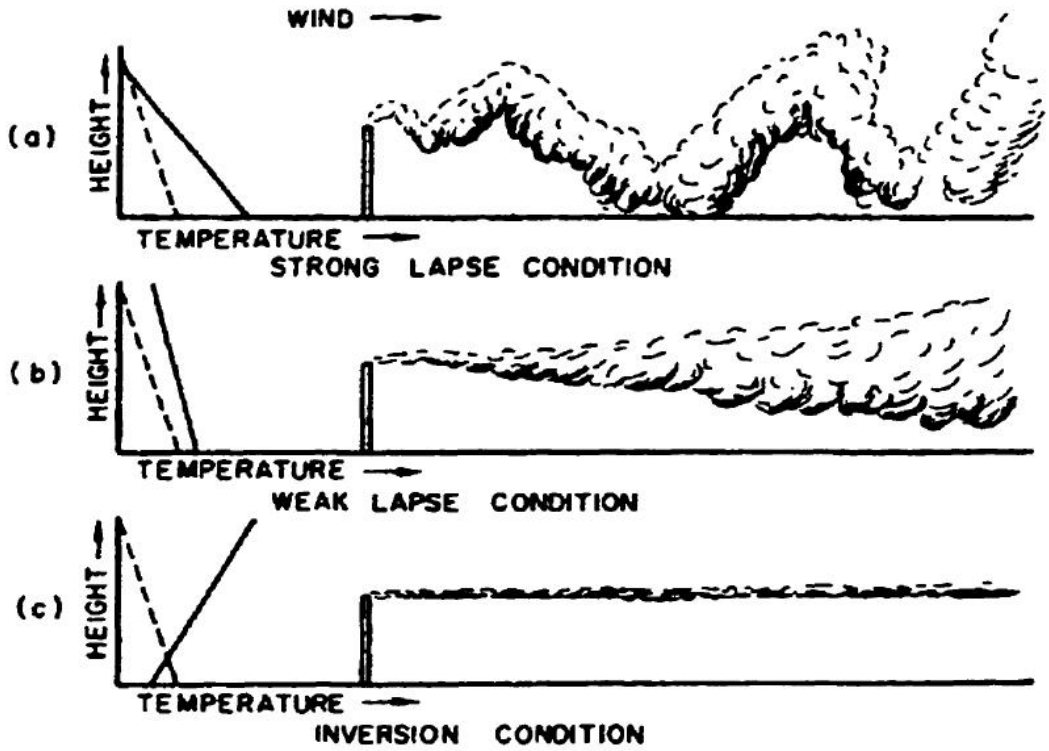

FIG. 2.2 – The effect of atmospheric stability on the dispersion of plumes. The adiabatic lapse rate is shown as a dashed-line, while typical vertical temperature profiles are shown as solid lines for (a) unstable conditions, (b) neutral conditions, and (c) stable conditions.

Dispersion in a stable atmosphere

In a stable atmosphere the plume is narrow and can be observed at long distances from the source, because the dispersion is reduced and consequently the plume is not diluted much. Usually the wind speed is relatively low and the variation in wind direction can be relatively large. The plume is said to be '*fanning*'. In the case of a ground-level source, like a field after application of pesticides, the plume is also very narrow and the concentration is relatively high close to the ground.

Dispersion in an unstable atmosphere

In an unstable atmosphere there are strong vertical movements. This does not only lead to faster dispersion and dilution, but causes also the plume to reach the surface at a relatively short distance from the source. The plume is said to be '*looping*' in this case. In the case of a ground-level sources the average concentration at ground-level is relatively low compared to the stable case, but at some distances during a short time relatively high concentrations can be observed.

Diffusion in a neutral atmosphere

In the neutral atmosphere the plume is somewhat wider than in a stable atmosphere, it is better mixed and cannot be observed over such long distances because it is diluted more rapidly by diffusion. In this case high concentrations are not observed close to the source as is the case in an unstable atmosphere. The plume is said to be '*coning*' in this case.

2.4 Wind characteristics

2.4.1 Wind Profile

Wind speed profile

The solid earth's and the ocean's surfaces constitute the lower boundary for atmospheric flow. Therefore the wind velocity decreases to zero with a transfer of momentum from the flow to the boundary (bottom friction). Inside the ABL, the wind speed increases with height up to the free atmosphere speed at an elevation usually referred to as the gradient height.

As mentioned previously, the wind speed near the surface is retarded by friction at the surface. By how much, will depend on the surface roughness. The wind speed at above about $500m$ is generally not influenced by the surface. At about $60m$ height the wind speed is influenced more by the surface roughness of a larger area (about $5 \times 5km^2$). At lower height the wind speed is more influenced by the local surface roughness.

In the inertial sublayer, the Reynolds stress $u'w'$, is used to define a typical turbulent velocity u_*, the friction velocity ($[m.s^{-1}]$), which is a measure of the mechanical turbulence :

$$u_* = \sqrt{-u'w'} \tag{2.3}$$

Measurements of the wind speed (in a neutral atmosphere), as a function of height have revealed that in the turbulent surface layer it obeys a logarithmic law, as all other boundary flows. The friction velocity, the viscous length and the wall distance allow to determine completely the logarithmic mean flow profile observed in the inertial sublayer.

$$\overline{u}(z) = \frac{u_*}{\kappa} \log\left(\frac{z-d}{z_0}\right) \tag{2.4}$$

In this equation, κ is the von Karman's constant (usually ≈ 0.4 [dimensionless]), z_0 is the surface roughness length ($[m]$, of the order of 1/10 of the height of the obstacles, vegetation, trees etc.), the extrapolated height at which the wind speed is 0, $\overline{u}(z)$ is the mean wind speed ($[m.s^{-1}]$) at height z, and d is called displacement height, because the logarithmic function is

shifted upwards when the density of roughness elements is large. Usually d is given as a fraction of roughness height.

With this equation it is possible to calculate the wind speed at one height from the wind speed at another height if the surface roughness is known. The wind speed profile can be described with the same type of function for stable and unstable conditions. It has then to be corrected somewhat so that the non-neutral situation is described correctly. Equation (2.4) is only valid up to a height of, typically, $100m$ but the present study stays well below this height. It should be noted that the surface roughness is not constant in agricultural areas, but depends on the heights of the crops, which vary during a year.

Wind direction profile

Not only the wind speed is influenced by the presence of the surface, but also the wind direction. In the free atmosphere the wind is approximately geostrophic (parallel to the isobars) while within the ABL the wind is affected by surface drag and turns across the isobars. The wind direction is often turned some 20 degrees counter-clockwise (towards the centre of the low pressure). This means that the origin of the air at greater heights is different from that at ground-level.

2.4.2 Effect on atmospheric transport

The existence of a wind speed profile influences the average speed at which a released compound is transported in the atmosphere. At some distance from the source part of the released compound has been transported upward by diffusion and encounters a higher wind speed than near the surface. This means that the average speed at which a compound is transported increases with the distance to the source until it is mixed over the whole mixing layer.

2.5 Conclusion

Finally, the local turbulence level, and thus the degree of mixing, depends on the local 'atmospheric stability' which in turn is characterized by 1) the magnitude of the wind speed 2) the surface roughness, and 3) the vertical temperature profile.

The 'free' geostrophic wind prevails above the ABL, and closer to the Earth's surface, within the strong turbulent ABL, the wind speed is gradually decreasing, due to the friction with the rough ground surface.

It is also important to note that atmospheric turbulence differs from turbulence generated in a laboratory or in pipe flow. In the atmosphere, convective turbulence coexists with mechanical turbulence. In fact, a wind tunnel environment closely approximates neutral atmospheric conditions.

Deuxième partie

LEVEL 1 : Vegetation

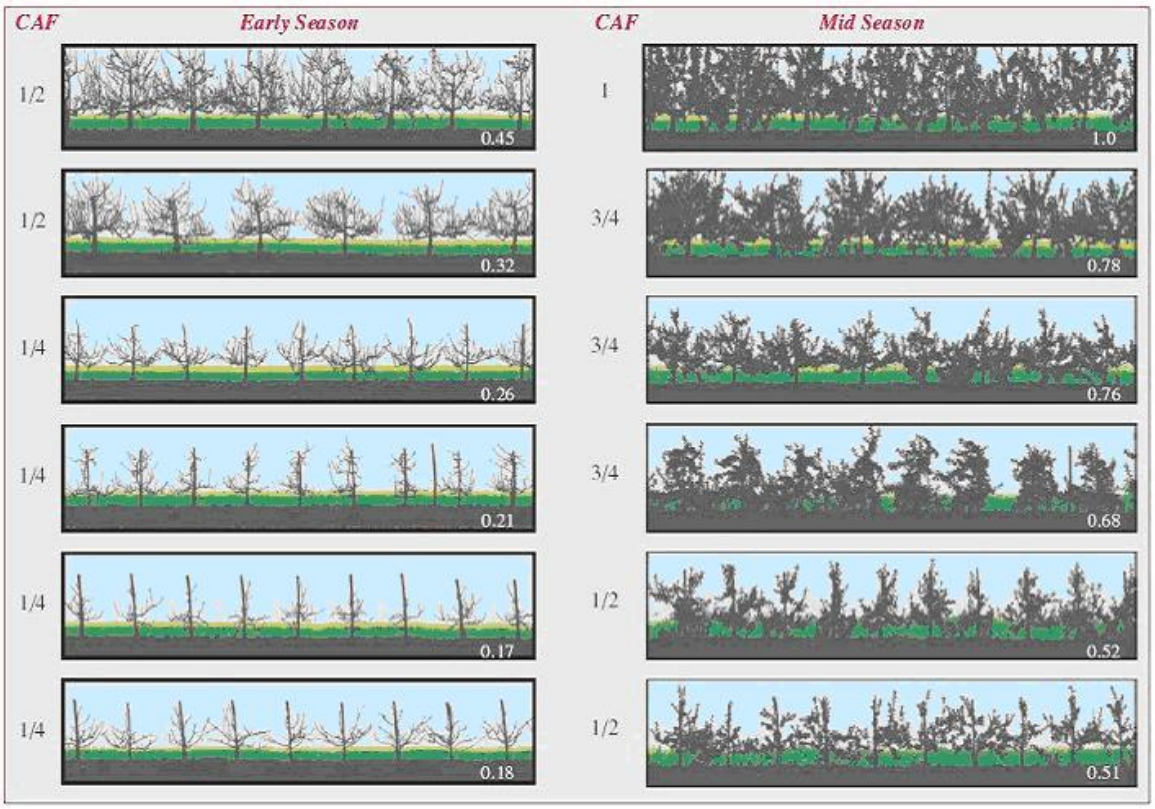

FIG. 2.3 – Exemple de variabilité au sein de la végétation.

Introduction

Contexte

La pénétration dans la végétation du flux d'air conditionne la qualité de la répartition sur le feuillage ainsi que les pertes de produit phytosanitaire dues aux gouttes qui ne sont pas interceptées. De par sa nature, la prise en compte la végétation dans la modélisation est source de complexité et les problèmes liés à cette canopée interviennent à de nombreuses échelles dans les phénomènes de dérive. Pour l'application, la géométrie, la structure et les caractéristiques de la cible sont les déterminants pour le choix du procédé d'application [3]. De plus, des variations spatiales et temporelles de ces propriétés sont toujours présentes dans les parcelles traitées. Tous ces éléments conditionnent de manière importante la dynamique initiale des pesticides dans le milieu naturel. C'est pourquoi la modélisation de la végétation représente un problème à part entière.

L'utilisation de la modélisation s'est imposée pour limiter les essais au champ, souvent très lourds à mettre en œuvre : ils demandent beaucoup de main d'œuvre et les analyses sont coûteuses. Ils sont, de plus difficilement reproductibles. La modélisation du phénomène met en jeu trois comportements : l'interaction du flux d'air avec la végétation, le transport de la pulvérisation et le dépôt des gouttes. A ce niveau, on choisit de ne pas prendre en compte le flux d'air dans le domaine extérieur au rang de vigne pour ne représenter que le comportement dans la canopée. On peut alors considérer que l'évaporation est négligeable ainsi que l'influence

du vent ou de la stabilité atmosphérique. Les autres conditions atmosphériques sont également négligées.

Cette étape, de représentation d'un écoulement à travers le couvert est donc indispensable pour l'étude de la dispersion des pesticides dans l'atmosphère, puisqu'elle influence et détermine la quantité directe perdue vers la couche limite atmosphérique et susceptible d'être transportée.

Dans ce contexte, il est nécessaire de fournir un outil simple pour représenter le rôle des caractéristiques du flux d'air et de la végétation afin d'envisager une optimisation des réglages et éventuellement des technologies.

Prise en compte de la végétation

L'étude de la littérarure sur la modélisation du couvert végétal et des écoulements associés, a permis d'identifier de nombreux modèles très différents les uns des autres. Plusieurs approches se distinguent suivant l'échelle à laquelle on étudie la dynamique des phénomènes. En effet, les rangs de vigne ont une influence immédiate sur le jet et les pertes instantanées vers l'atmosphère. Mais à des échelles supérieures, la végétation intervient également dans les phénomènes de dispersion par son influence sur la stucture du vent.

On peut ainsi citer deux approches différentes correspondant à deux échelles spatiales pertinentes, soit l'échelle d'un élément végétal, soit l'échelle macroscopique d'une portion de couvert. La vision dite globale considère le couvert végétal comme un tout et s'intéresse aux phénomènes de traînée et aux turbulences créées. La prise en compte de la végétation est, dans ce cas, souvent mesurée à une échelle suffisement grande pour pouvoir homogénéiser les variations et de manière à pouvoir traiter la canopée de manière statistique. On peut cependant remarquer que cette description d'une portion de couvert dépend elle-même de l'échelle considérée. A grande échelle lorsque la structure du vent est considèrée, cela amène souvent à résoudre explicitement l'écoulement dans la sous-couche rugueuse, définie par une canopée végétale, jusqu'à la surface du sol. Ce comportement des structures végétales et leur réponse au vent ont fait l'objet de nombreuses études tant aérodynamiques que comportementales .

A une échelle spatiale intermédiaire (celle d'une parcelle), on utilise souvent une approche assez simple basée sur une végétation homogène à densité de feuillage constante sur la profondeur. Plusieurs études ([8]) confirment qu'on peut alors représenter l'évolution de la vitesse et du dépôt dans la végétation par une loi de décroissance exponentielle (3.2.5). Or, c'est cette échelle qui est intéressante dans une approche de gestion des risques. Cette représentation peut donc être retenue pour l'étude des contaminations atmosphériques qui constitue l'étape suivante. Dans ces approches, un phénomène important est généralement négligé : il s'agit du **mouvement des feuilles**. Pourtant, selon les experts, l'intensité turbulente modifie de façon sensible le dépôt.

Au niveau local, le comportement de l'écoulement de pesticides à travers le feuillage reste malgré tout encore mal connu et les résultats numériques actuels ne collentpas toujours aux mesures en champ [48]. Des modèles d'écoulement traversant la végétation doivent par conséquent être développés.

Objectif et Méthode

L'effet de la végétation intervient donc essentiellement à deux niveaux dans l'étude de la dispersion. Au niveau local directement sur le jet et au niveau global, sur l'écoulement

atmosphérique en tant que rugosité. On s'intéresse ici plus particulièrement au niveau local.

L'objectif global de cette partie est la représentation de l'influence de la végétation sur le comportement d'un écoulement d'air. On recherche une approche générale et relativement simple utilisant toutes les informations diponibles a priori. Le comportement du flux d'air peut, en effet, être déterminé de manière empirique ou par des modèles mécanistes. On choisit d'associer les deux approches par le biais des techniques de problèms inverse. Cette approche doit permettre à la fois d'étudier des comportements complexes au niveau local, mais également de déterminer un comportement moyen pour l'échelle de niveau supérieur, c'est à dire la parcelle. On veut ensuite pouvoir intégrer et appliquer ce modèle, dans le cadre de la dérive, sur l'établissement du jet de pulvérisation situé au coeur même d'une vigne.

Cependant le caractère aléatoire des propriétés de la végétation (densité, répartition, disposition, taille, orientation des feuilles, ...), se répercute sur la nature de l'écoulement qui la traverse. Ces disparités qui peuvent d'un pied à l'autre à l'intérieur d'un même rang sont encore plus notables si on les observe à l'échelle de la parcelle toute entière. Le modèle doit pouvoir prédire l'effet sur l'écoulement qui représente au mieux les différents comportements possibles au sein des rangs de vignes, lors du traitement de la parcelle. A cette fin, il est nécessaire de considérer un traitement robuste qui limite la sensibilité du modèle devant ces variabilités intraparcellaires.

Pour atteindre ce but, on cherche à définir un "rang moyen" représentant le comportement de tous les rangs de végétation contenus dans la parcelle et qui permettra une représentation robuste de la vigne. On utilise une approche numérique, par application de techniques de contrôle optimal pour définir ce comportement moyen en dépit des variabiliés. L'aboutissement de ces recherches fournira un outil numérique pour quantifier les dépôts dans la végétation et les pertes, ce qui est indispensable pour optimiser les procédés.

Stucture de la partie

Tout d'abord, pour rendre compte de la difficulté du problème, on présente succintement, différentes méthodes utilisés dans la littérarure, pour modéliser les écoulements au sein de la végétation. L'énumération de ces approches permet de soulever les points importants liés à cette modélisation, et de choisir celle qui conviendra le mieux. Dans 3.2.4 par exemple, on montre les complications rencontrées lorsque l'on veut résoudre explicitement les équations générales de la mécanique des fluides à l'intérieur du couvert. Les sections 3.2.3 et 3.2.5 présentent les notions de base qui seront utilisés dans le modèle développé par la suite.

Dans le chapitre suivant (4) on va exposer l'approche utilisée pour l'étude de l'écoulement au sein d'un rang de vigne. Il s'agit d'un modèle monodimensionnel le long d'une ligne droite traversant la végétation. C'est ce modèle qui sera ensuite utilisé pour définir le comportement moyen à l'échelle de la parcelle. Plusieurs problèmes de controle optimal, sont présentés en application.

Mots clés : *Végétation, Estimation de paramètre, Milieu poreux, Ecoulement dans la canopée, Loi de Balance*

Keywords : *Vegetation, Parameter estimation, Porous medium, Canopy flow, Balance Law*

Chapitre 3

Canopy Flow Model

3.1 Introduction

Practical difficulties arise in drift dispersion due to a poor understanding of the air-flow interactions with different vegetative structures. In fact, vegetation canopy plays an important role in determining the amount of spray drift moving away from a sprayed area. The spray droplet movements are influenced by crop structures within the plot and also by the vegetation downwind of the sprayed area. While there have been numerous attempts to model these movements from both aerial and ground application, the inclusion of canopy or downwind vegetation parameters within these models have often been either somewhat simplistic or even non-existent [49].

At a local scale, combining the canopy models with spray drift application modelling enables strong and fundamental links to be made between the role of plant architecture and pesticide application processes. It could also be possible to greatly extend the predictive ability of various vegetative structures to minimise spray drift.

At a greater scale, by improving our understanding of the complex relationship between the pesticide droplets deposition on vegetative surfaces (e.g. forest, crop canopy, weeds, downwind buffer vegetation) it should be possible to develop and to improve pesticide application procedures. This will enable the effectiveness of plant protection products to be maximised while minimising risks to public health and the environment from agricultural spraying activities.

An understanding of these mechanisms is essential for a variety of applications in hydrology, biology, agriculture, and forestry, as well as being relevant to wider questions concerning the global balances of carbon dioxide and nitrogen. Because of these strong and diverse practical motives, a huge amount of work has already been done to analyse air flow behaviour within canopies. They have been intensively studied since the 1960s, mainly with the aim of providing insight into the processes of momentum and scalar exchange between biologically active plants and the atmosphere. However most research into turbulence of plant environment has been observational and empirical ; several decades of effort by many workers have produced no general and successful theory [50].

Most work was developed for bio-climatology concerns to characterize transfers within the *Canopy Sub-Layer* (CSL). Most often, the vegetation was supposed to be homogeneous in a horizontal plane and only the vertical dimension was considered. Recent research works have focused on local heterogeneities like e.g. landscape patterns, hills, windbreaks and forest edges.

This chapter is an attempt to present a consistent picture of flow dynamics models in simple canopies by recalling some of previous attempts for canopy flow modeling. Moreover, it allow

us, to present the basis for our model developped in chapter 4.

3.1.1 Difficulties : Variability-Structure

A plant canopy consists of numerous discrete elements such as leaves, stems, and branches, aggregated into complex structures, randomly oriented and distribued. One of the main difficulty is to take into account these random characteristics of the vegetation. This favoures the development of simplified [51] or empirical [52] based model. In addition, since canopy parameters are difficult to measure, it is impractical to explicitely account for the presence of within-$3D$-canopy structures.

3.1.2 Resistance due to vegetation : situation under consideration

The main effect on airflow of a crop is to alter the mean velocity. In fact, air flow changes abruptly when it encounters a canopy and fine geometric scales strongly affects the airflow. Interaction between flow and canopy act principally on two ways : the canopy drag force results in pressure loss in the air flow and air turbulence is modified. When the canopy interacts with the airflow above and within it, the following important aerodynamic processes occur [50] :

- **Momentum** is absorbed by drag
- **Scalar properties** are exchanged between the flow and the elements.
- Momentum and scalar properties are transported vertically
- Canopy elements generate **turbulent wakes**, which convert the MKE[1] into TKE at length scales characteristic of the elements.
- Most plants wave, thereby storing MKE as strain potential energy, to release it as TKE half a **waving cycle** later.

However, plant cover could be also simply seen as a porous obstacle to the approaching airflow, forcing air to flow through the crop at a reduced speed and accelerate over the top.

Drag

A common way to express the aerodynamic effect of a canopy is in terms of its resistance to the flow or drag. The drag is generated when a fluid moves through vegetation, creating velocity gradients and eddies that cause momentum losses. These losses are significant for a wide range of flow conditions, and existing techniques for the prediction of resistance do not take these into account, leading to underpredictions of drag force [53].

Drag is a complicated phenomena and explain it from a theory based entirely on fundamental principles is rather difficult. In fact, drag is a topic that is best explored experimentally. The drag depends on many factors and these dependences are very complex. One way to deal with it, is to characterize it by a single dimensionless variable, C_D. which allows to collect all the drag effects into a single equation. Thus, many studies have been carried out to determine the natural canopy drag coefficient.

The most common empirical and general formula for drag is (see 4.2.1) :

$$D = \frac{1}{2}\rho A_{ref} u^2 \left(R_e\right)^a \tag{3.1}$$

$$= \frac{1}{2}\rho A_{ref} u^2 \left(\frac{L_{ref} U_{ref}}{\nu}\right)^a \tag{3.2}$$

$$= \frac{1}{2}\rho A_{ref} u^2 C_D \qquad [N = kg.m.s^{-2}] \tag{3.3}$$

[1] Mean Kinetic Energy, $MKE = \frac{1}{2}(u^2+v^2+w^2)$ and Turbulent Kinetic Energy as $TKE = \frac{1}{2}(u'^2+v'^2+w'^2)$)

where

D = drag force(**SI** : $N = kg.m.s^{-2}$, $[ML/T^2]$).

ρ = fluid density (**SI** : $kg.m^{-3}$, $[M/L^3]$).

A_{ref} = reference area (**SI** : m^2, $[L^2]$).

u =approach velocity of the fluid (SI : $m.s^{-1}$, $[L/T]$).

R_e =Reynolds number (**SI** : [Dimensionless]) and (L_{ref}, U_{ref}) is the characteristic couple of a reference length and a reference velocity associated to the flow and that defines R_e.

Forces resulting from the vegetation resistance and the viscous dissipation include the cumulative effects of viscous dissipation among the stems, laminar boundary layers on the plant surfaces (skin drag), wake production (form drag losses generated by the vegetative elements), besides the physical interception of the fluid by the vegetation [53]. So drag force can be split into friction drag and profile drag. Thus, the parameterization could also be rewrite as (minus) the sum of the pressure and viscous forces on the vegetation :

$$F_D = \quad f_F + f_V \quad [N.m^{-3} = kg.m^{-2}.s^{-2}] \tag{3.4}$$

where F_D is the total drag force per unit volume, f_F is the form (or pressure) drag and f_V is the viscous drag.

The influence of canopy structure and variability of drag on momentum was discussed by [54]. The effective drag coefficient $C_{D_{leaf}}$, of a single leaf measured in wind tunnel changes according to leaf orientation and the scales of turbulence and intensity around the leaf [50]. However, [55] reported that the C_D value of a vegetation canopy is constant, i.e. it does not depend on air velocity neither on the position within the canopy $\mathbf{x}$ [56].

$$C_D = \quad C_D(u(x), \mathbf{x}) = \quad \text{cst} \tag{3.5}$$

Reference Area for canopy

The drag coefficient calculated in the equation (3.3) depends on how A_{ref} is defined. It is obvious that the influence of canopy structure affects the variability of drag. A closely related issue is the definition of reference vegetation area. An area reference is often selected arbitrarily but can significantly influence.

The frontal area of an object projected on a plane perpendicular to the flow is the most common reference area [57]. However the conventional application of this area is to solid objects whereas vegetation canopy is porous [57]. So, including a representative area in this equation presents some particular difficulty.

To characterise the vegetation density, the *leaf area density* (a_{LAD}) is used. This quantity is more precisely defined as the one-sided surface of plant parts projected in the direction $\mathbf{d}$ per unit volume V (total surface$(\mathbf{d}, V)$). In most of the study a_{LAD} represents better than the frontal area these different values of area associated with all the types of drag linked with vegetation.

An other classical structural parameter used to characterize the vegetation density is the a_{LAI} (the leaf area index). a_{LAI} was first defined in 1947 as the total one-sided area of photosynthetic tissue per unit ground surface area. Various other definitions exists and (some measurement approach - dependent) and it should be noted that these different definitions can result in significant differences between calculated a_{LAI} values.

An other definition for the total a_{LAI} of a plant stand, could be simply the integral, or summation, of the leaf area density ($a_{LAD}(r)$) of successive layers.

$$a_{LAD} = \quad a_{LAD}(\mathbf{d}, V) \tag{3.6}$$

$$= \frac{\text{total surface}(\mathbf{d}, V)}{V} \quad [m^2/m^3] \tag{3.7}$$

$$\tag{3.8}$$

$$a_{LAI} = \quad \int \; a_{LAD}(r)\mathrm{d}r \qquad [no\ unit] \tag{3.9}$$

$$\tag{3.10}$$

Many researchers have used the a_{LAI} rather than a_{LAD} for modelling airflow through and over vegetation. An obvious problem with using a_{LAI} in equation (3.3) is that the units are not consistent ; a_{LAD} is measured in units m^2m^{-3} whereas a_{LAI} have no units (m^2m^{-2}). a_{LAI} is a dimensionless variable. The drag coefficient is not a dimensionless value when a_{LAD} is substituted for a_{LAI} in equation (3.3) [57]. However, a_{LAD} has the convenient dimension $[m^{-1}]$ to represent the crop structural density in the aerodynamic drag force per unit volume of fluid. This measure of drag is ideal for evaluating momentum loss over a control volume. Spatial variations in a_{LAD} could be important. If we divide the canopy into multiple layers we will observe different amounts of leaf area in different layers.

In the literature, the direction r of projection is sometimes vertical, whereas for the description of the drag forces in 3.1 it should be perpendicular to the flow direction. If no other data is available, isotropy is assumed :

$$a_{LAD} = \quad a_{LAD}(x, y, z) \tag{3.11}$$

Estimation Methods

Leaf area is one of the most important biometeorological variables to be characterized and serve as input to crop modelling. The problem with all of the approaches for measuring this parameter is that they are difficult and time consuming to perform over large areas. So their use has some limitations. The leaf area density, a_{LAD} can obtained, for example, after gathering all leaves of the plant, by recording images of each leaf with a scanner and then by sizing them using image analysis tools.

3.2 Mathematical models of canopy flow

3.2.1 Diffusion approach

Most theoretical work has assumed that fluxes within a plant canopy are governed by the local diffusion equation [50]

$$Q_S = \quad -\rho K_S \frac{\partial \overline{s}}{\partial z} \tag{3.12}$$

where Q_S is the vertical flux density of a property with mean concentration $\overline{s}$ per unit mass, and where turbulent diffusivity K_S is specifiable in terms of local flow or canopy parameters. However, the assumptions underlying this equation have long been known to be questionable. Therefore, research has moved towards identifying the limitations of local-diffusion models and providing alternatives of greater physical reality.

Although the diffusion approach has fallen into disfavor among micrometeorologists and turbulence workers, it remains the foundation for a great deal of work on the plant microclimate. It has given approximate but useful insight into the way in which physical and biological factors combine to govern the transpiration and photosynthesis rates of a plant canopy, and has been used to parametrize turbulent transport in several computer models of the physical processes in crops [50].

3.2.2 Roughness parameterization

Most studies of canopy dynamics focus on the one dimensional vertical velocity profile of wind inside an homogeneous horizontal canopy. Early interpretations of canopy wind dynamics used a Planetary Boundary Layer (PBL) model representing the canopy surface as a topographic sheet [58]. It was hoped that it was possible to parametrize the vegetation canopies influence in terms of appropriate characteristic quantities which depend on 'the amount of roughness' presented by the canopy. In fact, as already evocated in 2.4 the mean velocity profile of flow over a plant canopy was found to depend on certain roughness parameters characteristic of the canopy.

The parameters help in understanding and quantifying the momentum and scalar processes occuring between the canopy and the atmosphere. Specific applications include the parametrisation of surface drag for use in atmospheric models, pollutant dispersal modelling and calculation of wind loads on buiding or trees.

This canopy *Land Surface Parameterization* (LSP) is mainly used in weather prediction and global change models. At these macroscopic scales, the vegetation is considered as a continuuous medium. The goal is to adjust turbulent boundary layers to a canopy of roughness element. Numerous investigators have attempted to quantify wind profiles within canopies using an analytical relation of the form :

$$\overline{u}(z) = u_h \exp\left(\alpha(\frac{z}{h} - 1)\right) \quad \text{(exponential law)} \tag{3.13}$$

where the phenomenological studies have parameterized the wind extinction coefficient as a function of canopy height (h), leaf area, and drag coefficients associated with the canopy and leaf elements. However, LSP does not account for complex structures within the canopy which have considerable effects on local air motion.

3.2.3 Porous Approach

The study of the airflow through permeable material is a topic of great importance due to its large number of technical applications, such as air infiltration in enclosed spaces. Despite the existence of important studies on this field, the subject is far from being fully understood. For a proper quantification of the phenomenon, it is necessary to know how the fluid motion is related to the driving forces and to the characteristics of the transmitting medium.

Convecting in porous media

It would be unrealistic to attempt to take into acount transfers on each leaf. The definition and design of the $3D$ domain of interest (leaves as solid bodies and air as fluid) is very complex. It lies into considering the crop vegetation as a multiply-connected porous medium. The traditional

approach to macroscopically characterise the airflow through real porous media is to use the Darcy-Forchheimer theory.

When a fluid is forced through a permeable medium (containing pores or apertures ; like airflow through crops) energy is lost, this causing the pressure to drop over the slab of the medium. The pressure drop over apertures is generally presented as being proportional to the square of fluid velocity. A term, which is linearly dependent on the fluid velocity, is added for extremely narrow apertures. So the crop exerts a drag force on the airflow, causing a net loss of momentum and this drag effect can be modelled as a function of leaf area density, the drag coefficient and the square of air velocity. The alteration of pressure field, mean air velocity and turbulence resulting from flow through a porous canopy can explain almost all the other crop effects. In a porous case, drag could be modeled as a sink term in the momentum conservation equation and as a source term for TKE.

This section begins with the derivation of a general equation for porous medium. The airflow in the crop cover is described by the porous medium approach proposed by *Darcy* and completed by *Forchheimer*.

For a porous medium, with Reynolds numbers being less than 1, the pressure drop is generally considered to be proportional to the fluid velocity (Darcy's law). Brinkman modified Darcy's equation by adding a second-order velocity term, in order to be consistent with no-slip conditions. However, it was soon verified that both Darcy's law and Brinkman's later correction were inconsistent with a higher Reynolds number. As a result, an extra squared fluid velocity term has been added to match the experimental results. The application of Darcy's law is the standard approach to characterize single phase fluid flow in homogeneous porous media. Basically, one simply assumes that a global index, permeability K_p, relates the average fluid velocity $\mathbf{u}$ through the pores with the pressure drop ΔP measured across the system as follows :

$$u = -\frac{K_p}{\mu}\frac{\partial P}{\partial x} \tag{3.14}$$

In a three dimensional (3-D) system equation (3.14) generalizes to :

$$\mathbf{u} = -\mu^{-1}\mathbf{K}_p\Delta\mathbf{P} \tag{3.15}$$

Equation (3.14) is for an isothermal fluid, moving with a slow steady velocity under the action of the pressure gradient. In these equations (3.14), (3.15) $\mathbf{P}$ is the pressure in $[Pa] = [N\ m^{-2}] = [kg\ s^{-2}m^{-1}]$; μ is the dynamic viscosity of the fluid in $[kg\ s^{-1}m^{-1}]$ $\mathbf{u}$ the speed of fluid in $[m\ s^{-1}]$; x the coordinate in the flow direction in $[m]$; and $\mathbf{K}_p$ the permeability of the porous medium in $[m^2]$.

Theoretical considerations

In spite of its great applicability, the concept of permeability as a global index for flow, which implies the validity of equation (3.14) should be restricted for Reynolds numbers ($Re = \rho u K^{0.5}/\mu$) smaller than unity as for larger Re numbers it has experimentally demonstrated the existence of a nonlinear flow regime. This motivated Forchheimer (1901) to add an extra squared fluid velocity term in Darcy's equation and equation (3.14) took the following form :

$$\frac{\partial P}{\partial x} = -\left(\frac{\mu}{K_p}u + \rho\left(\frac{Y}{K_p^{1/2}}\right)|u|u\right) \tag{3.16}$$

where ρ $[kg\ m^{-3}]$ is the fluid density and Y the non-linear momentum loss coefficient or inertial factor (dimensionless).In the the other view, at sufficiently low velocities, equation (3.16) is reduced to **Darcy's law**.

Equation (3.16) shows how fluid velocity is related to pressure drop, through the viscous resistance force, which appears due to the momentum transfer at the fluid interface (μ/K_p) and the pore inertia effects ($\rho Y/K_p^{1/2}$).

The term $\rho Y u^2/K_p^{1/2}$ can be interpreted as a second-order correction to account for the contribution of inertial forces in fluid flow. Equation (3.16) is not a purely empirical expression, since it can be derived from the Navier-Stokes equation for one-dimensional, steady incompressible flow of a Newtonian fluid in a rigid porous medium.

Crop aerodynamic properties were determined in a similar way with the screen [59]. For reasons of simplicity we assumed that pressure forces contributed to the major portion of total canopy drag. The momentum sink represented for equation (3.16), due to the drag effect of the crop, can be introduced as the source term in the Navier-Stokes equations. This form drag effect produced by the airflow through crops can also be modelled as a function of (a_{LAD}) and the square of air velocity [60] :

$$\frac{\partial P}{\partial x} = -C_{D_{veg}}\ a_{LAD}\ \rho\ u^2 \tag{3.17}$$

$$\left[kg\ s^{-2}m^{-2}\right] = [\,]\,[m^{-1}]\,[kg\ m^{-3}][m^2 s^{-2}] \tag{3.18}$$

where $C_{D_{veg}}$ is the isotropic vegetation drag coefficient.

If the surface density is known, the drag coefficient can be 'measured' using mean velocity profiles within the canopy and assuming homogeneous conditions. The values of a_{LAD}, $C_{D_{veg}}$, Y, and K_p of the porous medium can be related by combining equations (3.16) and (3.17) : From equations (3.16) and (3.18) we can deduce that :

$$\frac{Y}{\sqrt{K_p}} = a_{LAD} C_{D_{veg}} \tag{3.19}$$

From equation (3.19) it is obvious that crop aerodynamic characteristics can be determined if we know the pressure drop across the crop. Equation (3.19) is valid only at higher Reynolds numbers, when inertial forces causing turbulent flow are predominant and the quadratic drag term dominates on the right-hand side of equation (3.16) and the form drag due to solid obstacles is greater than the surface drag due to friction.

3.2.4 Averaging procedures for canopy flow

The analysis framework

The equation of motion for a single-phase flow in a general flow field (Navier-Stokes equation) can be written as

$$\rho\frac{\partial \mathbf{u}}{\partial t} + (\rho\mathbf{u}\cdot\nabla)\,\mathbf{u} = -\nabla\mathbf{P} + \mu\nabla^2\mathbf{u} \tag{3.20}$$

where $\mathbf{u}$ is the velocity vector, $\mathbf{P}$ the total pressure (with gravitational force per unit mass included), ρ the density, t the time and μ the dynamic viscosity.

Unfortunately, it is not correct to apply equation (3.20) in the description of the airflow though a permeable material (solid matrix with pores) because this equation is only valid for

the fluid inside the pores. To solve this problem one motion equation is needed for each pore, which is impractical.

For many years, standard free-air Reynolds equations were adapted for use in canopies, as explained in the previous section 3.2.3, by the adhoc addition of a source or drag term which was regarded as a smooth function of space. However, when attempts to write second-order closure models of canopy flow were made, the limitations of this approach quickly became apparent.

The paradox was resolved when [60] showed that a rigorous spatial averaging procedure, when applied to the moment equations obtained at a point in the canopy airspace, produced equations for the area-averaged flow field containing the required smooth source and drag terms as well as terms corresponding to the production of fine-scale 'wake turbulence'. The equations also contained extra 'dispersive flux' terms that had not been formally included in analyses up to that point and which were the spatial analogues of the Reynolds stresses that attend time averaging.

Equation (3.20) will be developed with the help of the methodology called "method of volume averaging", resulting in an equation valid over a small volumetric element, which is representative of the medium under study. The validity of the resulting approach is based on the following assumptions :

- (i) the medium is homogeneous at a macroscopic scale,
- (ii) the solid matrix is rigid,
- (iii) there are no chemical reactions between the solid matrix and the fluid, and
- (iv) the conditions are isothermal.

In several works, an analytical model of wind profile inside canopy is derived from $3D$-incompressible Navier-Stokes equations by space and time-averaging. The spatial averages used by [60] and further developed by [61] were averages over a horizontal plane. The more general volume average was subsequently introduced by [62] and [14].

Thus, the effects of the canopy do not appear explicitly in the conservation equations until a horizontal average is taken [60]. This is best done by horizontally averaging the time-averaged equations over an area large enough to eliminate variation caused by individual canopy elements.

A spatial average requires that the canopy be homogeneous over the averaged region, i.e. tree spacings, tree heights and foliage density should be approximately constant. This enables canopy effects as a whole to be well represented by the spatial average, despite considerable spatial variations in the flow within the canopy.

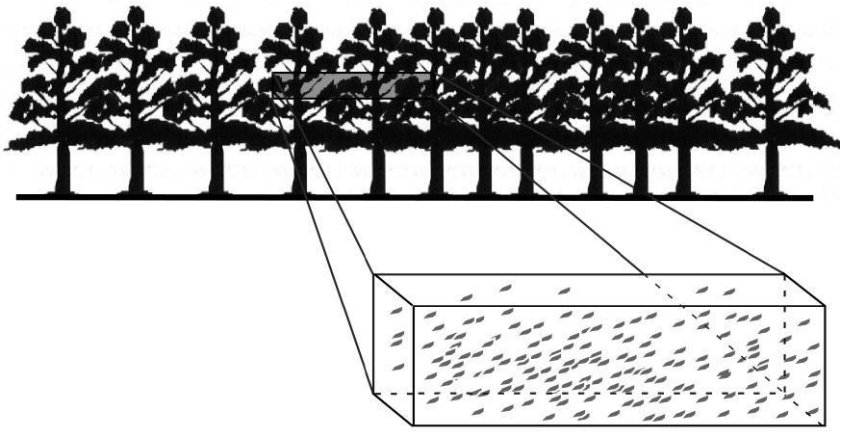

FIG. 3.1 – Spatial Averaging : Canopy representative elementary volume (REV). [63]

The advantage with this method compared with using roughness parameterization is that effects of the vegetation over the whole depth can be taken into account, instead of only affecting the velocity near the top of the canopy. The effects of the canopy appear explicitly in the equations with this procedure. The method used for the volume averaging is presented in the following.

Conservation equations

At any point in the roughness sublayer, the airflow obeys three-dimensionnal, time-averaged conservation equation for mass, momentum, and a passive property S with specific concentration s :

$$\frac{\partial \overline{u_i}}{\partial x_i} = 0 \qquad \text{Mass Conservation} \tag{3.21}$$

$$\frac{\partial \overline{u_i}}{\partial t} + \overline{u_j}\frac{\partial \overline{u_i}}{\partial x_j} + \frac{\partial}{\partial x_j}\overline{u_i' u_j'} = -\frac{1}{\rho}\frac{\partial \overline{p}}{\partial x_i} + \frac{g\overline{\theta}}{T_0}\delta_{i3} + \nu\nabla^2\overline{u_i} \qquad \text{Moment} \tag{3.22}$$

$$\frac{\partial \overline{s}}{\partial t} + \overline{u_j}\frac{\partial \overline{s}}{\partial x_j} + \frac{\partial}{\partial x_j}\overline{u_j' s'} = \kappa_S \nabla^2 \overline{s} \qquad \text{Transport} \tag{3.23}$$

Here u_i and x_i are velocity and position vectors, respectively, with $i = 1, 2$, and 3 denoting the longitudinal, lateral, and vertical directions relative to the mean wind. A right-handed rectangular Cartesian coordinate system is used, $x_i(x, y, z)$ with $x_1(x)$ aligned with the mean velocity and $x_3(z)$ normal to the ground surface. Velocity components are denoted by u_i, (u, v, w) with $u_1(u)$ the streamwise component and $u_3(w)$ the vertical one. t is time, ρ air density, p pressure without hydrostatic component, g acceleration due to gravity, θ deviation from a reference temperature that decreases adiabatically with height, T_0 an average absolute temperature, ν kinematic viscosity of air, and K_S the molecular diffusivity for the property s.

The time-averaging procedure has introduced the Reynolds-stress tensor $\overline{u_i' u_j'}$ and the vectorial turbulent flux $\overline{u_j' s'}$ of s. The momentum conservation equation includes no Coriolis-force term because it is usually negligible in the surface layer.

Spatial Averaging

All flow variables may be decomposed into their volume average and a departure therefrom. Let angle brackets denote a horizontal average, and double primes a departure of a time-averaged quantity therefrom

$$\phi_j = \langle \phi_j \rangle + \phi_j'', \tag{3.24}$$

where the departure satisfies :

$$\left\langle \phi_j''(x, t) \right\rangle = 0. \tag{3.25}$$

Combining both operators time and spatial, one defines a time-spatial decomposition

$$\overline{\phi} = \left\langle \overline{\phi} \right\rangle + \overline{\phi}'' \tag{3.26}$$

$$\phi = \overline{\phi} + \phi' = \left\langle \overline{\phi} \right\rangle + \overline{\phi}'' + \phi' \tag{3.27}$$

The volume average of a scalar or vector function ϕ_j is defined as :

$$\langle \phi_j \rangle (x,t) = \frac{1}{V} \int \int \int_V \phi_j(\mathbf{x}+\mathbf{r},t) \mathrm{d}^3\mathbf{r}, \tag{3.28}$$

where the averaging volume V, which excludes solid plant parts, consists of a horizontal slab, extensive enough in the horizontal to eliminate plant-to-plant variations in canopy structure but thin enough to preserve the characteristic variation of properties in the vertical.

Operator Commutation

While time-averaging and differentiation are commutative operations, this is not always the case for spatial averaging [61]. In the multiply-connected canopy airspace, differentiation and volume averaging do not commute for variables that are not constant at air-canopy interfaces. This is true in all cases for spatial differentiation and also for differentiation with respect to time in the case of a waving canopy. Instead it can be shown using Green's formula ([62],[14]) that :

$$\overline{\partial_i \phi} = \partial_i \overline{\phi}, \quad \text{but} \tag{3.29}$$

$$\langle \partial_i \phi \rangle \neq \partial_i \langle \phi \rangle \tag{3.30}$$

$$\left\langle \frac{\partial \phi_j}{\partial x_i} \right\rangle = \frac{\partial \langle \phi_j \rangle}{\partial x_i} - \frac{1}{V} \int \int_{S_I} \phi_j n_i \mathrm{d}S, \quad \text{spatial differentiation} \tag{3.31}$$

$$\left\langle \frac{\partial \phi_j}{\partial t} \right\rangle = \frac{\partial \langle \phi_j \rangle}{\partial t} - \frac{1}{V} \int \int_{S_I} \phi_j \nu_i n_i \mathrm{d}S, \quad \text{temporal differentiation} \tag{3.32}$$

where the surface S_I is the sum of all the solid plant surfaces that intersect the averaging volume V, n_i is the unit normal vector pointing away from S_I into V, and ν_i is the velocity of a point on the plant surface. In the free atmosphere, the operation of horizontal averaging commutes with spatial differentiation, as it is the case for time averaging.

Full analysis shows that if $\langle \phi \rangle$ is constant at the air-element interfaces, then averaging and differentiation commute so that $\left\langle \partial \overline{\phi} / \partial x_i \right\rangle = \partial \left\langle \overline{\phi} \right\rangle / \partial x_i$. Otherwise, they do not commute ; in particular, $\left\langle \partial \overline{\phi}'' / \partial x_i \right\rangle \neq 0$.

Application to the equations

Decomposing the mean quantities in the Reynolds equations ((3.21),(3.22),(3.23)) into a spatially averaged part and the its deviation, then averaging the equation in space leads to the time-spatial mean continuity and -momentum equations in a canopy [58].

$$\frac{\partial \langle \overline{u_i} \rangle}{\partial t} + \langle \overline{u_j} \rangle \frac{\partial \langle \overline{u_i} \rangle}{\partial x_j} = \frac{\partial \langle \overline{p} \rangle}{\partial x_i} + \frac{\partial \tau_{ij}}{\partial x_j} + f_{F_i} + f_{V_i} \tag{3.33}$$

where

$$\tau_{ij} = -\left\langle \overline{u_i' u_j'} \right\rangle - \left\langle \overline{u_i'' u_j''} \right\rangle + \nu \frac{\partial \left\langle \overline{u_i} \right\rangle}{\partial x_j} \tag{3.34}$$

$$f_{F_i} = -\frac{1}{V} \int \int_{S_I} \overline{p} n_i \mathrm{d}S \quad \text{(form/pressure drag)} \tag{3.35}$$

$$f_{V_i} = -\frac{\nu}{V} \int \int_{S_I} \frac{\partial \overline{u_i}}{\partial n} \mathrm{d}S \quad \text{(viscous drag)}. \tag{3.36}$$

In these equations p is the kinematic pressure and μ the kinematic viscosity. The volume averaged kinematic momentum flux tensor τ_{ij} includes the conventional turbulent and viscous stresses as well as the dispersive flux term, the second term on the RHS of (3.34), which results from any spatial correlations in the time-averaged velocity field.

In addition to the spatial-mean Reynolds stresses $\left\langle \overline{u_i' u_j'} \right\rangle$, spatial averaging introduces dispersive flux terms $\left\langle \overline{u}_i'' \overline{u}_j'' \right\rangle$ to the transport term of mean momentum. They are in general small compared to the Reynolds stresses, at least in the upper part and above the canopy layer [14].

The presence of terms f_{F_i} and f_{V_i} is a direct consequence of the non-commutivity of differentiation and volume averaging in the multiply-connected canopy airspace. f_{F_i} is (minus) the sum of the form or pressure drag forces and f_{V_i} is (minus) the sum of the viscous drag forces exerted on every surface element that intersects the averaging volume V. Together they constitute the *aerodynamic drag* on unit mass of air within V.

Once again, the system is underdetermined (not closed), since the additional flux and drag terms are unknown a priori. Turbulence models establish a relationship between these unknown quantities and the mean quantities.

Application to a spray model [51]

[51] describes the assumptions that are required to make the small-scale volume-averaged turbulent momentum equations mathematically tractable for a two-dimensional moving air-jet penetrating a crop canopy.

In common with many previous approaches to modelling air flows in crop canopies and other porous structures [14], all the flow properties of interest are defined in terms of a small-scale volume-average.

$$\psi = \overline{\langle \psi \rangle_s} + \langle \psi \rangle_s' + \psi'' \tag{3.37}$$

Then a typical form for the small-scale spatial-averaged turbulent momentum equations for predicting atmospheric boundary-layer driven airflow in a crop canopy has been given by [14]. The momentum equation for a 2D air-jet penetrating a crop canopy is assuming taken the same form as (3.33) :

$$\overline{\langle u \rangle_s} \frac{\partial \overline{\langle u \rangle_s}}{\partial x} + \overline{\langle v \rangle_s} \frac{\partial \overline{\langle u \rangle_s}}{\partial y} = -F_u - \frac{\partial}{\partial y} \overline{\langle u \rangle_s' \langle v \rangle_s'} \tag{3.38}$$

with (3.39)

$$F_u = a_{LAD} C_{D_{veg}} \overline{\langle u \rangle_s} \| \overline{\langle u \rangle_s} \| = B_{veg} \overline{\langle u \rangle_s} \| \overline{\langle u \rangle_s} \| \tag{3.40}$$

where $\overline{\langle u \rangle_s}$ and $\overline{\langle v \rangle_s}$ are time averages of small-scale volume-averaged velocities in orthogonal directions x and y respectively. The directional convention adopted uses x for distances in

the initial jet flow direction and this is normal to the direction y parallel with the row. F_u is the model used to represent the momentum losses due to small-scale flow separation and turbulent diffusion. Furthermore, it is commonly assumed that the crop structural density scaling parameter B_{veg} is proportional to area density i.e. $B_{veg} = C_{D_{veg}} \times a_{LAD}$, where a_{LAD} is the leaf area density and $C_{D_{veg}}$ is the drag factor that accounts for the effects of flow separation within the small-scale volume.

In addition to momentum losses due to small-scale turbulent diffusion, the turbulent diffusion losses at volumetric scales greater than the small-scale volume, are modelled as a gradient diffusion process

$$\frac{\partial}{\partial y}\overline{\langle u\rangle_s' \langle v\rangle_s'} = -K_s \frac{\partial^2 \overline{\langle u\rangle_s}}{\partial y^2} + \sigma_v l_{uv} \frac{\partial^2 \overline{\langle u\rangle_s}}{\partial y^2} \tag{3.41}$$

where $\sigma_v = \overline{\langle v\rangle_s' \langle v\rangle_s}^{1/2}$ is a turbulent velocity and l_{uv} is a suitable length-scale of turbulence .

Solution of theses equations

The approximate form of the solution of these equations is used to establish the relationship between the spatial distribution of the velocity, the jet width, the jet initial velocity and the crop density. An approximation of the solution of equation (3.38) is given as the following series expansion by Zwillinger ([64])

$$S(x,y) = \sum_{n=0}^{m} S_n(x,y) = S_0 \sum_{n=0}^{m} F_n(x) G_n(y) \tag{3.42}$$

where $S(x,y)$ is a arbitrary small-scale volume-averaged transport property in the region $-\Delta/2 < y < \Delta/2$ with boundaries $\mathrm{d}S/\mathrm{d}y = 0$ at $y = -\Delta/2$ and $y = \Delta/2$ for all x and Δ is the final jet width at large x . The Fourier series $G_n(y) = A_n \cos(2n\pi y/\Delta)$ with coefficients

$$A_0 = 2\int_0^{\delta/2} G(y)\mathrm{d}y/\Delta, \tag{3.43}$$

$$A_n = 4\int_0^{\delta/2} G(y)\cos(2n\pi y/\Delta)\mathrm{d}y/\Delta \tag{3.44}$$

where δ is the initial jet width, define the shape of the velocity profile normal to the initial flow direction.

The penetration profile function $F_n(x) = \exp(-b_n x)$ where $b_n = a_{1S}n^2 + a_{2S} + a_{3S}$ determines the total crop penetration of the air-jet. The parameter $a_{1S} = (2\pi c)^2 R/\delta$ determines the length of adjustment from the initial jet flow profile at $x = 0$ to the fully developed profile. The parameter $a_{2S} = C_{D_{veg}} a_{LAD}$, determines the influence of crop density. Finally, the parameter $a_{3S} \sim (V_s/U_0)^2/(4R\delta)$ determines the apparent increase in crop density produced by sprayer movement.

For the flow region where *similarity arguments* (see 5.5) apply to the profile $G_n(y)$ (i.e. beyond the initial flow development region where $G_n(y)$ has a universal form) the following approximation can be adopted for jet properties at $y = 0$

$$S(x,0) \sim S_0 \exp(-xb) \tag{3.45}$$

where $b = a_{1S} + a_{2S} + a_{3S}$ and S_0 is a constant. The air-jet centre-line velocity can therefore be used to estimate parameters S_0 and b by fitting equation (3.45) to measurements of $S(x,0)$ in the region beyond the origin .

We will see that this approach has several similar features with the one developped in 5.6 for this thesis.

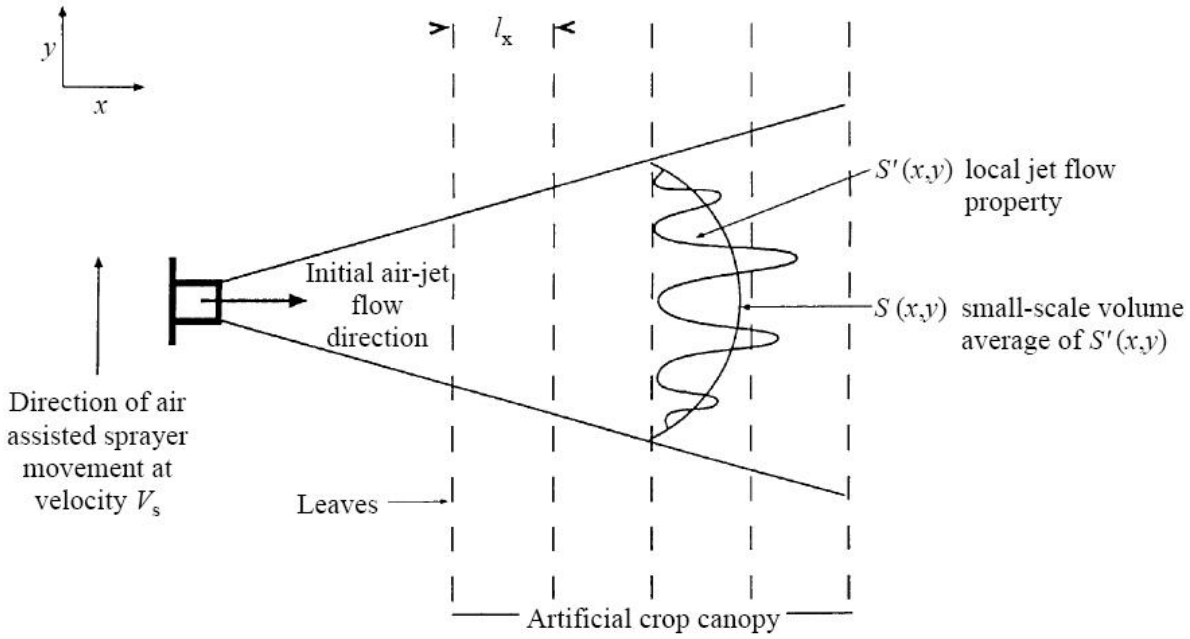

FIG. 3.2 – Plan view showing a two-dimensional air-jet which is penetrating an artificial crop canopy at the mid-height plane (x, y). The influence of small-scale volume averaging of local jet flow properties is also illustrated. From [51]

3.2.5 Combining spray and plant architectural models

Plant architecture informatics is an emerging discipline for the study of dynamic vegetation strucure in relation to environmental entities such as spray droplets. It can represent the entire developmental trajectories within plants and canopies. linked to dynamical systems. This formalism models plants or parts of plants as an assembly of components, each represented by a symbol with associated parameters called a module. A string of modules captures the architecture of a plant, by positioning the components relative to their neighbours, with a hierarchy of branching topology. This approach combined with particle trajectory models has been developed to determine when the tracked spray droplets collide with plant components [65].

Semi-Empirical Result

Several studies considered that the velocity decrease through the canopy follow an exponential law, that leads to [66] :

$$u(x) = u_e \exp(-C_D a_{LAD} x) \tag{3.46}$$

where $u(x)$ is the velocity profile at a given position x inside the canopy, and u_e, the mean velocity at the entrance of the canopy.

Then denoting L_{veg} the depth of the canopy and u_s the mean velocity just behind the canopy, the value of C_D is given by [66]

$$C_D = \frac{1}{a_{LAD} L_{veg}} \ln\left(\frac{u_e}{u_s}\right) \tag{3.47}$$

L_{veg} the depth of the canopy, u_s, the mean velocity just behind the canopy.

The current values for C_D in agreement with those found in literature are in the range $0.1<$ to < 0.5. The value of 0.5 corresponds to a single leaf perpendicular to the flow. The 0.3 value obtained is due to a shelter effect, caused by the surrounding leaves.

Chapitre 4

DriftX Module 1 : Canopy Flow Model

4.1 Motivation

4.1.1 Introduction

This section presents the development of a low complexity model for canopy flows. We use a *PDE* based model obtained by dimension reduction of the Navier-Stokes and transport equations. This step is used to study the obstruction effect of the canopy on the local flow and concentration field. The first objectif is to develop a low order model to describe the velocity, the distribution of the quantities sprayed within a canopy and the amount of species captured by the foliage. We want to reduce intuitive modelling using inverse design to identify the terms in the model recovering experimental data when available or direct simulations (4.3, p. 68).

With this aim, we present control problems for the assimilation of experimental data. It deals with the application of typical minimization methods based on dynamical systems to the solution of characteristic inverse problems. We show through a redefinition of the cost function ((4.16),(4.14)) that a multi-criteria problem could be considered. The approach aims also to define a single "mean row effect" as a robust representation of all rows on a parcel (4.3, p. 71) and which could be used as input in the next level of the platform.

4.1.2 Method

As our interest is on the row scale ($\sim$ row depth), the porous approach is used as explained in section 3.2.3. So the deceleration is described thanks to the drag force :

$$F_{D_{veg}} = \frac{1}{2}\rho\, a_{LAD}\, u^2\, C_{D_{veg}} \quad [N = kg.m.s^{-2}] \tag{4.1}$$

[67] found that the net effect of the drag was consistent for all of the data present in the literature, regardless of the vegetation type or flow medium (air or water for foodplain application). The section (3.1.2) has recalled that coefficient $C_{D_{veg}}$ contains many complex dependencies and is usually determined experimentally. Actually, the drag is only well known for a fixed individual isolated element perpendicular to the flow (3.2.5). In this case the reference value $C_{D_{veg}}$ is equal to 0.5. Obviously, within the canopy the leaves are not isolated and they are waving under the airflow. Actually, in the litterature $C_{D_{veg}} \in [0.1, 0.5]$.

Equation (4.1) requires the measurements or estimation of values for the drag coefficient $C_{D_{veg}}$ and the characteristic aera $A_{ref} = a_{LAD}$ of the vegetation. Sink terms parametrizations

are still under evaluation. This study presents a way to make numerical estimates of these coefficients.

Moreover, experimental data show additional effects that are not accounted for by area density alone and some studies expose a limitation in this common model ([56]). The influence of canopy elements and structure on the airflow needs to be then investigated with more complicated parameterization than the one used in common models (4.3, p. 73). This leads to the inverse problem of searching the best parametrization corresponding to a desired profile ("target").

This part concerns the study of velocity and concentration profiles, in function of the canopy distance penetration. A passive single-phase one-dimensional transport is assumed to model flow through the canopy layer. Our model is simpler than the Navier-Stokes equations. In a local reference frame (r, θ, z), it describes the velocity and the concentration $1D$-profile along a straight line inside the canopy (forming an angle θ with the ground supposed horizontal, see figure 4.1).The flow is not assumed to be horizontal or perpendicular to the canopy. This representation is expected to be sufficient to decribe the entire process.

The aim is to use as much as possible a priori information in the definition of the search space for the solution. Also, the approach aims to unify experimental and numerical information : when partial information being available on canopy effect and dispersion of species coming from spraying devices, a useful numerical method should assimilate and complete these information. We use inverse modelling for this parameter estimation problem. The parameters are found minimizing a cost function based on the difference between the observed and calculated solutions of the system.

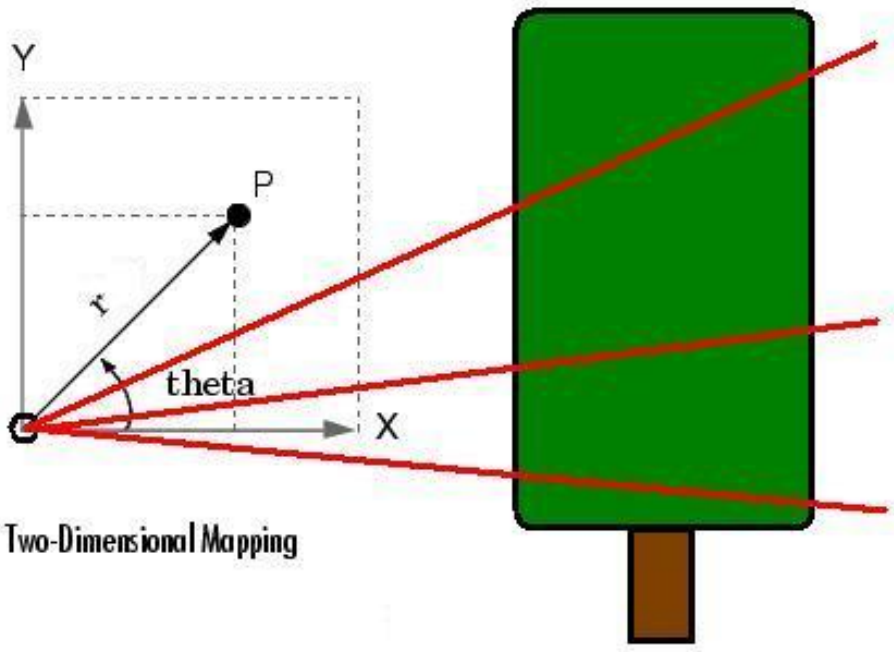

FIG. 4.1 – Representation of the reference frame. Different orientation of penetration inside a row. x is horizontal and parallel to the ground, z is parralel to the vineyard and y is vertical. Red lines indicates different orientation of the flow. $r = \sqrt{x^2 + y^2}$, $\theta = \arctan(y/x)$

4.2 Mathematical Setting

4.2.1 Dimensionnal Analysis

We apply the method of indices to the drag force. We consider that the drag force F_D per unit of volume depends only on the speed u, the characteristic length scale L_{ref}, the density ρ, and the dynamic viscosity μ. We then assume that the dependent variable F_D may be written in the form of a series of terms, each of which is a dimensionnally correct product of independent variables :

$$F_D = \sum_i c_i u^{\alpha_i} L_{ref}^{\beta_i} \rho^{\gamma_i} \mu^{\delta_i} \quad [N.m^{-3} = kg.m^{-2}.s^{-2}] \tag{4.2}$$

where the c_i are dimensionless constants. Dimensional homogeneity requires that :

$$[F_D] = [u^{\alpha_i} L_{ref}^{\beta_i} \rho^{\gamma_i} \mu^{\delta_i}] \tag{4.3}$$

which implies that

kg : $1 = \gamma_i + \delta_i$

m : $-2 = \alpha_i + \beta_i - 3\gamma_i - \delta_i$

s : $-2 = -\alpha_i - \delta_i$

Here we have 3 equations in 4 unknowns, so 3 unknowns may be expressed in terms of the other 1, and the i^{th} term may be written :

$$c_i u^{2-\delta_i} (L_{ref})^{-1-\delta_i} \rho^{1-\delta_i} \mu^{\delta_i} = \quad c_i u^2 \rho L_{ref}^{-1} \left(\frac{\rho}{\mu} u L_{ref} \right)^{-\delta_i} \tag{4.4}$$

Thus :

$$\frac{F_D}{\rho u^2 L_{ref}^{-1}} = \quad \sum_i c_i \left(\frac{u L_{ref}}{\nu} \right)^{-\delta_i} = \sum_i c_i \left(R_e \right)^{-\delta_i} \tag{4.5}$$

$$= \qquad \text{func} \left(\frac{u L_{ref}}{\nu} \right) = \text{func} \left(R_e \right) \tag{4.6}$$

The drag, made dimensionless by $\rho u^2 L_{ref}^{-1}$ is a function only of the Reynolds number (the dynamic viscosity μ and the kinematic viscosity ν, $[m^2 s^{-1}]$ are related by $\nu = \mu/\rho$). This suggests the investigator plot his observations in the form $\frac{F_D}{\rho u^2 L_{ref}}$ versus $\frac{u L_{ref}}{\nu}$ in the hope of finding a universal relationship.

Selection of the relevant parameters is the critical step. The process may rely on intuition, on limited data, or, most mechanically but most reliably, on a knowledge of the governing equations and their boundary and initial conditions (even if the latter cannot be solved). *Buckingham's pi theorem* states that physical laws are independent of the form of the units.

Using this kind of analysis, we will define in 4.3 a new parameterization for the drag term.

4.2.2 Problem statement : model equations and parameters

General form of state equations : Balance Law

In this part we treat with scalar viscous balance law with a nonlinear source term. Balance laws appear in a variety of applications that offer control or design possibilities, such as the design of airfoils, ducts and turbine blades, the control of traffic flow or the identification of parameters in chromatography or hydrodynamics [68]. The viscous balance law, for $u = u(r,t)$, are of the general following form (see C for the numerical resolution) :

$$u_t + f(u)_r = \varepsilon u_{rr} + g(u), \quad (r,t) \in \mathbb{R}^2,\ u \in \mathbb{R},\ \varepsilon \in \mathbb{R}^+ \tag{4.7}$$

Balance laws are extensions of hyperbolic conservation laws where viscosity ε and a source term g is added. These reaction terms can model chemical reactions, combustion or other interactions.

In many problems of fluid dynamics, the source term corresponds to the interaction with the surrounding medium, including the geometry and some internal forces (friction, gravity, Coriolis acceleration, etc..). It can dramatically change the long-time behaviour of the equation compared to hyperbolic conservation laws. In environmental problems, this interaction is often a very dominant term which characterizes the well balanced states.

Momentum : generalized forced viscous Bürgers equation

The state equation is the viscous forced Bürgers equation which represents typical first-order non-linear equation with right hand side (RHS). Burgers' equation is a useful test case for numerical methods due to its simplicity and predictable dynamics. This equation was designed originally to give a preliminary insight into the nature of turbulence. This one dimensional spatial model has recently raised much interest because of its multiple connections to a variety of three dimensional physical phenomena. Clearly, this rather oversimplified picture of the real situation has useful real-world applications in modeling ([69], [70], [71]).

$$\underbrace{\frac{Du}{Dt}}_{Lagrangian\ form} = \underbrace{\frac{\partial}{\partial t}u(r,t) + \frac{1}{2}\frac{\partial}{\partial r}(u(r,t)^2)}_{Eulerian\ flux/Conservative\ form}$$

In our particular problem the following sytem is considered :

$$\begin{aligned} (r,t) \in Q = [r_0, r_1] \times [0,T] \\ u(r,t)_t + 0.5(u(r,t)^2)_r - \nu u(r,t)_{rr} = F_u(u,r,t) \end{aligned} \tag{4.8}$$

where $f(u) = \frac{u^2}{2}$, $T \in]0,\infty]$ with initial, and boundary conditions given by

$$\begin{aligned} u(r,0) = u_0(r) = 0, \quad r \in [r_0, r_1] \\ u(r_0,t) = u_l(t) = u_l, \quad t \in [0,T] \end{aligned}$$

It models the momentum conservation equation for the velocity $u(r,t)$. In our model $u(r,t)$ is the velocity along a straight line and r represents the distance penetration inside the canopy. F_u is the sink term within the canopy due to the drag phenomena.

Scalar Transport

The classical one-dimensional transport equation for a passive scalar is used to simulate the mixing inside the row :

$$\begin{aligned} \frac{\partial c(r,t)}{\partial t} + u(r,t)\frac{\partial c(r,t)}{\partial r} - D\frac{\partial^2 c(r,t)}{\partial r^2} &= F_c(u,c,r,t) \\ c(r,0) &= c_0(r) = c_0 \\ c(r_0,t) &= c_l(t) = c_l \end{aligned} \tag{4.9}$$

where c is the concentration, u is the convection velocity, t is the time and r is the penetration distance. F_c is incorporated in the simulation to account for the mass sink effect of the canopy.

4.2.3 Inverse Problem

Inverse problem, starting from the observed data to plausible parameter values, are evaluated in terms of the cost of achieving an "exact solution" (target). It suggests that the payoff of achieving a solution should be balanced by cost, and in many cases, inexact answers may be the best. The state equations are based on (4.8) and (4.9).

Objective Function

We would like to recover a prescribed distribution u_{tar} by solving the following general control minimization problem :

$$(P) : \ inf\,\{J(F), F \in \Omega_{ad}\} \tag{4.10}$$

In our particular case, F is the sink term. We want to minimize the functional J, a cost function of the form :

$$J : \Omega_{ad} \rightarrow \mathbb{R}_+ \tag{4.11}$$

$$J(F) = \|u_F - u_{tar}\| \tag{4.12}$$

where Ω_{ad} is a functional space to be determined, u_F is the state solution of the state equation ((4.8) and (4.9) in our applications), and u_{tar}, the target state. Clearly, the problem (P) admits $F = F_{tar}$ as a global minimum and the corresponding value of J is then $J(F_{tar}) = 0$. But from a numerical point of view, the problem (P) is not easy to handle.

Adaptive Robust Control : Multi-criteria formulation

An adequate formulation for inverse problems is often by nature multi-criteria. A suitable minimization approach needs to recover particular characteristics which means that several functionals have to be minimized at the same time. To solve multi-criteria problems, different approaches are available [72].

We examine the situation where, (1) there exists more than one control for a system ($\left\{u_{tar}^{(i)}\right\}_i$) and (2) a hierarchy is associated with these controls ($\left\{\alpha^{(i)}\right\}_i$) ; thus, a multiobjective optimization problem arises. Mean-Square Error (MSE) is used to actually determine the coefficients and delivers optimum solution but taking into account realistic measurement conditions and uncertainties resulting from different error sources (measure,...). The convenient solution is selected with these following methods (average cost or worst cost) [73] :

– Case 1 : for instance, a possible approach consists in considering a linear combination of the associated cost function J_{LC} where $\alpha^{(i)}$ are positive coefficients.

$$(P_{LC}): \quad \min_F \{J_{LC}(F)\} \tag{4.13}$$

$$J_{LC}(F) = \sum_{i=1}^{n} \alpha^{(i)} \left\| u_F - u_{tar}^{(i)} \right\|_{L_2} \tag{4.14}$$

The weighted-sum of the n errors relatively to the n different target, $i \in [1, n]$. In a robust way, this method provides a framework to achieve the goal and also the criterion for the best solution of the system (average cost).

– Case 2, in an another approach, we can also consider the following min-max formulation for (P) :

$$(P_{WCE}): \quad \min_F \{J_{WCE}(F)\} \tag{4.15}$$

$$J_{WCE}(F) = \max_i \{\alpha^{(i)} \left\| u_F - u_{tar}^{(i)} \right\|_{L_2}\} \tag{4.16}$$

The minimization process of J_{WCE} corresponds then to the calculation of the efficient and optimal solution in the worst case considered. These methods are based in the concept of minimax (minimize the maximum error given the worst possible, worst case error).

These methods ensure an optimal solution at a required precision for a given computational cost. It provides a measure of control and quality of the solution. We then argue that these multicriteria formulation optimization problem greatly improves robustness properties of the solution of the inverse problem. Indeed, the two proposed functionals have complementary features, both necessary for a suitable solution of the problem. When dealing with a given inverse problem, a challenging task consists in finding these adequate functionals and the physical nature of the problem must then serve as a guideline.

4.3 Application to the present problem

We will carry out our analysis for the following class of optimal control problems where control appearing in the source term of equations (4.8) and (4.9).

Application to a parameter estimation problem

For this particular problem, the functions $u(t, r), c(t, r)$ are defined on $(t, r) \in \mathbb{R}_+ \times L_{veg}$, with $L_{veg} = [r_0, r_1]$ the depth of the canopy row. The objective is to see the behaviour of the model used in a simple case. No multicriteria approach is used at this stage.

The control is meant to achieve a prescribed state distribution u_{tar}^i. Based on experiments, these target functions can be estimated in analytical forms. This application uses a target space Ω_{tar} suggested by the observation (see 3.2.5) when the canopy is represented as an homogeneous single layer ($a_{LAD}(r, t) = cste$). In this case, the target functions $u_{tar}^i \in \Omega_{tar}$ could be considered of the following form :

$$u_{tar}^i(r) = u_l^i \exp\left(-\log\left(u_l^i/u_r^i\right) \left(\frac{r - r_0}{r_1 - r_0}\right)\right) \tag{4.17}$$

$$u_{tar}^i(r_0) = u_l^i, \qquad u_{tar}^i(r_1) = u_r^i = \beta_{veg} u_l^i \tag{4.18}$$

u^i_{tar} represents the different target objectives (see for example 4.2), u^i_l u^i_r are the velocity at the bounday of the domain (4.9), i.e. the mean veolcity before and behind the canopy and $\beta_{veg} \in [0, 1]$ is a cofficient depending of the vegetation density. It describes the velocity drop after the vegetation.

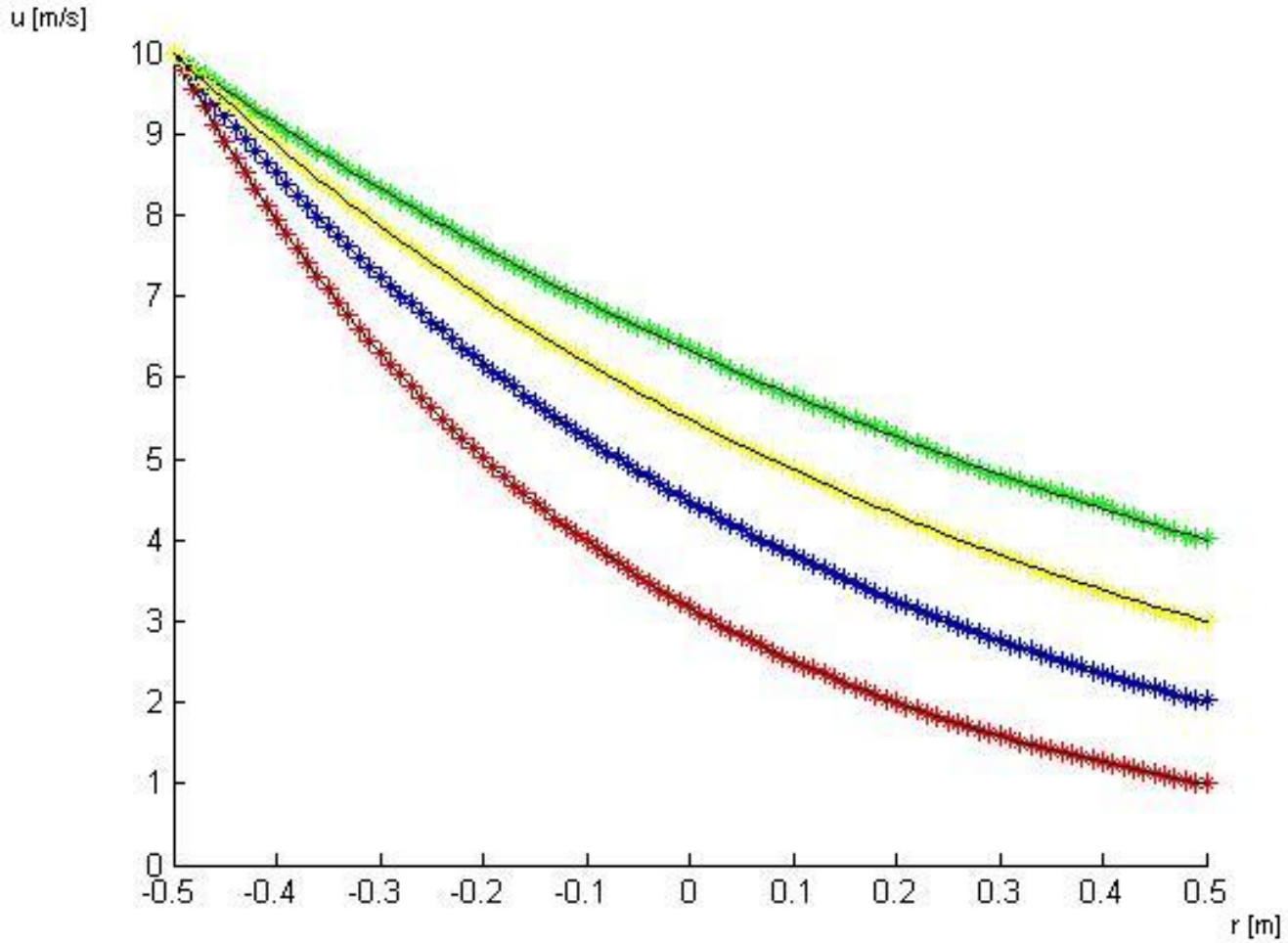

FIG. 4.2 – This figure represents several target flow profiles u^i_{tar} $(m\ s^{-1})$ (that are calculated with the semi experimental law (4.17), with $u^i = 4, 3, 2, 1$) plotted against the distance inside the vegetation r (m). For these target flows, the same initial condition is considered, $u^i_l = u_l = 10$ (ms^{-1}). The total domain represents a vegetation of $L_{veg} = 1$ meter depth (r_0, r_1), with $r_0 = -0.5$, $r_1 = 0.5$. For each profile target u^i_{tar} a minimization problem (4.22) is solved by resolution of the burger equation. The different control solutions u^i_{opt} are superposed to exact targets u^i_{tar} (black line profile). Each u^i_{opt} correponds to a different inverse problem and is defined by an optimal parameter $(a_{LAD} \times C_{D_{veg}})^i_{opt}$.

The solution of the equations (4.8) and (4.9) requires, among other things, the specification of vegetation characteristic functions a_{LAD} and $C_{D_{veg}}$. To reduce intuitive modelling the inverse design is used to identify the terms in the model recovering the experimental function shape given in (4.17) ([51],[52]). The sink term in (4.8) is assumed to have the following particular

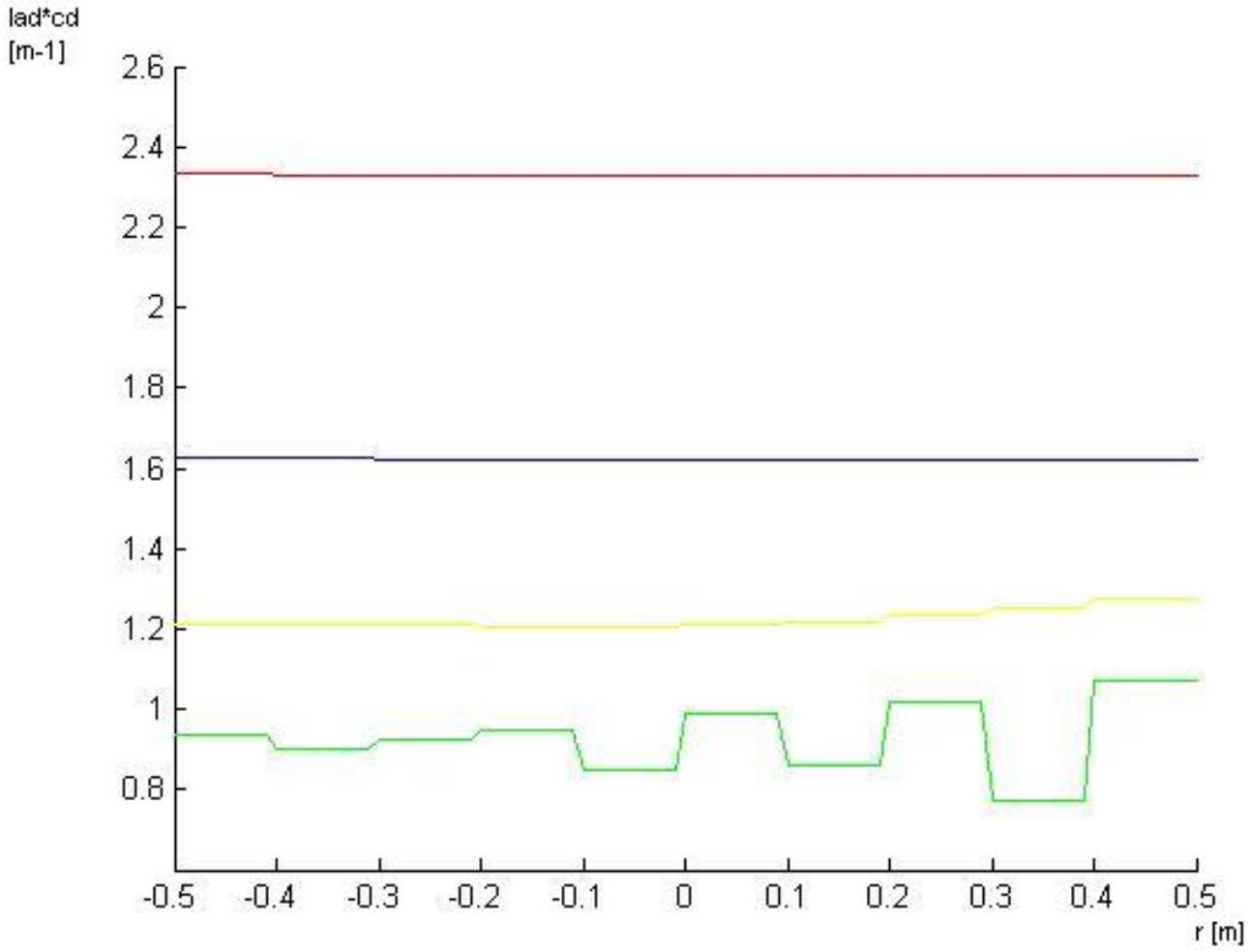

FIG. 4.3 – Optimal control $F^i_{u_{opt}} = (a_{LAD} \times C_{D_{veg}})^i_{opt}$ (m^{-1}) parameter corresponding to the flow profile u^i_{opt} presented in 4.2. It can be seen that, for our model, in the case of classical concave flow inside the vegetation, a quasi-constant parameter represents a reasonable aproximation. However, in the case of less convex flow, like for the green curve where the ratio β between the input and the output velocity is weaker, a constant parameter (that could be interpreted as a single homogeneous layer inside the canopy) is not sufficient to represent the good behaviour. It can be supposed that the product $(a_{LAD} \times C_{D_{veg}})$ need a more complicated behaviour that the constant one (variation in the vegetation density).

form :

$$F_u(u, r, t) = -\frac{1}{2}\, C_{D_{veg}}\, a_{LAD}\, u(r,t)|u(r,t)| \tag{4.19}$$

In fact, we could remark that, numerically, this source term depends only on a single free parameter equivalent to the product $C_{D_{veg}} \times a_{LAD}$. Numerically, it is equivalent to fix $C_{D_{veg}}$ and use a_{LAD} as a parameter, or to do the inverse. Only the admissible physical range of each parameter is different. So we can consider that $C_{D_{veg}} \times a_{LAD}$ is a single parameter varying over the full range of the product. Physically relevant solutions are limited to the following ranges of a_{LAD} and $C_{D_{veg}}$: minimize subject to $a_{LAD} \in [0, 12]$ and $C_{D_{veg}} \in [0.1, 0.5]$. So we consider product varying between $[0, 6]$.

We first assumes a simple functional form for the $a_{LAD} \times C_{D_{veg}}$ of a piece-wise discontinuous function. The interval $[r_0, r_1]$ is discretized into m sub-intervals. Physically it can be interpreted such as we let the row be a multilayered domain, where m layers are considered and a different value of a_{LAD} is possible for each layer. This representation naturally leads to the finite dimensional admissible space $\Omega_{ad} = \mathbb{R}^m$. The interest of this approximation is that, in practice, it grants more freedom to the canopy structure than the single homogeneous layer ($\rightarrow C_{D_{veg}}(r) \times a_{LAD}(r) = cst$). So the control F^i can be viewed as an element of $\mathbb{R}^m$.

$$F^i(r) = \sum_{k=1}^{m} \chi_{[r_k, r_{k+1}[}(r) \times (a_{LAD} \times C_{D_{veg}})_k^i \qquad [m^{-1}] \tag{4.20}$$

$$\text{where } (a_{LAD} \times C_{D_{veg}})_k^i \in \mathbb{R}^m \tag{4.21}$$

Where $\chi_{[r_k, r_{k+1}[}(r)$ is the characteristic function (or indicator function) $\chi_A : X \rightarrow \{0, 1\}$ which for every subset A of X, has value 1 at points of A and 0 at points of $X - A$. The inverse problem is then

$$\text{Find } \left(a_{LAD} \times C_{D_{veg}})_{u_{opt}}^i\right) \tag{4.22}$$

$$u_{opt} = min_u J^i(u) \tag{4.23}$$

$$\text{with } J^i(u) = \|u_{tar}^i - u\| \tag{4.24}$$

Figure 4.2 shows different targets profile u_{tar}^i and the optimal solution corresponding u_{opt}^i. Figure 4.3 shows the corresponding optimal control parameters F_{opt}^i. If the velocity has the exponantial form presented in 4.17, the product $a_{LAD}(r) \times C_{D_{veg}}(r)$ considered as almost constant is find to be an acceptable approximation when the ratio β_{veg} between input and output velocity is enough small $u_r^i/u_l^i < 0.25$. In these cases, solutions of the inverse problem reproduce in correct agreement compared to previously available approximate analytic functions obtained by assuming constant foliage distribution. So, in the case of a single homogeneous layer (i.e. $a_{LAD}(r) \times C_{D_{veg}} \sim$ constant), the classic model gives similar solution shape with experimental results.

Application to the definition of a mean row over a parcel

In the farm field, the crop is planted uniformly (e.g. vinerow) so that any study on a certain area of crop canopy can be extended to other parts of the field. However, on the other side, spatial variability is an irrenounceable element of natural and anthropic systems.

A good management corresponds to a reduced sensibility to variability in the vineyard. Its objective representation could be a significant advantage in terms of field work rationalisation, optimisation and quality improvement for pesticdes spraying. For this reason, a tool able to describe, to take into account for vineyard internal variability and to quantify the existing differences between plants and/or field sectors, is strongly desirable for producers and technicians.

New technologies for agrometeorological model applications integrate GIS (Geographical Information Systems) and RS (Remote Sensing) data techniques for canopy variability evaluation in vineyards [74]. Vineyard variability evaluation by RS is a field of study in continuous development, thanks to the advances in Very High Resolution (VHR) multispectral sensors designing. They could provide maps of spatial and temporal variation of the canopy at the vine row scale.

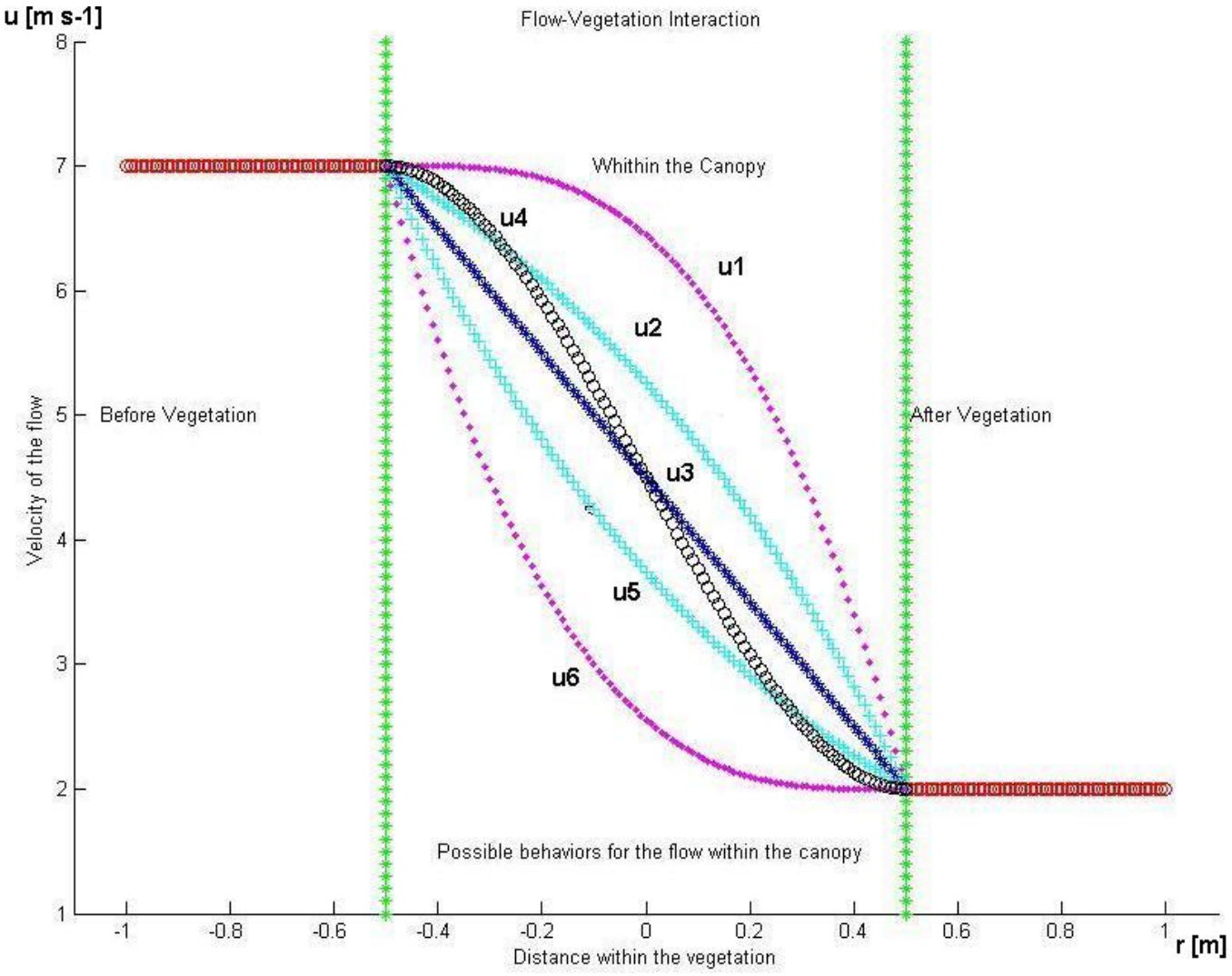

FIG. 4.4 – Example of several flow targets $\{u^j\}_{j=1,6}$ $(m\ s^{-1})$ profiles, which represent different possible behaviors in a sprayed area inside the vineyard row, for the velocity profile. Numerous factors could be responsible of these behaviors, such as nozzle axis orientation, vegetation structure variability, vegetation flexibility, shelter effect... In order to represent in the better way all these effects by a single profile, we should solve a robust optmization problem. This approach allow to control the error over the parcel thanks to the cost function.

As example, VIVES (VIneyard Variability Evaluation System), a component of the Bacchus system, uses a vine growing model (for the estimation of potential values of a_{LAI}, biomass and yield) and a series of geo-morphological layers, technical information and High Resolution images for the evaluation of existing differences and a detailed description of local variability. If these data encompass the parcel properties, it could be used as a representative benchmark of the parcel. A drift model could be then parameterized in terms of these readily measured field properties.

Our approach aims to define a "mean row effect" as a robust canopy representation. We want to use the cost function defined in (4.14) and (4.16), where more than one control and a hierarchy associated with these controls are considered. These multicriteria formulation optimization problem ensure a measure of control and quality of the solution and consequently improves its

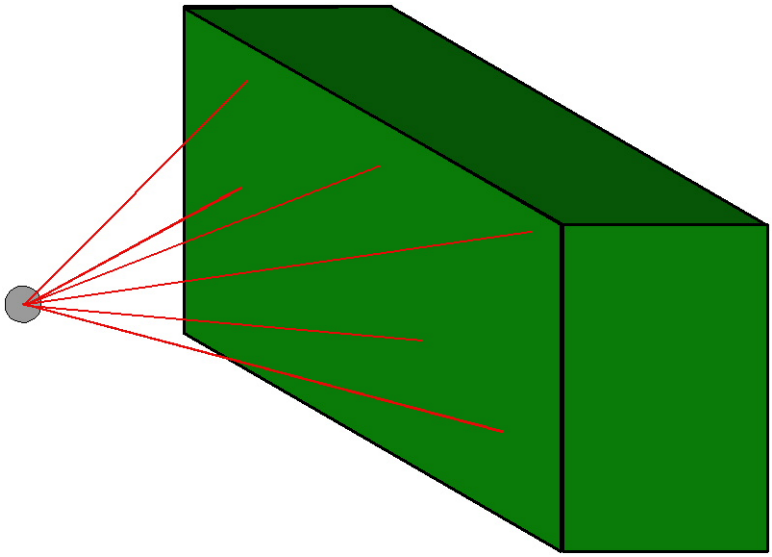

FIG. 4.5 – Penetration along straight line within a vineyard row following different orientation θ^j. We could consider these lines fsuch as the different nozzle axis orientation of the sprayer.

robustness properties.

Let us consider a set of target functions $\left\{u_{tar}^j\right\}_j$ as for example in figure 4.4 (or even 4.2). These different behaviors could result of different vegetation canopy stucture or different axis nozzle orientation, different flow direction not necessary perpendicular to the row. For example, $a_{LAD} = a_{LAD}(\theta)$ could be a directionnal parameter (see (3.6)), hence its value could be different following the flow orientation considered. Then different profile u_{tar}^j could be associated to these different $a_{LAD}(\theta^{(j)})$ corresponding to the angles of the axis nozzle with the ground, $\theta^{(j)}$ (see figure 4.5). These profiles could also depend, for example, on different vine growth rate due to the heterogeneity condition in the parcel (ground properties, sunshine duration...).

Then we set $\alpha^{(j)}$ the corresponding control weight coefficient. These coefficients $\alpha^{(j)}$ can represent the confidence according to the different values of a_{LAD}^j or the representativeness of these different values inside the parcel. So they associate a hierarchy to the different target. The objective is to find a control u_{opt}, such that u_{opt} is close to all the *targets* u_{tar}^j in the sens of one of the multicriteria approach presented in 4.2.3. The figure 4.8 show 2 examples of result for this problem. These optimal results could be considered over the parcel and used as robust profiles, in the sens that we know the maximum error which is given by the cost function considered.

Application to the common model limitation

The motivation for this problem could be found in the following where limitations of common models are evocated. First, we need to recognize that for crops with a high proportion of leaf cover the momentum and TKE losses are not always given by the conventional models [51]. In addition, the effect may become enhanced in a real crop when the leaves respond to forcing from the air flow. It depends on more rigid or low density crop structures. Moreover the shape of the velocity profile is also affected by fractional vegetation cover, leaf orientation, leaf size and shape, plant flexibility, shelter effect...The shelter effect, for example, is not completly understood ([58],[50]).

According to the existing model, errors occur from the deposition parameterization used in models due to the simplified assumption on canopy structure (a simple homogeneous single layer

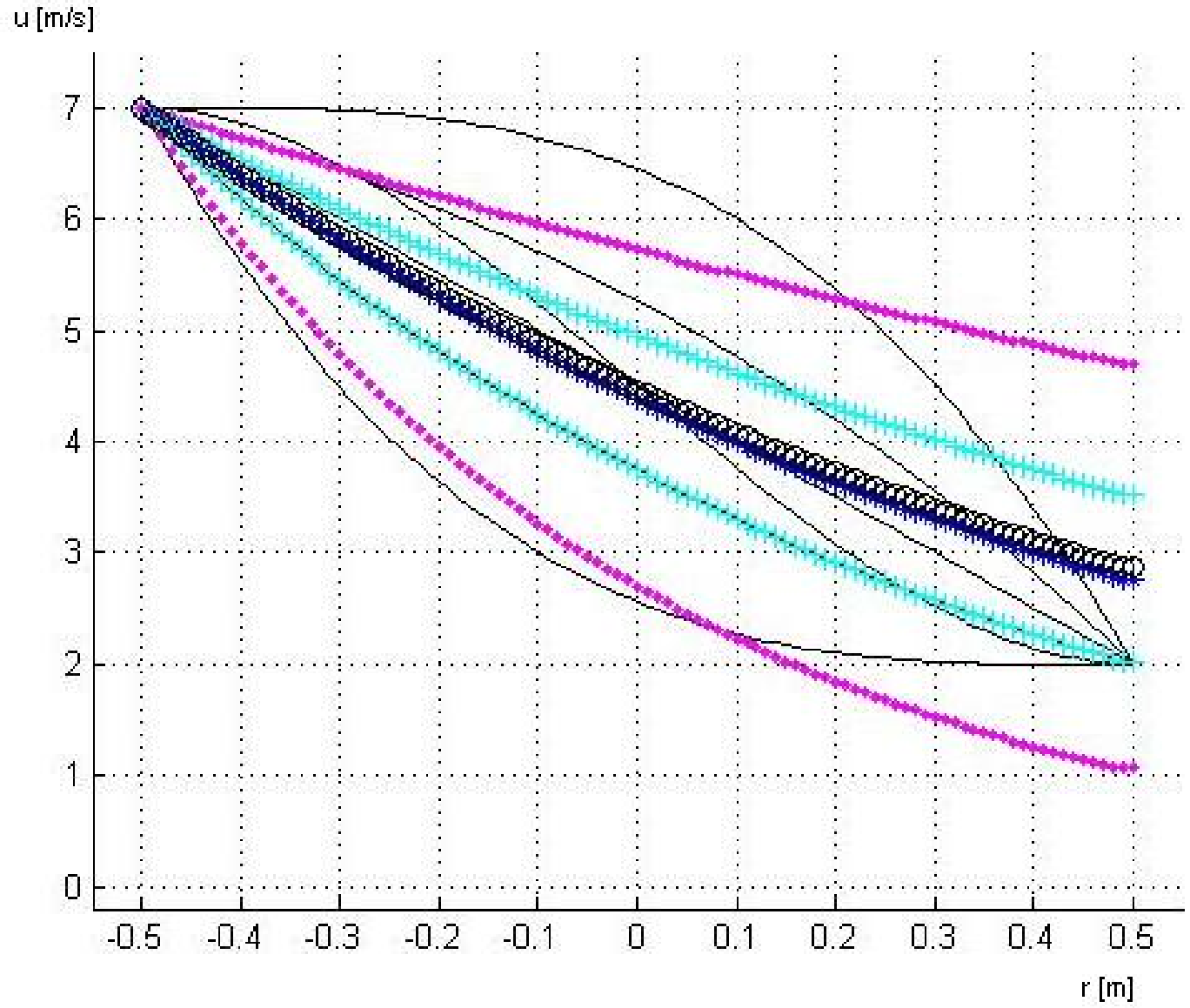

FIG. 4.6 – Optimal results for the targets $\{u^j\}_{j=1,6}$ $(m\ s^{-1})$ (original target are represented by thin black lines, see figure 4.4) using the classical model of drag with $a_0 = a_2 = 0$ and a_1 is constant.

with no flexibility is considered). These difficulties limit interest in these classical models and lead us to suggest some cheap and realistic alternatives. Current efforts are focusing on the effect of the improved parameterization for each type of canopy. But sink terms parametrizations are still under evaluation.

Therefore, we suggest in this section, an alternative crop density model for scaling air-jet flow losses within a crop. Our model has been developed to take into account additional effect of crop structure. We want to include different canopy structure and the effect of canopy elements on the flow by redefining the drag force as in [56], [51]. Our approach is to use the systematical decomposition approach of dimensionnal analysis for the drag, as presented in 4.2.1. The sink term could then be generalized for applying to heterogeneous cover with density depending on space and time. This new parameterization has the form of a series of terms and each of

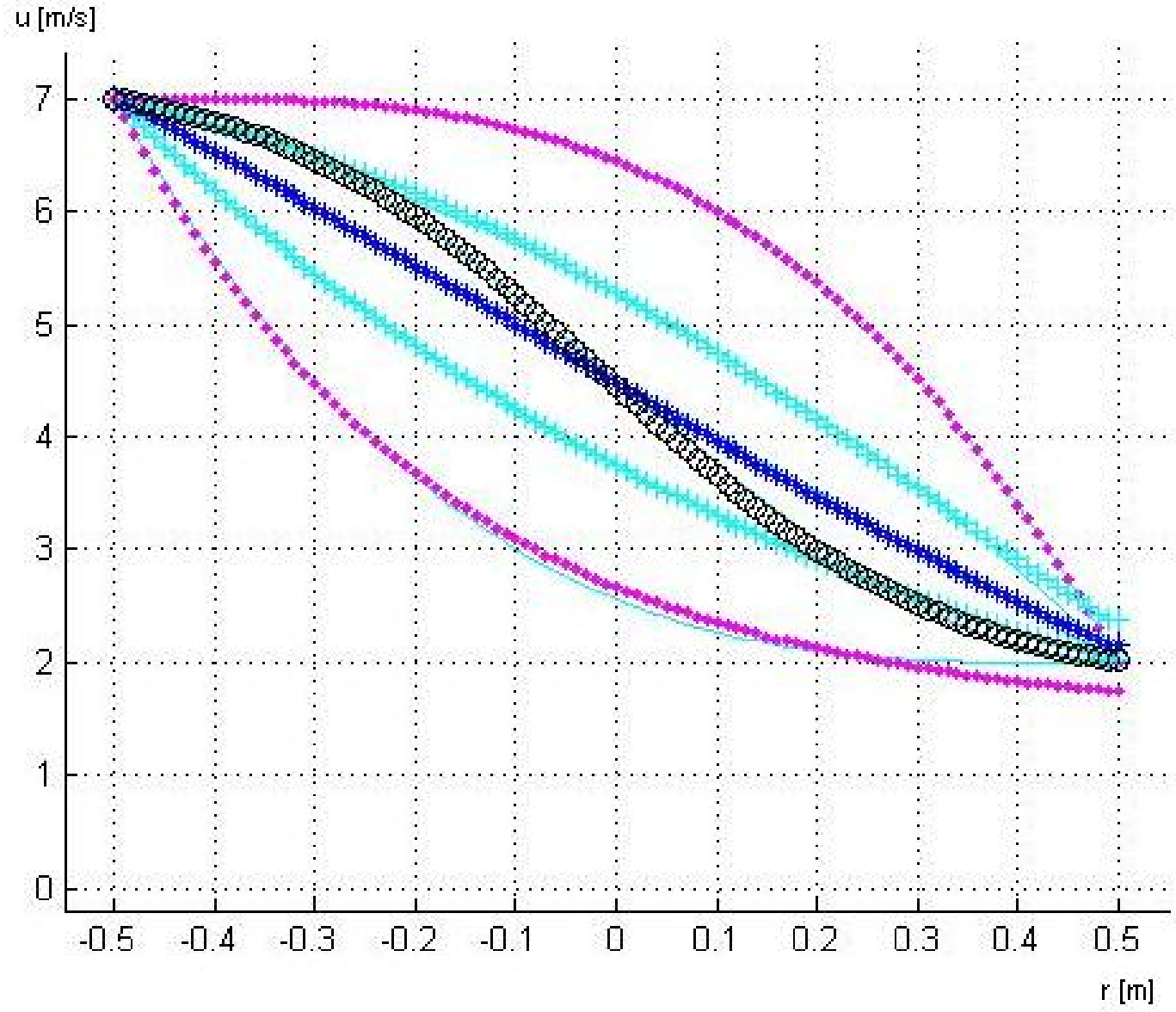

FIG. 4.7 – Optimal results for the targets $\{u^j\}_{j=1,6}$ using the new model 4.25 (a_0, a_1 and a_2 are constant). Optimal solutions in this case fit the targets in a better way than in the classical case 4.6.

which is a dimensionnally correct product of independent variables. The new following form is proposed for the sink term in (4.8) :

$$F_u(u,r,t) = -\tfrac{1}{2}u(r,t)\left[a_0(r,t) + a_1(r,t)|u(r,t)| + a_2(r,t)|u(r,t)|^2\right] \quad (4.25)$$

$$F_u(u,r,t) = \sum_{i=0}^{n} b_i \; u \; |u|^i \quad (4.26)$$

To close the model we need however to identify several coefficients a_i. If we set $a_0 = a_2 = 0$ and $a_1 = C_d \times a_{LAD}$, we retrieve the classical model of drag. This model extension seems to be natural when the dimensionnal analysis theory (section 4.2.1) and the porous theory (section 3.2.3) are used. Figures 4.6 and 4.7 show optimal results for different flow target profiles with the old and the new parameterization, respectively. It can be seen that with the

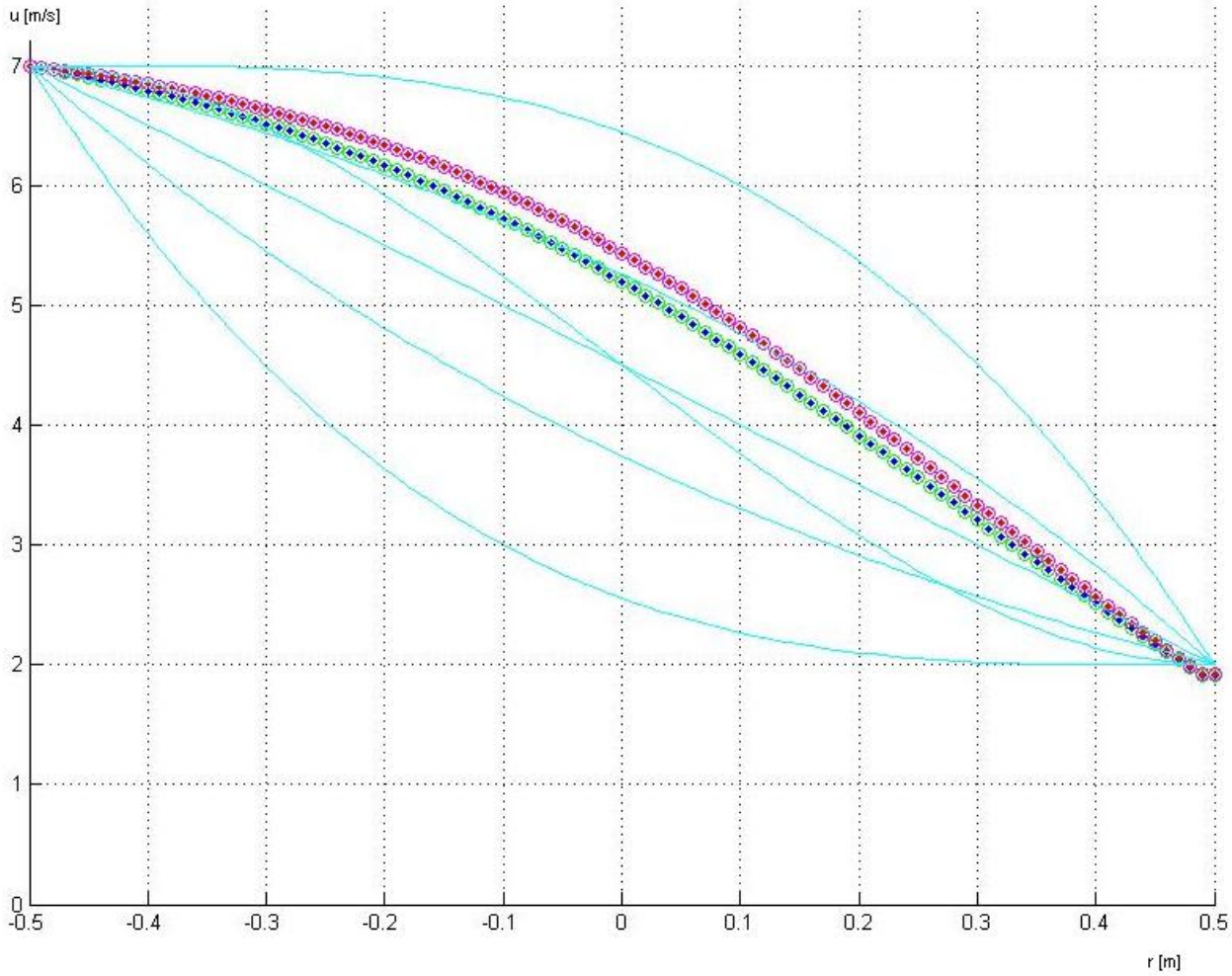

FIG. 4.8 – Robust optimal controls for the targets $\{u^j\}_{j=1,6}$ with the new parameterization model 4.25. The green curve represents the optimal solution in the "LC sens" (see 4.14) and the red one in the "WCE" sens (see 4.16). In these 2 cases the coefficients α^j are all set to 1.

old parameterization, the optimal results are far from the target objectives, except for the exponential decay target. It could be supposed that the control needs more degree of freedom as in the curve for $u_l = 10, u_r = 4$ ($\beta_{veg} = 0.4$) of figure 4.3 where a non constant parameter is the optimal control. The figure 4.7 shows that the new parameterization with more degree of freedom gives optimal results that are superposed with their targets. Hence a best control of the solution is possible to identify a robust behavior for the parcel.

4.4 Concluding Remarks

The objectif was to develop a model to describe the velocity and the distribution of the quantities sprayed within a canopy in order to be able to encompass the general features of the random heterogeneous porous media which is vegetative canopy. The described applications are idealized model problem in the sens that they allow to present the methodology. But they are limited in nature. That is why the results presented here are simple. The practical interest is essentially in the method. The scalar transport is not discussed because the methodology is

exactly the same as for the moment equation.

This is the first step for a basis framework of multi-scale modelling, where simulation are based on low order model. This part has presented an analysis of momentum equation along a straight line penetrating a crop canopy. The model illustrates basic aspects of canopy flow Typical inverse problems approach have been used in a basic way to overcome characteristics difficulties involved with canopy flow modelling.

Beyond this simplistic present 1D-modelling, such calculations could be useful to understand the complex effects of vegetation on air circulation in the canopy layer. They also could provide theoritical and physical guidance for computationaly intensive three-dimensional calculations. The same idea could easily be expanded to include more inputs, complex phenomen or extended to higher dimensions with a little more work. Described techniques are applicable to a broad range of cases and this range of applicability has not been fully explored. In fact, a substantially wider range of variation in these problems is possible. It allows to establish a scientific basis for improving canopy flow and architecture understanding.

Moreover, even though some techniques are available for estimating porosity rate, none offers a quick and easy way to obtain an estimate for the purposes of preliminary analysis and decision-making. The estimation methods presented here are easy to use and yield scientifically-based estimates using parameters representative of the prevailing site conditions.

It is shown that the common approach (exponential decay within an homogeneous single layer, equation (3.3)) exhibits a correct effect (in 4.3) and seems to be an acceptable representation when uncomplicated flow are considered with our model. Hence, the used resistance force in these cases gives an approximation of the canopy effect on air flow. The simulations (in 4.3) could explicitly consider variability in leaf area density in space. So it adds significant flexibility to the model and to the range of problems that can be studied. The calibration of free parameters had be done by comparison with experimental observations or semi-experimental law. An exemple of new formulation and calibration of the sink term had been proposed. More complex flow could be well reproduced by this new parameterization. However, the proposed model in this last inverse problem application missed of physical meaning. The different terms added in u and u^3 show just how it is possible to increase the degree of freedom. It is then possible to take account more complicated behaviour and to have a better control. Benefit of the new parameterization allow to better control the solution behaviour within the vegetation.

Some simple features could be added, such as the radial diffusion thanks to the term $\mu u_{zz}, \mu c_{zz}$ (where z is perpendicular to the flow direction r) in equations (4.8) and (4.9) in order to improve our model. The order of magnitude of the different term in the equation should be estimated.

These study show also that a correct definition of the minimization problem could help and needs to be studied before a direct application of brute force minimization approaches. In fact the choice of the cost function (for example the definition of the weight coefficient $\{\alpha_i\}_i$ could of importance for the robustness of the result.

The techniques developed may be linked to decisions support systems to maximise the effectiveness of plant protection products and minimise risks to the environment and public health from agricultural spraying activities. This model could be also used to recognize and classify canopy morphologies starting from some field data or experiments. In the scope of this thesis the more interesting application is probably the possibility to validate a robust canopy model which could be applied over the whole parcel, i.e. a profile that could be use inside all the vinerow and with an error that could be estimated by the cost function.

Troisième partie

LEVEL 2 : Sprayer

FIG. 4.9 – Air-assisted sprayer and nozzle output.

Introduction

Le but de cette partie est de présenter un modèle réduit simulant en champ proche, la pulvérisation de produits phytosanitaires sur des rangs de vigne. Il sera ainsi possible d'estimer les pertes directes engendrées dans la couche limite atmosphérique pendant l'application. On va s'attacher, en particulier, à décrire la distribution locale du champ de concentration.

Pour décrire l'écoulement issu d'un pulvérisateur, on utilise les solutions de similitudes classiques pour les jets libres turbulents. Ce choix permet de réduire considérablement la complexité du modèle. Cette étape, spécifique au problème de la dispersion des pesticides, permet donc de quantifier les émissions vers l'atmosphère. Elle est par conséquent déterminante pour le modèle de dispersion puisqu'elle fournit une condition d'entrée, en caractérisant la source, au niveau de modélisation suivant qui sera décrit dans la partie IV.

Le problème lié au terme source

Généralités

En amont de la modélisation de la dispersion atmosphérique d'une substance, il convient généralement de caractériser un "terme source". On entend par "terme source", tout ce qui conditionne la formation du nuage, c'est-à-dire les propriétés de la source d'émission initiale éventuellement modifiées par son environnement. Par exemple, la source d'émission initiale est

caractérisée par le type de produit (état physique, quantité,...), le débit (conditionné par sa pression, sa température,...), la vitesse initiale...

Son "environnement proche" est par exemple la présence d'un mur (jet dit "impactant"), d'un local de confinement, etc. qui influencent directement le devenir du terme source initial (devenir de la fraction liquide, évaporation de la flaque etc.). Cet environnement a été l'objet de la partie précédente, concernant la représentation des rangs de vigne.

Il faut souligner l'importance de la quantification du terme source. Quel que soit l'outil de calcul utilisé pour modéliser le transport, la caractérisation du terme source doit être la meilleure possible. En effet, le phénomène physique qui en résulte (la dispersion atmosphérique en l'occurrence) ne peut être correctement appréhendé si le terme source n'a pas été bien évalué.

Ce terme est souvent occulté ou mal pris en compte car il nécessite une compréhension approfondie des phénomènes impliqués. Généralement, la détermination du terme source peut s'effectuer soit forfaitairement[1], soit de manière spécifique (par exemple via l'utilisation d'un outil intégral qui caractérise le terme source[2]). A l'heure actuelle et compte tenu des avancées des codes de calculs, une détermination forfaitaire du terme source est de moins en moins adaptée.

Cette étape va donc permettre de connaître les caractéristiques de la source d'émission (énergie cinétique, direction du rejet, durée, conditions ...) et d'estimer le terme source associé.

Représentation du jet de pulvérsation

Dans la modélisation utilisée, chaque jet issu d'une buse du pulvérisateur est représenté par un jet libre turbulent. Le parti pris a été, encore une fois, de tenter une modélisation la plus simple possible. Ainsi, il a été choisi de représenter la végétation de manière globale, en ne prenant en compte que sa géométrie (ramenée à un parallélépipède) et la densité de feuillage. A l'intérieur de la canopée, on se sert de l'étude sur le comportement du flux d'air effectuée au niveau précédent (partie II), pour représenter les modifications induites sur le spray par la végétation.

Pour le flux d'air, on utilise la simulation d'un jet libre axisymétrique, et notamment les solutions analytiques de similitudes qui lui sont associées. Cette hypothèse de symétrie, implique une isotropie et une homogénéité dans l'établissement du jet et dans le développement de la turbulence dans les directions orthogonales à l'axe de la buse. Dans la partie précédente (chapitre 4), l'étude réalisée va permettre de décrire la dynamique de ce jet au sein du couvert le long de l'axe de la buse. On réintroduit cette information, afin de prendre en compte la présence du rang de vigne (modélisé comme un milieu poreux homogène). Une comparaison des résultats du modèle a été réalisée avec les méthodes expérimentales menées par [3].

La recherche bibliographique a permis de mettre en lumière les limites de la théorie (cf. 5.3.2). Par ailleurs ces limites démontrent la consitance et la cohérence de la recherche menée au Cemagref, car elles permettent de mettre en évidence les besoins de travaux sur la formation des jets de pulvérisation, comme ceux réalisés par [75] sur les phénomènes de fragmentation.

[1] Par exemple dans le cas d'une fuite, assurer que, quelle que soit la brèche initiale, il y aura une évaporation de 30%, le reste faisant une flaque au sol.

[2] Par exemple la détermination d'un débit par le calcul via un outil intégral à partir de la vitesse et du débit moyen des gouttelettes pour un rejet di-phasique.

FIG. 4.10 – Experimental estmation of spray losses with an air-assisted sprayer.

Plan

Le début de cette partie est consacré à l'étude des jets turbulents, et résume les connaissances existantes sur ces écoulements classiques.

On montre ensuite la démarche permettant d'arriver aux équations de couche limite, gouvenant l'écoulement du jet, en partant des équations générales de Navier-Stokes, par une analyse sur les ordres de grandeurs des différents termes des équations. L'étape suivante introduit les arguments provenant de l'analyse dimensionnelle, autorisant un déduction des solutions analytiques.

Enfin, le dernier chapitre décrit l'application de ces concepts au modèle utilisé et explique leur utilisation dans cette thèse.

Mots clés : *Théorie des jets turbulents, champ proche, transport scalaire, solutions de similitudes, terme source*

Keywords : *Turbulent jet theory, near field, mixing transport, similarity solution, source term*

"Everything should be made as simple as possible, but not simpler."

[Albert Einstein (1879-1955)]

Chapitre 5

Turbulent Jet Theory

5.1 Introduction

In order to provide a simple and robust tool for estimate the source term, the spray flow must be described. An axisymmetric free turbulent round jet, or 'simple jet', was chosen for this purpose. The characteristics of such jets are widely reported in the literature for a variety of flow and boundary conditions (bounded and free geometries) with numerous experimental and computational investigations of jet behaviour.

5.1.1 Short literature review

Turbulent jet dynamics

Jets belong to the classical prototype of turbulent free shear flows and occur in a large number of engineering and environmental situations. They are driven purely by momentum supplied at the source. There are fairly simple to create, and are, therefore, frequently used as models for experimental and computational testing purposes ([77], [78], [79], [80], [81]).

Besides the theoretical value of the turbulent jet, there are many practical applications which may be single-phase or two-phases. It provides the basis for modeling a variety of practical and natural flows, including combustion, waste disposal, cooling towers,... ([82] ; [79] ; [83]). They are deceptively simple flows and their numerical simulation is a challenging task (e.g., [80]).

However, its simple geometry makes it an attractive subject for the study of turbulence (see for example [84] and [85] for comprehensive reviews). For as long as turbulence has been known, turbulent jets have been investigated extensively to understand just how turbulence is generated at the expense of the mean motion and how it is dissipated.

Many experimental investigations have been carried out in order to get more insight in the characteristics of turbulent phenomena. As examples we may mention here [86] and [87].

A lot of studies are based on the $K-\varepsilon$ turbulence closure model or its variants (e.g., [88] , [80]). But the standard $K-\varepsilon$ model has not been found to be very successful in predicting jet characteristics ([80]).

Turbulent jet mixing

Apart from its dynamics, turbulent jet flow has been also widely studied for its mixing properties. In fact, together with the fluid flow one may also emit a substance from the orifice. The dispersed phase is transported and mixed by the jet fluid.

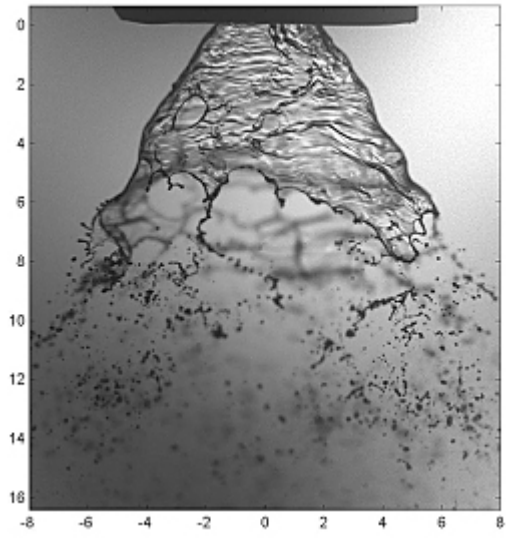

FIG. 5.1 – Droplet formation from a turbulent nozzle. (Source : Cemagref)

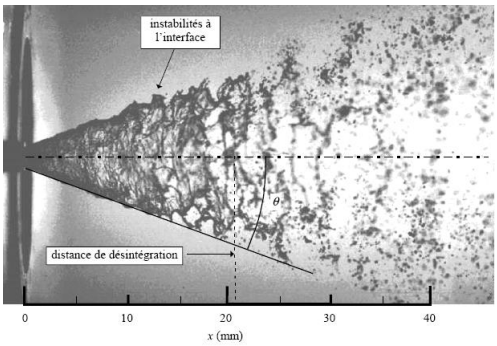

FIG. 5.2 – Photography of the cone-jet. (Source : [76])

The dispersed phase may either have its own dynamics or behave as a passive (scalar) mixed quantity, which means that it does not contribute to the jet dynamics. The substance is usually taken to be passive [89]. It is thus carried along passively by the flow while being dispersed by the turbulence.

Apart from a fundamental interest in the mixing processes within a turbulent jet, a study of jet mixing is also of much practical importance. For instance, jet flows in combination with turbulent mixing can be found in many industrial applications, e.g. injection of fuel in combustion chambers, propulsion systems for aircraft and spacecraft, spraying and mixing devices but also many combustion flames can in essence be considered as turbulent mixing jets. Acquiring knowledge about the turbulent transport is therefore useful for the design of these applications.

5.2 Jet Theory

5.2.1 Fundamentals of Turbulent Jets

Our particular subject of inquiry here is the axisymmetric turbulent jet. When a fluid is issued from a circular orifice, at a sufficiently high Reynolds number, a round turbulent jet results. If the jet does not feel the presence of the boundaries of the surrounding medium (e.g. not influenced by the presence of side walls), it is called a free turbulent jet and is a well-known class of self-preserving shear flow and their structure has been extensively documented.

One of the focus has been on the similarity theory that claims that, on every position downstream along the jet axis, the flow variables can be described by a single function, provided that they are scaled properly. Although the similarity approach seems straightforward, its application in particular to jet flow has not been without controversy ; for a recent discussion we refer to [90] (see also 5.3.2).

Fluid issued from a circular orifice forms an axisymmetric laminar shear layer. Above a certain Reynolds number, which must be determined experimentally (order of magnitude 500),

FIG. 5.3 – An example of turbulent jet, visualised with fluorescein (from [91]).

the shear layer becomes unstable and forms ring vortices. Adjacent vortices pair off and break up which leads to a turbulent flow. The jet starts spreading outwards by engulfing ambient fluid. The instability process is known in literature as *Kelvin-Helmholtz instability* [92].

The mentioned Reynolds number of the jet is defined as :

$$R_{e_{jet}} = \frac{\rho \overline{U_{jet}} d_{jet}}{\mu} \tag{5.1}$$

in which ρ is the fluid density, $\overline{U_{jet}}$ the mean jet velocity at the outlet, d_{jet} is the diameter of the jet tube (or nozzle) and μ the dynamic viscosity of the fluid.

Because of entrainment, the volume rate of the flow past any section in the jet increases in the x direction and the mean speed of the jet at its centerline decreases. The region of finite thickness which forms on the boundary of the jets is termed the turbulent jet boundary layer and is characterized by a continuous distribution of velocity, temperature and constituents [84]. In the vicinity of the jet boundary layer, large velocity gradients are present and so the terminology shear flow can be used [93]. Characteristically, free shear layer flows, and therefore free jets, are highly unstable.

5.2.2 Entrainment in Free Jets

As the jet spreads, fluid from the surroundings is drawn radially towards the jet across its conical surface. This process is known as entrainment. Entrainment is important in many practical situations ; for example, it controls the flow pattern in combustion chambers and furnaces. Also, many mixing devices in the chemical industry rely on entrainment for their effectiveness. To improve the efficiency of these devices and processes, it is important to gain insight into this process.

The process of entrainment in turbulent jets is understood to occur in three phases. The first step, known as the induction phase, involves the engulfment of ambient fluid driven by the Biot-Savart-induced velocity of large vortices residing at the edge of the jet. The inducted flow, although still irrotational, forms a part of the moving turbulent flow. Subsequent turbulent straining of the inducted flow reduces its spatial scale to a small enough value at which viscous diffusion dominates (diastrophy). Finally, viscous diffusion enables the inducted fluid to mix at

the molecular level with the turbulent flow (infusion). Obviously, any mechanism that interferes with the induction process will also affect entrainment.

The entrainment behavior of free-shear flows is influenced by a number of internal and external parameters. For example, these could include density stratification of the host fluid, buoyancy addition to the jet (both at source and off source), ambient pressure gradient, and the effect of other body forces. Classical entrainment mechanisms are abundantly described in the literature for ordinary jets.

5.3 Free Jet structure

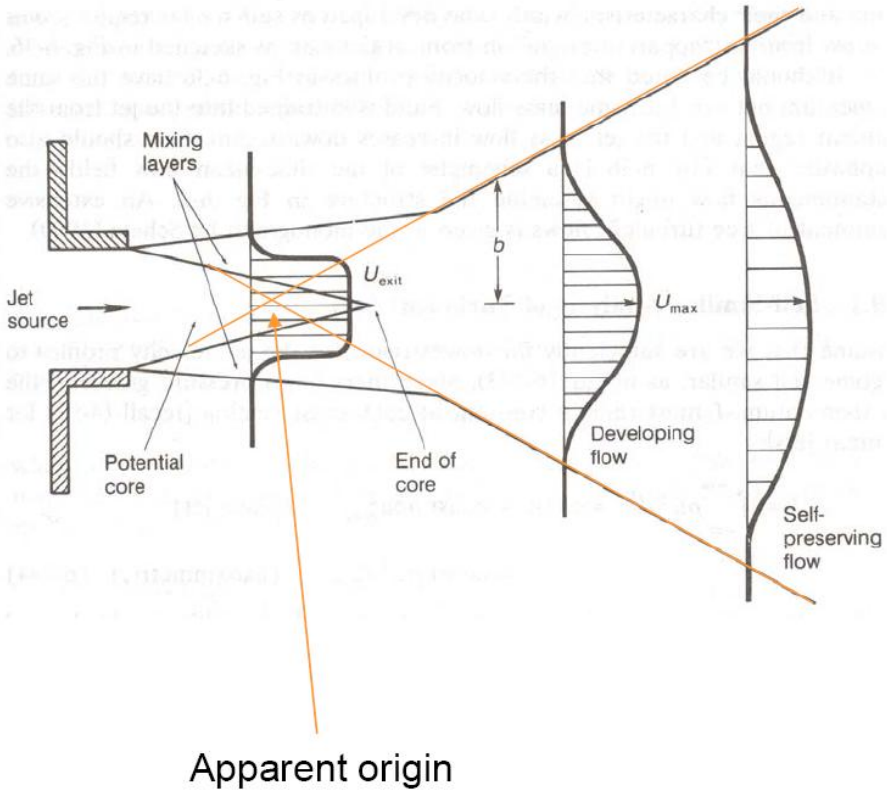

FIG. 5.4 – Sketch of a free turbulent jet structure [91].

5.3.1 Jet expansion zones

Classically, the development of a free jet is characterised by several regimes and divided into several zones, related to centerline velocity decay : the zone of flow establishment (ZFE) near the jet orifice, followed by the zone of established flow (ZEF) far away (see figure 5.3 and 5.4).

Zone of flow establishment (ZFE)

The ZFE has been less investigated than the ZEF. One of the probable reasons is that no suitable theory is available for the ZFE because of the dependence of flow structure on the jet orifice geometry.

A jet emerging from a nozzle will initially maintain a constant velocity U_{jet} to a downstream distance x_{core1}, before the turbulence generated on the boundaries of the jet penetrates to the jet axis and causes the jet velocity decay [85]. This region of constant velocity is in the form of a cone, and is known as the potential core.

Numerous investigators take the potential core region as the ZFE. However, other studies ([94]) argued that there is a transition region after the potential core before the jet becomes self-similar in the ZEF. So this zone could be divided into 2 sub-zones :

- zone 1, $0 < x/d_{jet} < x_{core1}$ a canonical zone where centerline velocity is equal to outlet velocity, where x is the axial distance measured from the orifice and d_{jet} is the orifice diameter.
- zone 2, $x_{core1} < x/d_{jet} < x_{core2}$ a transition zone where the velocity starts to decrease, often approximated as proportional to $x^{-0.5}$.

Zone of established flow (ZEF)

Observations show that, after some distance from the source, the flow is turbulent, expands conically, and appears as if originating from a point source. In this fully developed region, the radial distribution of the axial velocity at any value of x has the same profile, (the shape of mean horizontal profiles become independent of the axial location [78] when the velocities are normalised (when normalized by the appropriate velocity and length scales in the flow) and plotted against a dimensionless radial distance. For this reason, the fully developed region of flow is also referred to as 'self-similar'.

Self-preservation means a continuing similarity in turbulent structure during the decay or development of a turbulent flow, i.e. there is equilibrium between viscous decay and the generation of turbulent energy through turbulent shear stresses.

In fact, in some cases, the instantaneous flow field is three-dimensional, highly complex, and varies from one instant to another. However, when averaged over a period that is much larger than the timescale given by l/U (the *eddy turnover time*), where l and U are characteristic length and velocity scales in the flow, the resulting mean flow field is steady and two-dimensional.

The characteristics of a turbulent free jet in the ZEF have been the subject of many investigations. And consequently, the mean and turbulent flow properties in this region have been measured by several investigators. [95] performed a comprehensive study of the self-similar region of a round jet and reported moments, energy balance, intermittency, microscales, and integral scales.

[95] argued that a given body of fluid is said to be in a self-preserving state when all of its turbulent components (u', v', and w') are in equilibrium. They indicated that self-similarity is reached in steps. First, the mean velocity becomes similar, which leads to certain production of the axial fluctuating component u'. Experiments showed that the u' component attained self-similarity at $x/d_{jet} \approx 40$ and v' component became self-similar only at $x/d_{jet} \approx 70$.

As the ZFE, this zone could be subdivided into 2 subzones :

- zone 3, the self-preserving zone, where transverse velocity profiles are similar at different values of x and velocity decay is assumed to be proportional to x^{-1} ; and
- zone 4, the jet terminal zone, where the centerline velocity rapidly decreases. Despite this zone has been studied by several researchers, its different mechanisms are still not very well understood.

In brief, beyond the potential core region and the transition zone, the flow is considered to be fully developed [85]. The mean velocity profiles, turbulence intensities, and shear stresses at

various axial stations in the ZEF collapse onto a single profile.

Centerline velocity in the ZEF of the jet can be calculated from equations based on the principle of momentum conservation along the jet. Assuming that the momentum flux in the axial direction is conserved, the jet centerline velocity in the fully developed region decays with x [85]. In fact, the momentum contained within the jet remains constant at any streamwise cross section.

5.3.2 Dependance on the Initial Conditions

The key to the growth rate of jets is a topic that has created much excitement, and a lot of argument, in the past. There is some documentation on the effect of initial conditions on round jets.

There has been an extensive debate on the question whether the self-similarity is universal, implying that the spreading rate, α_{jet}, has the same value in every jet experiment. However, some recent numerical studies show a strong dependence of the velocity profile on initial conditions [90] which agrees with the analysis of [96].

Although classical analysis suggests that the self-similar state depends only on the exit momentum flux, different experimenters have noted a range of values for the self-similarity parameters and [96] has argued that, in fact, there are multiple self-similar states, uniquely determined by the initial conditions, principally the precise form of the exit velocity profile. This view is supported by comparisons with relatively recent experiments.

It has been found that there exists significant differences between jet flows having different initial conditions (e.g. top-hat, fully-developed turbulent, etc.).

[96] discovered a shortcoming in the original similarity theory which implicitly assumed that the self-preserving state was independent of the details of the initial conditions. The analysis showed that there exists a multiplicity of self-preserving states for a particular type of flow and that each state is uniquely determined by the initial conditions.

5.4 Equations of motion and their self-similar solution

The velocity field of an incompressible turbulent jet is governed by the general Navier-Stokes equations already given in the chapter 3 (see 3.2.4). In vectorial convention they become :

$$\nabla \cdot \mathbf{u} = 0 \tag{5.2}$$

$$\frac{\partial \mathbf{u}}{\partial t} + (\mathbf{u} \cdot \nabla)\,\mathbf{u} = -\frac{1}{\rho} p + \nu \Delta \mathbf{u} \tag{5.3}$$

where $\mathbf{u}$ is the velocity vector, p the pressure, and ρ and ν are the density and kinematic viscosity of the fluid, respectively.

The passive scalar c in this flow is governed by the following transport equation (see 1.2.4) :

$$\frac{\partial c}{\partial t} + \nabla \cdot (\mathbf{u} c) = D \nabla^2 c \tag{5.4}$$

where D is the molecular diffusion coefficient.

5.4.1 Governing Equation for Axisymmetric (round) jets

Assumptions

Here a steady-state behavior of a turbulent round jet is considered. The stationary and axisymmetric turbulent jet can be conveniently described with the help of a cylindrical coordinate system. The coordinate system and associated notation used are (r, θ, x), in which $\overline{u}$ is the mean velocity component directed along the jet axis x, $\overline{v}$ the mean velocity in the radial direction r and $\overline{p}$ the mean pressure (the overbar denotes time-averaged quantities). The contribution of the viscous terms is neglected based on the assumption that the Reynolds number is sufficiently high.

The flow is symmetrical about longitudinal axis of the jet, passing through the center of the orifice, also referred as the centerline. Due to the axisymmtric nature of the flow, $\overline{w}, w = 0$ but not necessarily the root-mean-square of its fluctuations ($\overline{w'^2}$).

Cylindrical steady momentum equations

Applying the Reynolds decomposition and neglecting the molecular terms (viscous or molecular shear stress usually can be neglected in comparison with turbulent eddy stresses throughout the entire flow field, at large Reynolds number, $R_{e_{jet}} >> 1$, $D\nabla^2 c = 0$), 2D time-averaged Navier-Stokes equations (Reynolds equations) for a stationary axisymmetric geometry in cylindrical coordinates become (using the incompressibility condition) [87] :

$$\frac{\partial \bar{u}\,\overline{u}}{\partial x} + \frac{1}{r}\frac{\partial r\overline{u}\,\overline{v}}{\partial r} = -\frac{1}{\rho}\frac{\partial \overline{p}}{\partial x} - \frac{\partial \overline{u'u'}}{\partial x} - \frac{1}{r}\frac{\partial r\overline{u'v'}}{\partial r}, \text{ (x-moment)} \tag{5.5}$$

$$\frac{\partial \bar{u}\,\overline{v}}{\partial x} + \frac{1}{r}\frac{\partial \overline{v}\,\overline{v}}{\partial r} = -\frac{1}{\rho}\frac{\partial \overline{p}}{\partial r} - \frac{1}{r}\frac{\partial r\overline{v'v'}}{\partial r} - \frac{\partial \overline{u'v'}}{\partial x} \text{ (r-moment)} \tag{5.6}$$

$$\frac{\partial \overline{u}}{\partial x} + \frac{1}{r}\frac{\partial r\overline{v}}{\partial r} = 0 \text{ (mass/continuity)} \tag{5.7}$$

Equation (5.7) describes the conservation of mass (continuity equation in cylindrical coordinates). The LHS in the equation (5.5) could be rewriten :

$$\frac{\partial \bar{u}\,\overline{u}}{\partial x} + \frac{1}{r}\frac{\partial r\overline{u}\,\overline{v}}{\partial r} = 2\overline{u}\frac{\partial \overline{u}}{\partial x} + \overline{u}\frac{1}{r}\frac{\partial r\ \overline{v}}{\partial r} + \frac{\overline{v}}{r}\frac{r\partial \overline{u}}{\partial r} \tag{5.8}$$

$$= \overline{u}\frac{\partial \overline{u}}{\partial x} + \overline{v}\frac{\partial \overline{u}}{\partial r} + \overline{u}\underbrace{\left[\frac{\partial \overline{u}}{\partial x} + \frac{1}{r}\frac{\partial r\overline{v}}{\partial r}\right]}_{0} \tag{5.9}$$

The equation (5.5) is equivalent to :

$$\bar{u}\frac{\partial\ \overline{u}}{\partial x} + \overline{v}\frac{\partial \overline{u}}{\partial r} = -\frac{1}{\rho}\frac{\partial \overline{p}}{\partial x} - \frac{\partial \overline{u'u'}}{\partial x} - \frac{1}{r}\frac{\partial r\overline{u'v'}}{\partial r} \tag{5.10}$$

5.4.2 Boundary-layer assumption

The equations for $\overline{u}$ and $\overline{v}$ can be obtained from (5.2) and (5.3) after some manipulation and after application of the so-called boundary-layer approximation [78].

In the self-similar region of the flows under consideration, the traditional approach is to first perform an order of magnitude analysis of the Navier-Stokes equations as [97] to obtain the simplified streamwise momentum equation. This boundary layer approximation allows a substantial reduction in the number of terms. The resulting terms are then scaled using the appropriate length and velocity scales. Further, by invoking conservation of momentum for jets, one can obtain the streamwise variation of width and centerline velocity.

The free turbulent motion of a jet has an important property in common with boundary-layer motion, the width of the jet, δ, is small relative to x (downstream extent/longitudinal distance >> transverse extent/width of mixing zone), and the velocity gradient in the radial direction is large relative to the x direction. Therefore, a Prandtl's boundary layer type of approximation applies.

The jet flow develops as a function of the downstream direction, x, with characteristic length scale $\mathcal{L}_x$. This development is very slow in comparison to the development in the radial direction, r, with characteristic length scale l_r. Thus,

$$\frac{\partial}{\partial x} \approx \frac{1}{\mathcal{L}_x} << \quad \frac{\partial}{\partial r} \approx \frac{1}{l_r} \tag{5.11}$$

$$\tag{5.12}$$

Furthermore, the mean axial velocity $\overline{u}$, is scaled by a characteristic velocity scale $u_{\mathcal{L}_x}$ and the mean radial velocity $\overline{v}$ is scaled according to (5.7) by $u_{\mathcal{L}_x}\frac{l_r}{L_x}$. The turbulent terms u_i' are scaled by the macro scale $\mathcal{U}_{turb}$: $\overline{u_i'u_j'} \sim \mathcal{U}_{turb}^2$.

$$\frac{\partial \overline{u}}{\partial x} = \mathcal{O}\left(\frac{u_{\mathcal{L}_x}}{\mathcal{L}_x}\right) \tag{5.13}$$

It is hypothesized that the ratio between these two scales is determined by ([91]) :

$$\frac{\mathcal{U}_{turb}^2}{u_{\mathcal{L}_x}^2} = \quad \mathcal{O}\left(\frac{l_r}{L_x}\right) \tag{5.14}$$

From the Navier-Stokes equations, an approximation of the momentum equation for conservation in the x-direction (5.5) can be derived by applying this scaling and thereafter neglecting the terms with a relatively small order of magnitude. The following equation is then obtained :

$$\overline{u}\frac{\partial \overline{u}}{\partial x} + \overline{v}\frac{\partial \overline{u}}{\partial r} = \quad -\frac{1}{r}\frac{\partial r\overline{u'v'}}{\partial r} \text{ cylindrical boundary-layer equations} \tag{5.15}$$

This equation and the continuity equation (5.7), are the so-called boundary-layer equations. Note that it is assumed that the pressure outside the turbulent area is constant. The term $\overline{u'v'}$ is the *Reynolds shear stress*, which can be interpreted as the transport in the r-direction of momentum in the x-direction and denotes the covariance of the velocity fluctuations. As it concerns an extra unknown variable, an extra relation is needed to solve this equation analytically (closure-problem see 1.3.2).

For this type of flow the largest values of u', v' and the Reynolds stress $\overline{-u'v'}$ are found in the region where the mean gradient $\frac{\partial \overline{u}}{\partial r}$ is largest emphasizing the intimate connection between

turbulence production and sheared mean flow. Also, the mean velocity gradient is zero at the centerline of the jet and hence no turbulence is produced here. However, the values of u' and v' do not decrease significantly because strong eddy mixing transports fluid from nearby regions of high turbulence production towards and across the centerline. By symmetry the value of $\overline{-u'v'}$ has to be zero at the centerline of the jet since the shear stress must change sign.

In the next sections a possible solution of this equation of motion is formulated. First, a mathematical description of the flow field is introduced assuming self-similarity.

5.5 Self-similarity

One essential assumption in the theory describing a turbulent jet is that during the development of the flow in the downstream direction, the turbulence maintains its structure. In other words : the jet is self-similar. By definition : if all velocities are reduced by one velocity scale and all dimensions by one length scale, the flow patterns expressed in the reduced quantities become identical [78]. As a consequence, the following mathematical description of the flow field can be applied :

$$\overline{u}(r,x) = u_{\mathcal{L}_x}(x) f\left(\frac{r}{l_r(x)}\right) \tag{5.16}$$

$$\overline{-u'v'} = \mathcal{U}^2_{turb}(x) g\left(\frac{r}{l_r(x)}\right) \tag{5.17}$$

$$\eta = \frac{r}{l_r(x)} \tag{5.18}$$

The $u_{\mathcal{L}_x}$ is usually taken to be equal to the value of the mean velocity on the jet axis. The length scale l_r is frequently defined as the radial distance where the mean velocity is equal to half the centerline velocity.

A streamfunction is introduced (which fulfils the continuity equation[1]) to integrate the continuity equation (5.7) :

$$\overline{u} = \frac{1}{r}\frac{\partial \psi}{\partial r} \tag{5.19}$$

$$\overline{v} = -\frac{1}{r}\frac{\partial \psi}{\partial x} \tag{5.20}$$

The condition of self-similarity applied to the stream function ψ leads to the following description of the flow field :

$$\psi(r,x) = u_{\mathcal{L}_x}(x) l_r^2(x) F(\eta) \tag{5.21}$$

$$\tag{5.22}$$

with $f(\eta) = F'(\eta)/\eta$.

[1] $\frac{\partial \overline{u}}{\partial x} + \frac{1}{r}\frac{\partial r\overline{v}}{\partial r} = \frac{\partial}{\partial x}\left(\frac{1}{r}\frac{\partial \psi}{\partial r}\right) + \frac{1}{r}\frac{\partial}{\partial r}\left(-r\frac{1}{r}\frac{\partial \psi}{\partial x}\right) = \frac{1}{r}\frac{\partial^2 \psi}{\partial x \partial r} - \frac{1}{r}\frac{\partial^2 \psi}{\partial r \partial x} = 0$

Substitution of ψ in (5.17), leads to the following relation for the velocities :

$$\overline{u} = u_{\mathcal{L}_x} \frac{F'(\eta)}{\eta} = u_{\mathcal{L}_x} f(\eta) \tag{5.23}$$

$$\overline{v} = u_{\mathcal{L}_x} \frac{\partial l_r}{\partial x} \left(F'(\eta) - \frac{F(\eta)}{\eta} \right) \tag{5.24}$$

Normalising $f(\eta)$ with $f(0) = 1$, makes $u_{\mathcal{L}_x}$ the velocity at the centreline of the jet.

The conservation of axial momentum flux which can be derived by integrating (5.10) across a plane perpendicular to the jet axis leads to the relation $u_{\mathcal{L}_x}(x) l_r(x) =$ constant.

$$I = 2\pi \int_0^\infty \overline{u}^2 r \mathrm{d}r, \tag{5.25}$$

$$= 2\pi u_{\mathcal{L}_x}^2 l_r^2 \int_0^\infty \eta f^2(\eta) \mathrm{d}\eta = I_0 \tag{5.26}$$

in which I_0 is the initial momentum flux. In order to have a constant momentum flux, it is obvious that the product $u_{\mathcal{L}_x} l_r$ must be constant. Substituting the expressions for the velocities (5.24) in the equation of motion (5.15) and applying $(1/u_{\mathcal{L}_x})\mathrm{d}u_{\mathcal{L}_x}/\mathrm{d}_x = -(1/l_r)\mathrm{d}l_r/\mathrm{d}x$, which follows from $u_{\mathcal{L}_x} l_r =$ constant, the equation of motion reads :

$$-\frac{u_{\mathcal{L}_x}^2}{\mathcal{U}_{turb}^2} \frac{\mathrm{d}l_r}{\mathrm{d}x} \left\{ \left(\frac{F'}{\eta} \right)^2 + \frac{F}{\eta} \frac{\mathrm{d}}{\mathrm{d}\eta} \left(\frac{F'}{\eta} \right) \right\} = \frac{1}{\eta} \frac{\mathrm{d}}{\mathrm{d}\eta} (\eta g) \tag{5.27}$$

Consequently, a self-similar solution of the equation of motion is only possible if :

$$\frac{u_{\mathcal{L}_x}^2}{\mathcal{U}_{turb}^2} \frac{\mathrm{d}l_r(x)}{\mathrm{d}x} = c_{ste} = \text{ constant} \tag{5.28}$$

The ratio $\frac{u_{\mathcal{L}_x}}{\mathcal{U}_{turb}}$ is assumed to be constant in the self-similar region, as only a single velocity scale is needed to describe the flow field. In view of the fact that the only constraint to be satisfied by the solution is conservation of momentum flux, (5.27) implies that the constant c_{ste} must be universal, i.e. independent of the flow details near the orifice. To proceed some further assumptions must be made. The most straightforward one is to take $u_{\mathcal{L}_x} = \mathcal{U}_{turb}$ in (5.28) (see e.g. [97]). It then follows immediately that

$$\frac{\mathrm{d}l_r}{\mathrm{d}x} = \frac{\mathcal{U}_{turb}^2}{u_{\mathcal{L}_x}^2} = \text{ constant} \tag{5.29}$$

which implies that the length scale is a universal function of x. In other words all jets have in their similarity region the same spreading rate irrespective of the initial conditions. The existence of a universal spreading rate has been questioned by [96] who argues that there is no argument to assume that (5.29) is correct. He then proceeds by assuming $u_{L_x} \neq \mathcal{U}_{turb}$ so that the spreading rate of a jet is not universal. This viewpoint seems to be supported by recent numerical simulations reported by [90] to which we refer for further discussion on the similarity of the mean velocity and also of turbulence statistics.

Combined with $u_{\mathcal{L}_x} l_r = c_{ste}$, the following scaling relations for the width and centreline velocity of the jet may be applied :

$$l_r = \frac{\mathcal{U}_{turb}^2}{u_{\mathcal{L}_x}^2} (x - x_0) = \alpha (x - x_0) \tag{5.30}$$

$$u_{\mathcal{L}_x} = \frac{c_{ste}}{\alpha (x - x_0)} \tag{5.31}$$

in which α is the spreading rate of the jet ($\mathrm{d}l_r/\mathrm{d}x$) and x_0 is the x-coordinate from which the self-similar part of the jet virtually originates. Here, we will further concentrate on the similarity of the concentration profile.

Equation of transport

To get insight in the turbulent transport processes within the jet, we use the Reynolds-averaged transport equation describing the mixing of a passive dispersed phase which reads

$$\frac{\partial \overline{u}\overline{c}}{\partial x} + \frac{1}{r}\frac{\partial r\overline{v}\,\overline{c}}{\partial r} = \frac{\partial \overline{u'c'}}{\partial x} - \frac{1}{r}\frac{\partial r\overline{v'c'}}{\partial r} \text{ or} \tag{5.32}$$

$$\overline{u}\frac{\partial \overline{c}}{\partial x} + \overline{v}\frac{\partial \overline{v}}{\partial r} = -\frac{\partial}{\partial r}\left(r\overline{v'c'}\right) \tag{5.33}$$

where again $\overline{v'c'}$ is the turbulent flux of the scalar and where the molecular diffusion term has been neglected based on the assumption of a sufficiently large Reynolds number.

Under the same assumptions as used for the derivation of moment equation, we can also obtain an equation for the mean concentration profile. Let us again look for a similarity solution given by

$$\overline{c}(r,z) = c_{\mathcal{L}_x}(x)h(\eta) \tag{5.34}$$

$$\overline{v'c'} = \mathcal{U}_{turb}(x)\mathcal{C}_{turb}(x)k(\eta) \tag{5.35}$$

$$\eta = \frac{r}{l_{r_c}(x)} \tag{5.36}$$

where $c_{\mathcal{L}_x}$ is a scale for the mean concentration and $\mathcal{C}_{turb}$ a scale for the concentration fluctuations. Similar to the velocity scale $u_{\mathcal{L}_x}$, $c_{\mathcal{L}_x}$ is taken equal to the mean concentration value at the jet axis. The $\mathcal{C}_{turb}(x)$ is a length scale for the concentration profile which in principle does not have to be equal to the length scale for the velocity profile. We first consider the consequences of conservation of concentration flux which can be derived from (5.33) by integration across a plane perpendicular to the jet axis and which reads

$$\int_0^\infty \overline{cu} r \mathrm{d}r = \frac{Q_0}{2\pi} \tag{5.37}$$

where Q_0 is the source strength of concentration introduced at the orifice. Substitution of the similarity solution (5.16) and (5.34) into (5.37) leads to the conclusion that similarity can only be satisfied when $l_{r_c}(x) \approx l_r(x)$ and without loss of generality we take $l_{r_c}(x) \equiv l_r(x)$. One should realize however, that this choice means that at $l_r(x)$ the mean concentration is not necessarily equal to half the enterline concentration. With this result for $l_{r_c}(x)$ and with $u_{\mathcal{L}_x} l_r$ =constant we find from (5.37) that $c_{\mathcal{L}_x} l_r$ is also a constant. Substituting the similarity expressions for mean concentration and the mean velocity profile into equation (5.33), we find after using the relationships between $u_{\mathcal{L}_x}$, $c_{\mathcal{L}_x}$ and l_r derived above, the following equation :

$$\frac{u_{\mathcal{L}_x}\mathcal{C}_{turb}}{c_{\mathcal{L}_x}\mathcal{U}_{turb}}\frac{\mathrm{d}}{\mathrm{d}\eta}(\eta k) \tag{5.38}$$

We see that similarity is only possible when

$$\frac{u_{\mathcal{L}_x}\mathcal{C}_{turb}}{c_{\mathcal{L}_x}\mathcal{U}_{turb}} = c_2 \tag{5.39}$$

with c_2 as another universal constant. Integrating (5.38) we get

$$\frac{Fh}{\eta k} = \frac{1}{c_2} \tag{5.40}$$

where we have used the boundary condition that $F(0) = 0$. If we assume that $u_{\mathcal{L}_x} = \mathcal{U}_{turb}$ we find that $\mathcal{C}_{turb}/c_{\mathcal{L}_x} = c_2$ and hence the normalized scalar concentration in the far field is completely independent of the conditions at the jet nozzle. Previously, we stated that it is very unlikely that $u_{\mathcal{L}_x} = \mathcal{U}_{turb}$, thus $\mathcal{C}_{turb} \neq c_2 c_{\mathcal{L}_x}$ which implies that the scalar concentration in the far field, like the velocity field, depends on the conditions at the jet nozzle ([96], [90]).

Mean centreline decay

In brief, beyond the potential core region and the transition zone, the flow is considered to be fully developed [85]. These flows have the same characteristics and profile shapes when employing the appropriate scaling. Hence, at sufficient distances from the nozzle, the mean concentration profiles, turbulence intensities, and shear stresses at various axial stations in the ZEF collapse onto a single profile. Dimensional arguments together with experimental observations suggest forms for the mean flow variables, which are known as similarity solutions [91, 81, 98, 51].

Assuming that the momentum flux in the axial direction is conserved, the mean jet centerline concentration in the fully developed region decays with x [85] is typically modelled by a simple decay equation such as given by

$$\frac{c_0}{c_{centerline}(x)} = \frac{1}{K_{dec_{jet}}} \left(\frac{x - x_0}{d_{jet}} \right) \tag{5.41}$$

In this equation, c_0 is the jet exit concentration, $c_{centerline}(x)$ is the local mean centreline concentration, $K_{dec_{jet}}$ is the concentration decay coefficient, d_{jet} is the nozzle diameter, x is the coordinate in the axial direction, and x_0 is the distance from the nozzle opening to the virtual origin of the jet. The parameter x_0 has a positive value if the virtual origin is in front of the nozzle. Table 5.1 lists some frequently cited measurement results for comparison purposes. For example, these previous research results indicate that the measured $K_{dec_{jet}}$ values are generally around 6.

5.6 Application

The methodology described above describing a single jet issued from one nozzle is applied to derive the direct drift from the air assisted sprayer used in the experience. One looks, in a cylindrical frame (x, r, θ), for local injection solutions of the form :

$$\frac{c_{jet}(x, r, \theta)}{c_{centerline}(x, r)} = f_{rad}\left(\frac{r}{x}\right) \tag{5.42}$$

where the search space is built using the assumption that f_{rad} has a given shape.

This dispersion model is based on statistical theoretical basis that makes them successful in many outdoor applications and furnishes a simple analytical solution that needs much less computational power than CFD. This approach based on the self-similarity concept does not include discretization of the transport equation but requires a large number of simplification steps. Example of the solution obtained is shown in figure 5.7.

Investigator	Substance	$R_{e_{d_{jet}}}$ $\times 10^{-4}$	Decay rate ($K_{dec_{jet}}$)	$\frac{x_0}{d_{jet}}$	Spread rate (K_s)	Initial condition
[99][a]	water	2.19	5.84	-0.98	0.106	Top hat
[78]	—	—	5.90	-0.50	0.080	—
Wygnanski & Fiedler (1969)	air	10	5.70	3	0.086	—
Rodi (1982)	—	8.7	5.90	—	0.086	—
Panchapakesan & Lumley (1993)	air	1.1	6.06	-2.50	0.096	Top hat
[87] LDA	air	9.55	5.80	4	0.094	Top hat
[87] SHW	air	9.55	5.90	2.70	0.102	Top hat

TAB. 5.1 – Comparison of decay results for a free round jet [99].

[a]Note that this study investigates a vertical axisymmetric jet.

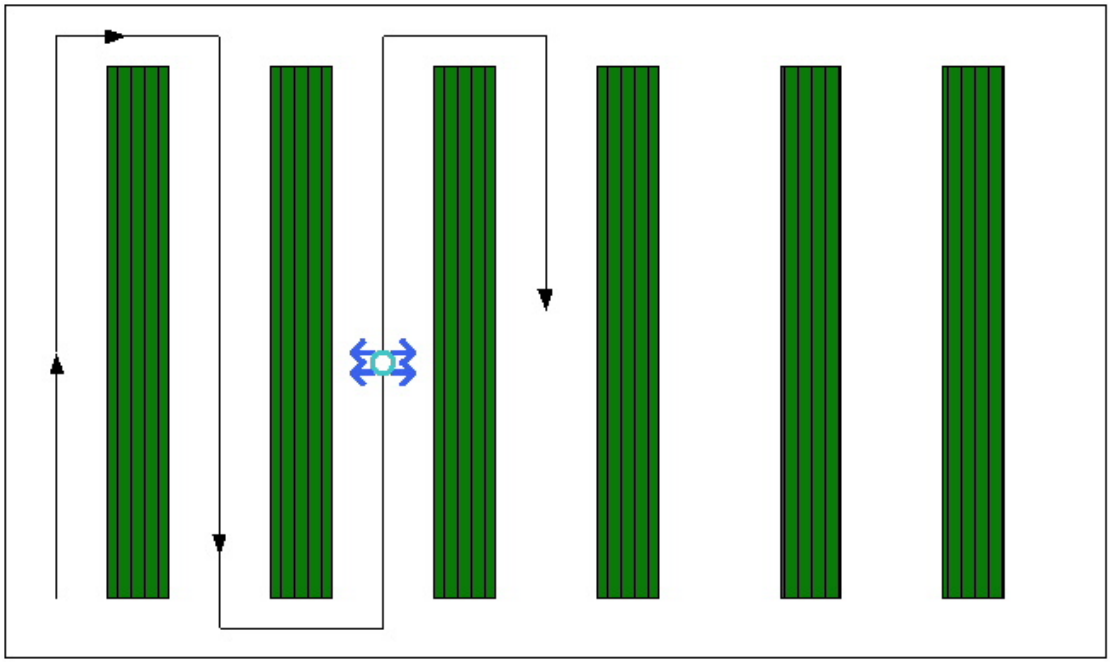

FIG. 5.5 – Sketch of the vehicule trajectory between rows.

5.6.1 Application to a vineyard spray

The equation (5.42)above describing a single jet issued from one nozzle is applied to compute the direct drift from the air assisted sprayer used in the experience. Another feature must be added to represent the jet behaviour within the vine row. The structure of the artificial row used in the experimental part is well identified and assimilited to an homogeneous porous medium [100]. As usually for natural canopy [56, 57], this medium is caracterised by two parameters, the leaf area density (A_{LAD}) and the canopy drag coefficient (C_D).

Mid to late-season vineyard canopies have significant opaqueness. A shade netting, with an apparent porosity of about 34% was used to represent this crop. The energy loss coefficient C_p and the global efficiency factor Eff of this net had been evaluated as a single-layer in the past by using a small wind-tunnel. These physiscal values were determined by [100] (cf table 5.6.1).

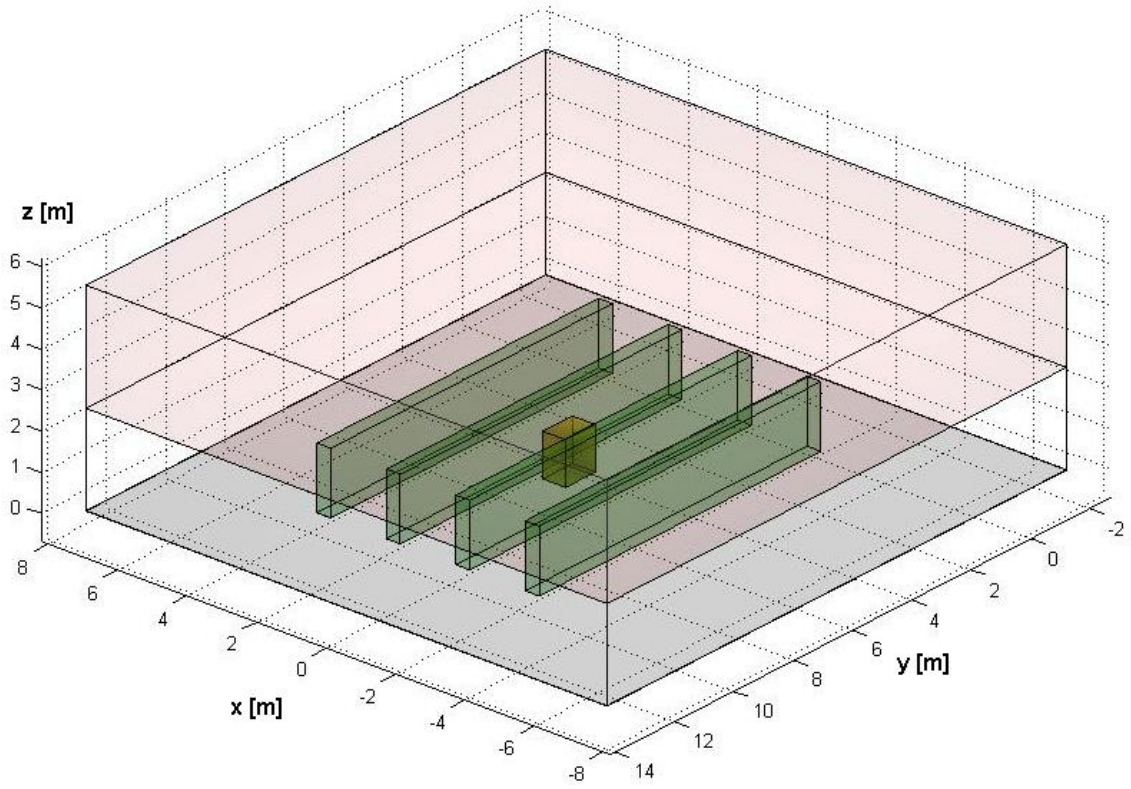

FIG. 5.6 – Representation of the computational domain. The domain is separated in two part (under and above z_0. The four vinerow are in green and the sprayer is at the center of the domain in yellow. This figure shows how the real experiment is reproduced by the code, see 5.6.3 and 5.11

Net parameter	Measurement method	Values processed	Observed values
Apparent porosity	Image processing	% of holes per surface unit	$\varepsilon \approx 34\%$
Energy loss coefficient for a net angle α towards the wind direction	Small wind tunnel	$C_p = \dfrac{\Delta p}{\frac{1}{2}\rho U^2}$	$C_p(\alpha = 90°) = 3.07$
			$C_p(\alpha = 60°) = 2.34$

TAB. 5.2 – Artificial canopy net characteristics as a single-layer [100].

When considering the interaction between turbulent axisymetric jets and porous walls, very few information is available. This fundamental problem in fluid mechanics is still not fully understood [101]. [51] presented a mathematical description for an air-jet penetrating a uniform crop canopy. This analysis showed that the velocity decay is exponential with respect to penetration distance, and depends mainly on the couple of constant (A_{LAD}, C_D) associated to the canopy. This approach was used in our model and we defined a function c_{canopy} that describes the evolution of the concentration on the axis sprayer inside the canopy layer [102].

The concentration along the centerline axis for a single turbulent jet issued from one nozzle of an airblast sprayer oriented towards a canopy row, $c_{centerline}$, is now defined by the following

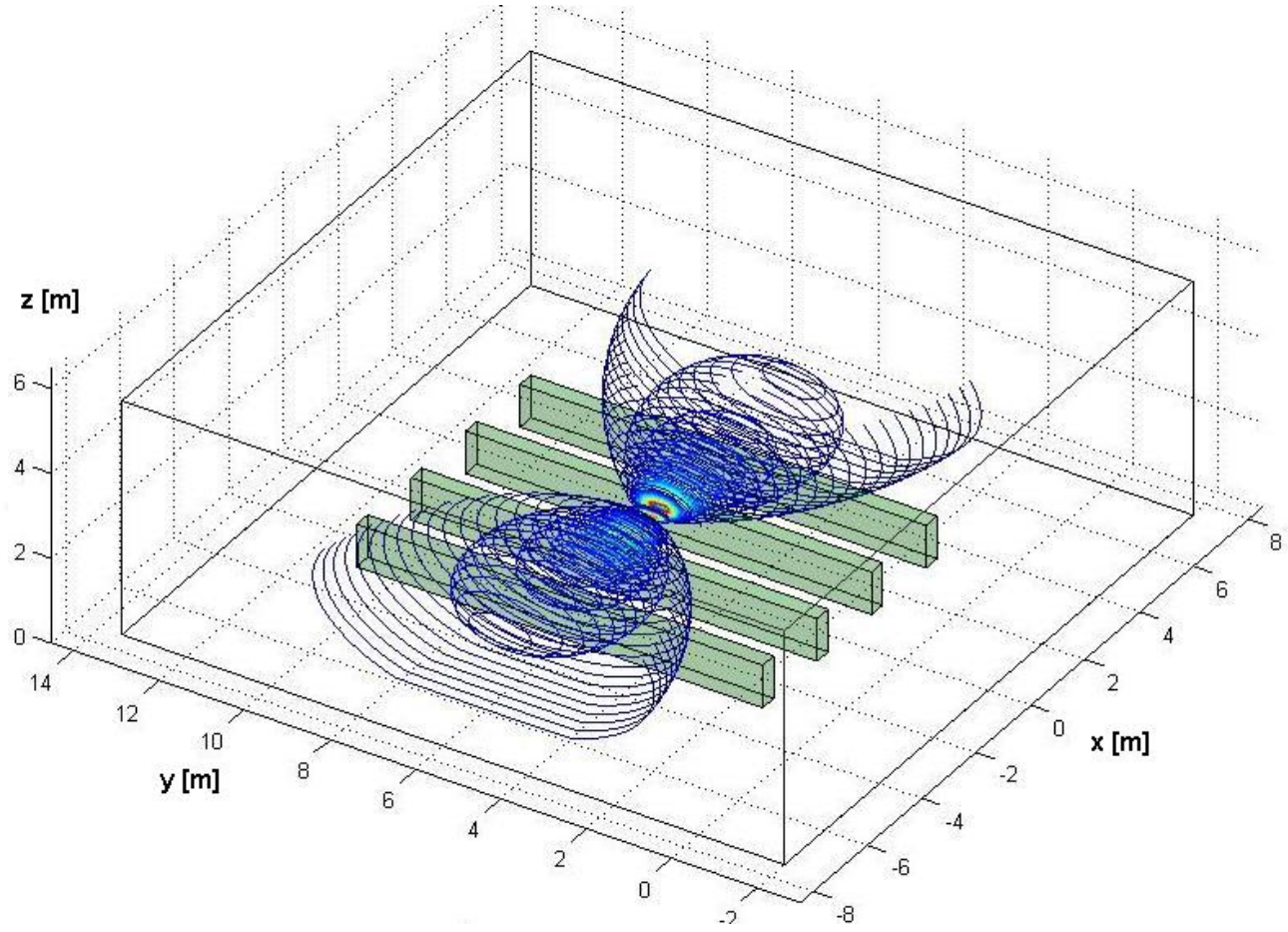

FIG. 5.7 – Similitude solution : simulation exemple of 3D-concentration field of a round turbulent free jet using the similarity assumption. The contour in the figure show the shape of the concentration field issued from an horizontal nozzle during one time step Δt.

piecewise function which is continuous :

$$c_{centerline}(x) = \begin{cases} c_{canopy}(x) = & c_{row} \exp\left(-d(x) A_{LAD}\ C_D\right) \text{ , inside the canopy} \\ c_{free}(x) = & c_0 \frac{K_{c_{jet}}}{x - x_0} \text{ , otherwise} \end{cases} \tag{5.43}$$

where x_0 indicates the virtual origin of the jet, c_0 the initial concentration (at the oulet nozzle), $K_{c_{jet}}$ is the centerline concentration decay coefficient, $d(x)$ the penetration distance inside the vegetation along the jet axis, and c_{row} the concentration on the nozzle axis at the canopy entrance x_e ($d(x_e) = 0$ and $c_{free}(x_e) = c_0 \frac{K_{c_{jet}}}{x_e - x_0} = c_{row} = c_{canopy}(x_e)$).

In the considered experiment, the crop structure is well identified because of its artificial nature. So the couple (A_{LAD}, C_D) and the function shape is assumed to be the same for all the jets issued from the different nozzles of the sprayer. But the shape of the function c_{canopy} could be easily modify, or even changed, to consider more complicated features, such as the ones encountered in natural environment. Canopy geometry and structure, inhomogeneous density, leaves size, shape and orientation, etc. could all consequently be taking account by modifying the parameter values $(K_{c_{jet}}, x_0)$or the function shape of c_{canopy}, which could be non in en exponential form.

The figure 5.8 shows the behaviour of the function $c_{centerline}$, with vine rows or without.

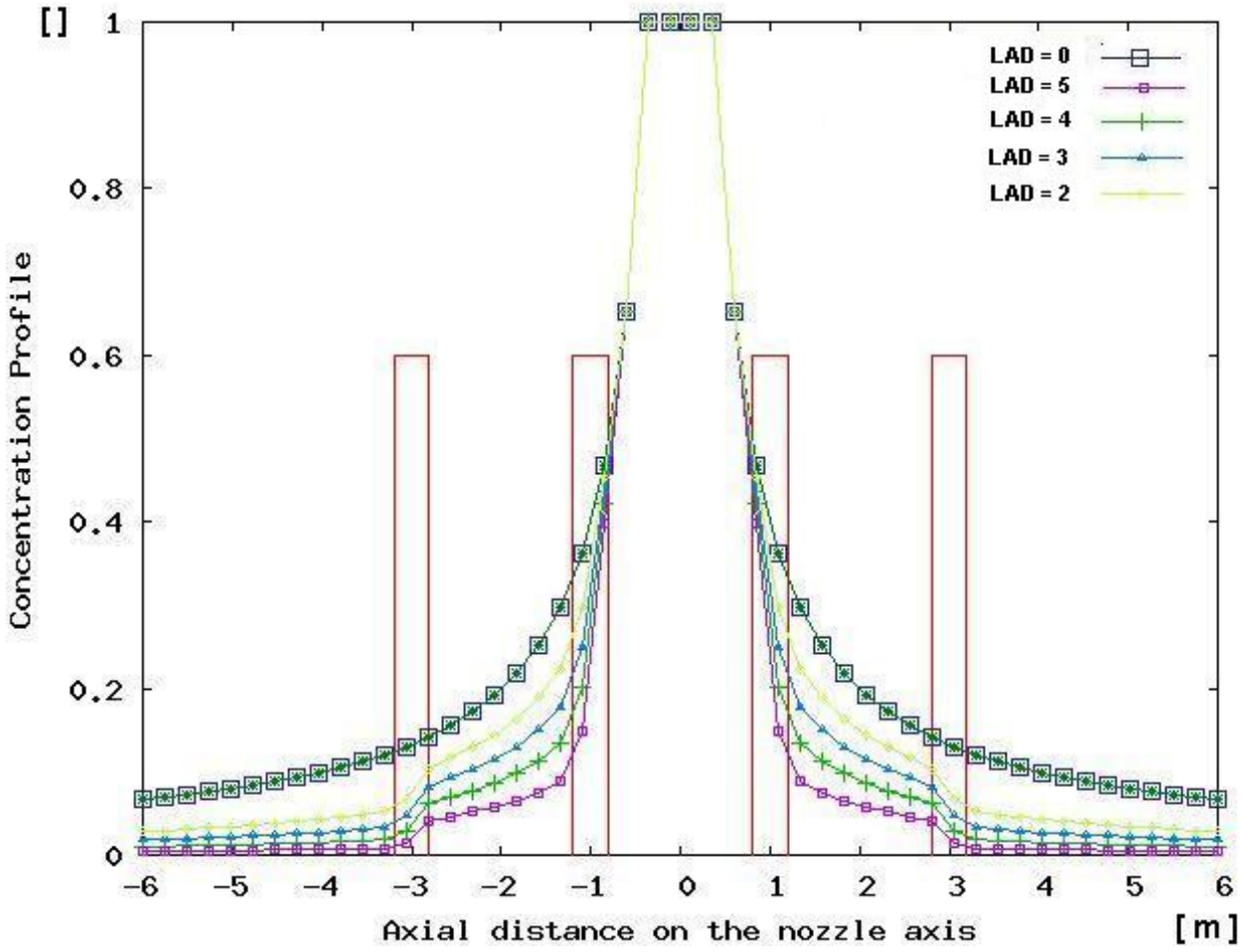

FIG. 5.8 – Normalized centerline concentration for different density vegetation along the nozzle axis. The concentration is ploted relatively to the nozzle distance and profiles are normalized by the maximum concentrationalong the nozzle axis. This figure shows also a comparison of the profiles with ($a_{LAD} > 0$) and without ($a_{LAD} = 0$) the presence of vegetation canopy. In the presence of canopy the different a_{LAD} used are approximatively 5,4,3 and 2 (m^{-1}). The location of the rows is indicated by a schematic rectangular representation in order to facilitate the interpretation of the figure. The axis nozzle is parralel to the ground ($x \sim x_{cart}$). This comparison of the centerline concentration profiles for different A_{LAD} show the model sensitivity to the canopy density.

In the absence of vine rows ($d(x) = 0, A_{LAD} = 0$ everywhere), the function c_{free} given by the classical jet theory [89] as explained in the previous section, is valid everywhere and the decay rate along the nozzle axis is always in the order of $1/x$. When vine rows are present the decay rate of the mean centreline concentration becomes more important at downstream locations where the canopy is present, i.e. where $c_{centerline}$ has the exponential form of c_{canopy}.

Assuming an isotropic turbulence, the steady-state turbulent flow field and its concentration distribution are based on a similitude solution. As in almost all the studies that use this principle ([89, 81]), it is assumed that the mean concentration profile in the radial direction, f_{rad}, has a Gaussian shape. The 3D concentration scalar field issued from one nozzle is then described by

the following equation :

$$c_{jet}(x,r,\theta) = \quad c_{centerline}(x) f_{rad}\left(\frac{r}{x}\right) \quad \text{with} \tag{5.44}$$

$$f_{rad}\left(\frac{r}{x}\right) = \quad \exp\left(-\alpha_{Jet}\left(\tfrac{r}{x}\right)^2\right) \tag{5.45}$$

where α_{Jet} is the spread rate of the jet.

One essential assumption in this model describing a single spray jet is that, during the development of the flow in the downstream direction, the turbulence maintains its general structure, even inside the vegetation. Canopy presence modify the xaial behaviour of the flow but not the radial one. The radial dispersion stays Gaussian outside and inside the vegetation. This is a strong assumption that must should be verified experimentally. However if the gaussian shape is not convenient, the radial behaviour f_{rad} could be easily changed to better fit the reallity, without modify completly the model. A possibility is to define α_{Jet} as a function of $d(x)$.

5.6.2 Losses Calculation

We need to define another reference frame (x_{cart}, y, z) in order to encompass the different jets issued from the sprayer. Instantaneous spray losses toward the atmosphere are computed in a this new cartesian frame where (x_{cart}, y) is the horizontal plane parallel to the ground, z design the vertical direction, z_0 being the height of the canopy row.

One important hypothesis, as said before, is to assume two different time scales based on the injection velocity and the velocity at which the injection source moves. The injection velocity being much higher, one assumes the local concentration at the outlet of the injection device to be established instantaneously. So, the transient of the jet establishment is not considered. This instantaneous local flow field is devoted to vanish immediately and not to affect the overall atmospheric circulation. This injection velocity is only designed to determine the part of the pollutant leaving near-ground area and being candidate for transport over large distances.

So 2 separated time-scale are considered :

– the time t based on the injection source movement and

– τ with $\Delta\tau << \Delta t$,

We note $T_{spray} = \sum_{j=1}^{n_T} \Delta t^j$ the total time of the spaying treatment. Thanks to this assumption, during the interval Δt^j, the spray jet is assumed to be stationary, the vehicule is supposed static, and so the jet is uniform over $(\Delta x, \Delta t^j)$ where Δx is the space interval corresponding to Δt^j and the sprayer velocity.

Mass Repartition

During a computational time step Δt^j, the mass sprayed by the nozzle i, $M^i_{\Delta t^j}$, is defined as :

$$M^i_{\Delta t^j} = \quad \int_V c^i_{flux} \mathrm{d}V \qquad [kg] = \left[kg.m^{-3}\right]\left[m^3\right] \tag{5.46}$$

$$= \int_{\Delta t^j}\int_V c_{\Delta t^j} \mathrm{d}V \mathrm{d}t \quad \left[kg.m^{-3}.s^{-1}\right][s]\left[m^3\right] \tag{5.47}$$

$$= Q^i_0 \Delta t^j \qquad \left[kg.s^{-1}\right][s] \tag{5.48}$$

$$\tag{5.49}$$

where Q_0^i is the ejection rate of the nozzle i (is not dependant of the interval considered, supposed constant $Q_0^{i,j} = Q_0^i$ over T_{spray}), V is a volume enough large to encompass the spray and $c^i_{\Delta t^j}$ is defined as :

$$\begin{aligned} c^i_{\Delta t}(x_{cart}, y, z) &= \frac{c^i_{flux}(x_{cart}, y, z)}{\int_V c^i_{flux}(x_{cart}, y, z)\mathrm{d}V} \times Q_0^i && (5.50)\\ &= c^i_{flux}(x_{cart}, y, z) \times \frac{Q_0^i}{\int_V c^i_{flux}(x_{cart}, y, z)\mathrm{d}V} && (5.51)\\ & && (5.52)\\ &= c^i_{flux}(x_{cart}, y, z) \times coeff^i && (5.53)\\ \left[kg.m^{-3}.s^{-1}\right] &= \left[kg.m^{-3}\right]\left[kg.s^{-1}/kg\right] && (5.54) \end{aligned}$$

c^i_{flux} gives the shape of the concentration field end the term $coeff^i$ calibrates this distribution in order to respect the mass conservation. $c_{\Delta t^j}$ has the dimension $[kg.m^{-3}.s^{-1}]$, is constant during Δt^j. The shape of c^i_{flux} is given by c_{jet}. The calibration term is then defined as :

$$coeff^i = \frac{Q_0^i}{\int_V c_{flux}(x_{cart}, y, z)\mathrm{d}V} \quad \left[s^{-1}\right] \tag{5.55}$$

Now, we consider the total concentration issued from n the nozzle at the time $t + \Delta t^j$:

$$\begin{aligned} c_{loc}(x_{cart}, y, z, t + \Delta t^j) = \; & c_{loc}(x_{cart}, y, z, t) \; + \; \sum_i^n c^i_{\Delta t^j}(x_{cart}, y, z)\Delta t^j && (5.56)\\ \left[kg.m^{-3}\right] = \; & \left[kg.m^{-3}\right] \; + \; \left[kg.m^{-3}s^{-1}\right][s] && (5.57)\\ & && (5.58) \end{aligned}$$

$$\begin{aligned} \frac{c_{loc}(x_{cart}, y, z, t + \Delta t^j) - c_{loc}(x_{cart}, y, z, t)}{\Delta t^j} = \; & \textstyle\sum_i^n c^i_{flux}(x_{cart}, y, z) && (5.59)\\ & \times coeff^i && (5.60) \end{aligned}$$

If $\mathrm{d}S = \mathrm{d}x_{cart}\mathrm{d}y$ we could say that $M_{loss}(\Delta t^j)$ the mass losses during a time Δt^j by one nozzle is

$$\begin{aligned} M^i_{loss}(\Delta t^j) &= \textstyle\int_{\Delta t^j}\int_{z>z_0}\int_S \left(c^i_{\Delta t^j}\right)\mathrm{d}S\mathrm{d}z\mathrm{d}t \quad [kg] && (5.61)\\ &= \Delta t^j \left(\textstyle\int_{z>z_0}\int_S c_{\Delta t^j}\mathrm{d}S\mathrm{d}z\right) \quad [kg] && (5.62) \end{aligned}$$

By applying the same procedure for each nozzle, the sum of the total losses M^{tot}_{loss} during T_{spray} is then evaluated.

$$M^{tot}_{loss} = \int_{z_0}^{+\infty}\int_{-\infty}^{+\infty}\int_{-\infty}^{+\infty} c_{loc}\left(x_{cart}, y, z, T_{spray}\right)\mathrm{d}x_{cart}\mathrm{d}y\mathrm{d}z \tag{5.63}$$

This quantity determines a source term as the non-target amount of pesticide that leaves the local system, i.e. the crop canopy and rows at a height z_0. This is the source term of the level 3 model of DriftX that computes mesoscale atmospheric dispersion.

Flux

If we consider the classical approach used, the total mass losses during Δt^j could be calculated by integrated upward flux, i.e. the total mass balance over the plane $x-y$ at z_0 :

$$M_{loss}(\Delta t^j) = \int_{\Delta t^j} \int_S (wc_{loc}) \mathrm{d}S \ \mathrm{d}t \tag{5.64}$$

where w represent the vertical velocity towards the atmosphere perpendicular to the ground. Physically, this means that $M_{loss}(\Delta t^j)$ equals the total mass of scalar (the time-integrated mass flux) crossing the $x-y$ plane just above of z_0 during Δt^j.

During this interval the sprayer is assumed to be static at a given point of the domain. By the shape of the concenration field (exponential form), the release is localized in space so that the integral over Δt^j is finite. Moreover the flow is assumed to be stationnary :

$$\int_{\Delta t^j} \int_S (wc_{loc}) \ \mathrm{d}S \ \mathrm{d}t = \Delta t^j \int_S (wc_{loc}) \ \mathrm{d}S \qquad [kg] \tag{5.65}$$

From (5.62) we have also :

$$M_{loss}(\Delta t^j) = \Delta t^j \left(\int_{z>z_0} \int_S \sum_i^n c^i_{\Delta t^j} \mathrm{d}S\mathrm{d}z \right) \tag{5.66}$$

Then from (5.65) and (5.66) we can write :

$$\int_S (wc_{loc}) \ \mathrm{d}S \approx \int_{z>z_0} \int_S \left(\sum_i^n c^i_{\Delta t^j} \right) \mathrm{d}S\mathrm{d}z \tag{5.67}$$

5.6.3 Numerical Implementation

The code was written in FORTRAN77 and can be run on any personal computer in real-time computation (a few seconds) which permits a substantial computation time-saving. To represent the analytical similitude solution, the whole domain is discretized into a uniform mesh prescribed by the user. The numerical implementation considers that each nozzle produces an independent turbulent jet described by the equation (5.44). It is assumed that there is no interaction between the different jet.

All the geometric parameters used above (domain size, position, size and row characteristics) are set as input variables and an automated method is employed to replicate the computation domain according to the parameters provided by the user. The sprayer ride is simulated by nozzles movements at each time step, parallely to the row, in the $y-z$ plane (x-coordinate $= 0$).

5.7 Field tests

5.7.1 Test organisation

The experimental approach was based on the use of classical 2 mm diameter passive collectors and fluorescent tracer dye to assess near-field pesticide emissions to the air during spraying process [103]. The spray losses were assessed at 2.5 meter from soil. An artificial vineyard was built from shade nettings with an apparent porosity of 34%. Row spacing and crop height were

FIG. 5.9 – Aerial photography of the real experience.

2 meters each. The artificial plot was made of four $8m$ long rows oriented along the North-South direction.

An axial air-assisted sprayer Fisher Turbo 561 -Berthoud Ltd.- was used. The tractor forward speed was set at 5.1 $km\ h^{-1}$. The air output stream was explored with a 3D ultrasonic sensor. Its main features are shown in Fig.5.10. Mean air volumetric flow was of 3.3 $m^3\ s^{-1}$ and averaged air velocity 12.8 $m\ s^{-1}$. Two sets of nozzles were tested, at a 10 bar operating pressure : Albuz ATR white hollow cones and Conejet green hollow cones. Spray characteristics of these nozzles are shown in Table 5.3.

Nozzle	$D_{V.10}$	$D_{V.50}$	$D_{V.90}$	Vol. >100 μm	Flow rate	Spray Quality
Green	72	134	180	74%	1.00 $l\ min^{-1}$	Fine
White	28	65	135	24%	0.38 $l\ min^{-1}$	Very Fine

TAB. 5.3 – Droplet diameter (μm) for 10% ($D_{V.10}$) , 50% ($D_{V.50}$) and 90% ($D_{V.90}$) of cumulative volume, spray volume with droplet diameter greater than 100 μm (Vol. >100 μm). Spray Quality is derived from the BCPC classification system. All information was obtained from manufacturers reports and the measurements were performed with a laser diffraction instrument.

Three runs were carried out for both set of nozzles. Microclimatic state was characterized by wind speed and temperature measurements from a 3D anemometer system. Wet bulb temperature depression and stability parameter were also calculated. The stability parameter is

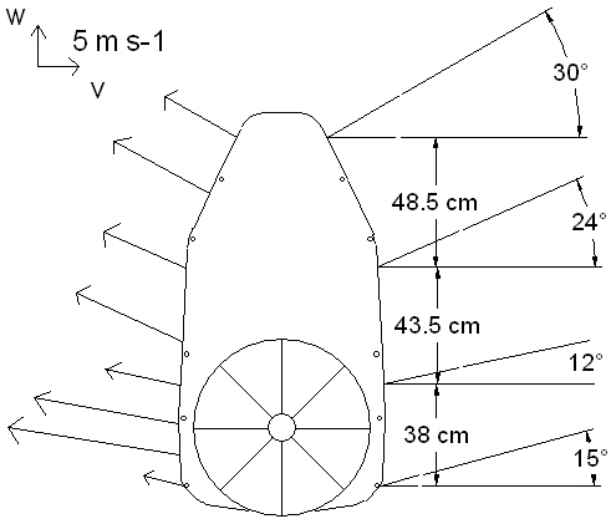

FIG. 5.10 – Schematic view of sprayer : air output velocity vectors (left) and orientation (right)

Spray Quality	Wind Speed	Temperature	Δ T	z/L
Fine	0.30 $m\ s^{-1}$	17.38 °C	2.41 °C	-1.23
Very Fine	0.72 $m\ s^{-1}$	17.38 °C	4.47 °C	0.23

TAB. 5.4 – Microclimatic conditions during each test series

given by the relation h/L_M, where h is the height of the 3D anemometer (four meter) and L_M is the Monin-Obukhov length.

The experiments were run between 5 :00 am and 7 :00 am on July 13^{th} 2005, in an experimental plot of Cemagref at Montpellier, France. The averaged microclimatic conditions are show in Table 5.4. These conditions correspond to influential variables for upward spray emission [103].

Although during very fine spraying, the microclimatic conditions could be more favorable to upward spray movement, all values registered are into the recommendable range to minimize the spray drift and evaporation risks [104], therefore, only operational sprayer conditions and crop configuration could affect spray emissions.

5.7.2 Spray flow estimation

An horizontal measurement plane was setup at 2.5 m from the ground (Fig. 5.11) to intercept upward spray losses. This plane was made of five 12-meter long PVC lines, parallel to the rows. The separation between the lines was of two meters. During each run, the sprayer was driven four times on the central inter-row to increase the amount of deposited spray and decrease random effects.

The spray liquid was an aqueous solution of 1 $g\ l^{-1}$ of Brilliant Sulpho-Flavine (BSF) as fluorecent tracer dye and 0.1% of non-ionic surfactant.

Captured liquid volumes of spray were estimated from the amount of liquid captured by the PVC lines. Once the droplets on the lines had evaporated, each line was washed using 200 ml of tap water.

The spray volume removed from the lines (V_i, in ml) was determined from the relationship

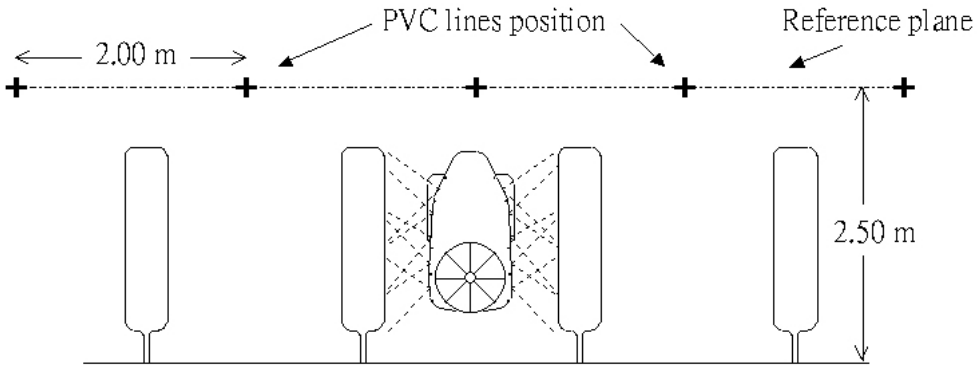

FIG. 5.11 – PVC line and reference plane position in artificial crop plot

between spray mixture and line wash solution concentrations, that were obtained by fluorometry reading. The specific flux (S_i, in $ml\ mm^{-1}$) was then calculated as in equation 5.68, where d is the collector diameter (2 mm).

$$S_i = \frac{V_i}{d} \tag{5.68}$$

Then airborne spray quantity in ml (Q) crossing the measurement plane during the spraying, can be calculated as :

$$Q = \sum_{i=1}^{n} \frac{1}{2} \left[S_i + S_{i+1}\right] \left[h_{i+1} - h_i\right] \tag{5.69}$$

The term $[h_{i+1} - h_i]$ is the distance between each line (2000 mm). The amounts of spray flux are then normalised by the amount of spray applied to the crop so that atmospheric loss is defined as a percentage of the total amount of spray used in each test.

5.8 Results and Discussion

5.8.1 Field Test

The losses, evaluated at 2.5 meter from the ground were of 6.14% for fine spray and 10.95% for very fine spraying (averaged values), the variation coefficients were 5.93% and 10.84% respectively. During the conditions observed, with small wind speed and atmospheric stability, normalised losses are 44% larger for very fine spray than for fine spray.

A relative symmetrical plume is observed with 85% of losses concentrated in a range of four meters (two meters in each direction from the central inter-row) ; this range is defined by two maximum peaks. A minimum peak, distinct to zero, was observed on the central line. During very fine spraying the cloud is more sensible to mechanical displacement due to wind speed than during fine spraying, even with very small wind velocity values.

Then, taking into account that the collector efficiency stands between 78 and 100% [105, 106, 107, 103], measured spray losses directly sent to the air could be between 6.1 and 7.9% for fine spray and between 11.0 and 14.0% for very fine spray during calm atmosphere and non evaporative conditions.

The variations observed between both spray qualities is assessed to correspond to the gravity effect on droplet dynamics : small droplets follow the air stream whereas coarse droplets are deposited within the canopy and on the ground. This effect is also shown by the losses distribution profiles (fig. 5.12).

5.8.2 Simulation Test

The simulation configuration try to fit as best as possible the real experimental field geometry and sprayer characteristics presented in the precedent section and in the article [103]. Numerical parameters correspond to the experimental values described in section 5.7. In particular, the nozzle characteristics (number, locations, orientations, diameters, ejection rates) are set to the experimental data and used as input parameters to compute the turbulent jet.

In this computation, the domain is a rectangular channel of $6m$ (longitudinal) $\times 12m$ (traverse) $\times 3m$ (vertical) size which encompassed the real domain field (see 5.11). Four rectangular pavements of size $6m \times 0.4m \times 1.m$ represent the vineyard row, supposed as an uniform medium. The current values for C_D are in agreement with those found in literature which are in the range $0.1 < to < 0.5$. The value of 0.5 corresponds to a single leaf perpendicular to the flow. The 0.3 value obtained is due to a shelter effect, caused by the surrounding leaves and is the one used in the simulation.

The figure 5.12 shows a first comparison between experimental values and model output. It could be seen in (5.12) that a perfect symmetry is observed in the plane $x - z$ with the model. This is natural since there is no meteorological parameter (wind,...) consideration. In this simulation test, the proportion of deposits that are captured by the vine canopy foliage is about 30%. The quantity lost as drift is around 12% of the total amount sprayed.

5.8.3 Discussion

Several strong modelling assumptions have been made in order to find simple analytical solutions. However, it must be kept in mind that the reality is by far more complex. These simplifications neglect the importance of influential parameters and phenomena such as wind, canopy oscillations, jets interactions, droplet spectrum (effect of gravity and drag), density, temperature and possible effects due to the evaporation on the droplets. Forward speed and wind velocity within the vine rows are considered to be constant and their values are supposed not to affect the ejection speed. Moreover, [108] also showed that some differences between spray jet and typical gas jet exists.

More complex algorithms, such as models based on Computational Fluid Dynamics are possible alternatives. They are instead more precise, however they require a lot of information that are not necessarily available, are computationally expensive to run and often affected by numerical errors. In addition, to make proper use of these model needs greatly increase the level of user understanding and numerical solutions cannot be easily “interpreted” as more simple model. Moreover, although the input data requirements and level of sophistication increase with the more advanced models, a more complex model does not necessarily lead to predictions that are more accurate : as the number of input variables goes up in the advanced models, the room for input data error increases. A lot of practical application such as risk or scenarii analysis, inverse problems (data assimilation, sensitivity analysis,...), involves several thousand of model evaluation . So the model complexity reduction is a determinent feature for these operationnal applications.

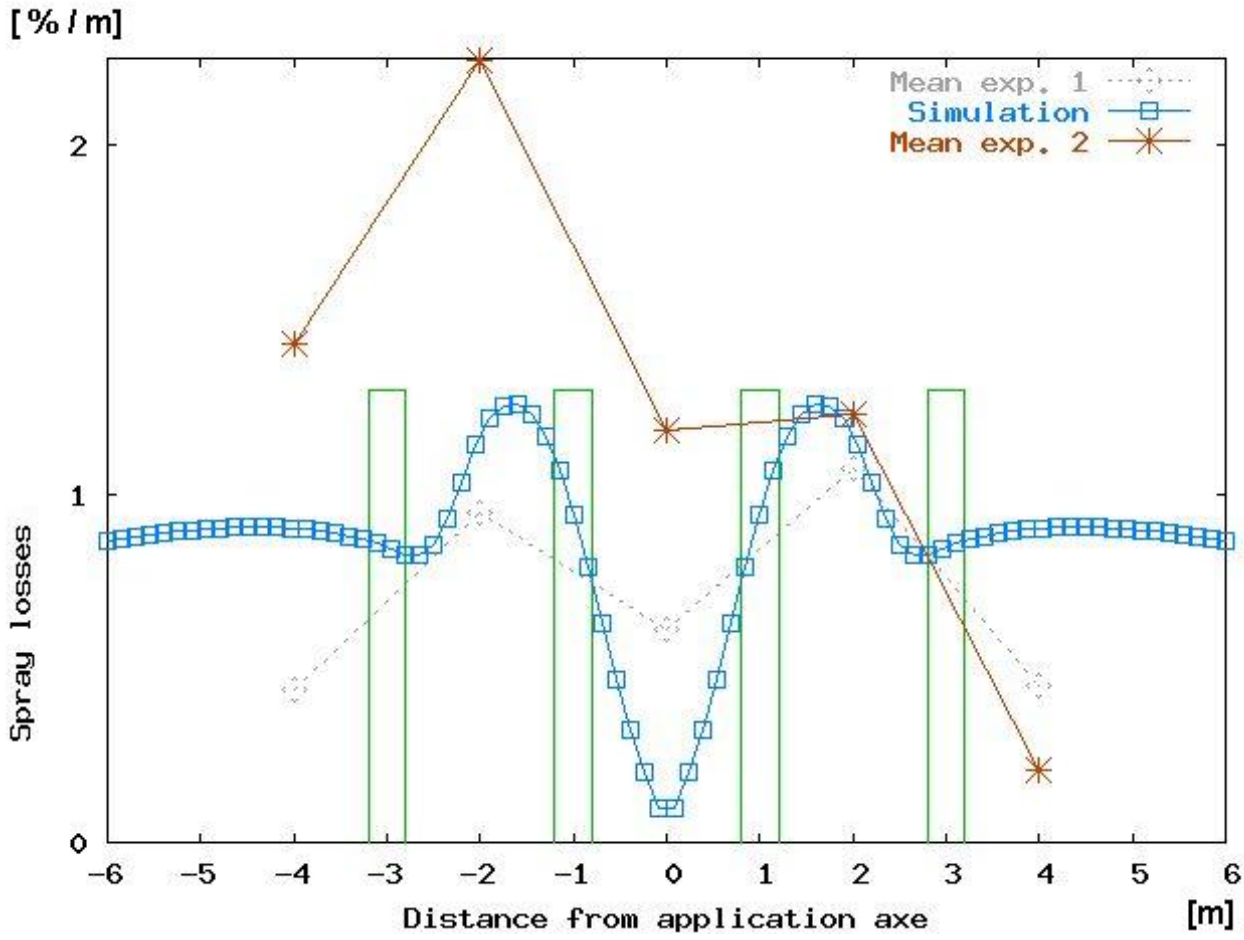

FIG. 5.12 – Pesticide air losses relatively to the distance from the sprayer : comparison of numerical (Simulation) and experimental data (Mean exp.1, data with fine spraying and Mean exp.2, data with very fine spraying). The total mass losses M_{loss}^{tot} is the integral under the curve which represents quantity in % m^{-1} of the global mass sprayed. Vertical straight lines indicate the location of the rows such as in figure 5.8.

For example, recent studies suggested a great dependance of turbulent jet flow on the initial conditions [99]. Initial velocity profiles issued from a nozzle has a great importance in the flow establishment, and is seldom provided by the manufacturer. In fact, usable data is often incomplete and accurate simulations are consequently ineffective.

Very fine and fine spray droplet size distributions give different drift losses in the experimental part. But the model considers only passive scalar transport, as notified in section 2, and doesn't take account for the size distribution. We made this choice because our experience show that the nozzle orientation seems to have more influence.

However thanks to the complexity of the model, inverse problems could be afterwards solve in very short time in order to find robust parameter for the different classes. For example it is possible to modify the parameters x_0, $K_{c_{jet}}$ that defines the decay on the centerline and on α_{jet} that influences the radial behaviour. These parameters could be modified to better take into account for some important factor that are negliged by the model.

The effects of a vertical porous layer on a turbulent round jet discharging from a nozzle into quiescent ambient air, is not still understood. In fact, free jets and wall-impinging jets are

well-known classes of shear flows. But it appears to be only few studies on the intermediate cases. This porous layer could produce significant differences in growth rates of the jet because the half-widths could develop not uniformly. The conservation of the flow stucture (similitude assumption inside the vegetation), is also a strong approximation, but the real behavior of the flow inside a real crop stays inaccessible. In addition, interactions between the different jets are not taken into account, and no cross-flow effect is represented. Moreover, a reduction in entrainment into the jet would be anticipated as a consequence of the restricted contact volume inside the porous media. In such jets, significant modifications of the usual jet motion occur, due to the porous medium and entirely new and unexplained flow phenomena may arise which require altogether different analytical approaches and robust assimilation.

Despite of all these simplifications, the results of the model seems to give a correct order of magnitude compared with the measurements, as shown in figure 5.12. An overestimation is observed with the model compared with fine spraying experimental results, where 74% of spray volume is made of droplets greater than 100 μm.

5.9 Conclusion

Dealing with a complex chain of events, simulation programs can be used to gain a statistical representation of the likely outcome. Although difficult to develop, simulation models can be less costly and more controllable than field trials. However experimental field are indispensable in order to validate the theoretical approaches and to allow robust assimilation. To determine the relative effects of various factors on spray droplets, computer simulations could be useful tools.

Overall, spraying models should be seen as a tool aiding planning and analysis. It is unlikely that they can ever provide a completely accurate picture of what really happens because of the stochastic nature of spray dropler generation and deposition.

The model does not take into account possible wind speed effect on near-to-sprayer dispersion and transport of spray, as well as gravity effect on diverse droplet sizes. However, it is possible to simulate the main characteristics of sprayer, like air and nozzle outlet orientation, forward speed and canopy geometry effects on the performance of a pesticide source. Field experiments have the limitation that wind conditions cannot be controlled and can vary during a single pass with a sprayer. The effect of meteorological condition on drift have been discussed in [109]. Terrain and vegetation variations among drift measurement sites also influence local wind conditions and drift deposits.

The model presented here can compute spray losses magnitude from experimental setting data selected by the user. The calculation time is really short and thus highly reduced in comparison with classical CFD approaches. In spite of the numerous modelling assumptions, both approaches seem to give interesting preliminary results. The results agreed weakly, due to model limitations to accurately describe all the processes, but they obtained important information on near field spray and on a source term quantity.

Simple feature should be add to the model in order to better fit the real conditions of spraying. To better represent the impact of a jet on a porous wall, the screen effect should be represented. To this goal, a simple feature could be add to our model in this way :

$$(1-\gamma)c_{\text{canopy-jet}} + \gamma c_{\text{wall-jet}} = c_{\text{porous-jet}} \tag{5.70}$$

where γ is a function of the crop porosity and $c_{\text{canopy-jet}}$ is the model presented in this paper (see (5.44)). In the wall jet model $c_{\text{wall-jet}}$ the same analytical approach as for the free jet can be used,

i.e. analytical self similar solution could be finded. Moreover, simple boundary conditions could easily incorporated in our model such as in analytical gaussian model in atmospheric dispersion. For example the ground deposit can be easlily calculated by definition of the percentage of ground reflexion. At least, the wind effect and the interaction between the different air jets from the different nozzles could also be taken into account by analytical crossflow jet solution.

In order to validate this model definitively, additional comparisons with experimental trials would be desirable using several sprayers and other configurations in droplet spectra and air-flow setting. More theoretical and experiemntal studies are necessary in order to characterise the effects of a porous layer on a neutrally-buoyant turbulent round jet discharging into a stagnant air. The inclusion into the model of the micro-meteorological variables like wind speed and orientation, spray granulometry, other sprayer setting and possible cross-flow effect in the zones near to the sprayer will allow to improve the predictions with the aim to contribute to support the further performance of DRIFTX.

Quatrième partie

LEVEL 3 : Dispersion

Introduction

Ce dernier niveau de la plateforme présentée concerne le transport longue distance. Un terme source a été identifié grâce aux étapes précédentes et le but est maintenant d'estimer la dispersion de cette source par l'écoulement atmosphérique. Dans l'optique de garder une modélisation à complexité réduite, le choix a été fait de travailler avec des modèles analytiques comme celui décrit dans la partie introductive (1.5). En effet il faut garder à l'esprit qu'étant donné la complexité du problème et la nature des données d'entrées disponibles, seule la représentation de comportements moyens semble réaliste.

Comme l'a rappelé le chapitre 2, la dispersion des particules s'effectue en grande majorité dans les basses couches de l'atmosphère. Elle dépend essentiellement de l'état de l'atmosphère (turbulence, stratification atmosphérique,...) et des caractéristiques de la surface terrestre (topographie, orographie).

Le problème des solutions analytiques classiques est qu'elles nécessitent souvent des hypothèses fortes, notamment sur les conditions atmosphériques et la nature de la topographie (champ de vitesse atmosphérique uniforme stationnaire, et non prise en compte de l'effet topographique). Cela implique d'importantes restrictions quant à leur champ d'application. Cependant pour ces cas simples les solutions sont connues et bien identifiées (il existe de nombreuses paramétrisations issues de la bibliographie, cf E.1.3). On propose donc de généraliser ce type de solutions, afin de pouvoir traîter le cas des champs de vitesse non uniformes et des topographies plus complexes.

Le modèle developpé est basé sur l'adaptation d'un modèle analytique dans une nouvelle métrique généralisée (non symétrique) basée sur les temps de parcours, et dans laquelle on a incorporé la physique du problème considéré, c'est à dire l'influence de la topographie et du champ de vent. Cette approche est générale et peut être adaptée à d'autres types de solutions (cf 1.4.2).

Plan

La première partie, très générale, traite des outils de modélisation et permet d'exposer les grandes lignes sur la simulation de la dispersion atmosphérique. Elle permet par ailleurs de rappeler l'intérêt et le fonctionnement de ces outils tant du point de vue de l'utilisateur que par rapport aux concepts physiques.

Il existe de nombreux modèles pour la description mathématique de la dispersion atmosphérique. Une revue succinte des principaux types de modèles couramment utilisés est ensuite présentée. Les modèles sont tellement nombreux qu'il n'est pas possible d'être exhaustif dans le recensement des outils. Il s'agit juste de présenter les grandes familles et les principes qui les sous-tendent.

Enfin, le modèle développé dans le cadre de cette thèse, et les principes sur lesquels il est basé fera l'objet de la dernière partie.

Mots clés : *Modèles de Dispersion Atmosphérique, Modèle à complexité réduite, geométrie non symétrique, identification des sources*

Keywords : *Atmospheric Dispersion Modeling, Reduced order modelling, non symmetric geometry, source identification*

"As as far as the laws of physics-mathematics refer to reality, they are not certain ; as far as they are certain, they do not refers to reality"

[Albert Einstein]

Chapitre 6

Theory and Objectives of Atmospheric Pollution Dispersion Modelling

In the last decades, interest in studying pollutant dispersion has considerably increased as a consequence of the environmental problems caused by industrial development. Several analytical (see 1.4.2), numerical and hybrid methods were used to solve tranport problems [64]. The choice of a model depends on the specific objectives.

Models of environmental processes are approximate representations of reality. Each model involves a set of tradeoffs, taking into account objectives : for instance, it is used to aid understanding, to estimate changes that might occur or to determine which areas might be affected. Research in numerical contaminant transport modeling is intense, both in the broad scope of study, and in the large quantity of information published each year. This part first summarizes why *Atmospheric Dispersion Modelling* (ADM or AQM for Air Quality Modelling) is needed and how it works. It then describes the main categories of modern atmospheric dispersion models.

Nowadays atmospheric dispersion scientists and modellers seek to characterize air pollution spread in terms of important parameters representing the actual state of the atmosphere. A part of the model selection problem is then understanding which transformations and removal processes are of concern. Hence, part of the problem of model selection is knowing the scales of the various transport and diffusion processes. The vertical scale has already been presented in the chapter 2. The horizontal and temporal atmospheric scales will be briefly described.

6.1 Air Quality Modelling

6.1.1 Introduction and Motivation

Because air pollution can't be measure in every place where it occurs, models are used to simulate the dispersion of air pollutants away from emission sources, and to estimate ground level pollution concentrations. Air pollution models are routinely used in environmental impact assessments, risk analysis and emergency planning, and source apportionment studies. In many countries appropriate regulations provide a societal mandate to assess and manage air pollution levels to protect human health and the environment, requiring the development of effective emissions control strategies. Models are also designed to optimize the costs of control strategy implementation.

Consequently, air quality simulation tools are important for regulatory, policy, and environmental research communities. From these previous remarks, the need for well designed software is obvious if one wants to use advanced methods in a safe, efficient and perennial framework.

6.1.2 Structure of an ADM

Air dispersion models are mathematical representations of the atmospheric processes which operate on a set of input data and produce output that describe the pollutant concentration of the region. Current comprehensive and practical air pollution modelling systems gather main components and consists of several functional structural levels :

- **a set of inputs and parameters :**
  - Meteorological conditions, such as wind speed and direction, the amount of atmospheric turbulence (stability class), the ambient air temperature and mixing height, the height to the bottom of any inversion aloft...(see chapter 2)
  - Emissions parameters, such as source location and height, source diameter, source exit velocity, gas exit temperature, emission rate/mass flow rate...(see chapter 5).
  - Surface roughness, terrain elevations and the location, height and width of any obstructions (such as buildings, forests or other structures) in the path of the emitted plume.
- **preprocessors for inputs** (database exploitation...)
- **a set of assumptions and approximations** that reduce the actual physical problem to an idealised one that retain the most important features of the actual problem.
- **basic mathematical relations** and auxiliary conditions that describe the idealised physical system. Typically, they are two components :
  - *balance equations* (employing the principles of thermodynamics, chemical kinetics and transport phenomena).
  - *constitutive equations* (that determine the value of physico-chemical parameters and are often derived from statistical mechanics considerations). It also includes the physical parameterizations (turbulence closure, deposition velocities, etc. see chapter 1).
- **computational schemes** used to solve the basic equations (the numerical core of the transport model).
- **computer program or code** that actually perform the calculations.
- **postprocessors** for outputs (see E.2). Many also include a post-processor module for graphing the output data and/or plotting the area impacted by the air pollutants on maps. The resulting calculations for air pollutant concentrations are often expressed as an air pollutant concentration contour map in order to show the spatial variation in contaminant levels over a wide area under study. In this way the contour lines can overlay sensitive receptor locations and reveal the spatial relationship of air pollutants to areas of interest. These are high levels methods, in which the model is simply viewed as a function, such as the ensemble forcasts or data assimilation.

These components are usually combined and mixed in a single system. This conception blends components which natures are completely different.

6.1.3 Model Requirements & Limitations

Dispersion models range from the dispersion of passive tracers at small scales (a few hundred meters) to the simulation of aerosol continental (or even global) scale ; from simple paper

based models, providing information in the form of graphs and tables, to advanced computer programmes. However, the proliferation of air pollution research and models to date has made it necessary to read specialized journals and conference proceedings to keep up with developments. The activities share common features (at least for the transport) but there is still strong diversity due to the dedicated add-ons. Moreover, within a given application, there is some diversity in the field involved, from chemical to meteorological fields, and in the goals, e.g. forecasts or data assimilation. While models developed for water environment are often adaptable to other situation with minor modifications, the portability of air quality model is rather limited [110]. A single atmospheric model is seldom applicable universally.

There are several competing requirements in the design of an air pollution model. A model must capture the essential physics of the dispersion process and provide reasonable and repeatable estimates of downwind concentrations.

The most complex models may take too long to run, or require too much input data in a real emergency, in which case a simple but good quality model may be much more practical and still provide the answers urgently needed by the decision makers exercising emergency management. In addition, efficient software is necessary because of the high computational costs.

To a large extent, the accuracy of the model depends upon the detailed knowledge of inputs and the data quality being used. It is also a fact that complex models are not always significantly more accurate than simpler models, and that no model produces results of a quality better than the quality of the input data they require to work. As the number of input variables goes up in

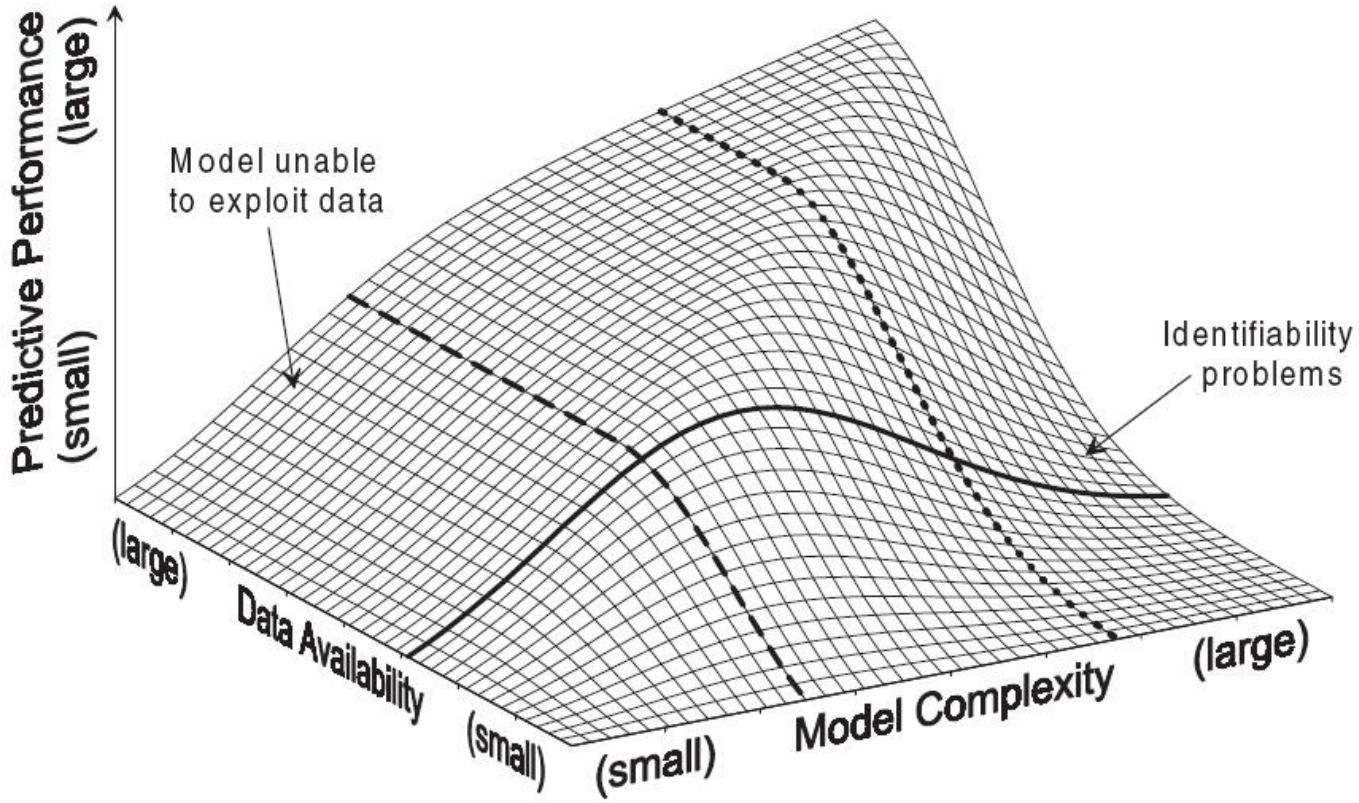

FIG. 6.1 – Schematic diagram of the relationship between model complexity, data availability and predictive performance, from [111].

the advanced models, the room for input data error increases 6.1. In addition, the level of user

understanding must increase to make proper use of the model. So it is desirable to keep these input requirements to a minimum, and simplicity is an important asset in any model.

While ADM are the best tools currently available for evaluating proposed pollution control strategies, it is very important to recognize that uncertainties in the model components and in the input data used by the models can have a serious impact on the model predictions. Even with very precise information, there will always be a degree of uncertainty associated with the model estimates, due to the variability of weather patterns and pollution emission conditions. Standard statistical procedures have been developed for expressing the uncertainty and variability of the predicted results when comparing them to measured concentrations. Regulatory models must also undergo extensive quality assurance, including the evaluation of the model under several scenarios using benchmark data.

The maturity of the models allows to use complex methods such as the data assimilation methods or ensemble forcasts. A well designed modelling system should allow to apply and test these methods without endless developments. One should also stress the large amount of data processed. It requires **safe** and **robust** software. All models should have a fully documented account of the equation algorithms used and their conversion into valid software (i.e., traceability).

The conclusions exposed in this preceding paragraph, concerning the quality of the results provided by the various approaches of modelling, must be the subject of some reserves. Indeed, the quality of the results of a model of dispersion depends on many factors relating to the model in itself, but also to the way in which it is implemented. These various factors are : intrinsic quality of the model, adequacy between the model and the problem to be treated, quality of the data, expertise of the user.

It is necessary to be conscious that a "good" model is not enough to provide good results. It is in general the good adequacy of the preceding factors, which makes it possible to obtain the best results. To illustrate this point, it is interesting to analyse the results of the exercises of intercomparison and validation of models of dispersion, which are regularly carried out by the scientific community. It is not rare to observe that two users, using the same model and seeking to simulate the same episode, obtain results for the concentration different from a factor of 10.

6.2 General Air Pollution Model Types Classification

6.2.1 Introduction

Models describing the dispersion and transport of air pollutants in the atmosphere can be distinguished on many grounds, for example :

- on the **spatial scale**,
- on the **temporal scale** (episodic models, (statistical) long-term models),
- on the **treatment of the transport equations** (Eulerian, Lagrangian models,...),
- on the **treatment of various processes** (add-ons such as chemistry, wet and dry deposition),
- on the **complexity** of the approach 6.2.1.
- on their **type of application**
  The first and most widely used application is 'Environmental impact studies'. In this category, dispersion models are used for Government and regulatory bodies control and assessment on environmental loads coming from industrial and energy production emis-

sions. The second type of application is 'probabilistic assessment studies' - where, for example, the annual mean or the monthly peak concentrations over an area are investigated. The third type of application is a real-time assessment model. This is of interest for the real-time monitoring of pollution states, decision support concerning accidents, and for assessing the present or near future state of pollution.

	Gaussian model	**Lagrangian model**	**Eulerian model**
CPU time for a scenario	$<$ 1 minute	A few minutes to 1 hour	$>$ 1 hour

TAB. 6.1 – Order of magnitude of the computing times necessary for a scenario, for the various types of models.

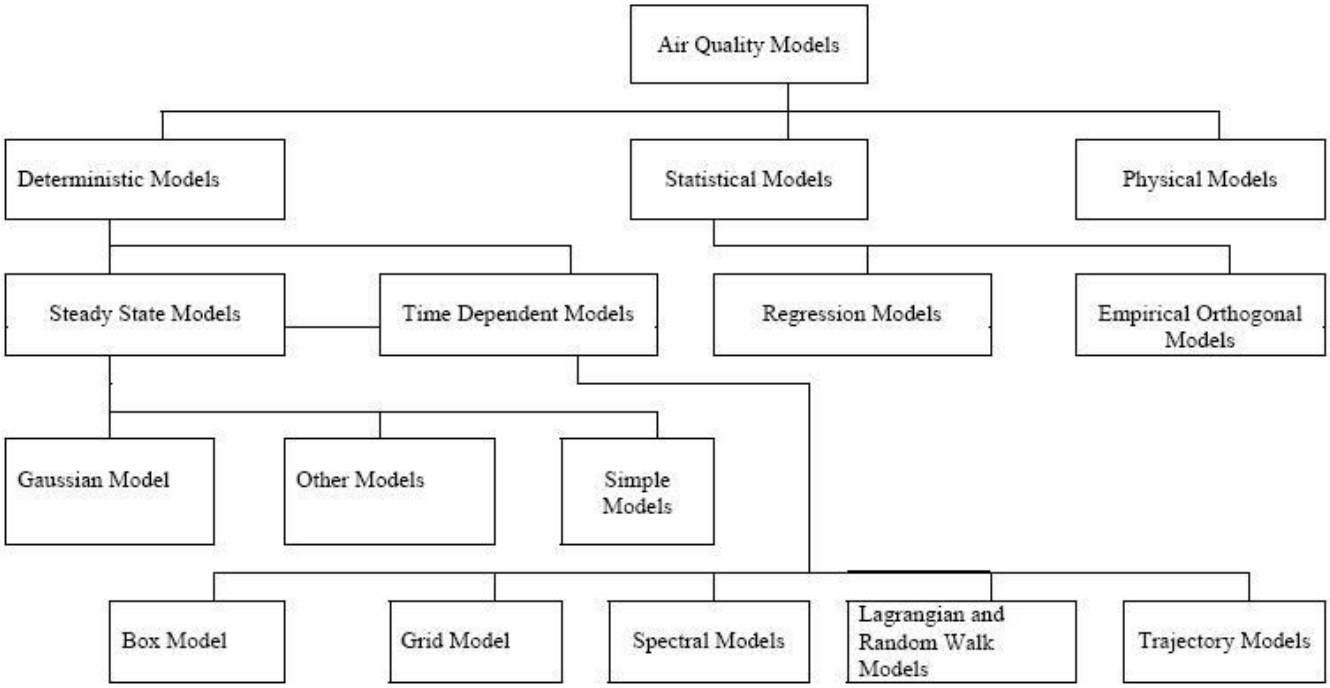

FIG. 6.2 – Example of Air Classification Models (from [110]).

6.2.2 Practical Atmospheric Dispersion Models

A gallery of air pollution model types treatment is presented in figure 6.2 and their applications areas are listed in tab. 6.2 (see also D.1).

Statistical models

In spite of considerable conceptual differences within this category, all these models are chracterised by drastic simplifications and a high degree of empirical parameterizations. These models are very useful for real-time short-term forecasting of concentrations and need very small computational efforts.

Scale of atmospheric process	Microscale	Mesoscale	Macroscale	
Scale of dispersion phenomenon	Local	Local-to-regional	Regional-to-continental	Global
Model type				
Plume-Rise	1,2,4			
Gaussian	1,2,4	1,2		
Semi-Empirical	1,2,3,4	1,2,4		
Eulerian	1,2,4	2,3,4	2,4	2,4
Lagrangian	4	4	2,4	
Chemical	(1,2,)4	2,3,4	2,4	2,4
Receptor		2,4		
Stochastic		2,4		

TAB. 6.2 – Application areas of various air pollution model categories depending on the scale of the dispersion phenomenon (1 : regulatory purposes ; 2 : policy support ; 3 : public information ; 4 : scientific research) from [112].

Several techniques are used to achive this goal, e.g., frequency distribution analysis, box models, time series analysis, Box Jenkins, various kinds of parametric models, spectral analysis, etc. They are intrinsically limited because they do not establish cause-effect relationships.

Deterministic Dispersion Model Gallery :

A deterministic model is based on determining a numerical solution to the governing equations of fluid flow and transport, typically systems of parabolic partial differential equation derived through either

- Eulerian types
- Lagrangian types
- Hybrid types

Gaussian plume and puff models.

This is the most common type air pollution model used to estimate the concentrations from sources at locations from tens of meters to a few kilometers. It is based on the assumption that the shape of the plume and the distribution of material within the plume, at each downwind distance, has independent Gaussian distributions both in the horizontal and in the vertical (these models are described in 1.5). They have been modified to incorporate special dispersion cases (segmented Gaussian plume models, puff-splitting, low wind conditions...) For example, [39] uses a Gaussian dispersion model to describe a modeling framework for quantifying all of the airborne pathways, consisting of components describing the source, dispersion, and deposition phases of each pathway.

Lagrangian Particle Models.

This type of transport methods represents transport on a moving frame of reference by directly moving parcels of solute mass along pathlines. Lagrangian methods track a contaminant plume through a given velocity field using particles to represent discrete packets of solute mass. Dispersion is modelled by adding a random component to the particle trajectory at each time step. Concentrations are recovered at the end of the simulation by summing the mass in each cell (the number of particles) and dividing by the cell volume. Random walk models are

representative of this class.

Lagrangian methods are useful for locating the spatial extent of a contaminant plume or for deriving concentration fields for plumes of small extent. Numerical diffusion is avoided and those models can handle non-homogeneous atmospheric structures. This description in fluid element that follow the instantaneous flow typically requires a large number of particles to build up some statistical significance in the simulation. Hence for larger problems, the method requires large numbers of particles and small time steps to avoid statistical fluctuations and particle trajectory errors. This can make Lagrangian methods computationally heavy to implement. In addition, Lagrangian methods tend to have difficulty representing complex boundary conditions and/ or solute chemistry. Much effort has been put into the development of these non-Gaussian models [113, 114].

Eulerian Grid Models.
Eulerian methods attempt to solve the ADE directly on a fixed grid. However, these methods are generally susceptible to numerical dispersion or spurious oscillations, especially when advection dominates. A lot of numerical methods for modeling of solute transport rely heavily upon this fixed spatial grid representation and solve numerically all the terms of equation system (e.g., finite difference, finite element, flux-limiting schemes, finite volume methods,...) over a large number of grid points. As a consequence, all existing methods for transport simulation are also strongly limited by the scale of the modeled physical domain. The concentration values are obtained at the grid points and are averages in time and space according to the chosen time step and grid size. Grid models are mostly used for the simulation of episodes, because the computational effort connected with their application is large. Such models are usually embedded in prognostic meteorological models. Advanced Eulerian models include refined sub-models for the description of turbulence (e.g. second-order closure models and large-eddy simulation models).

Hybrid types.
Hybrid types incorporate features of Lagrangian types into an Eulerian framework. The combined use of Lagrangian methods for advection and Eulerian methods for dispersion and/or reaction are referred to as *Eulerian-Lagrangian* (EL) methods. E-L methods, sometimes called operator-splitting methods, split the advection and diffusion/reaction portions of the ADE, solving the advection portion using Lagrangian methods and the balance of the equation using Eulerian methods. By utilizing the strengths of each solution type, E-L methods have a good balance between computational efficiency and numerical accuracy. However, also due to the split nature of the method, errors from both types of solution methods can be present.

Spectral Model
The spectral models differ from grid models in that the equation is transformed into Fourier space and then solved. The advantage here is that one avoids numerical truncation errors. There does not seem to be an advantage in computational efforts.

Streamline method
An alternative to traditional Eulerian, Lagrangian, or EL methods is the deterministic streamline method, which was developed primarily in the petroleum engineering field [115]. The method uses streamlines (the paths of particle trajectories in a steady-state flow field) as the primary frame of reference. A transformed 1-dimensional equation is solved along each streamline.

6.3 Atmospheric Dispersion at different scales

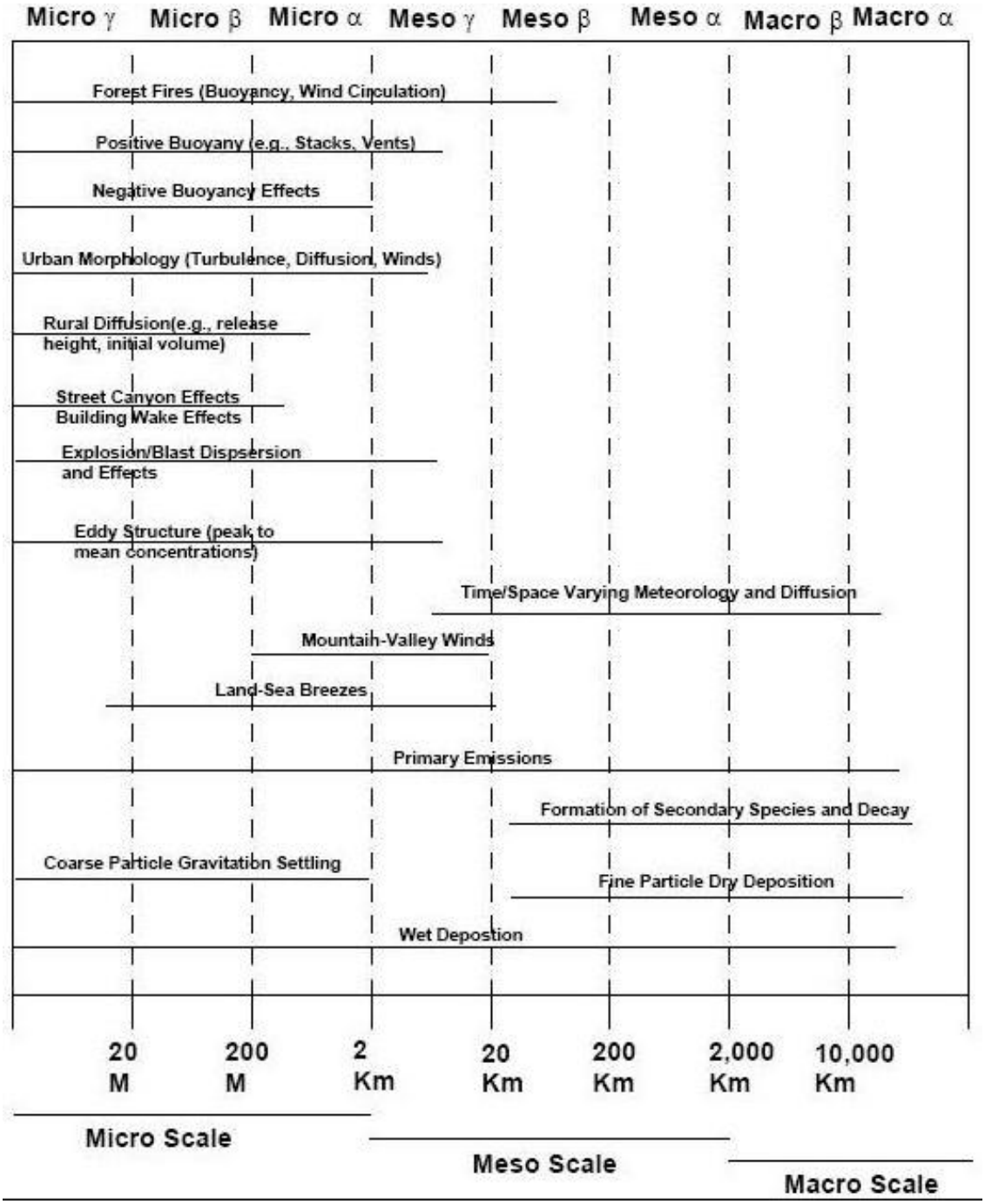

FIG. 6.3 – Depiction of varying horizontal scale transport and diffusion processes likely to be of most concern (from [37]).

6.3.1 Introduction

Air pollution dispersion phenomena are decisively influenced by atmospheric processes which are commonly classified with regard to their spatial scale. Figure 6.3, which depicts some of the

major atmospheric processes typically addressed in transport and dispersion models, illustrates that not all processes are of interest at all scales (see D.2). Many of the processes of interest for near-field impact assessment become of less importance for problems involving longer transport distances.

However, these scales are all interconnected. Large-scale atmospheric processes drive smaller scale processes as energy is transferred from large to small scales. Conversely, small-scale processes can organize to develop large-scale systems. Despite of this, statistical methods separate different scales linked to different physical processes.

So the choice of horizontal scale plays an important role in the formulation and selection of an atmospheric model. According to hierarchy theory, describing effects at some scale (the scale of interest) requires at least three levels (scales) for both comprehensiveness and conciseness : (1) the next smaller scale, which provides information up to the scale of interest, (2) the scale of interest, which constrains processes at the next lower scale and provides information up to the next larger scale, and (3) the next larger scale, which constrains processes at the scale of interest.

6.3.2 Horizontal and temporal scales of atmospheric processes

Local scale or Microscale

In general, air flow may vary in a quite complex way with horizontal position (especially over complex terrain) and with time. It depends strongly on the detailed surface characteristics (i.e. form of buildings, their orientation with regard to the wind direction etc.). On the local scale, effects of the underlying surface with its topographical features also tends to be important, each tree, house and hill exerts drag on the air, and heat and moisture profiles of the air becomes important. In view of the complex nature of such effect, local scale dispersion phenomena are mainly described with robust 'simple' models in the case of practical applications.

Mesoscale

Meso is Greek for 'in between' and refers to atmospheric phenomenon which occurs on horizontal scales large enough that the hydrostatic approximation is a valid assumption (usually it is on scales bigger $> 2km$) ; yet small enough ($< 2000km$) that larger (synoptic) scale geostrophic and gradient winds can approximate the regional wind circulation. The flow configuration is depending both on the hydrodynamic effects (e.g. flow channelling, roughness effects) and inhomogeneties of the energy balance (mainly due to the spatial variation of area characteristics (e.g. land use, vegetation, water), but also as a consequence of terrain orientation and slope).

From the air pollution point of view, thermal effects are the most interresting, as they are of particular importance at times of a weak synoptic forcing, i.e bad ventilation conditions.

Large scale or Macroscale

At this scale, the atmospheric flow is mainly associated with sypnoptic phenomena, i.e. the geographical distribution of pressure systems. Such phenomena are mainly due to large-scale inhomogeneties of the surface energy balance. Global and the majority of regional-to-continental scale dispersion phenomena are related to macroscale atmospheric processes, for which the hydrostatic approximation can be considered as valid. The regional winds (in particular its direction) vary with an average periodicity of about $3 - 7$ days.

6.4 Conclusion

Pollutants in the atmosphere are subject to myriad transport processes and transformation pathways that control their composition and levels. The successful application of a model is thus one of knowing what questions are being posed, what capabilities are present in the models, and what the tradeoff consequences are as one tailors the application of the model to a particular situation. A model can be envisioned as a tool that can be used in a variety of ways. To apply a tool successfully takes wisdom (i.e., experiMential knowledge as well as academic knowledge).

Numerical-model operating ranges are limited by the choice of governing equations, the numerical methods used to solve the governing equations, the scales of the surface or atmospheric forcing and the atmospheric response, the specified resolution and domain size, and the available computer resources. And, although the input data requirements and level of sophistication increase with the more advanced models, it does not necessarily lead to predictions that are more accurate.

In practice, most estimates of dispersion from continuous point sources are based on the Gaussian approach. The Gaussian model is an easy and fast method which, however, cannot properly simulate complex nonhomogeneous conditions. It does not require complex meteorological input, and describes the diffusive transport in an Eulerian framework, making easy use of the Eulerian nature of measurements. The input parameters of the Gaussian plume model are frequently related to simple turbulence typing schemes and stability classes. For these reasons they are still widely used by the environmental agencies all over the world for regulatory applications. However, because of their well known intrinsic limits, the reliability of a Gaussian model strongly depends on the way the dispersion parameters are determined and the model's ability to reproduce experimental dispersion data.

As a consequence, the major part of applications to practical problems are currently done by using the Gaussian model, and great deal of empirical work has been done do determinate the dispersion parameter appropriate to the ABL under various meteorological conditions and to extend the basic formulation of this model and its range of applicability.

In the next chapter a new modeling approach is introduced to overcome these limits. Within this framework, it is possible to develop operational analytical models that employ some of the presented analytical solutions in 1.4.2.

Taking all of the previous aspects presented in this chapter under consideration, one can conclude that ADM depends on

- a definition (or redefinition) of the information to be gained or the decision to be made ;
- the selection of the scales of interest (vertical, horizontal, temporal) ;
- the observation which needs an appropriately sampled estimate of the variance of the properties observed.
- a knowledge of the physical processes that likely should be treated for the intended purpose ;
- an appreciation of the uncertainty associated with the tradeoffs made in the model's construction ; and
- the limits of predictability associated with any modeling system for the scale of interest.

In all cases the circulation in the lower layers is decoupled from the synoptic flow and appears to be mainly determined by local and mesoscale terrain features. The transport phenomena considered in this study cover horizontal scales in the range from ~ 2 to $\sim 20km$ (usually addressed as meso-γ), and time scales of few hours. Microscale dispersion problems as well as regional to large scale pollution problems are not taken into account in this context.

Chapitre 7

Application to DriftX : Module3

This level is the last part of the integrated set in the proposal platform Drift-X. This study use mathematical tools, such as control theory, to establish a scientific basis and a realistic low cost transport model. The objective of this part is to evaluate some adaptation of analytical solutions to better take into account the characteristics of the ground-topography/wind, as those model proved their efficiency in aerial pollution dispersion.

One aims to model pesticide transport in turbulent atmospheric flows with very low calculation cost and needs to be able to perform statistical analysis. However available information on data is highly incomplete and rather statistical. In addition, the number of parameters involved is very large. Dimension reduction, reduced order modelling (see A) and Monte Carlo simulations are being natural.

This chapter explains how a parameterized reduced order model has been built to reduce the search space for the solution using a priori and experimental information (see A). This model is defined with parameters solving minimization problem (see E). The passive transport problem in an environment driven by travels distance is considered. Similitude solutions are used in a non symmetric metric for the transport over long distances. The approach does not require the solution of any PDE and therefore is mesh free. It also permits to access the solution in one point without computing the whole solution.

As said in previous part, the near field (to the injection device) search space is built using experimental observations and turbulent jet theory. Once this local solution is known, the amount of specie (7.2) leaving the atmospheric sub-layer is evaluated.

This quantity is candidate for long distance transport using similitude solutions for mixing layers and plumes [116].

These are well known in cartesian metrics (e.g. gaussian model in 1.5 and E.1). However, they cannot properly simulate complex nonhomogeneous conditions. An original contribution here is the generalization of these solutions in a non symmetric travel-time based metric (section 7.1.3) to account for non uniform winds.

Once the atmospheric flow field is known (section 7.2.1), it is used to built migration times on a coarse mesh (section 7.3). These transport times are then used to define a non symmetric geometry (section 7.4) on which one applies similitude solutions for dispersion. This is achieved including a model to account for the impact of the topography on the dispersion (section 7.2.2).

Better assimilation of wind or concentration measurements by the model might therefore impact as well the wind definition, the topography impact model, the migration time definition, and also the coefficient in the similarity solution used for the dispersion.

Constraints are added such that solutions built with this approach are solution of the direct

model (i.e. flow equations and transport model for a passive scalar). In particular, the divergence free condition for the generated winds (see 7.2.1), conservation, positivity and linearity of the solution of transport equations are requested.

For this meso-scale impact assessment, the transport times are sufficiently short that the chemical species being modeled can usually be treated as inert. However, whether the chemical or radioactive species can be treated as inert depends on the species.

7.1 Generalized geometry

In this section we explain how a non-Riemannian metric has been built for wind transport. It is showed how the intuitive space can be modified to take into account for complex transportation effect which distort topological and metrical relations.

7.1.1 Generalized distance in geography

Generalized metric are often used in geography [117]. Consider the set of all places which could be reached within one hour from where someone is. The outer edge of this set forms a geographical "space" of one hour radius (see figure 7.1). This isochronic map most probably has holes, and probably consists of disjoint pieces, shape depends on the place and time of day. This environment, as a geometry, seems more complicated than the Riemannian geometry.

7.1.2 Distance Definition

The essential features of the notion of distance are :
– a finite or infinite set of distinct, definable objects, and
– a rule or set of rules for determining the degree of separation of object pairs (a "measure").
In addition objects and rules may vary over time, the measure may be process- or activity-related and will generally be numeric. In a classical symmetric geometry the distance function between two points A and B verifies

$$\text{Positivity :} \quad d(A,B) \geq 0 \ \forall A,B \tag{7.1}$$

$$\text{Discrimination ("non degenerate" distance) :} \quad d(A,B) = 0 \ \Rightarrow \ A = B, \tag{7.2}$$

$$\text{Symmetry :} \quad d(A,B) \ = \ d(B,A), \tag{7.3}$$

$$\text{Triangle Inequality :} \quad d(A,B) \leq d(A,C) + d(C,B) \tag{7.4}$$

But the distance function can be non uniform with anisotropy (the unit spheres being ellipsoids).

7.1.3 Generalized distance and Non-symmetric geometry

For example, in a chosen metric $\mathcal{M}_{mesh}$ the distance between A and B could be given by :

$$d_{\mathcal{M}_{mesh}}(AB) = \int_0^1 \left({}^t\overrightarrow{AB} \ \mathcal{M}_{mesh}(A + t\overrightarrow{AB})\overrightarrow{AB} \right)^{1/2} dt \tag{7.5}$$

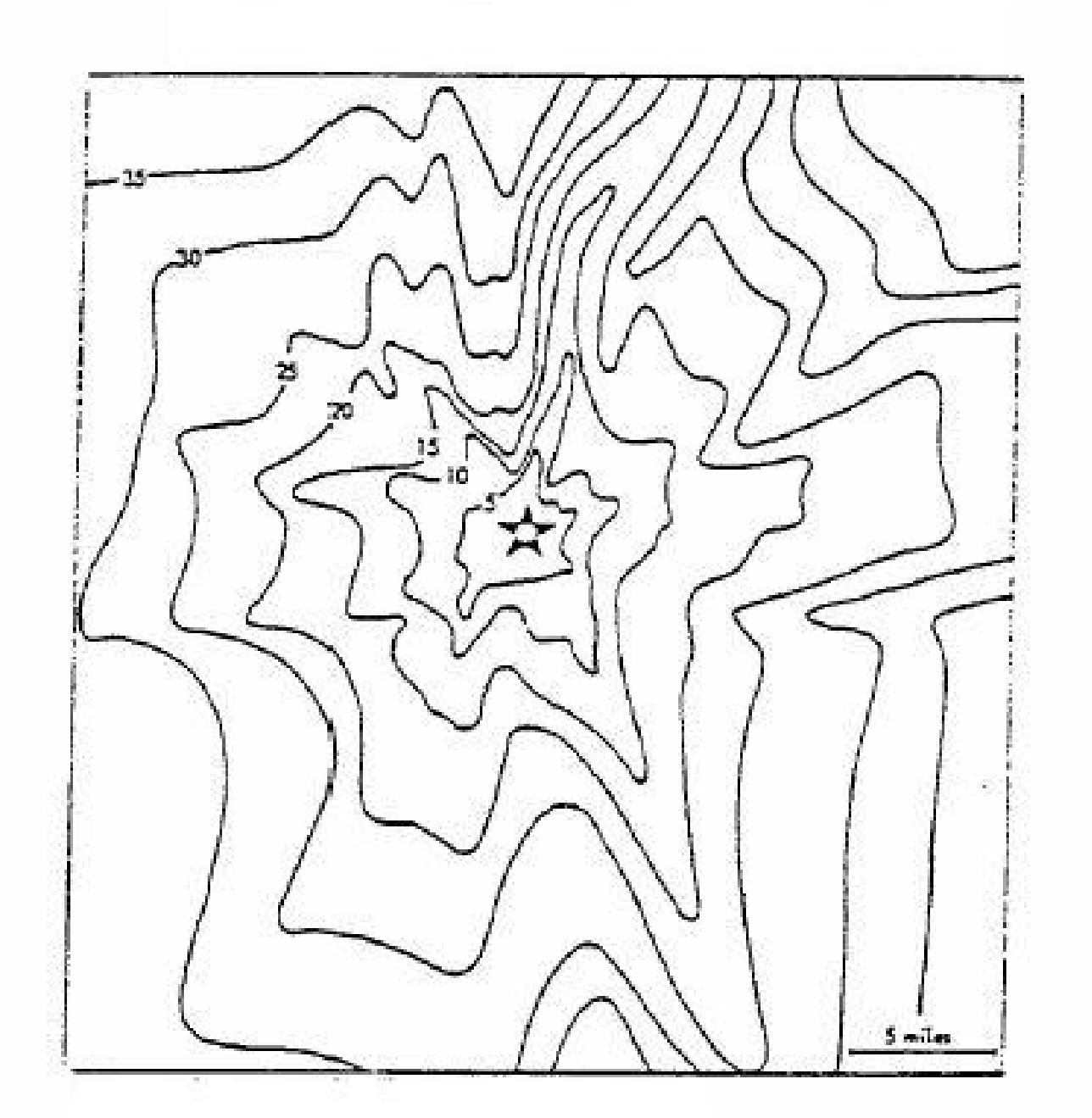

FIG. 7.1 – Isochronic map typical example : The map of travel times from central Dallas. Five-minute isochrones. From Departement of traffic control cited by [117]

where $\mathcal{M}_{mesh}$ is positive definite and symmetric in symmetric geometries. With $\mathcal{M}_{mesh} = I$, one recovers the Euclidean geometry and variable $\mathcal{M}_{mesh}$ permits to account for anisotropy and non uniformity of the distance function.

This approach has been widely used for mesh adaptation for steady and unsteady phenomenon [118, 119, 120] linking the metric to the Hessian of the solution. This definition of the metric permits to equi-distribute the interpolation error over a given mesh and therefore monitor the quality of the solution.

Consider now the following distance function definition :

If A is *upwind* with respect to B then

$$d_{wind}(B, A) = \infty \quad \text{and} \tag{7.6}$$

$$d_{wind}(A, B) = \int_A^{B^\perp} \frac{\mathrm{d}s}{u} = T_{mig} \tag{7.7}$$

T_{mig} is the **migration time** from A to $B^\perp$ along the characteristic passing by A. u is the local velocity along this characteristic and is by definition tangent to the characteristic. $B^\perp$ denotes the projection of B over this characteristic in the Euclidean metric defined by the distance d_E.

One supposes that this characteristic is unique hence avoiding sources and attraction points in the flow field. In case of non uniqueness of this projection, one chooses the direction of the projection which satisfies best the constraint $(\mathbf{u} \cdot \nabla c_{glob} = 0)$ in B. Here subscript $_{glob}$ reads for global and mentions long distance transport.

7.2 Flow field & Wind statistics

7.2.1 Practical flow field calculation

It should be keept in mind that in realistic configurations, one has very little information on the details of the atmospheric flow compared to the accuracy one would like for the transport. As an example, the flow will be described probably by less than one point by several square kilometers.

The near to ground flow field is built from observation data as solution of the following system :

$$\mathbf{u} = \nabla\phi, \tag{7.8}$$

$$-\Delta\phi = \sum_{i=1,\dots n_{obs}} \|\nabla\phi(x_i) - \mathbf{u}_{obs}(x_i)\| \tag{7.9}$$

where ϕ is a scalar potential and n_{obs} the number of observation points. The observations are close to the ground at $z = H$ and this construction gives a map of the flow near the ground.

This is completed in the vertical direction using generalized wall functions for turbulent flows (see [121, 122] and section 2.4) :

$$(\mathbf{u} \cdot \tau)^+ = (\mathbf{u} \cdot \tau)/u_\tau = f_{wind}(z^+) = f_{wind}(z_\tau/\nu) \tag{7.10}$$

where $\tau = \mathbf{u_H}/\|\mathbf{u_H}\|$ is the local tangent unit vector to the ground in the direction of the flow and $(\mathbf{u} \cdot \mathbf{n}_{(z=H)} = 0)$ is assumed if $\mathbf{n}$ is the normal to the ground.

This is a non linear equation giving u_τ , the friction velocity, knowing $(\mathbf{u} \cdot \tau)_H$ and is used in turn to define the horizontal velocity $\mathbf{u} \cdot \tau = u_\tau f_{wind}(z^+)$ for $z > H$. This construction gives two components of the flow and the divergence free condition implies the third component is constant and therefore it vanishes as it is supposed zero at $z = H$. This construction can be improved but it is expected to be sufficient for the level of accuracy required. In presence of ground variations, the flow is locally rotated to remain parallel to the ground.

7.2.2 Ground variations

At this point one accounts for the topography or ground variations $((x, y) \to \psi(x, y))$ in the prediction model above. These are available from *digital terrain models* (**DTM**) [123]. Despite

this plays an important role in the dispersion process, it is obviously hopeless to target direct simulation based on a detailed ground description. One should mention that ground variations effects are implicitly present in observation data for wind and transport as mentioned in the introduction.

However, as it was said, observations are quite incomplete and, to improve the predictive capacity of the model, one needs to model the dependency between ground variations and migration time. Therefore, in addition to the mentioned assimilation problem, one scales the migration times used for transport over large distances by a positive monotonic decreasing function $f_{topo}(\phi)$ with $f_{topo}(0) = 1$ where

$$\phi = (\nabla_{x,y}\psi.\mathbf{u_H})/\left\|u_H\right\| \tag{7.11}$$

where $\mathbf{u_H}$ is the 'close to ground' constructed flow field based on the assimilated observations.

7.3 Long range transport

The input condition

The basic premise of the work is that there is a time-scale separation. The spraying process can be divided into two zones ; close to the nozzle where droplet movement is influenced by the sprayer (c_{loc},$\mathbf{u}_{loc}$),and at distance from the sprayer where droplet movement is controlled by prevailing meteorological conditions (c_{glob},$\mathbf{u}$). Once a droplet moves far enough from the spray nozzle it will move entirely under the influence of the meteorological conditions. At this stage the spray concentration in the air is low so the influence of the droplets on the local air turbulence is negligible.

The modelling in the previous part gives a local distribution for the advected quantities (see chapters 4, 5 and figure 7.2). The quantities candidate for a transport over large distances are now considered. It is supposed that those are given by

$$c^+(x,y) = \int_{z>H} c_{loc}dz \quad \text{or} \quad c^+(x,y) = \mathbf{u}_{loc}{}^+ c_{loc} \tag{7.12}$$

where $H \sim 2-3m$ and $u^+_{loc} = max(0, (\mathbf{u}_{loc}.\vec{z})/\|\mathbf{u}_{loc}\|)$.

The total quantity being transported is given by

$$M_C = \int_{\mathbb{R}^2} c^+(x,y)\mathrm{d}\sigma \tag{7.13}$$

which should be conserved by the reduced-order transport model built and for which c^+ is the input condition.

Shape of the solution

One aims now to again reduce the search space for the solution. The primary factors influencing the dispersion of a neutral plume are advection by the wind and turbulent mixing. The simplest model of this process is to assume that the plume advects downwind and spreads out in the horizontal and vertical directions (slender plume approximation, cf. section 1.5.1).

Hence, the distribution of a passive scalar c_{glob}, emitted from a given point and transported by a uniform plane flow field $\mathbf{u} = (U, 0, 0)$ along x coordinate, is given by :

$$c_{glob}(x,y,z) = c_{axis}(x) f_{rad}(\sqrt{y^2+z^2}, \delta(x)) \tag{7.14}$$

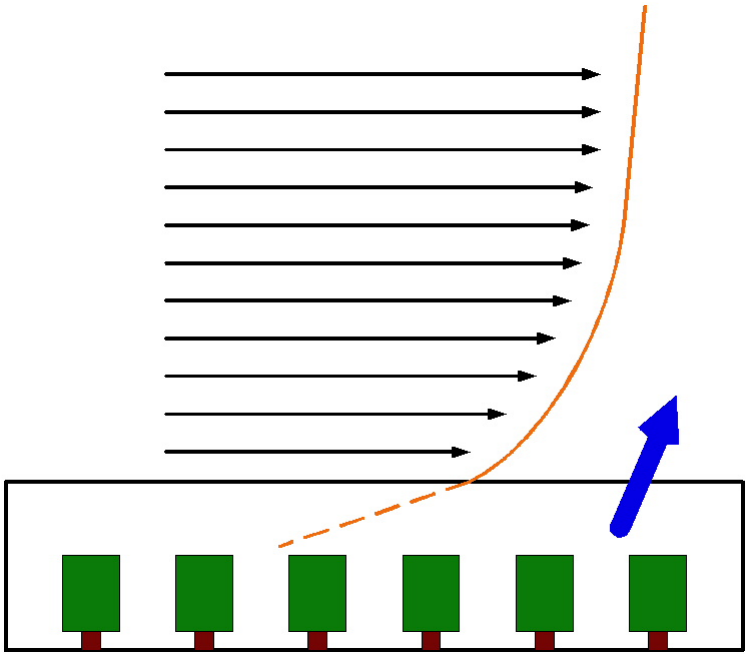

FIG. 7.2 – Sketch of instantaneous spray losses above the parcel. The vertical wind field profile is aslo represented. The box represent the system that encompass the 2 first level of DriftX. Two different time scales are identified, based on the injection velocity and the velocity at which the injection source moves. The injection velocity being much higher, one assumes the local concentration at the outlet of the injection device to be established instantaneously. This instantaneous local flow field is devoted to vanish immediately and not to affect the overall atmospheric circulation. This injection velocity is only designed to determine the part of the pollutant leaving near-ground area and being candidate for transport over large distances.

where $r = \sqrt{y^2 + z^2}$

$$c_{axis}(x) \sim exp(-a(U)x) \quad \text{and} \quad f_{rad}(\sqrt{y^2+z^2}, \delta(x)) \sim \exp(-b(U, \delta(x))r) \tag{7.15}$$

c_{axis} is the behavior along the plume central axis and here subscript $_{glob}$ reads for global and mentions long distance transport. $\delta(x)$ characterizes the thickness of the distribution at a given x coordinate. An analogy exists with plane or axisymmetric mixing layers and neutral plumes where δ is parabolic for a laminar jet and linear in turbulent cases (see figure 7.3, [124, 116], chapters 5, B.2 and apendice B.2). The shape of the function $\delta(x)$ drives the level of turbulence within the flow. $a(.)$ is a positive monotonic decreasing function and $b(.,.)$ is positive, monotonic increasing in U and decreasing in δ. In a uniform atmospheric flow field, this solution can be used for the transport of c^+ above (see E for the calibration of the different parameter).

One would like to generalize this solution in a non-symmetric metric defined by migration times based on the flow field and hence treat the case of variable flow fields.

As we said, our approach aims to provide the solution at a given point without calculating the whole solution. Being in point B, one needs an estimation of the migration time from the source in A to B using the construction described in 7.2.1.

The construction of characteristics is avoided using an iterative polynomial definition for a characteristic $s(t) = (x(t), y(t), z(t))$, $t \in [0, 1]$, starting from a third order polynomial function

verifying for each coordinate :

$$P_n(0) = x_A, \tag{7.16}$$
$$P_n(1) = x_B, \tag{7.17}$$
$$P'_n(0) = u^1_A, \tag{7.18}$$
$$P'_n(1) = u^1_B \qquad \text{(and same for } y \text{ and } z) \tag{7.19}$$

If $P'_n(\zeta) \neq u^1(x = P_n(\zeta))$ this new point should be assimilated by the construction increasing by one the polynomial order. $\zeta \in]0, 1[$ is chosen randomly. The migration time is computed over this polynomial approximation of the characteristic.

Here the approximation $B^\perp = B$ ($B^\perp$ is defined as in 7.1.3) is made which means the characteristic passing by A passes exactly by B which is unlikely. In a uniform flow, this means the angle between the central axis and AB is supposed small (cosine near 1). One introduces therefore a correction factor of $2/3 = 0.636$ on the calculated times. This is the stochastic averaged cosine value for a white noise for angles between 0 and π.

Then $d^\perp_E$ is defined as the Euclidean distance in the normal direction local to the characteristic at $B^\perp$ (i.e. along direction $BB^\perp$). The following approximation is made, $d^\perp_E \sim d_E(B, B^*)$ where B^* is the projection of B over the vector $\overline{u}_{char}$ the averaged velocity along the polynomial characteristic. This approach gives satisfactory results for smooth atmospheric flow fields which is the domain of interest of this study as no phyto treatments is in principle applied when the wind is too strong or if the temperature is too high. This also makes that the polynomial construction above gives satisfaction with low order polynomials.

7.4 Generalized plume solution

Once this distance is built, it is assumed that the distribution of a passive scalar transported by a flow $\mathbf{u}$ can be written as (see figure 7.4) :

$$c_{glob}(B) = c_{axis}(d_{wind}(A, B)) f_{rad}(d^\perp_E, \delta(d_{wind}(A, B))) \tag{7.20}$$

7.5 Inverse Problem

At this level, two types of inverse problem have been treated. The first inverse problem is for parameter identification in the model above assimilating either experimental data or partial data available. In particular, the unknown parameters in the global transport model come from the solution of a minimization problem (see chapter E). The second is a source identification problem. Similar work exist for the assimilation of data in ground water motion models.

7.5.1 Parameter Identification

Partial data are available on the wind $\mathbf{u}_{obs}$ and transported species c_{obs} measured by localized apparatus. The numerical model should therefore reproduce these after simulation. A prediction model ($p \longrightarrow \{\mathbf{u}(p), c(p, \mathbf{u})\}$) should use p solution of a minimization problem for :

$$\min_{p \in \mathcal{O}} \{J(p)\} \tag{7.21}$$
$$J(p, \mathbf{u}_{obs}, c_{obs}) = \|\mathbf{u}(p) - \mathbf{u}_{obs}\| + \|c(p, \mathbf{u})) - c_{obs}\| \tag{7.22}$$

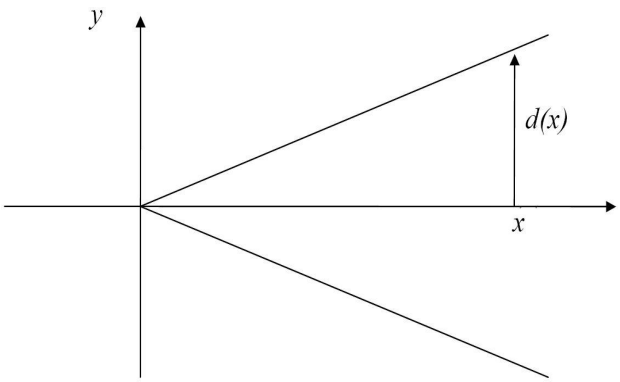

FIG. 7.3 – Transport in an Euclidean reference frame (x, y) by an constant uniform wind field. In this figure, x represents the distance along the axis and $d(x) = r = \sqrt{y^2 + z^2}$ is the radial distance to the axis plume.

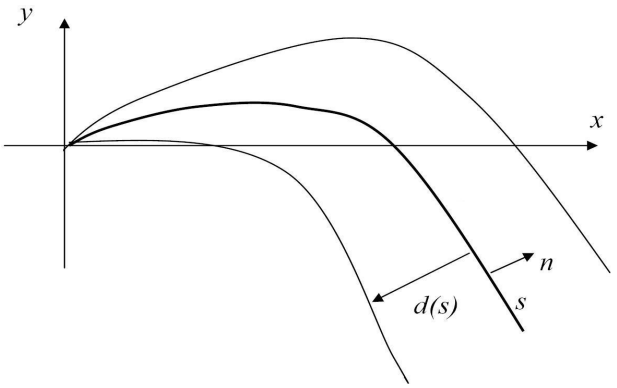

FIG. 7.4 – Solution in the new generalized metric based on the travel transport time. (s, n) is a local coordinate system along the characteristic. With $s = d_{wind}(A, B)$ the distance along the characteristic, and $d(s)$ the radial distance to this characteristic.

where p gathers all independant variables in the model, including simulation domain description, topography and injection source details. $\mathbf{u}(p)$ is the calculated divergence free flow used for the transport and the calculation of $c(p, \mathbf{u})$. We will show how to build a parameterized reduced order model to reduce the search space for the solution using a priori and experimental information. $\|\cdot\|$ is a discrete L^2 norm over the measurements points.

In this work, $\mathbf{u}(p)$ is the completion of available wind measurements ($\mathbf{u}_{obs}$) over the domain described in 7.2.1 (by divergence free construction procedure used to complete available partial (wind) measurements). The calculated divergence free flow is used for the transport and the calculation of $c(p, \mathbf{u}(p))$.

7.5.2 Source Identification

Once the model is established, the second inverse problem of interest is the identification of possible sources of an observed pollution. This region is defined as where J'_p is large. In this case, the parameter p is the location of the different sources (crops). An example is shown in figure 7.10.

7.6 Numerical Results

The application of low complexity transport model to several flow condition is shown. These typical application concern ground level concentration. Examples also show typical configuration input of DriftX, multi-source configurations as well as sensitivity analysis of detected pollution. This is useful for both source identification and risk analysis.

Numerical examples show a comparison of our approach with a PDE based simulation (Fig. 7.5). A regular mesh on a cartesian frame is used with $\Delta x = \Delta y = 1km$. The DriftX solution is calculated over the whole domain, at the node of the DNS mesh for the comparison. This is a first approach, with classical DNS resolution over a flat topography and needs further analysis. But from a first point of view the results seem to show the same trends. Our similitude approach

reduces the evaluation cost of the solution in one point of a factor around $10^3 - 10^4$ compared to the global calculation (here a mesh of around 1000 points is used) . This ratio growths in a quadratic way in 2D and in cubic one in 3D, with the problem size.

The pesticide transport problem is multiscale as it shown in figures 7.6. We can cite some characteristic dimensions such as the nozzle diameter ($\approx$ 10cm), the vinerow dimension and their spacing (few meters), the parcel dimension (few hundreds meters) and the catchment area of several thousands of km. It is obvious that considering only one scale with an adaptive mesh refinement around the sprayed area would be unrealistic in the configuration shown in 7.6. Typical agricol fields (Fig. 7.6 on the right) of $0.01 \sim 0.1 km^2$ have been considered in a region of $400 km^2$. Rows are spaced by about $1.5m$. The pesticide source sprayer moves at a speed of around $1m/s$ and the injection velocity is taken at 7 to $10m/s$ for a typical spraying of $100 kg/km^2$.

The transport-based (which is different in every point and anisotropic) and the classical Euclidean distances have been reported for a given point in Fig. 7.7. Contours represent isochronic lines of transport travel time such as in the figure 7.1. This result show five-minute isochrones from the sprayed area (in blue) with an interpolated wind field of the order of $3m\ s^{-1}$.

Mono and multi source situations (Fig. (7.5) and (7.8)) are considered and examples of the constructed flow field are shown together with the wind measurement points assimilated by the model (Fig. (7.6) and (7.8)).

The impact of ground variations on the advected species is shown in Fig. (7.9). A uniform wind field of $3ms^{-1}$ is considered and modified by the topography. The comparison with the transport in the flat topography case shows how the plume symmetry is broken in the presence of ground variation.

As the developed model is highly efficient in computing time and storage space, the model permit to identify the source of an observed pollution in short time. An example of source identification problem is shown in Fig. (7.10).

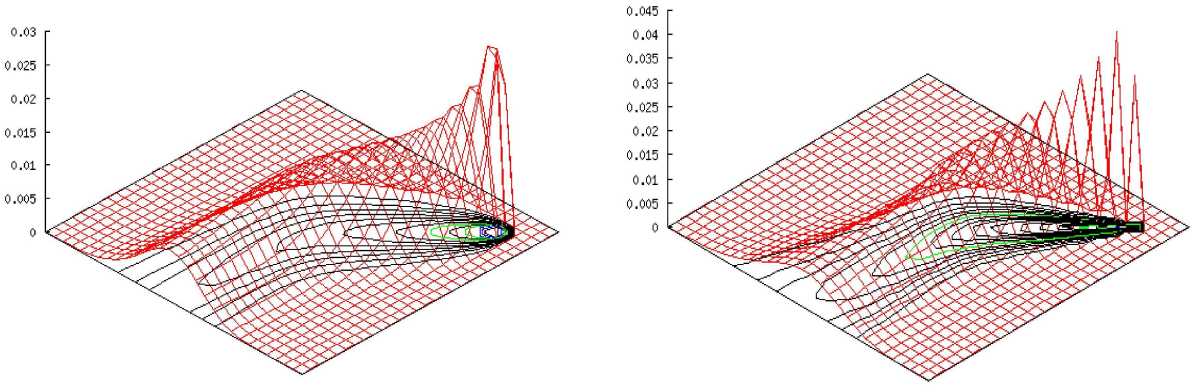

FIG. 7.5 – Generalized similitude solution (right) for a 2-point based wind (similar to Fig. 7.6) compared to a direct simulation with a PDE based on a transport-diffusion-deposition by Finite Element model for the same interpolated wind field. The calculation domain represents an area of $30 km^2$. The quantity transported are in kg. The similitude solution has been evaluated on all the nodes of the finite element mesh for comparison.

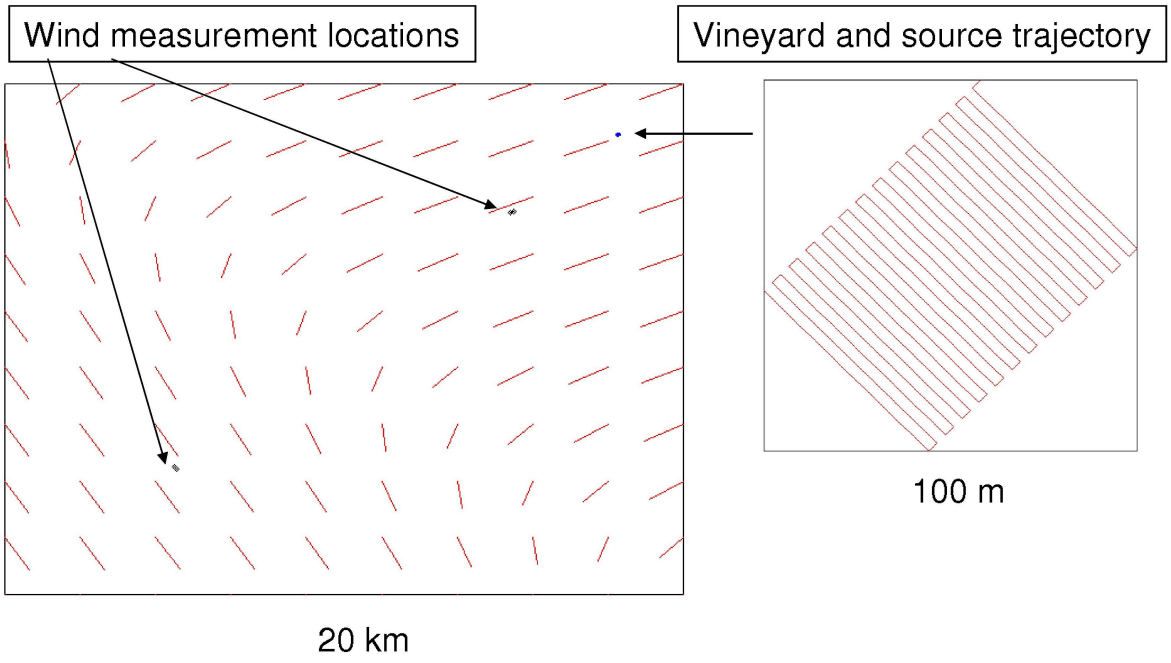

FIG. 7.6 – Typical trajectory of the vehicle in a culture of $10000m^2$ and the location of this field in a calculation domain of $400km^2$. Wind measurements based on two points have been reported together with the constructed divergence free flow field at $z = H \sim 3m$.

7.7 Concluding Remarks

A low-complexity model has been presented for the prediction of passive scalar dispersion in atmospheric flows for environmental and agricultural applications. The solution search space has been reduced using a priori physical information. A non symmetric metric based on migration times has been used to generalize injection and plume similitude solutions in the context of variable flow fields. Data assimilation has been used to define the flow field and the parameters in the dispersion model. Sensitivity analysis has been used together with this low-complexity modelling to introduce robustness issues in the prediction. In addition to the data assimilation inverse problem, inverse source reconstruction has been considered as a natural demand in environmental survilance. Current work concerns the introduction of stochastic analysis in the present model to produce regional parametric risk maps using Monte Carlo simulations which become achievable thanks to the low calculation cost of the approach.

The increase in processing velocity allows that the solution may be obtained in real time. The reduction in the amount of memory required to perform the necessary tasks in order to obtain the solution are important. Moreover the analytical expressions can be easily manipulated in post-processing and also the discretization of the domain may not be necessary in some cases.

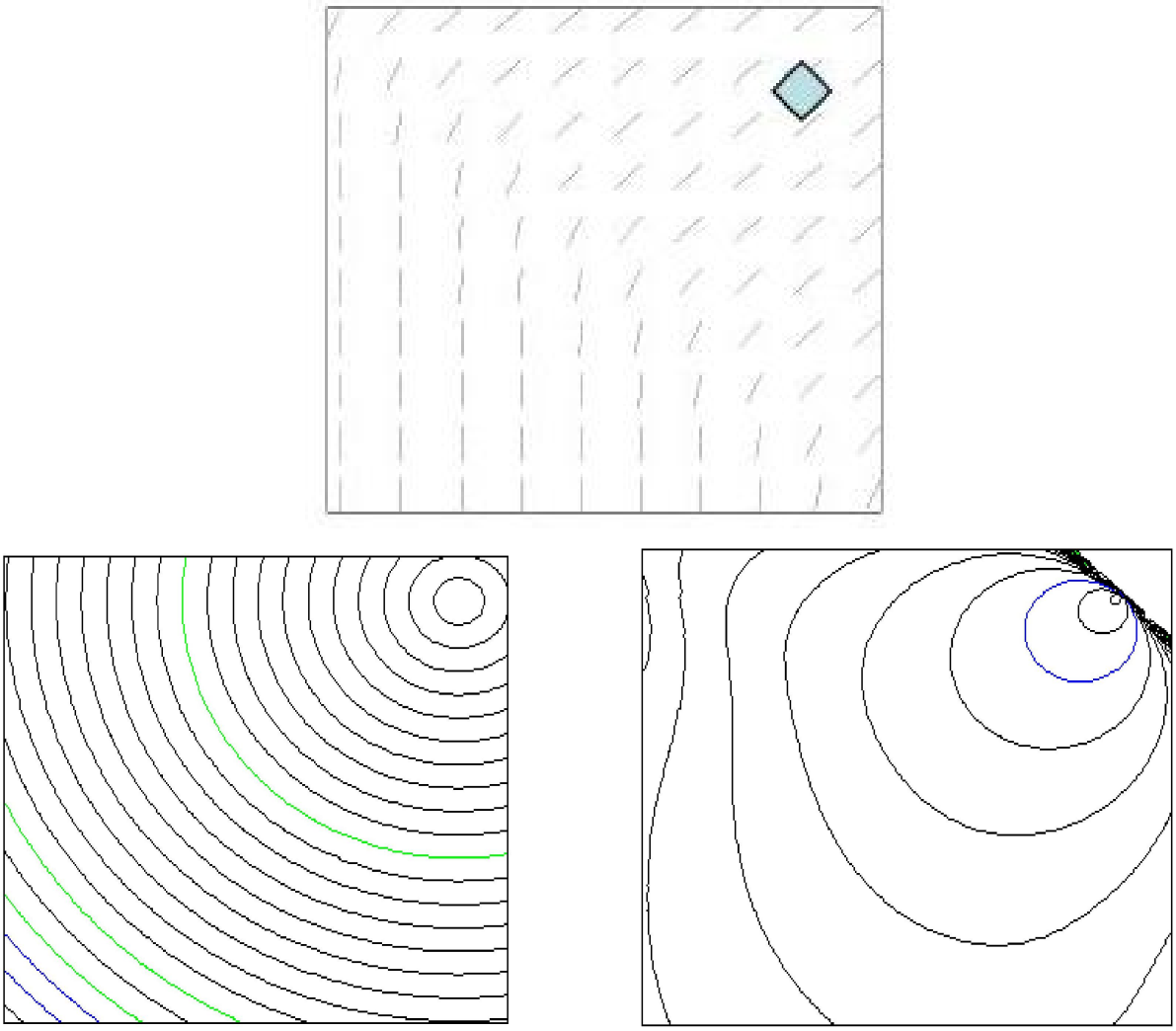

FIG. 7.7 – Examples of symmetric Euclidean and non symmetric travel time based distances over a domain of $25km^2$. The corresponding wind field is plotted above. The distance are calculated from the parcel represented in blue on the windfield.

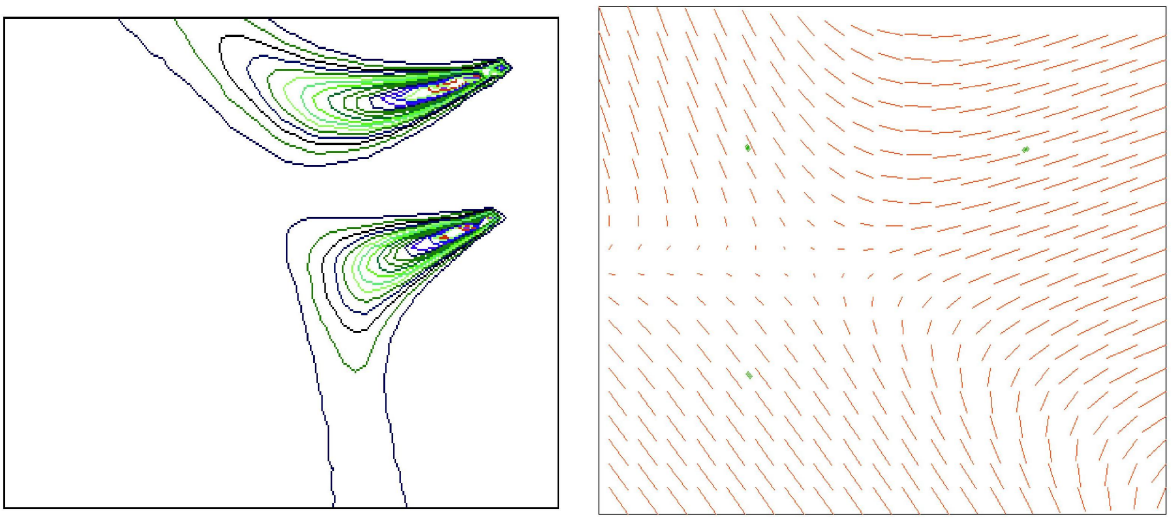

FIG. 7.8 – Regions affected from the treatment of two sources. The isolines represents normalized concentrations by the maximaum concentration. The domain calculation represents $25km^2$. The flow field has been built from three points of measurement indicated on the picture (right).

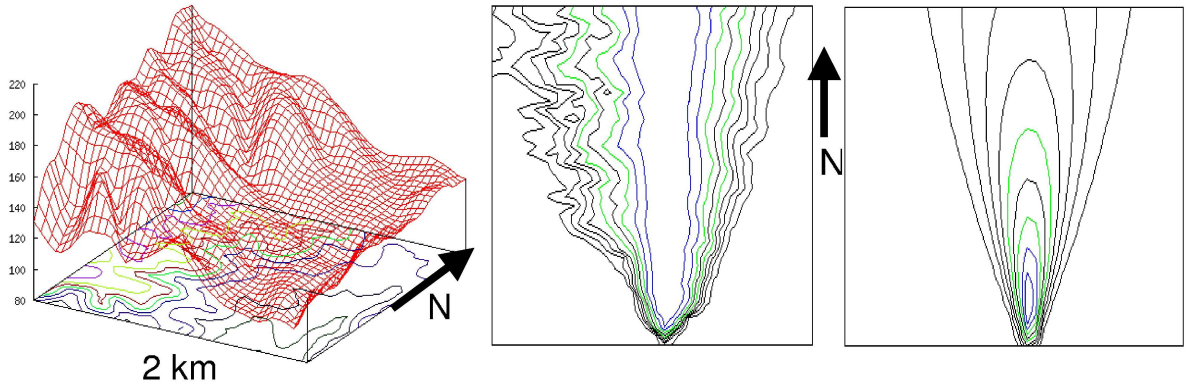

FIG. 7.9 – Left : a typical digital terrain model (x and y coordinates range over $2km$). Dispersion in a uniform north wind with (middle) and without (right) the ground model (7.2.2). Concentration are normalized by the maximum concentration.

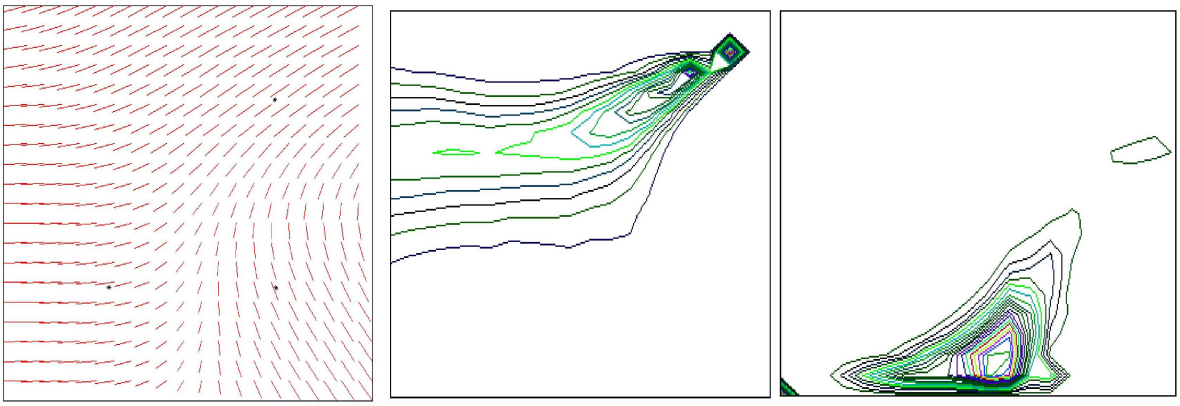

FIG. 7.10 – Left : constructed flow field over a domain of $25km^2$ from 3 observation points. Middle : dispersion from a vineyard. Right : sensitivity analysis for a dispersion detected on the lower left corner. One can therefore give possible origins of a pollution.

CONCLUSIONS

Conclusion Générale et Perspectives

Rappels

Les recherches sur la prédiction de la dispersion atmosphérique des produits phytosanitaires sont devenues une grande priorité. Leur utilisation dans les pratiques agricoles, et leur dissémination dans l'environnement entraîne un risque encore mal évalué sur notre écosystème et sur la santé publique.

Pour répondre à un besoin certain, que ce soit en terme de stratégie d'aménagement durable du territoire ou de prévention de la contamination, la modélisation numérique peut se révéler un outil puissant. Les outils de modélisation sont, par exemple, un moyen parmi d'autres pour préciser, vérifier ou conforter des solutions techniques proposées ou retenues dans le cadre de la maîtrise des risques.

Cependant, la modélisation numérique des phénomènes physiques ne saurait se suffire à elle même. Elle doit impérativement être accompagnée d'une démarche expérimentale. Il faut également rappeler qu'au delà des résultats de la modélisation (et même en amont des calculs), c'est en partie la compétence du modélisateur à la fois vis à vis du modèle lui-même que vis à vis des phénomènes à modéliser qui est d'importance.

L'acquisition de logiciels industriels est souvent coûteuse. De plus, les codes ne sont souvent pas disponibles et les documentations peu explicites, voire parfois absconses. Le temps nécessaire à leur bonne assimilation peut également demander des efforts importants. Ces logiciels qui s'utilisent comme des boites noires ont rarement été developpés spécifiquement pour la problématique traitée et ne sont donc pas nécessairement adaptés (ou necessitent un travail conséquent pour le faire).

Afin de s'affranchir de ces considérations, on a voulu développer un logiciel dédié grâce à une méthodologie innovante, par le biais d'une modélisation mathématique simplifiée de phénomènes environnementaux. D'une manière générale, il convient souvent de commencer par un modèle simple qui permettra de déterminer ensuite où il est nécessaire d'affiner les investigations.

Bilan

Cette première approche réalisée au Cemagref, permet de poser les bases théoriques et tente d'apporter une vue d'ensemble sur les problèmes liés à la modélisation de la dérive aérienne des pesticides. L'état d'avancement du projet de développement d'un modèle de dispersion atmosphérique, appliqué spécifiquement à la dérive aérienne des produits phytosanitaires, a été présenté. Des réponses simples ont été proposées, avec comme motivation finale, l'apport d'éléments d'information supplémentaires pouvant contribuer à une limitation et une meilleure gestion de la pollution.

Il faut cependant garder à l'esprit que le modèle présenté reste un outil préliminaire propre aux conditions dans lesquelles il a été mis au point et mérite donc une analyse approfondie par

le biais de différentes techniques.

Le travail a consisté à rechercher et utiliser les connaissances existantes, et à leur appliquer des raisonnements et des aspects méthodologiques classiques issus des mathématiques. Ainsi, à partir de l'observation de l'environnement, et des phénomènes qui s'y déroulent, on a voulu inclure toute cette information connue "à priori" (assimilation de lois expérimentales ou semi-expérimentales) afin de réduire la complexité des problèmes traités.

Au travers des différents développements qui ont été décrits, différents concepts de modélisation ont été balayés. On a eu recours à plusieurs modèles couplés, agissant à différents niveaux d'échelle. Ainsi, ils diffèrent tant pour l'objet auquel ils s'appliquent, que pour le formalisme choisi et pour l'utilisation qui en est faite.

L'objet principal des modèles développés est de représenter des phénomènes physiques. Pour représenter ces processus, le formalisme suivi passe par des modèles déterministes s'appuyant pour beaucoup sur les équations de la mécanique des fluides. Différentes représentations mathématiques ont été utilisées.

Enfin, les modèles développés diffèrent par leur domaine d'application. La complexité a rendu nécessaire le développement d'une approche multi-échelles. L'approche adoptée a été de développer en parallèle, plusieurs modèles et systèmes d'équations pour prendre en compte les différents processus physiques mis en jeu dans la dispersion des particules, à plusieurs échelles. Dans les applications qui ont été traitées, on a eu recours à au moins deux échelles de modélisation : une échelle de détail à laquelle certains phénomènes sont décrits précisément (petite échelle, celle d'une parcelle de vignes) et une échelle plus globale qui correspond à celle des résultats attendus (de l'ordre d'un bassin versant, échelle méso de quelques km).

Chaque modèle ou partie de modèle qui a été conçu a donc des spécificités et des objectifs qui lui sont propres. On ne saurait les utiliser dans un autre contexte. On peut par ailleurs remarquer que, sur certains aspects, approche expérimentale et modélisation se confondent en cela que ces modèles peuvent être considérés comme des outils d'expérimentation virtuelle. C'est en effet la complexité des phénomènes qui a rendu nécessaire le développement de ces modèles, la démarche de modélisation a fourni des solutions là où la démarche expérimentale aurait atteint ses limites du fait de la difficulté à maîtriser l'ensemble des variables.

L'un des buts implicites était d'étendre le domaine de validité de certains modèles connus et identifiés dans des cas précis, à des configurations plus complexes et pus générales. Pour cela, l'accent a été mis sur l'élaboration d'un modèle numérique simplifié capable, à terme, d'intégrer des champs de vent non uniformes et la topographie.

L'innovation porte sur la possibilité de retrouver les résultats connus pour les situations académiques dont les paramétrisations ont été identifiées (telles que pour des vents uniformes sur des zones plates, un exemple est traité en annexe chapitre E), tout en permettant d'inclure des phénomènes météorologiques et topographiques plus complexes.

La démarche de réduction des temps de calculs, a amené à reconsidérer la modélisation, en concentrant les efforts sur la description des phénomènes essentiels. Pour atteindre cet objectif, une revue des connaissances et des modèles déjà développés a été effectuée à chaque étape de la modélisation. Ce recensement de l'existant a permis d'identifier les paramètres les plus importants et les outils les mieux adaptés aux problèmes traités, ainsi que de procéder à une analyse critique des hypothèses sur lesquelles ils reposent.

La construction de cette plateforme a requis d'une part la description du couvert végétal et de son influence sur le flux de pulvérisation (cf partie II), et d'autre part celle des caractéristiques de la distribution des pesticides en champ proche (cf partie III) puis en champ lointain (cf partie IV). Ainsi, un modèle pour la détermination du terme source a été mis au point, puis le modèle

de transport proprement dit a été développé.

Cette aproche originale permet de prédire le devenir des polluants dans l'atmosphère et introduit de façon implicite la prise en compte de conditions météorologiques plus complexes et de la topographie, grâce à leur action sur les temps de de parcours. Il est conçu pour être un outil de prévision dans le cadre de la gestion des risques, mais il peut également été utilisé par problème inverse pour délimiter une zone d'enquête.

Perspectives et recommandations pour la poursuite des recherches

Il est nécessaire de réfléchir dès maintenant, aux améliorations futures possibles. Cela nécessite tout d'abord d'estimer les besoins des réseaux de surveillance en matière de simulation.

Ces améliorations passent également par un approfondissement de la connaissance des phénomènes physiques et chimiques mis en jeu dans les divers processus, afin d'améliorer la modélisation physique, ce qui n'était pas le but premier de cette thèse. Ainsi, l'amélioration du modèle doit suivre en parallèle l'évolution constante du savoir accumulé. Du fait de l'état des connaissances actuelles du champ d'application considéré, les voies de recherches pour l'amélioration du modèle sont vastes. Les améliorations futures sont donc en partie fonction des progrès dans la compréhension des processus (nouveaux résultats expérimentaux ou numériques facilement assimilables...). Les paramétrisations physiques des modèles peuvent notamment être améliorées, grâce à l'études de ces processus.

La recherche d'un modèle plus apte à décrire la dispersion de polluants particulaires passe par exemple par une meilleure connaissance du type de polluant transporté, ainsi que de ses possibles transformations au cours de son trajet dans le milieu dans lequel il transite. Dans le cas des pesticides, la diversité des produits utilisés et l'ajout des surfactants qui ont leurs propriétés propres rend cette tâche difficile. La prise en compte des processus typiquement rencontrés dans le dépôt, le transport des particules de pesticides et leurs interactions avec le domaine environnant (chimie, micro-physique,...) doit donc faire l'objet d'une attention plus particulière.

Il s'avère, par exemple, que les particules mesurées dans l'air sont souvent des particules émises de longue date. Ceci explique la tendance des modèles à minimiser significativement la concentration en particules. Le temps de résidence des particules dans l'air devient donc un paramètre important.

Un des problèmes récurrents pour ce type d'application sur la qualité de l'air est la quantité et la qualité des observations expérimentales disponibles. Lors de la phase applicative, nous avons été confrontés à la difficulté de trouver des campagnes de mesures en extérieur suffisamment bien renseignées pour servir à la validation d'un modèle. De telles campagnes gagneraient à être effectuées. Par exemple pour l'évaluation du terme source, d'autres essais sont souhaitables afin d'étendre la validation du modèle, notamment en termes de concentration et de flux, dans et au-dessus du couvert. L'absence d'observation impose la plus grande prudence vis-à-vis des résultats, c'est-à-dire qu'elle nécessite une estimation de l'incertitude. En sortie de modèle, les concentrations qui ne sont pas contrôlées par des observations sont en effet peu fiables.

En ce qui concerne l'étude de la végétation, la prise en compte des effets d'abri et d'écran pourrait améliorer les prévisions du modèle. Par ailleurs, l'impact des gouttes sur les feuilles qui détermine le pourcentage de la population qui sera piégée, ainsi que la capacité des feuilles à retenir le produit (modèle de captation), sont d'autres phénomènes déterminants pour évaluer l'efficacité des traitements.

La démarche proposée dans cette thèse peut être envisagée pour optimiser les flux dans la végétation vis à vis des dépôts, des pertes ou des deux simultanément.

Il faut enfin garder en mémoire que le modèle qui a été développé au niveau 2, n'a été confronté qu'à des mesures réalisées sur un seul pulvérisateur et un seul type de rang artificiel. L'utilisation de l'outil sur d'autres types de machines demandera des adaptations qui réclameront une identification expérimentale des valeurs des variables d'entrée (et éventuellement une modification de leur représentation dans le modèle) puis ensuite un validation sur des mesures en conditions réelles.

Il sera ensuite nécessaire de proposer des descriptions analytiques ou de paramétrer les fonctions déjà proposées à l'intérieur du modèle pour diverses technologies et différents réglages puis pour d'autres végétations. Ce travail pourra s'appuyer sur des données descriptives des flux de différents types de pulvérisateurs : un tel jeu de données est en cours de constitution sur tout le parc de machines d'un bassin versant. Le travail devra mettre en évidence des fonctions génériques de description des flux émis soit pour toutes les machines soit pour les différentes technologies. Le modèle pourra alors être proposé pour calculer les pertes au niveau d'une parcelle dans différentes configurations, puis au niveau d'un bassin versant.

Dans l'étude des pertes vers l'air, ni la méthode expérimentale ni le modèle ne prennent en compte **l'évaporation des gouttes**. Or, l'analyse de résultats expérimentaux, montrent que dans des conditions favorisant l'évaporation, les quantités de gouttes piégées au dessus d'une parcelle par les fils peuvent être anormalement faibles. Par ailleurs, la prise en compte de l'évaporation permettrait d'approfondir les approches classiques de calcul des quantités déportées par dérive (celles qui se déposent à proximité de la parcelle traitée). En effet, l'évaporation n'est en général pas prise en compte alors que ce phénomène joue probablement un rôle important, surtout dans les régions où les traitements se font dans des conditions relativement chaudes et sèches comme c'est le cas dans les pays du pourtour méditerranéen. Dans la soufflerie du Cemagref équipée d'un système de climatisation, cette étude pourrait être abordée par une approche expérimentale en conditions contrôlées.

Une autre amélioration possible est la création d'un module de transition champ proche-champ lointain qui assurerait l'interface entre les deux champs et la continuité physique des quantités modélisées. Le problème d'un tel modèle est qu'il est fortement dépendant des deux formulations (de champ proche et de champ lontain), et dégraderait la forme modulaire du code. Un tel module permettrait par contre une meilleure compréhension des phénomènes ayant lieu à l'interface des champs.

Comme il est par ailleurs prévu de coupler le dernier niveau du modèle (dispersion atmosphérique) avec des Modèles Numériques de Terrain (MNT) (cf thèse Nicolas Bozon) pour assimiler les données topographiques, une autre perspective à ce travail peut être de proposer l'établissement de scenarii en fonction des données descriptives des répartitions spatio-temporelles des applications (quel produit, sur quelle parcelle, à quel moment). De telles études de la répartition des applications sont menées par d'autres équipes du Cemagref : les approches peuvent faire l'objet d'un travail de couplage pour proposer un outil de prévision des contaminations à l'échelle d'une petite région.

Par ailleurs, la prise en compte de la topographie est un des éléments qui doit être amélioré. Elle est limitée à la prise en compte de certains effets élémentaires provoqués par des topographies simples. Néanmoins, le problème se complique dès lors que l'on s'intéresse à des surfaces accidentées ou hétérogènes (différentes végétations, relief, lacs, etc.) où une modélisation dans les trois directions de l'espace est nécessaire. La complexité de cette modélisation résulte d'une part, de l'aspect aléatoire et fluctuant de la turbulence devant être traitée en 3D, et d'autre part

de la difficulté à caractériser les conditions de forçage extérieur à plus grandes échelles. Celles-ci nécessitent le plus souvent des modèles traitant des échelles plus larges et intégrant des processus continentaux voire globaux. Les phénomènes les plus complexes interviennent lorsque le rayonnement solaire est couplé avec les caractéristiques topographiques (obstacles/colline, rugosités, lac-mer/brise de mer).

On peut aussi envisager d'utiliser cet outil pour tester l'influence de différents aménagements ou l'exposition de divers milieux à risque. Cette perspective suppose de caractériser les différents types d'aménagement vis-à-vis de leur influence sur la dispersion du nuage de pesticides. L'étude des haies qui modifient les flux d'air et « filtrent » les particules devra alors être approfondie. On pourra également analyser le rôle des bandes enherbées ou des zones non cultivées (zones tampons).

Rendre la simulation possible pour un environnement de type urbain, dans lequel la topographie est très singulière, est particulièrement difficile. Les phénomènes doivent souvent être traités différemment dans le cas d'une atmosphère rurale ou urbaine. Par conséquent, un modèle capable de résoudre les problèmes de dispersion de particules en zone rurale est difficilement transposable à des zones urbaines.

La température, qui joue un rôle important dans les échanges turbulents atmosphériques est prise en compte très simplement et de manière indirecte au travers de la stabilité atmosphérique. Elle nécessite une modélisation plus fine étant donné son importance sur les phénomènes météorologiques losqu'elle est couplée avec la topographie. Les polluants évoluent sous l'effet combiné de la dynamique atmosphérique et des réactions chimiques pour lesquelles la radiation solaire joue un rôle important.

Le modèle développé s'est montré pertinent, dans différentes configurations simples. Une étude critique plus approfondie doit être envisagée pour confirmer et vérifier la pertinence de la démarche développée. Un complément de validation est donc absolument nécessaire au modèle. L'étude paramétrique des grandeurs physiques conditionnant la dispersion atmosphérique ou les autres modèles est un champ d'investigation nécessaire à cette validation.

Une comparaison du modèle présenté, par exemple, avec d'autres modèles "plus matures" et dont les résultats ont déjà été validés est indispensable pour permettre de discuter des résultats obtenus. Mais cette inter-comparaison des modèles pose de nombreuses difficultés et nécessite notamment une normalisation des entrées-sorties.

Cinquième partie

APPENDICES

Annexe A

Reduced-order modeling

A.1 Principles

Modeling and simulation of dynamical systems is a very important task in the engineering sciences - and differential equations have proven to be one of the most sucessful means of modeling such systems. Solutions of (nonlinear) complex systems are expensive with respect to both storage and CPU costs. As a result, it is difficult if not impossible to deal with a number of situations such as : parametric studies of state solutions ; optimization and control problems (multiple state solutions) ; and feedback control settings (real-time state solutions).

Not surprisingly, a lot of attention has been paid to reducing the costs of the nonlinear state solutions by using reduced-order models for the state ; these are low-dimensional approximations to the state. Reduced-order modeling has been and remains a very active research direction in many seemingly disparate fields. To obtain a simpler model, there is basically two choices :

- The use of experience and engineering intuition to generate a simpler and thus more tractable model, or
- to employ approximation procedures based on mathematics to perform the model reduction.

A.2 Reduced-Order Modelling

Consider the calculation of a state variable $\mathbf{U}(\mathbf{x})$, function of independent variables $\mathbf{x}$. Our aim is to define a suitable search space for the solution $\mathbf{U}(\mathbf{x})$ instead of considering a general function space. The search space can be restricted, by limiting the possible choices of the basis function. This former approach is what one does in finite element methods, for instance, where the solution is expressed in some subspace $\mathbf{S}(\{\mathbf{W}_N\})$ described by the functional basis chosen $\mathbf{W}_N$, with the quality of the solution being monitored either through the mesh quality (h-methods where the polynomial degree is fixed and the mesh is refined) or increasing the order of the finite element (p-methods where the mesh is fixed and the spectral order of the ansatz functions is increased) [125]. In all cases, the size of the problem is large $1 << N < \infty$ and if the approach is consistent, the projected solution tends to the exact solution when $N \longrightarrow \infty$.

In a low-complexity approach, one replace the calculation of $\mathbf{U}(\mathbf{x})$ by a projection over a subspace $\mathbf{S}(\mathbf{w}_n)$ generated this time, for instance, by $\mathbf{w}_n$, a family of solutions ("snapshots") of the initial full direct model ($\mathbf{x} \longrightarrow \mathbf{U}(\mathbf{x})$). In particular, one aims $n << N$.

One aims to use a priori information in the definition of the search space for the solution

and avoid the solution of partial differential equations. In our approach, one aims to remove the calculation of the snapshots as this is not always an easy task. One would like to take advantage of what one knows on the physic of the problem and replace the direct model $\mathbf{x} \longrightarrow \mathbf{U}(\mathbf{x})$ by an approximate model $\mathbf{x} \longrightarrow \mathbf{u}(\mathbf{x})$ easier to evaluate.

Annexe B

Derivations of the Gaussian Plume dispersion model

B.1 Derivation of the Gaussian Plume dispersion model

This paragraph presents the derivation of the Gaussian Plume Dispersion model for a pollutant release from a ground source. This is accomplished by a *K-diffusion* equation given by equation :

$$\frac{\partial c}{\partial t} = K_{c_x}\frac{\partial^2 c}{\partial x^2} + K_{c_y}\frac{\partial^2 c}{\partial y^2} + K_{c_z}\frac{\partial^2 c}{\partial z^2}, \tag{B.1}$$

where $c(x, y, , z, t)$ is the ensemble-average concentration ($[kgm^{-3}]$), M is the mass of contaminant released $t = 0$ ($[kg]$), x, y, z are the coordinates relative to the centre of mass of the plume ($[m]$),

The usual practice is to adopt a coordinate system where the x-axis is along the direction of the mean wind, U, the y-axis is in the cross-wind direction, i.e. perpendicular to the x-axis and horizontal, and the z-axis is vertical. The following conditions are added :

– initial conditions :

$$c(x, y, z, 0) = 0, \text{ for } x \neq 0, y \neq 0, z \neq 0 \tag{B.2}$$

– boundary conditions : Pollutant concentration tends to zero at large distances from the source $c \to 0$ as $|x|, |y|, z \to +\infty$

$$c(\pm\infty) \longrightarrow 0; \nabla c(\pm\infty, t) \longrightarrow 0 \tag{B.3}$$

– continuity :

$$\int_{-\infty}^{+\infty}\int_{-\infty}^{+\infty}\int_{-\infty}^{+\infty} c(x, y, z, t)\mathrm{d}x\mathrm{d}y\mathrm{d}z = M \tag{B.4}$$

where M is the mass of the release $[kg]$.

The forward and reverse three-dimensional Fourier transform of the species is given by :

$$F(\boldsymbol{k}, t) = \frac{1}{(2\pi)^{3/2}}\int_{-\infty}^{+\infty}\int_{-\infty}^{+\infty}\int_{-\infty}^{+\infty} c(\mathbf{x}, t)\exp(-i\boldsymbol{k}\cdot\boldsymbol{x})\mathrm{d}x\mathrm{d}y\mathrm{d}z \tag{B.5}$$

$$c(\boldsymbol{x},t) = \frac{1}{(2\pi)^{3/2}} \int_{-\infty}^{+\infty} \int_{-\infty}^{+\infty} \int_{-\infty}^{+\infty} F(\boldsymbol{k},t) \exp(-i\boldsymbol{k}\cdot\boldsymbol{x}) \mathrm{d}k_x \mathrm{d}k_y \mathrm{d}k_z \tag{B.6}$$

The derivative of equation (B.5) with respect to time is

$$\frac{\partial F}{\partial t} = \frac{1}{(2\pi)^{3/2}} \int_{-\infty}^{+\infty} \int_{-\infty}^{+\infty} \int_{-\infty}^{+\infty} \frac{\partial c(\mathbf{x},t)}{\partial t} \exp(-i\boldsymbol{k}\cdot\boldsymbol{x}) \mathrm{d}x\mathrm{d}y\mathrm{d}z \tag{B.7}$$

Substitution of equation (B.1) gives

$$\frac{\partial F}{\partial t} = \frac{1}{(2\pi)^{3/2}} \int_{-\infty}^{+\infty} \int_{-\infty}^{+\infty} \int_{-\infty}^{+\infty} \left[K_{X_c} \frac{\partial^2 c}{\partial x^2} + K_{Y_c} \frac{\partial^2 c}{\partial y^2} + K_{Z_c} \frac{\partial^2 c}{\partial z^2} \right] \exp(-i\boldsymbol{k}\cdot\boldsymbol{x}) \mathrm{d}x\mathrm{d}y\mathrm{d}z \tag{B.8}$$

Evaluation of the integral term in equation (B.8) for the x-component can be found as follows

$$\int_{-\infty}^{+\infty} \int_{-\infty}^{+\infty} \int_{-\infty}^{+\infty} \frac{\partial^2 c}{\partial x^2} \exp(-i\boldsymbol{k}\cdot\boldsymbol{x}) \mathrm{d}x\mathrm{d}y\mathrm{d}z = \tag{B.9}$$

$$\int_{-\infty}^{+\infty} \int_{-\infty}^{+\infty} \left(\int_{-\infty}^{+\infty} \frac{\partial^2 c}{\partial x^2} \exp(-ik_x x) \mathrm{d}x \right) \exp(-ik_y y) \exp(-ik_z z) \mathrm{d}y\mathrm{d}z \tag{B.10}$$

The inner-integal can be solved by integrating by parts

$$\int_{-\infty}^{+\infty} \frac{\partial^2 c}{\partial x^2} \exp(-ik_x x) \mathrm{d}x = \exp(-ik_x x) \frac{\partial c}{\partial x}\bigg|_{-\infty}^{+\infty} + (ik) \int_{-\infty}^{+\infty} \frac{\partial c}{\partial x} \exp(-ik_x x) \mathrm{d}x \tag{B.11}$$

The first term in this equation can be neglected since the boundary condition specified by equation (B.3) indicates that this term is approximated zero. Integrating the second term by parts and enforcing the same boundary conditions gives

$$\int_{-\infty}^{+\infty} \frac{\partial^2 c}{\partial x^2} \exp(-ik_x x) \mathrm{d}x = \quad (ik_x) \exp(-ik_x x) c|_{-\infty}^{+\infty} + (ik_x)^2 \textstyle\int_{-\infty}^{+\infty} x \exp(-ik_x x) \mathrm{d}x \tag{B.12}$$

$$= \qquad (ik_x)^2 \textstyle\int_{-\infty}^{+\infty} c \exp(-ik_x x) \mathrm{d}x \tag{B.13}$$

Substitution of this result back into equation (B.10) gives

$$\int_{-\infty}^{+\infty} \int_{-\infty}^{+\infty} \int_{-\infty}^{+\infty} \frac{\partial^2 c(x,t)}{\partial x^2} \exp(-i\boldsymbol{k}\cdot\boldsymbol{x}) \mathrm{d}x\mathrm{d}y\mathrm{d}z = \tag{B.14}$$

$$\int_{-\infty}^{+\infty} \int_{-\infty}^{+\infty} \left((ik_x)^2 \int_{-\infty}^{+\infty} c \exp(-ik_x x) \mathrm{d}x \right) \exp(-ik_y y) \exp(-ik_z z) \mathrm{d}y\mathrm{d}z = \tag{B.15}$$

$$\int_{-\infty}^{+\infty} \int_{-\infty}^{+\infty} \int_{-\infty}^{+\infty} (ik_x)^2 c \exp(-ik_x x) \exp(-ik_y y) \exp(-ik_z z) \mathrm{d}x\mathrm{d}y\mathrm{d}z = \tag{B.16}$$

$$\int_{-\infty}^{+\infty} \int_{-\infty}^{+\infty} \int_{-\infty}^{+\infty} (ik_x)^2 c \exp(-i\boldsymbol{k}\cdot\boldsymbol{x}) \mathrm{d}x\mathrm{d}y\mathrm{d}z \tag{B.17}$$

Repeating this procedure for the y- and z-componets of the species concentration c results in

$$\int_{-\infty}^{+\infty} \int_{-\infty}^{+\infty} \int_{-\infty}^{+\infty} \frac{\partial^2 c}{\partial y^2} \exp(-i\boldsymbol{k}\cdot\boldsymbol{x}) \mathrm{d}x\mathrm{d}y\mathrm{d}z = \int_{-\infty}^{+\infty} \int_{-\infty}^{+\infty} \int_{-\infty}^{+\infty} (ik_y)^2 c \exp(-i\boldsymbol{k}\cdot\boldsymbol{x}) \mathrm{d}x\mathrm{d}y\mathrm{d} \tag{B.18}$$

$$\int_{-\infty}^{+\infty}\int_{-\infty}^{+\infty}\int_{-\infty}^{+\infty}\frac{\partial^2 c}{\partial z^2}\exp(-i\boldsymbol{k}\cdot\boldsymbol{x})\mathrm{d}x\mathrm{d}y\mathrm{d}z = \int_{-\infty}^{+\infty}\int_{-\infty}^{+\infty}\int_{-\infty}^{+\infty}(ik_z)^2 c\exp(-i\boldsymbol{k}\cdot\boldsymbol{x})\mathrm{d}x\mathrm{d}y\mathrm{d}z \quad \text{(B.19)}$$

Substitution of (B.17), (B.18), and (B.19) back into equation (B.8) gives

$$\frac{\partial F}{\partial t} = \frac{1}{(2\pi)^{3/2}}(K_{c_x}k_x^2 + K_{c_y}k_y^2 + K_{c_z}k_z^2)\int_{-\infty}^{+\infty}\int_{-\infty}^{+\infty}\int_{-\infty}^{+\infty} c\exp(-i\boldsymbol{k}\cdot\boldsymbol{x})\mathrm{d}x\mathrm{d}y\mathrm{d}z \quad \text{(B.20)}$$

Using the defintion (B.5) for F, the above equation reduces to

$$\frac{\partial F}{\partial t} = -(K_{c_x}k_x^2 + K_{c_y}k_y^2 + K_{c_z}k_z^2)F \quad \text{(B.21)}$$

Which can be integrated as

$$\begin{aligned}
\frac{\partial}{\partial t}(\log(F)) &= -(K_{c_x}k_x^2 + K_{c_y}k_y^2 + K_{c_z}k_z^2) && \text{(B.22)}\\
\log(F) &= -(K_{c_x}k_x^2 + K_{c_y}k_y^2 + K_{c_z}k_z^2)t + A(k) && \text{(B.23)}\\
F(\boldsymbol{k},t) &= B\exp\left[-(K_{c_x}k_x^2 + K_{c_y}k_y^2 + K_{c_z}k_z^2)t\right] && \text{(B.24)}\\
&= B\exp(-(K_{c_x}k_x^2)t)\exp(-(K_{c_x}k_x^2)t)\exp(-(K_{c_x}k_x^2)t) && \text{(B.25)}
\end{aligned}$$

The initial condition given by (B.2), the definition of F given by (B.5) and the continuity equation are used to define the constant B as

$$\begin{aligned}
F(\mathbf{k},0) &= B && \text{(B.26)}\\
&= \tfrac{1}{(2\pi)^{3/2}}\int_{-\infty}^{+\infty}\int_{-\infty}^{+\infty}\int_{-\infty}^{+\infty} c(\mathbf{x},0)\exp(i\mathbf{k}\cdot\mathbf{x})\mathrm{d}x\mathrm{d}y\mathrm{d}z && \text{(B.27)}\\
&= \lim_{\epsilon\to 0}\tfrac{1}{(2\pi)^{3/2}}\int_{-\epsilon}^{+\epsilon}\int_{-\epsilon}^{+\epsilon}\int_{-\epsilon}^{+\epsilon} c(\mathbf{x},0)\mathrm{d}x\mathrm{d}y\mathrm{d}z = \tfrac{M}{(2\pi)^{3/2}} && \text{(B.28)}
\end{aligned}$$

Therefore, equation (B.25) is given by

$$F(\mathbf{k},t) = \frac{M}{(2\pi)^{3/2}}\exp\left(-K_{C_x}k_x^2t\right)\exp\left(-K_{C_y}k_y^2t\right)\exp\left(-K_{C_z}k_z^2t\right) \quad \text{(B.29)}$$

To determine $c(\mathbf{x},t)$, substitute equation (B.29) into equation (B.6) and solve :

$$\begin{aligned}
c(\mathbf{x},t) = {} & \tfrac{M}{(2\pi)^{3/2}}\int_{-\infty}^{+\infty}\int_{-\infty}^{+\infty}\int_{-\infty}^{+\infty}\exp\left(-K_{C_x}k_x^2t\right)\exp\left(-K_{C_y}k_y^2t\right)\exp\left(-K_{C_z}k_z^2t\right) && \text{(B.30)}\\
& \times\exp\left(i\mathbf{k}\cdot\mathbf{x}\right)\mathrm{d}k_x\mathrm{d}k_y\mathrm{d}k_z && \text{(B.31)}\\
= {} & \tfrac{M}{(2\pi)^{3/2}}\left(\int_{-\infty}^{+\infty}\exp\left(-K_{C_x}k_x^2t\right)\mathrm{d}k_x\right)\left(\int_{-\infty}^{+\infty}\exp\left(-K_{C_y}k_y^2t\right)\mathrm{d}k_y\right) && \text{(B.32)}\\
& \times\left(\int_{-\infty}^{+\infty}\exp\left(-K_{C_z}k_z^2t\right)\mathrm{d}k_z\right) && \text{(B.33)}
\end{aligned}$$

The individial integrations are carried out as follows :

$$\begin{aligned}
&\int_{-\infty}^{+\infty}\exp\left(-K_{C_x}k_x^2t\right)\exp(\mathbf{i}k_xx)\mathrm{d}k_x = && \text{(B.34)}\\
&\int_{-\infty}^{+\infty}\exp\left(-K_{C_x}k_x^2t\right)\left[cos(k_xx) + \mathbf{i}sin(k_xx)\right]\mathrm{d}k_x && \text{(B.35)}\\
&= \int_{-\infty}^{+\infty}\exp -K_{C_x}k_x^2tcos(k_xx)\mathrm{d}k_x && \text{(B.36)}\\
&+\mathbf{i}\int_{-\infty}^{+\infty}\exp -K_{C_x}k_x^2tsin(k_xx)\mathrm{d}k_x && \text{(B.37)}
\end{aligned}$$

Note that the integration over infinite limits of an odd function is zero. Continuing then gives

$$\int_{-\infty}^{+\infty} \exp\left(-K_{C_x} k_x^2 t\right) \exp(\mathbf{i} k_x x) \mathrm{d}k_x = \int_{-\infty}^{+\infty} \exp\left(-K_{C_x} k_x^2 t\right) cos(k_x x) \mathrm{d}k_x \tag{B.38}$$

$$= \left[\frac{\pi^{1/2}}{(K_{C_x} t)^{1/2}} \exp\left(-\frac{x^2}{4k_x t}\right)\right] \tag{B.39}$$

$$= \frac{2\pi}{\sqrt{4\pi K_{C_x} t}} \exp\left(-\frac{x^2}{4k_x t}\right) \tag{B.40}$$

$$= \frac{2\pi}{\sqrt{2\pi}\sigma_x} \exp\left(-\frac{x^2}{2\sigma_x^2}\right) \tag{B.41}$$

Repeating this procedure for the y- and z-components gives

$$\int_{-\infty}^{+\infty} \exp\left(-K_{C_y} k_y^2 t\right) \exp(\mathbf{i} k_y y) \mathrm{d}k_y = \frac{2\pi}{\sqrt{2\pi}\sigma_y} \exp\left(-\frac{y^2}{2\sigma_y^2}\right) \tag{B.42}$$

$$\int_{-\infty}^{+\infty} \exp\left(-K_{C_z} k_z^2 t\right) \exp(\mathbf{i} k_z z) \mathrm{d}k_z = \frac{2\pi}{\sqrt{2\pi}\sigma_z} \exp\left(-\frac{z^2}{2\sigma_z^2}\right) \tag{B.43}$$

Substituting equations (B.41), (B.42), and (B.43) into equation (B.33) gives finally

$$c(\mathbf{x}, t) = \frac{M}{(2\pi)^{3/2} \sigma_x \sigma_y \sigma_z} \exp\left[-\left(\frac{x^2}{2\sigma_x^2} + \frac{y^2}{2\sigma_y^2} + \frac{z^2}{2\sigma_z^2}\right)\right] \tag{B.44}$$

This is the Gaussian Plume equation for a ground-level pollutant release. σ_x, σ_y, and σ_z represent the standard deviations (the spread of the plume and also known as the dispersion coefficients $[m]$) of the Gaussian distribution in the x, y and z directions. They increase downstream, i.e. $\sigma_x = \sigma_x(x)$, $\sigma_y = \sigma_y(x)$ and $\sigma_z = \sigma_z(x)$. These functions determine the nature of the result and have to be estimated empirically. They are also often given in the following form :

$$\sigma_x = \sqrt{2K_{x_c} t},\ \sigma_y = \sqrt{2K_{y_c} t},\ \sigma_z = \sqrt{2K_{z_c} t} \tag{B.45}$$

B.2 Self-similar approach

For simplicity of presentation, only one-dimensional spreading is considered. Assume that $Q([kg\ s^{-1}])$ are emitted over a line of length H parallel to the y-axis. There are no solid boundaries. The governing equation for the mean concentration then becomes

$$\overline{u} \frac{\partial \overline{c}}{\partial x} = K_x \frac{\partial^2 \overline{c}}{\partial z^2} \tag{B.46}$$

which is identical to the unsteady heat equation if we recognize that $t = x/\overline{u}$.

The initial and boundary conditions determine the solution. Many solutions of equation (B.46) are given in advanced heat transfer books.

An alternative way to show the rationale behind the solution used in (B.1), is to seek self-similar solutions. By "self-similar" one means solutions that depend on one independent variable only, which is a combination of the two dependent variables t and z. Most slender turbulent

flows are self-similar for the velocity and the scalar fields (see also 5.5)). Let be a function $f_c(\eta)$, such that

$$\overline{c} = c_0 f_c(\eta) \tag{B.47}$$

$$\eta = \frac{z}{\sigma} \tag{B.48}$$

with c_0 and s being a function of x only. The quantity c_0 is a characteristic scale of the concentration, while σ is a characteristic width of the plume, both as yet undetermined.

The following transformation rules are used :

$$\frac{\partial f_c}{\partial x} = \frac{\partial f_c}{\partial \eta}\frac{\partial \eta}{\partial x} \tag{B.49}$$

$$\frac{\partial \overline{c}}{\partial z} = \frac{\partial \overline{c}}{\partial \eta}\frac{1}{\sigma} \tag{B.50}$$

and from equation (B.48)

$$\frac{\partial \eta}{\partial x} = -\frac{\eta}{\sigma}\frac{\partial \sigma}{\partial x} \tag{B.51}$$

Using the above and substituting equation (B.47) and (B.48) in (B.46) gives :

$$\left(\overline{u}\frac{\mathrm{d}c_0}{\mathrm{d}x}\right) f_c + \left(-\frac{\overline{u}c_0}{\sigma}\frac{\mathrm{d}\sigma}{\mathrm{d}x}\right)\eta\frac{\mathrm{d}f_c}{\mathrm{d}\eta} = \left(\frac{Kc_0}{\sigma^2}\right)\frac{\mathrm{d}^2 f_c}{\mathrm{d}\eta^2} \quad \Leftrightarrow \tag{B.52}$$

$$\frac{\mathrm{d}^2 f_c}{\mathrm{d}\eta^2} + \left(\frac{\overline{u}\sigma}{K}\frac{\mathrm{d}\sigma}{\mathrm{d}x}\right)\eta - \left(\frac{\overline{u}\sigma^2}{Kc_0}\frac{\mathrm{d}c_0}{\mathrm{d}x}\right) f_c = 0 \tag{B.53}$$

If self-similar solutions are wanted, the terms in brackets in equation (B.53) must be independent of x, i.e. constants. Let us consider the term $\frac{\overline{u}\sigma}{K}\frac{\mathrm{d}\sigma}{\mathrm{d}x}$ first. Without loss of generality, it could be said that this constant is unity (if it were anything else, σ could be altered so that it is). This results in :

$$\frac{\overline{u}\sigma}{K}\frac{\mathrm{d}\sigma}{\mathrm{d}x} = 1 \Leftrightarrow K = \frac{\overline{u}}{2}\frac{\mathrm{d}\sigma^2}{\mathrm{d}x} \tag{B.54}$$

For long times, K is constant and equation (B.54) gives that $\sigma^2 = 2K\frac{x}{\overline{u}}$., i.e. we recovered equation (B.45).

For short times, the diffusivity is proportional to u' and the characteristic length of eddies inside the plume. This is σ, i.e. the width of the plume itself, since the plume cannot be mixed by eddies greater than its size (see 1.1.5). So for short times, $K = u'\sigma$, which gives $\sigma = \frac{u'}{\overline{u}}x$. The way how the width of the plume grows with x is also determined : for long times, $\sigma \sim x^{1/2}$, while for short times $\sigma \sim x$.

The second requirement for self-similar solutions is that the term $\frac{\overline{u}\sigma^2}{Kc_0}\frac{\mathrm{d}c_0}{\mathrm{d}x}$ be independent of x. $\mathrm{d}c_0/\mathrm{d}x$ can relate to $\mathrm{d}\sigma/\mathrm{d}x$ by examining the overall conservation of mass of the (inert)

pollutant. Integrating across any section of the plume gives

$$\int_{-\infty}^{\infty} \overline{c}\mathrm{d}z = \frac{Q}{\overline{u}H} \Leftrightarrow c_0\sigma \int_{-\infty}^{\infty} f_c(\eta)\mathrm{d}\eta = \frac{Q}{\overline{u}H} \tag{B.55}$$

Denote the integral above by I_0. Since it is a function of η only, it is independent of x. Therefore, $c_0\sigma$ is a constant, which gives that

$$\frac{1}{c_0}\frac{\mathrm{d}c_0}{\mathrm{d}x} = -\frac{1}{\sigma}\frac{\mathrm{d}\sigma}{\mathrm{d}x} \tag{B.56}$$

Therefore, equation (B.53) becomes

$$\frac{\mathrm{d}^2 f_c}{\mathrm{d}\eta^2} + \eta\frac{\mathrm{d}f_c}{\mathrm{d}\eta} + f = 0 \tag{B.57}$$

with boundary conditions

$$f_c(0) = 1, \quad f_c'(0) = 0 \tag{B.58}$$

and the solution should obey $f_c(\pm\infty) \to 0$. It is very easy to confirm that a function satisfying all the above is

$$f(\eta) = \exp(-\eta^2/2) \tag{B.59}$$

(This can also be derived by solving equation (B.57) directly). From equation (B.55), it is also found that $c_0 \sim \sigma^{-1}$, i.e. the characteristic scale of the pollutant concentration decreases as $x^{-1/2}$ for long times and as x^{-1} for short times. The problem is almost solved now. The mean concentration is given by

$$\overline{c} = \frac{1}{I_0}\frac{Q/H}{\overline{u}\sigma} f_c(\eta) \tag{B.60}$$

Using equation (B.59) and the fact that

$$I_0 = \int_{-\infty}^{\infty} \exp^{(-\eta^2)}\mathrm{d}\eta = \frac{1}{\sqrt{2\pi}} \tag{B.61}$$

Equation (B.62) gives the final result for the concentration :

$$\overline{c} = \frac{Q/H}{\sqrt{2\pi}\overline{u}\sigma}\exp^{(-\frac{z^2}{\sigma^2})} \tag{B.62}$$

It has been shown how the concept of self-similarity and the overall conservation of pollutant mass gave the scaling of characteristic width and centerline concentration with downwind distance. This approach can be extended to more dimensions. For example, for two dimensional spreading, put $\overline{c} = c_0 f(\eta)g(\zeta)$ with $\eta = z/\sigma_z$ and $\zeta = y/\sigma_y$. Repeating the procedure to seek self-similar solutions will result in the 2D Gaussian equation.

B.3 Laplace transform approach

To solve the 1D-ADE for $f(x,t)$ as an initial value problem, start with a Laplace transform in time

$$\int_0^\infty \exp(i\omega t)\left[\frac{\partial f}{\partial t} + u\frac{\partial f}{\partial x} - D\frac{\partial^2 f}{\partial x^2}\right]\mathrm{d}t = \quad 0 \quad \mathcal{I}m(\omega) > 0 \tag{B.63}$$

The condition $\mathcal{I}m(\omega) > 0$ is here mandatory to ensure causality. Integrate the first term by parts and substitute a Dirac function $f(t,0) = f_0(x) = \delta(x - x_0)$ for the initial condition

$$f\exp(i\omega t)|_0^\infty + \int_0^\infty \exp(i\omega t)\left[-i\omega t + u\frac{\partial f}{\partial x} - D\frac{\partial^2 f}{\partial x^2}\right]\mathrm{d}t \tag{B.64}$$

$$-\delta(x - x_0) + \left[-i\omega f(x,\omega) + u\frac{\partial f(x,\omega)}{\partial x} - D\frac{\partial^2 f(x,\omega)}{\partial x^2}\right] \tag{B.65}$$

using here the notation $f(x,\omega)$ for the Laplace transform in time of $f(x,t)$. Spatial derivatives can be dealt with a simple Fourier transform

$$\int_{-\infty}^\infty \exp(ikt)\left[-\delta(x - x_0) - i\omega f(x,\omega) - iukf(x,\omega) + Dk^2 f(x,\omega)\right]\mathrm{d}x \tag{B.66}$$

which yields an explicit solution for the Fourier-Laplace transformed function

$$f(k,\omega) = \frac{i\exp(-ikx_0)}{\omega + uk + iDk^2} \tag{B.67}$$

This has a pole in the complex plane for $\omega = -uk - iDk^2$ and needs to be taken into account when inverting the Laplace transform

$$f(k,t) = \int_{-\infty+iC}^{+\infty+iC} \tfrac{1}{2\pi}\exp(-i\omega t)\left(\frac{-i\exp(-ikx_0)}{\omega + uk + iDk^2}\right)\mathrm{d}\omega \quad C > 0 \tag{B.68}$$

$$= 2\pi i\left(-\frac{i}{2\pi}\exp(-i[-uk - iDk^2]t)\exp(-ikx_0)\right) \tag{B.69}$$

$$= \exp(ik[ut - x_0])\exp(-Dk^2 t) \tag{B.70}$$

where the *residue theorem* has been used to calculate the integral along the positive real frequencies and closing the contour in the positive half plane where the Laplace integral decays exponentially. Inverting the Fourier integral

$$f(x,t) = \int_{-\infty}^{+\infty} \tfrac{1}{2\pi}\exp(ikx)\left[\exp(ik(ut - x_0))\exp(-Dk^2 t)\right]\mathrm{d}k \tag{B.71}$$

$$= \frac{1}{2\pi}\int_{-\infty}^{+\infty} \exp\left[ik\exp(x - x_0 + ut)\exp(-Dk^2 t)\right]\mathrm{d}k \tag{B.72}$$

$$\tag{B.73}$$

Using the following formula

$$\int_{-\infty}^{+\infty} \exp(-p^2x^2)\exp(\pm qx)\mathrm{d}x = \frac{\sqrt{\pi}}{p}\exp\left(\frac{q^2}{4p^2}\right) \quad p > 0 \tag{B.74}$$

with $p = Dt$ and $q = i(x - x_0 + ut)$, this finally yields the explicit solution

$$f(x,t) = \frac{1}{2\sqrt{\pi Dt}} \exp\left(-\frac{(x - x_0 + ut)^2}{4Dt}\right) \tag{B.75}$$

It shows explicitly the characteristic $x - x_0 + ut = 0$.

Annexe C

Numerical implementation for the burger equation

We use an possible extension of upwind scheme for the numerical resolution. This is not the only one approach possible. There exits an abundant litterature on the first-order non linear hyperbolic equation resolution. This problem is often difficult. We consider the following Burgers equation :

$$u_t + uu_r = \nu u_{rr} + g(u, r) \tag{C.1}$$
$$u_t + 0.5(u^2)_r = g(u, r), \text{ sur } (-1, 1) \tag{C.2}$$
$$u(t, r_0) = u_0(t), \ u(0, r_0) = 0 \tag{C.3}$$

The resolution could be made by considering the non conservative form :

$$\frac{\partial u}{\partial t} + u\frac{\partial u}{\partial r} = g(u, r) \tag{C.4}$$

The numerical treatment use finite dimensional space and finite difference. The interval $[r_0, r_1]$ is discretizing in k sub-intervals. Then, one has $k+1$ points of discretization. If uniform discretization with constant spatial step $\Delta x = h$ are considered and we note $(t^{n+1} - t^n) = \Delta t$, then we have

$$\frac{\partial u(x_i, t^n)}{\partial t} = \frac{u_i^{n+1} - u_i^n}{\Delta t} - \text{ (forward order 1, time)} \tag{C.5}$$
$$\frac{\partial u(x_i, t^n)}{\partial x} = \frac{u_{i+1}^n - u_{i-1}^n}{2h} - \frac{h^2}{6}u'''(\theta_i) \text{ (central order 1, spatial)} \tag{C.6}$$
$$\frac{\partial^2 u(x_i, t^n)}{\partial x^2} = \frac{u_{i+1}^n - 2u_i^n + u_{i-1}^n}{2h} + \frac{h^2}{12}u^{(4)}(\theta_i) \text{ (central order 2, spatial)} \tag{C.7}$$

Then,

$$u(x_i, t^n)u_x(x_i, t^n) = \frac{1}{2}(u(x_i, t^n)^2)_x \sim \frac{1}{2}\frac{(u_{i+1}^n)^2 - (u_{i-1}^n)^2}{2h} \tag{C.8}$$

$$u_i^{n+1} = u_i^n + \Delta t\left(-\frac{1}{2}\frac{(u_{i+1}^n)^2 - (u_{i-1}^n)^2}{2h} + \nu\frac{u_{i+1}^n - 2u_i^n + u_{i-1}^n}{h^2} + g(u_i^n, x_i^n)\right) \tag{C.9}$$

We use this stabilized sheme with a particularly simple Runge-Kutta time integrator introduced by Jameson-Schmidt-Turkel (R-K3 [JST]). The idea is each time step is divided into s substeps, which taken together approximate the update to s'th order.

Taylor's theorem tell us that :

$$u(t+\mathrm{d}t) = \left(1 + \frac{\mathrm{d}t}{1!}\left\{\frac{d}{\mathrm{d}t}\right\} + \frac{\mathrm{d}t^2}{2!}\left\{\frac{d}{\mathrm{d}t}^2\right\} + ... + \frac{\mathrm{d}t^s}{s!}\left\{\frac{d}{\mathrm{d}t}^s\right\}\right) u(t) + \frac{\mathrm{d}t^{s+1}}{(s+1)!}\left\{\frac{d^{s+1}u}{\mathrm{d}t^{s+1}}\right\}(t^*)$$
$$\text{for some } t^* \in [t, t+\mathrm{d}t]$$

We will compute an approximate update as :

$$u(t+\mathrm{d}t) \approx \left(1 + \frac{\mathrm{d}t}{1!}\left\{\frac{d}{\mathrm{d}t}\right\} + \frac{\mathrm{d}t^2}{2!}\left\{\frac{d}{\mathrm{d}t}^2\right\} + ... + \frac{\mathrm{d}t^s}{s!}\left\{\frac{d}{\mathrm{d}t}^s\right\}\right) u(t) \tag{C.10}$$

The numerical scheme will look like

$$u^{n+1} = \left(1 + \frac{\mathrm{d}t}{1!}\left\{\frac{d}{\mathrm{d}t}\right\} + \frac{\mathrm{d}t^2}{2!}\left\{\frac{d}{\mathrm{d}t}^2\right\} + ... + \frac{\mathrm{d}t^s}{s!}\left\{\frac{d}{\mathrm{d}t}^s\right\}\right) u^n \tag{C.11}$$

We then factorize the polynomial derivative term :

$$u^{n+1} = u^n + \frac{\mathrm{d}t}{s}\frac{\mathrm{d}}{\mathrm{d}t}\left(u^n + \frac{\mathrm{d}t}{s-1}\frac{\mathrm{d}}{\mathrm{d}t}\left(\frac{\mathrm{d}t}{s-2}\frac{\mathrm{d}}{\mathrm{d}t}\left(\ldots\left(u^n + \frac{\mathrm{d}t}{1}\frac{\mathrm{d}u^n}{\mathrm{d}t}\right)\right)\right)\right) \tag{C.12}$$

(Factorized Scheme) (C.13)

Algorithm (Jameson-Schmidt-Turkel (JST), multi stage Runge-Kutta explicit time-stepping integration scheme)

$$\text{Set } u = u^n \tag{C.14}$$
$$\text{For } k = p : -1, 1 \tag{C.15}$$
$$C \leftarrow u^n + \frac{\mathrm{d}t}{k}\frac{\mathrm{d}u}{\mathrm{d}t} \tag{C.16}$$
$$\text{End-for} \tag{C.17}$$
$$u^{n+1} = u^n \tag{C.18}$$

The scheme becomes for $p = 0, 1, 2; n = 1, ...$:

$$u_j^0 = \text{given}, \tag{C.19}$$
$$u_j^{n+1,p+1} = u_j^n - \frac{\Delta t}{3-p+1}\left(u_j^{n,p}\frac{u_{j+1}^{n,p} - u_{j-1}^{n,p}}{2\Delta x} - \mu_j^{n,p}\frac{u_{j+1}^{n,p} - 2u_j^{n,p} + u_{j-1}^{n,p}}{\Delta x^2} - g(u_j^{n,p})\right) \tag{C.20}$$
$$u_j^{n+1} = u_j^{n,3} \tag{C.21}$$

where we choose an numerical visosity given by :

$$\mu_j^{n,p} = \frac{max\left(\|u_{j-1}^{n,p}\|, \|u_j^{n,p}\|, \|u_{j+1}^{n,p}\|\right)\Delta x}{2} \tag{C.22}$$

Moreover we use an extension of the classical CFL stability condition (Courant Friedrichs Levy $\frac{c\Delta t}{\Delta x} \leq 1$), considering the variation of u and the source term presence :

$$\Delta t = min_j \left(\frac{\Delta x}{max\big(\|u_{j+1}^{n,p}\|, \|u_{j-1}^{n,p}\|, \|u_j^{n,p}\|, \|u_{j+1}^{n,p}\|, \Delta x \|g_j^{n,p}\|\big)} \right) \tag{C.23}$$

Annexe D

Compléments

D.1 Caractéristiques des modèles de dispersion atmosphérique

	Modèle gaussien	*Modèle intégral*	*Modèle 3D (CFD)*	***Essai sur terrain***	***Essai sur maquette***
Principaux avantages	Facilité de mise en oeuvre Coût peu élevé	Facilité de mise en oeuvre Cout peu élevé Densité (lourd, léger) thermique	Champ d'application étendu Débits variables Relief Rendu pedagogique excellent	Approche la plus fidele : tous les phénomènes physiques sont pris en compte	Bonne reproduction de la géometrie et de la météo reproductibilité
Principales difficultés	1) Conditions météorologiques qui jouent un rôle essentiel au moment d'un rejet 2) Caractéristique du terme source 3) Caractéristiques d'un éventuel jet (direction, présence d'obstacles,...) 4) Conditions de perte de confinement 5) Débit a la source 6) Obstacles et même en general de relief non pris en compte / terrain plat		1) 2) 3) 4) 5) Coût élevé Difficultés de mise en oeuvre, données detaillées a réunir Nécessite des compétences (cout de M.O.) Raccordement cartographique entre 2D/3D	Coût tres élevé Difficultés pratiques : disponibilités d'un terrain, météo le jour de l'essai et reproductibilité des essais.	Cout tres eleve
Principales limitations	conditions météorologiques champ lointain moyennes (distance de l'ordre de 100 m a une dizaine de km de la source) et terrain plat nuages ne s'eloignant pas trop du sol (a cause des cisaillement verticaux) vents de direction constante et de vitesse non nulle vitesse de vent supérieure a 1 ms^{-1}	valable a condition que la concentration soit homogène à l'interieur du nuage champ lointain (distance de l'ordre de 20 m a une dizaine de km de la source / 0-20 m au cas pas cas) vents de direction constante et de vitesse non nulle vitesse de vent supérieure a $1ms^{-1}$	Dépendent de la qualité des données d'entrée liées aux conditions et aux limites du problème a traiter (topographie, profils verticaux de vents et de température, etc.). Non prise en compte de la phase di-phasique (souvent)		Limitations pratiques du principe de similitude $\Rightarrow$ corrections
Evolution prévisible	Pas d'évolution fondamentale au niveau des hypothèses Plus large diffusion	Pas d'évolution fondamentale au niveau des hypothèses Plus large diffusion	Améliorations : modélisation physique (rejets di-phasiques), ergonomie Validation en rejet accidentel Baisse du coût : modèle, machine	Utilisation orientée plus vers la validation de modèles 3D que vers la reponse directe	Utilisation orientée plus vers la validation de modèles 3D que vers la reponse directe
	Développement de systèmes d'alerte couplés avec des stations météorologiques				

TAB. D.1 – Tableau"récapitulatif" avantages/inconvénients de différents modèles de dispersion.

D.2 Compléments sur les échelles de la dynamique atmosphérique

La gamme d'échelles couverte par les différents niveaux de modélisation est relativement large. Il convient de préciser les échelles temporelles pertinentes de l'atmosphère et des phénomènes qui sont étudiés dans cette étude, notemment ceux de la partie IV. Il est possible d'avoir une bonne appréciation des échelles caractéristiques des phénomènes étudiés en considérant les fréquences fondamentales des écoulements atmosphériques.

D.2.1 Fréquence de Brünt-Väisälä

Une notion importante pour la compréhension de la structure verticale de la basse atmosphère est la notion de stabilité verticale (voir 2.2). Cette notion est à relier directement à la notion de flottabilité d'une parcelle d'air. Cette flottabilité, expression de la stratification verticale de l'atmosphère, est parfois caractérisée par la fréquence de Brünt-Väisälä :

$$N = \left(\frac{g}{\theta_0} \frac{\partial \theta}{\partial z} \right)^{1/2} \tag{D.1}$$

Cette fréquence est associée aux oscillations verticales d'une parcelle d'air dans une atmosphère stratifiée de l'ordre de $10^{-2} s^{-1}$). On peut également définir les 2 fréquences suivantes :

- la fréquence inertielle, F, associée au mouvement de rotation de la Terre et à la force de Coriolis (de l'ordre de $10^{-4} s^{-1}$),
- la fréquence planétaire, P, associée à l'effet β, variation de la force de Coriolis selon la latitude (de l'ordre de $10^{-6} s^{-1}$).

Ces trois fréquences sont respectivement associées à des périodes de l'ordre de la minute, de quelques heures et de la semaine. On peut alors définir les échelles atmosphériques selon la fréquence f, qui correspond à l'inverse d'un temps de réponse de l'écoulement à un forçage :

- petite échelle : $f > N$,
- méso :$F < f < N$,
- synoptique : $P < f < F$,
- planétaire : $f < P$.

En réalité les échelles se superposent et les intéractions entre échelles conduisent aux phénomènes observés dans l'atmosphère. Il y a cependant des échelles de temps dominantes dans l'atmosphère : l'échelle de la journée, associée au cycle diurne du rayonnement solaire, et l'échelle de l'année, associée au cycle annuel dû au changement de l'axe de rotation de la Terre par rapport au Soleil. Ces échelles de temps sont principalement des échelles de forçage extérieur à l'atmosphère.

Les échelles qui sont plus particulièrement pertinentes pour l'étude de la pollution atmosphérique dans le cadre de ce travail de thèse sont essentiellement les échelles méso. L'échelle méso joue un rôle important dans le transfert d'énergie des grandes échelles vers les petites échelles. Cette large gamme d'échelles étant continue, elle impose une réprésentation correcte de l'ensemble des échelles pour prétendre obtenir des simulations numériques réalistes.

Les systèmes atmosphériques à l'échelle régionale (méso) peuvent être divisés en deux catégories :

- (i) ceux forcés principalement par les inhomogénéités de la surface du sol (systèmes induits par le terrain et/ou sa physiographie) et

– (ii) ceux forcés principalement par les instabilités produites par des perturbations à plus grande échelle (systèmes induits par la situation synoptique).

La première catégorie comprend des phénomènes comme les brises de mer, les brises de terre, les vents de vallée, les circulations en milieu urbain et les écoulements forcés sur un terrain rugueux. La deuxième catégorie inclut les ouragans et les paquets de nuages. Les sources de ces circulations à méso échelle sont géographiquement fixes avec des échelles de temps de l'ordre de quelques heures. Bien que ces systèmes ne se déplacent généralement pas loin de leur point d'origine, ils requièrent une représentation spatiale et temporelle détaillée des conditions extérieures.

On peut privilégier des fréquences de coupure sur le vent pour choisir une échelle de résolution. A partir de vitesses de vent mesurées près du sol, on peut reporter l'occurence d'observations du vent en fonction de la fréquence des tourbillons et de leur temps de vie. Ce mode d'illustration permet de séparer les contributions "synoptiques" des contributions "turbulentes" et montre que le choix de l'échelle est fortement guidé par l'observation. Pour éviter au mieux les erreurs dans les résultats de modélisation, il semble évident de "couper" la résolution au niveau d'une période temporelle de l'ordre de l'heure.

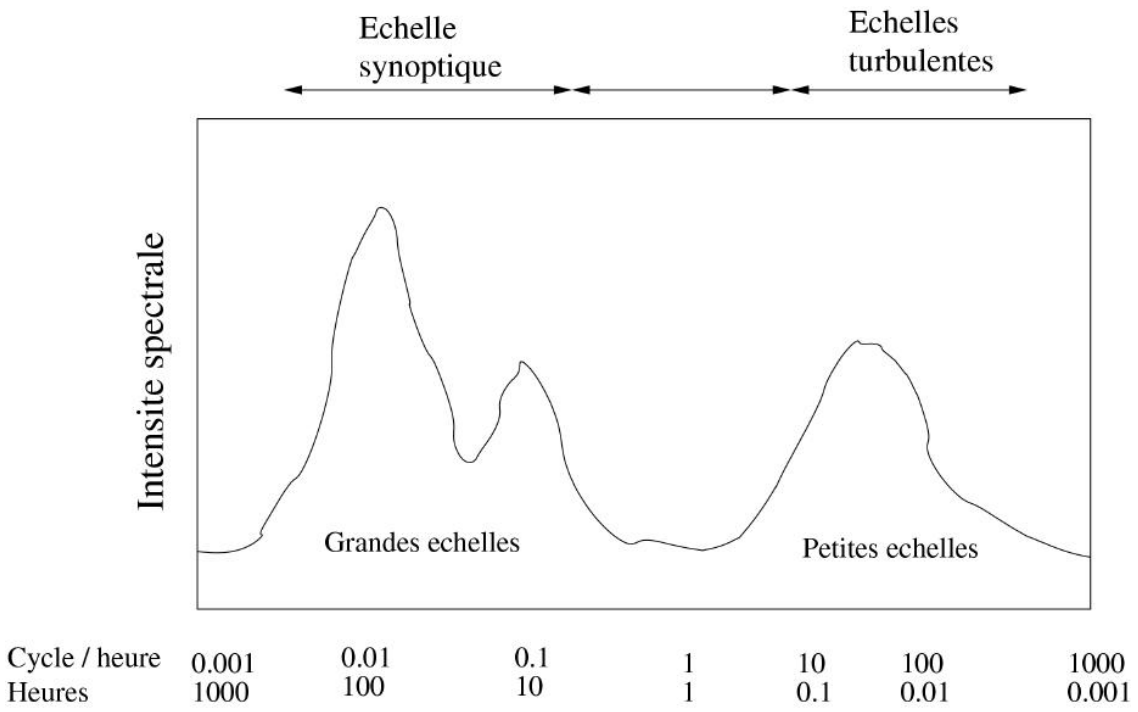

FIG. D.1 – Spectre schématique de vitesse du vent, d'après Van der Hoven (1957).

Echelle spatiale Horizontale L_H	Echelle temporelle T_s temporelle	Stull (1988) [44]	Pielke (1984) [45]	Orlanski (1975)	Thunis and Bornstein (1996)	Phénomènes atmosphériques
10000 km	1 mois	Macro	Synoptique	Macro-α	Macro-β	Circulation générale, ondes longues
2000 km	1 semaine			Macro-β	Macro-β	Cyclones synoptiques
200 km	1 jour	Méso	Méso	Méso-α	Macro-γ	Fronts, ouragans
				Méso-β	Méso-β	Jets de basse couche, lignes de grains, brises de mer, vents locaux vents de montagne, brises effets urbains
20 km	1 heure	Méso	Micro	Méso-γ	Méso-γ	Orages, turbulence en air clair
2 km		Méso/Micro	Micro	Micro-α	Méso-δ	Nuages, tornades, écoulements catabatiques circulations urbaines
200 m	30 min	Micro	Micro	Micro-β	Micro-β	Panaches, sillages, trombes d'eau, tourbillons, cumulus
20 m	1 min	Micro			Micro-γ	panaches (cheminées), micro-turbulence
2 m	1 s			Micro-γ	Micro-δ	Turbulence, ondes sonores

TAB. D.2 – nalyse d'échelles en météorologie : définition des échelles atmosphériques. Depuis le début des années 70, de nombreuses classifications ont été proposées. L_H est l'échelle de longueur horizontale. Tableau extrait et adapté de [126] et [127]

D.2.2 Nombre de Richardson et stabilité

Le rapport du terme de cisaillement sur le terme de flottabilité définit le nombre de Richardson R_{if} qui fournit un autre moyen de décrire la stabilité de l'atmosphère :

- $R_{if} > 0$ atmosphère stable
- $R_{if} = 0$ atmosphère neutre
- $R_{if} < 0$ atmosphère instable

Une interprétation de ce rapport "flottabilité"/"cisaillement" montre que lorsque le cisaillement est positif (on est dans l'atmosphère libre), le rapport est positif et l'atmosphère est stable. Plus on se rapproche de la surface, plus la flottabilité est négative et grande, et plus R_{if} est négatif et grand : on est en atmosphère instable.

Annexe E

Exemple de calage du modèle de dispersion

E.1 Paramétrisations

E.1.1 Description de la turbulence

La turbulence dans la couche limite atmosphérique peut être appréhendée par :
- une description continue de la turbulence suivant la théorie de similitude de Monin-Obukhov (1954),
- ou une description discrète de la turbulence suivant la Classification de Pasquill.

Les paramétrisations associées permettent également le calcul des coefficients de dispersion utilisés pour les formulations du champ lointain. On présente un exemple de calage pour des conditions de vent uniforme stationnaire et de topographie plate (cas d'application des modèles de dispersion gaussien). On détermine ainsi les paramètres qui permettent de retrouver les résultats d'un modèle de dispersion Gaussien classique pour une classe de stabilité fixée.

E.1.2 Détermination des écarts-types

Dans le cas d'un rejet continu et d'une vitesse de vent suffisamment importante pour que le phénomène de diffusion dans la direction du vent soit négligeable devant le phénomène de convection (hypothèse d'un modèle à panache Gaussien, cf "slender approximation" section 1.5.1), on cherche à calculer les paramètres du modèle présenté dans la section 7. A partir de campagnes de mesures sur des rejets de produits, des formules ont été etablies pour le modèle gaussien, donnant la valeur des ecarts-types en fonction :
- de la distance d'éloignement de la source de rejet (Pasquill, Turner, Briggs, Hosker) ;
- du temps de transfert (Doury).

Les ecarts types ont été calés pour des rejets relativement importants à la source (au minimum de l'ordre de la tonne), et pour des distances de dispersion de l'ordre de la dizaine de kilomètres au maximum. Ils dependent :
- de la distance à la source ou de la durée de transfert ;
- des caractéristiques de la structure de l'atmosphere (stabilité,...) ;
- et de la rugosité du site.

On peut remarquer que ces paramétrisations sont toutes très proches et donc à peu près équivalentes au vu de leur précision réelle.

E.1.3 Conditions retenues pour un rejet au sol

Dans le cadre des études de dangers, les conditions de stabilité atmosphérique généralement retenues pour des rejets au niveau du sol sont de type D (neutre) et F (très stable) au sens de Pasquill, respectivement associées à des vitesses de vent de 5 et $3m/s$ (E.1). Dans certaines configurations de rejet et particulièrement pour les rejets en altitude (cheminée), les conditions défavorables peuvent être différentes de celles caractérisées par le couple $(F, 3m/s)$ généralement admises comme conduisant aux distances les plus pénalisantes pour les rejets à proximité du sol.

	Stabilité atmosphérique	**Vitesses du vent considérées** [m/s]
Rejet horizontal au niveau du sol	D	5 (conditions médianes)
	F	3 (conditions défavorables)
Rejet vertical ou rejet de gaz léger	A	3
	B	3 et 5
	C	5 et 10
	D	5 (conditions médianes) et 10
	E	3
	F	3

TAB. E.1 – Conditions météorologiques retenues

Sur le territoire métropolitain, la température de l'atmosphère et du sol peut être fixée à 20°C pour les conditions de stabilité atmosphérique comprise entre A et E, et à 15°C pour la condition de stabilité atmosphérique F. L'humidité relative peut être retenue égale à 70%. En effet, sauf cas particuliers, l'influence de ces deux paramètres n'est pas dimensionnante pour des variations classiques.

Conditions favorables aux traitements phytosanitaires

Dans tous les cas d'application, on cherche à réaliser des pulvérisations dans des conditions favorables, en évitant au maximums les pertes diverses. Compte tenu des risques, il convient de traiter au bon moment et les conditions atmosphériques doivent donc présenter le moins de risques possible (température, vent, risque de pluie...). La décision de traitement doit donc etre prise en s'appuyant sur les conditions suivantes :

- ne pas traiter par temps de pluie (risque de lessivage, ruissellement).
- ne pas traiter par grand vent, afin d'éviter toute dérive de produit.
- ne pas traiter par trop forte chaleur. Elle peut provoquer la formation de vapeurs toxiques et des phenomènes de phytotoxicite, même a distance.

E.1.4 Application

Pasquill a proposé une description en 6 classes notées de A à F, d'une atmosphère très instable (forte diffusion turbulente à une atmosphère très stable (présence éventuelle d'inversions de température). Dans cette classification, l'atmosphère est neutre par vent fort (D) tandis que l'instabilité sera associée à un vent faible et une énergie thermique près du sol disponible (A, B ou C). Dans les autres cas, l'atmosphère sera stable (E ou F), par exemple la nuit. La classe

de Pasquill est déterminée suivant les mesures météorologiques disponibles ou prise par défaut à D afin de majorer les pertes.

La loi de dispersion pour σ_y, utilisé dans le modèle gaussien en cas de stabilité neutre (D) est :

$$TH = 0.017453293[c - d\log(x)],\ x \text{ en } km \tag{E.1}$$
$$\sigma_y = \frac{1}{0.00215} x \tan(TH) \tag{E.2}$$
$$= 465.11628(x)\tan(TH),\ x \text{ en } km \tag{E.3}$$
$$\tag{E.4}$$

Le modèle développé est ensuite calé par problème inverse afin de déterminer les paramètres qui minimisent l'écart avec le modèle gaussien. Il existe de nombreux algorithmes d'optimisation globale ; on a choisit ici de travailler avec BMO, développé au laboratoire ACSIOM par Benjamin Ivorra et Bijan Mohammadi pour résoudre le problème de minimisation.

E.2 Exploitation du modèle

Afin de rendre le modèle plus accessble, une interface graphique a été développée avec la collaboration de Nicolas Bozon (cf figure E.1). Cette interface permet l'utilisation des résultats de manière automatique en les transformant sous forme statique (format image) ou sous fome d'une couche dynamique utilisable par un SIG (Système d'Information Graphique utilisant un format shape). Un guide utilsateur ainsi qu'une page web (*http ://www.drift-x.com*) sont également en cours de développement.

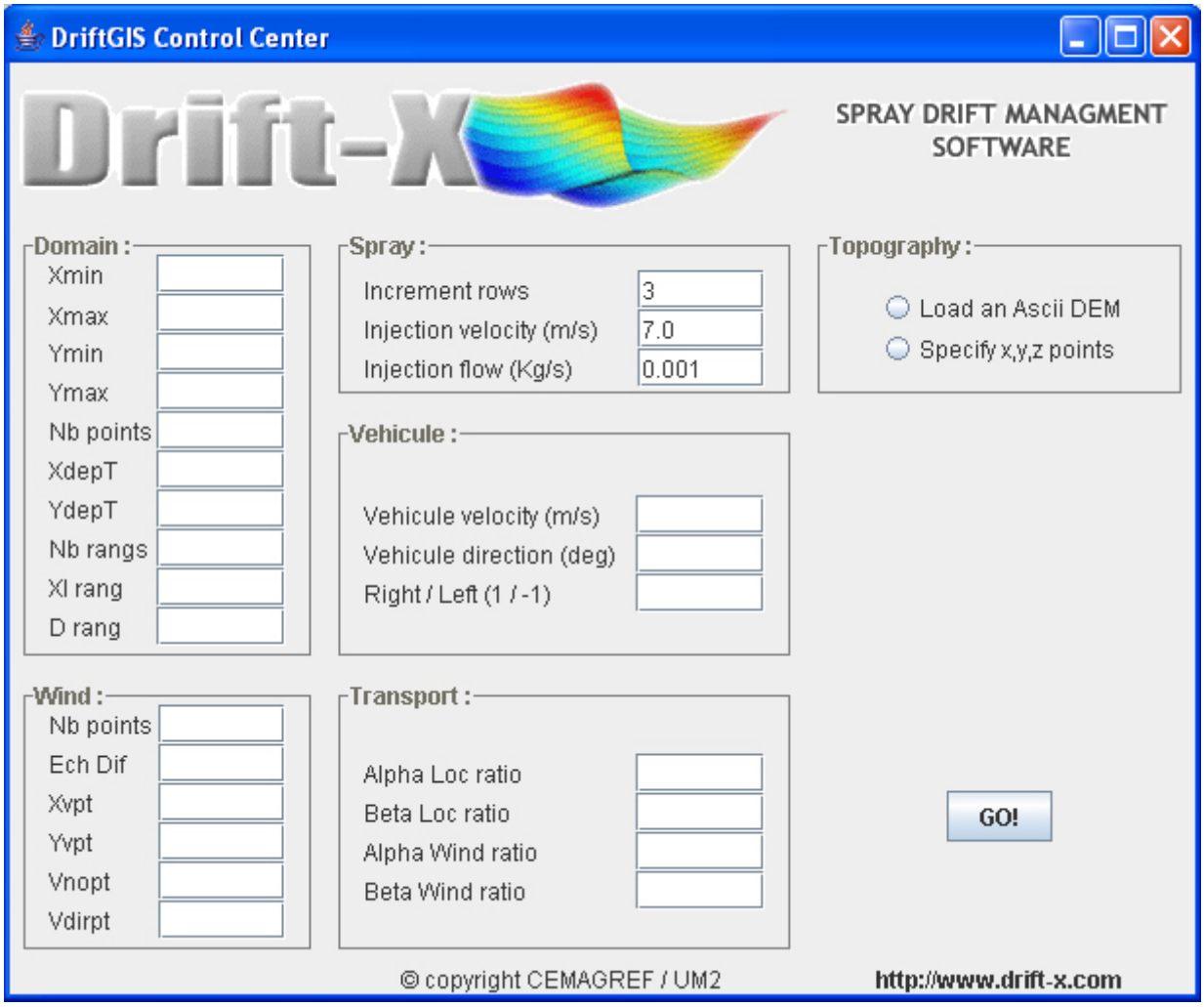

FIG. E.1 – Capture d'écran de l'interface graphique réalisée en Java en collaboration avec Nicolas Bozon pour le modèle de transport longue distance. Une interface graphique réalisé sous Matlab est également en cours de réalisation pour le modèle en champ proche.

Annexe F

Distance

F.0.1 Generalized geometry and Non-symmetric geometry

A lot of distances notions are used in real-world applications. Depending on context, the distances are either practical ones, used in daily life and work outside of science. For example, many studies have also employed various metrics for evaluating model performance in ADM [128].

Generalized metric are often used in geography [117]. Consider the set of all places which could be reached within one hour from where someone is. The outer edge of this set forms a geographical "space" of one hour radius. This isochronic map most probably has holes, and probably consists of disjoint pieces, shape depends on the place and time of day. This environment, as a geometry, seems more complicated than the Riemannian geometry.

We will fromalize these preliminary remarks. In a classical symmetric geometry the distance function between two points A and B verifies

$$\text{Positivity :} \quad d(A,B) \geq 0 \ \forall A,B \tag{F.1}$$

$$\text{Discrimination ("non degenerate") :} \quad d(A,B) = 0 \ \Rightarrow \ A = B, \tag{F.2}$$

$$\text{Symmetry :} \quad d(A,B) \ = \ d(B,A), \tag{F.3}$$

$$\text{Triangle Inequality :} \quad d(A,B) \leq d(A,C) + d(C,B) \tag{F.4}$$

But the distance function can be non uniform with anisotropy. For example, in a chosen metric $\mathcal{M}_{mesh}$ the distance between A and B could be given by :

$$d_{\mathcal{M}_{mesh}}(AB) = \int_0^1 \left({}^t\overrightarrow{AB} \ \mathcal{M}_{mesh}(A + t\overrightarrow{AB})\overrightarrow{AB} \right)^{1/2} dt \tag{F.5}$$

where $\mathcal{M}_{mesh}$ is positive definite and symmetric in symmetric geometries. With $\mathcal{M}_{mesh} = I$, one recovers the Euclidean geometry and variable $\mathcal{M}_{mesh}$ permits to account for anisotropy and non uniformity of the distance function. This approach has been widely used for mesh adaptation for steady and unsteady phenomenon [118, 119, 120] linking the metric to the Hessian of the solution. This definition of the metric permits to equi-distribute the interpolation error over a given mesh and therefore monitor the quality of the solution.

The "physical" distance between any two points A and B on a manifold $\mathbf{M}$ could be measured

by a Riemannian metric μ :

$$dist(A,B) = \inf_{\sigma_{AB}} \{L(\sigma_{AB})\} = \inf_{\sigma_{AB}} \left\{ \int_{\sigma_{AB}} \mathrm{d}s \right\} \tag{F.6}$$

$$= \inf_{\sigma_{AB}} \left\{ \int_{\sigma_{AB}} \sqrt{\mu_{\sigma_{AB}}(\dot{\sigma_{AB}}, \dot{\sigma_{AB}})}\, \mathrm{d}\tau \right\}, \quad \text{where } \dot{\sigma_{AB}} = \frac{\mathrm{d}\sigma_{AB}}{\mathrm{d}\tau} \tag{F.7}$$

Genarally, the infimum is taken over all admissible piecewise smooth curves $\sigma_{AB}(\tau)$ from A to B. The integral does not depend on the parameterization τ. In the previous approach (F.5) σ_{AB} is simply the segment AB.

The integrand $\sqrt{\mu_{\sigma_{AB}}(\dot{\sigma_{AB}}, \dot{\sigma_{AB}})}\mathrm{d}\tau = \mathrm{d}s = \|\mathrm{d}s/\mathrm{d}\tau\|_\mu \mathrm{d}\tau$ is the length of a tiny segment of the curve $\sigma(\tau)$, and the parameter τ may have nothing to do with actual travel time.

In the particular case considered in the following context, σ_{AB} is assumed known and fixed to γ_{AB} a particular path or trajectory (not necessary equal to the minimum).

To get the amount of time it takes to traverse this segment $\mathrm{d}s$, that length could be divided by the travel speed v_c. In general, it depends on the location $\mathbf{x} = \gamma_{AB}(\tau) \in \mathcal{M}$, the direction of the corresponding instantaneous tangent $\mathbf{y} = \dot{\gamma}_{AB}(\tau) \in T_{\mathbf{x}}\mathcal{M}$ and $T\mathcal{M} =:= \{\cup T_{\mathbf{x}}\mathcal{M} | \mathbf{x} \in \mathcal{M}\}$, and most likely the time t of the day. But this is not considered here, $v_c(\mathbf{x}, \mathbf{y}, t) = v_c(\mathbf{x}, \mathbf{y})$. Since only the direction of $\mathbf{y}$ matters, v_c should satisfy $v_c(\mathbf{x}, \lambda\mathbf{y}) = v_c(\mathbf{x}, \mathbf{y})$ for all $\lambda > 0$.

Then the travel time from A to B is :

$$time(A,B) = \int_{\gamma_{AB}} \frac{1}{v_c(\mathbf{x}, \mathbf{y})} \sqrt{\mu_{\gamma_{AB}}(\dot{\gamma}_{AB}, \dot{\gamma}_{AB})}\, \mathrm{d}s \tag{F.8}$$

The new integrand is of the type

$$F(\mathbf{x}, \mathbf{y}) = \frac{1}{v_c(\mathbf{x}, \mathbf{y})} \sqrt{\mu_{\mathbf{x}}(\mathbf{y}, \mathbf{y})} = \sqrt{\frac{\mu_{\mathbf{x}}(\mathbf{y}, \mathbf{y})}{v_c^2(\mathbf{x}, \mathbf{y})}} \tag{F.9}$$

It represents the time required for traveling along $\mathbf{y}$, from the point $\mathbf{x}$. The quantity inside the radical is typically not even rational in $\mathbf{y}$; it is a quadratic function of $\mathbf{y}$ if and only if v_c has no $\mathbf{y}$ dependence, and in that case F is said to be Riemannian.

Distances of this kind are usually known in literature as Finsler distances. Besides being a natural generalization of Riemannian geometry, Smooth Finsler geometry has numerous applications in mathematics and physics and have been widely studied in the framework of differential geometry. The literature on the subject is wide ; an introduction is supplied, for instance, by [129].

Finsler metrics become often relevant when one asks for the travel time from A to B, rather than physical distance. In practical applications, Finsler metrics are mandated whenever the speed of propagation is direction dependent.

For example, Finsler metric is used in Physics from the point of view of the geometric optics, where it describes the propagation of waves in a medium which is both anisotropic and inhomogeneous. Riemannian geometry, on the other hand, corresponds to the wave propagation in a medium, which although may be inhomogeneous, is isotropic. Finsler metric are also used in Computer Vision [130] and in Economy application (Kristaly).Intuitively, it also could be seen as travel time distance across a Riemannian landscape under windy conditions.

Formally, a Finsler metric is a continuous function $F : T\mathcal{M} \to [0, \infty)$ with the following properties.

– (1) Regularity : F is smooth on $T\mathcal{M}\backslash 0 := \{(\mathbf{x}, \mathbf{y}) \in T\mathcal{M} | \mathbf{y} \neq 0\}$.
– (2) Positive homogeneity : $F(\mathbf{x}, \lambda\mathbf{y}) = \lambda F(\mathbf{x}, \mathbf{y})$ for all $\lambda > 0$.
– (3) Strong convexity : the fundamental tensor $g_{ij} := \partial^2_{y^i y^j} y^i y^j \left(\frac{1}{2}F^2\right)$ is positive definite at all $(x, \mathbf{y}) \in T\mathcal{M}\backslash 0$.

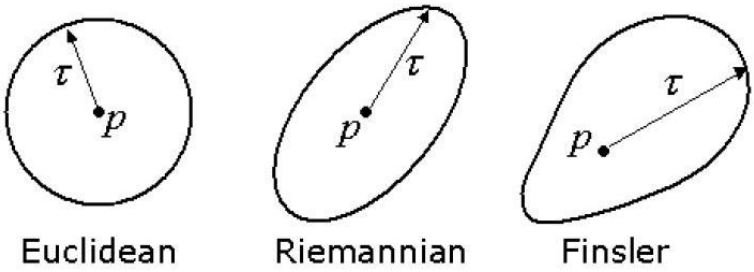

FIG. F.1 – Local distance maps. The Figure shows some examples of local distance maps of Finsler metric, including Euclidean and Riemannian metrics as special cases.

F.0.2 Application to a plane wind distance

In our particular case, v_c is represented by the projection of the local wind velocity $\pi_{wind}(\mathbf{u}(\mathbf{x})) = \mathbf{u}_p(\mathbf{x})$ on the curve trajectory direction on γ_{AB}. The Riemannian metric μ considered in this case is simply the Euclidean metric on the flat space $\mathbb{R}^2 = (x, y)$, i.e. $\mu = Id_{\mathbb{R}^2}$, hence $\|\cdot\|_\mu = \|\cdot\|_{\mathcal{E}_{\mathbb{R}\in}}$. The horizontal local travel time on, $\tau_{h-wind_{AB}}(\mathbf{x})$ (within the plane xy) at $\mathbf{x} = \gamma_{AB}(\tau)$ is then defined by :

$$\tau_{h-wind_{AB}}(\mathbf{x}) = \frac{\|\dot{\gamma}_{AB}(\tau)\|_\mathcal{E}}{\|\mathbf{u}_p(\mathbf{x})\|_\mathcal{E}} = \frac{\|\dot{\gamma}_{AB}(\tau)\|_\mathcal{E}}{\left(\frac{\mathbf{u}(\mathbf{x}) \cdot \dot{\gamma}_{AB}(\tau)}{\|\dot{\gamma}_{AB}(\tau)\|_\mathcal{E}}\right)}$$

Consequently, the travel time metrics becomes :

$$time_{wind}(A, B) = \int_{\gamma_{AB}} \frac{1}{\left(\frac{\mathbf{u}(\mathbf{x}) \cdot \dot{\gamma}_{AB}(\tau)}{\|\dot{\gamma}_{AB}(\tau)\|_\mathcal{E}}\right)} \|\dot{\gamma}_{AB}(\tau)\|_\mathcal{E} \mathrm{d}\tau$$

And F_{wind} that represent the metric is defined by

$$F_{wind}(\mathbf{x}, \mathbf{y}) = \frac{1}{\mathbf{u}(\mathbf{x}) \cdot \frac{\mathbf{y}}{\|\mathbf{y}\|_\mathcal{E}}} \sqrt{\mu_{Id_{\mathbb{R}^2}}(\mathbf{y}, \mathbf{y})} \tag{F.10}$$

where $\sqrt{\mu_{Id_{\mathbb{R}^2}}(\mathbf{y}, \mathbf{y})} = \|\mathbf{y}\|_\mathcal{E}$

In $\mathbb{R}^2$, the generalized Wind Metric Tensor associated is represented by the following matrix $\mathcal{M}_{wind}(\gamma(\tau)) =$

$$\begin{bmatrix} \dfrac{\sqrt{\dot{x}^2(\tau)+\dot{y}^2(\tau)}}{u(x(\tau),y(\tau))\dot{x}(\tau)+v(x(\tau),y(\tau))\dot{y}(\tau)} & 0 \\ 0 & \dfrac{\sqrt{\dot{x}^2(\tau)+\dot{y}^2(\tau)}}{u(x(\tau),y(\tau))\dot{x}(\tau)+v(x(\tau),y(\tau))\dot{y}(\tau)} \end{bmatrix}$$

Pratically we can consider the following distance function definition :

$time(A,B)_{wind} = T_{mig}(A,B)$

$$\begin{cases} \int_{\gamma_{AB}} \|\dot{\gamma}_{AB}\|_{\mathcal{M}_{wind}} \, \mathrm{d}t & \text{if } (\mathbf{u}\cdot\dot{\gamma}_{AB})(\mathbf{x}) > 0 \ \forall \mathbf{x} \\ & \text{if A is upwind with respect to B then} \\ +\infty, & \text{else} \end{cases}$$

In our model, we consider that $T_{mig}(A,B)$ is the migration time from A to $B^{\perp}$ along the characteristic γ_{AB} passing by A. $B^{\perp}$ denotes the projection of B over this characteristic in the Euclidean metric. $\mathbf{u}_p$ is the local velocity along this characteristic and is by definition tangent to the characteristic. One supposes that this characteristic is unique hence avoiding sources and attraction points in the flow field. In case of non uniqueness of this projection, one chooses the direction of the projection which satisfies best the constraint $(\mathbf{u}_p \cdot c = 0)$ in B.

Bibliographie

[1] Wagner W.C. Sustainable agriculture : how to sustain a production system in a changing environnement. *International Journal for Parasitology*, 29 :1–5, 1999.

[2] Zhang N., Wang M., and Wang N. Precision agriculture - a worldwide overview. *Computers and Electronics in Agriculture*, 36, 2002.

[3] Gil Pinto Yvan. *Caractérisation expérimentale des émissions de pesticides vers l'air pendant les pulvérisations viticoles.* PhD thesis, Montpellier SupAgro, 2007.

[4] G. Pergher and R. Gubiani. The effect of spray application rate and airflow rate on foliar deposition in a hedgerow vineyard. *Journal of Agricultural Engineering Research*, 61 :205–216, 1995.

[5] Salyani M. Spray technology research for orchard applications. *Acta Horticulturae*, 372 :67–74, 1994.

[6] R.E. Gaskin, D.W. Manktelow, and G.S. Elliott. New adjuvant technology for pesticide use on wine grapes. In *55th Conference Proceedings of the New Zealand Plant Protection Society Incorporated*, 2002.

[7] Michael Wilson, editor. *Optimising Pesticide Use.* Wiley Series in Agrochemicals and Plant Protection, England, 2003.

[8] Carole Sinfort. Link between experimental research and modelisation for the optimisation of agricultural spraying processes, hdr accreditation to supervise research. Technical report, Cemagref SupAgro, Montpellier, 2006.

[9] S. R. Hanna, J. C. Chang, and M. E. Fernau. Monte carlo estimates of uncertainties in predictions by a photochemical grid model (uam-iv) due to uncertainties in input variables. *Atmos. Env.*, 32(21) :3,619–3,628, 1998.

[10] Z. Hanna, S.R.and Lu, H. C. Frey, N. Wheeler, J. Vukovich, S. Arunachalam, M. Fernau, and D. A. Hansen. Uncertainties in predicted ozone concentrations due to input uncertainties for the uam-v photochemical grid model applied to the july 1995 otag domain. *Atmos. Env.*, 35(5) :891–903, 2001.

[11] Mallet Vivien. *Estimation de l'incertitude et prévision d'ensemble avec un modèle de chimie-transport. Application à la simulation numérique de la qualité de l'air.* PhD thesis, Ecole nationale des ponts et chaussées, Paris, 2005.

[12] Willem A.H. Asman. Modelling atmospheric transport and deposition of pesticides up to 2 km from a source. Report Pesticides Research 57, Danish Environmental Protection Agency, Copenhagen, Denmark, 2001. In : Asman, W.A.H., Felding, G., Kudsk, P., Larsen, J., Mathiassen, S., Spliid, N.H. : Pesticides in air and in precipitation and effects on plant communities.

[13] Gail Tonnesen, Jay Olaguer, Michelle Bergin, Ted Russell, Adel Hanna, Paul Makar, Dick Derwent, and Zion Wang. Air quality models. RAS Draft as of 11/26/98, March 2004.

[14] M. R. Raupach, P. A. Coppin, and B. J. Legg. Experiments on scalar dispersion within a model plant canopy part i : The turbulence structure. *Bound. Layer Meteorol.*, 35 :21–52, 1986.

[15] P.A. Coppin, M.R. Raupach, and B.J. Legg. Experiments on scalar dispersion within a model plant canopy, part ii : An elevated plane source. *Boundary Layer Meteorol.*, 35 :167–191, 1986.

[16] B.J. Legg, M.R. Raupach, and P.A. Coppin. Experiments on scalar dispersion within a model plant canopy, part iii : An elevated line source. *Bound. Layer Meteorol.*, 35 :277–302, 1986.

[17] H.S. Carslaw and J.C. Jaeger. *Conduction of Heat in Solids.* Oxford University Press, London, 1971.

[18] Van Genuchten and W.J. Alves. Analytical solutions of the onedimensional convective-dispersive solute transport equation. Technical Bulletin 1661, US Department of Agriculture, 1982.

[19] O. F. T. Roberts. The theoretical scattering of smoke in a turbulent atmosphere. *Proc. Roy. Soc.*, 104 :640–648, 1923.

[20] F. Nieuwstadt. An analytical solution of the time-dependent, one-dimensional diffusion equation in the atmospheric boundary layer. *Atmospheric Environment*, 14 :1361–1364, 1980.

[21] W. Koch. A solution of the two-dimensional atmospheric diffusion equation with height-dependent diffusion coefficients including ground level absoption. *Atmospheric Environment*, 23(8) :1729–1732, 1989.

[22] Water Resources Research, editor. *Solutions for Miscible Displacement of Soil Water with TimeDependent Velocity and Dispersion Coefficients*, volume 36(6). Proceedings, Soil Science Society of America, 1972.

[23] D.A. Barry and Sposito G. Analytical solution of a convection dispersion model with timedependent transport coefficients. *Water Resources Research*, 25(12) :24072416, 1989.

[24] H.A. Basha and ElHabel F.S. Analytical solution of the onedimensional timedependent transport equation. *Water Resources Research*, 29(9) :32093214, 1993.

[25] Zoppou C. and Knight J. H. Analytical solution of the spatially variable coefficient advective-diffusion equation in one-, two- and three-dimensions. Mathematics Research Report MRR 056, CSIRO, Australia, 1997. CMA, ANU, 0200.

[26] S.R. Yates. An analytical solution for onedimensional transport in porous media with an exponential dispersion function. *Water Resources Research*, 28(8) :21492154, 1992.

[27] Zabadal J. R. and Poffal C. A. Solution of the multidimensional diffusion equation using lies symmetries : simulation of pollutant dispersion in the atmosphere. *Engenharia Térmica (Thermal Engineering)*, 4(2) :197–204, October 2005. ISSN : 1676-1790.

[28] J.R. Philip. Some exact solutions of convectiondiffusion and diffusion equations. *Water Resources Research*, 30(12) :35453551, 1994.

[29] M.M. Aral and B. Liao. Analytical solutions for twodimensional transport equation with timedependent dispersion coefficients. *Journal of Hydrologic Engineering, American Society of Civil Engineers*, 1(1) :2032, 1996.

[30] C. Chrysikopoulous, L. Hildermann, and P. Roberts. A 3-dimensional steady-state atmospheric dispersion deposition model for emission from a ground area source. *Atmospheric Environment*, Part A, 26A :747–757, 1992.

[31] Sharan M., Singh M.P., and Yadav A.K. Mathematical model for atmospheric dispersion in low winds with eddy diffusivities as linear functions of downwind distance. *Atmospheric Environment*, 30(7) :1137–1145(9), 1996. ISSN 1352-2310.

[32] Shara M., Yadav A.K., Singh M.P., Agarwal P., and Nigam S. A mathematical model for the dispersion of air pollutants in low wind conditions. *Atmospheric Environment*, 30(8) :1209–1220(12), April 1996.

[33] Davidson M. Moreira, Marco T. Vilhena, Tiziano Tirabassi, Camila Costa, and Bardo Bodmann. Simulation of pollutant dispersion in the atmosphere by the laplace transform : The admm approach. *Journal Water, Air, & Soil Pollution*, 177(1-4) :411–439, November 2006.

[34] T. Tirabassi. Operational advanced air pollution modeling. *Pure and Applied Geophysics*, 160(1-2) :5–16, 2003.

[35] G. T. Csanady. *Turbulent Diffusion in the Environment.* Reidel Publishing Company, Dordrecht, Holland, 1973.

[36] S. Williamson and Mills Don. *Fundamentals of Air Pollution.* Addison-Wesley Publishing Company, Dordrecht, Holland, 1973.

[37] Samuel P.Williamson. Federal research and development needs and priorities for atmospheric transport and diffusion modeling. Technical report, Office of the Federal Coordinator for Meteorological Services and Supporting Research (OFCM), September 2004.

[38] De Vito Timothy J. *Modeling Aerosol puff concentration distributions from point sources using artificial neutral networks.* PhD thesis, Faculty of the Royal Military College of Canada, Department of National Defence, July 2000.

[39] M.R. Raupach, P.R. Briggs, N. Ahmad, and V.E. Edge. Endosulfan transport : Ii. modeling airborne dispersal and deposition by spray and vapor. *Journal Environ. Qual.*, 30 :729–740, 2001.

[40] Sachdev Jai Singh. *A review of dispersion modellingand particle trajectories in atmospheric flows*. PhD thesis, University of Toronto, 2000.

[41] Hargreaves David Michael. *Analytical and Experimental Studies of Vehicle Pollution Dispersion*. University of nottingham, Université de Nice Sophia-Antipolis, October 1997.

[42] S. Hanna, G. Briggs, , and R. Hosker. *Handbook on Atmospheric Diffusion*. Springfield, National Technical Information Center U.S. Dept of Energy, 1982.

[43] F. A. Gifford. *In Lectures on Air Pollution and Environmental Impact Analysis*, chapter Atmospheric Dispersion Models on Air Pollution Applications, pages 35–58. American Meteorological Society, d. a haugen edition, 1975.

[44] R. B. Stull. *An Introduction to Boundary Layer Meteorology*. Kluwer Academic Press, Dordrecht, 1988.

[45] R. A. Pielke. *Mesoscale Meteorological Modeling*. Academic Press, Dordrecht, 1984.

[46] Fabian Krzikalla. *Numerical Investigation of the Interaction between Wind and Forest under Heterogeneous Conditions*. PhD thesis, Institute for Hydromechanics, University of Karlsruhe, INRA-EPHYSE, 2005.

[47] ed. D.A. Haugen, editor. *Similarity laws and scale relations in planetary boundary layers.* in : Workshop on micrometeorology, AMS, 1973.

[48] Julien Dupuy. Simulation numérique de l'écoulement de pesticide dans un modèle de vigne. Master's thesis, Université Laval, Canada, 2006.

[49] Gary Dorr, Jim Hanan, Nicholas Woods, Paul Kleinmeulman, and Stephen Adkins Barry Noller. Combining spray drift and plant architecture modelling. In Washington State University, editor, *Proceedings of the International Conference on Pesticide Application for Drift Management*, pages 297–301, 2004.

[50] M.R. Raupach and A.S. Thom. Turbulence in and above plant canopies. *Ann. Rev. Fluid Mech.*, 13 :97–129, 1981.

[51] P.J. Walklate, K.-L. Weiner, and C.S. Parkin. Analysis of and Experimental Measurements Made on a Moving Air-Assisted Sprayer with Two-Dimensional Air-Jets Penetrating a Uniform Crop Canopy. *Journal of Agricultural Engineering Research*, 63 :365–378, 1996.

[52] Arthur Da Silva. *Modélisation numérique des dépôts de produits phytosanitaires*. PhD thesis, USTL. Université des sciences et techniques du Languedoc, Montpellier 2 - Cemagref, Montpellier, 2003.

[53] Craig Fischenich. Resistance Due to Vegetation. Technical Note (TN) TN-EMRRP-SR-07, Ecosystem Management and Restoration Research Program (EMRRP), May 2000.

[54] D.H. Bache. Momentum transfer to plant canopies : influence of structure and variable drag. *Atmospheric Ennvironment*, 20 :1369–1378, 1986.

[55] T P Meyers and U K T Paw. Testing of a higher-order closure model for airflow within and above plant canopies. *Boundary-Layer Meteorology*, 37 :297–311, 1986.

[56] F.D. Molina-Aiz, D.L. Valera, A.J. Ávarez, and A. Madue no. A wind tunnel study of airflow through horticultural crops : Determination of the drag coefficient. *Biosystems Engineering*, 4(12) :447–457, 2006.

[57] Craig Fischenich and Syndi Dudley. Determining Drag Coefficients and Area for Vegetation. Technical Note (TN) ERDC TN-EMRRP-SR-08, Ecosystem Management and Restoration Research Program (EMRRP), February 2000.

[58] John Finnigan. Turbulence in plant canopies. *Annual Review Fluid Mech.*, 32 :519–571, 2000.

[59] T. Bartzanas, T Boulard, and C. Kittas. Numerical simulation of the airflow and temperature distribution in a tunnel greenhouse equipped with insect-proof screen in the openings. *Computers and Electronics in Agriculture*, 34 :207–221, 2002.

[60] N. Robert Wilson and Roger H. Shaw. A higher order closure model for canopy flow. *Journal of Applied Meteorology*, 16(11) :1197–1205, 1977.

[61] M. R. Raupach and R. H. Shaw. Averaging procedures for flow within vegetation canopies. *Boundary-Layer Meteorology*, 22 :79–90, 1982.

[62] JJ. Finnigan. *Hutchinson BA, Hicks BB. (eds). The Forest-Atmosphere Interaction.*, chapter Turbulent transport in flexible plant canopies., pages 443–480. D. Reidel Publishing Company, Dordrecht, The Netherlands, 1985.

[63] Alexandre Petroff. *Mechanistic study of aerosol dry deposition on vegetated canopies.* PhD thesis, Université de la Méditerranée - Aix-Marseille II, IRPHE - Institut de Recherche sur les Phénomènes Hors Equilibre, IRSN - Institut de radioprotection et de sûreté nucléaire, 2005.

[64] D. Zwillinger. *Handbook of Differential Equations.* Academic Press., 1997.

[65] G. J. Dorr, J. S. Hanan, N. Woods, S. W. Adkins, P. A. Kleinmeulman, P. Ricci, and B. N. Noller. Combining spray drift and plant architecture modeling to minimise environmental and public health risk of pesticide application. In *International Congress on Modelling and Simulation Advances and Applications for Management and Decision Making.* The Modelling and Simulation Society of Aust & New Zealand, 2005.

[66] Arthur Da Silva, Carole Sinfort, Cyril Tinet, Daniel Pierrat, and Serge Huberson. A lagrangian model for spray behaviour within vine canopies. *Journal of Aerosol Science*, AS3921 :1–17, 2005.

[67] J.C. Fischenich. *Velocity and resistance in densely vegetated floodways.* PhD thesis, Colorado State University, University Press, Fort Collins, CO., 1996.

[68] 75-90 ESAIM : Proceedings, Vol. 6, editor. *Riemann Solvers for some Hyperbolic Problems with a Source Term.* Actes du 30ème Congrès d'Analyse Numérique : CANum'98, 1999.

[69] Varadhan Ravi and Joseph R. Williams. Estimation of infiltration rate in the vadose zone : Compilation of simple mathematical models volume i. Technical Report EPA/600/R-97/128a, Environmental Protection Agency, United States, 1998.

[70] J.H. Clothier, B.E.and Knight and I. White. Burgers' equation : Application to field constant-flux infiltration. *Soil Science*, 132(4) :255–261, 1981.

[71] R.G. Hills and Warrick A.W. Burger's equation : A solution for soil water flow in a finite length. *Water Resources Research*, 29(4) :1179–1184, 1993.

[72] Garret N. Vanderplaats. *Numerical optimization techniques for engineering design.* McGraw-Hill, 2001.

[73] A. Cabot and B. Mohammadi. Incomplete sensitivities and cost function reformulation leading to multi-criteria investigation of inverse problems. *Optim.Control Appl.Meth.*, 24 :73–84, 2003.

[74] Dainelli Niccolo, Conese Claudio, Rapi Bernardo, and Maurizio Romani. Integration of gis and rs techniques for canopy variability evaluation in vineyards. COST 718 - New technologies for agrometeorological model applications, CNR Research Area - Polo Scientifico di Sesto Fiorentino, Bacchus project, 2005.

[75] Magali De Luca. *Contribution to the modelling of pesticide spraying in order to reduce pollutions.* PhD thesis, Cemagref, Montpellier, 2007.

[76] Zamuner Bernard. *Experimental and numerical study of a burning spray achieved by a liquid-gas coaxial injector.* PhD thesis, Ecole Centrale Paris, 1995.

[77] J. S. Turner. *Buoyancy Effects in Fluids.* Cambridge University Press, 1973.

[78] Hinze J.O. *Turbulence.* McGraw-Hill, New York, 1975.

[79] Chen and Rodi W. *Vertical Turbulent Buoyant Jets.* Pergamon Press, 1980.

[80] J. R. Cho and Chung M. K. k-ϵ-γ equation turbulence model. *A. J. Fluid Mech.*, 237 :301–322, 1992.

[81] G.S. Bhat and A. Krothapalli. Simulation of a round jet and a plume in a regional atmospheric model. *Monthly Weather Review*, 128(12) :4108–4117, December 2000.

[82] H.B. Fisher, List E. J., Koh R.C.Y., Imberger J., and Brooks N.H. *Mixing in Inland and Coastal Waters.* Academic Press, 1979.

[83] A. Arakawa and Schubert W. H. Interaction of a cloud ensemble with the large-scale environment. part i. *J. Atmos. Sci.*, 31 :674–701, 1974.

[84] Abramovich G.N. *The Theory of Turbulent Jets.* The MIT Press, Cambridge, Massachusetts, 1963. Translation by Scripta Technica.

[85] N. Rajaratnam. Turbulent jets. Elsevier Scientific Publishing Company, Amsterdam, 1976.

[86] Panchapakesan N.R. and Lumley J.L. Turbulence measurements in axisymmetric jets of air and helium. part 1. air jet. *J. Fluid Mech.*, 246 :197–224, 1993.

[87] Hussein H.J., Capp S.P., and George W.K. Velocity measurements in a high reynolds number, momentum-conserving, axisymmetric, turbulent jet. *J. Fluid Mech.*, 258 :31–76, 1994.

[88] C. J. Chen and Chen C. H. On prediction and unified correction for decay of vertical buoyant jets. *Trans. ASME : J. Heat Transfer*, 101 :532–537, 1979.

[89] C.L. Lubbers, G. Brethouwer, and B.J. Boersma. Simulation of the mixing of a passive scalar in a round turbulent jet. *Fluid Dynamics Research*, 28 :189–208, 2001.

[90] Boersma B.J., Brethouwer G., and Nieuwstadt F.T.M. A numerical investigation on the effect of the in flow conditions on the self-similar region of a round jet. *Phys. Fluids*, 10 :899–909, 1998.

[91] Ramses Kaijen. Turbulent mixing of oil droplets in a round water jet. Technical Report MEAH 237, Laboratory for Aero & Hydrodynamics, Delft University of Technology, Netherlands, October 2004. Graduation Project.

[92] F.T.M. Nieuwstadt. *Turbulentie*. Epsilon Uitgaven, Utrecht, 1998.

[93] Versteeg H.K. and Malalasekera W. *An Introduction to Computational Fluid Dynamics, The Finite Volume Method*. Longman Group Ltd., Essex, England, 1995.

[94] L.W. Browne, R.A. Antonia, and A.J. Chambers. The interaction regions of a turbulent jet. *J. Fluid Mech.*, 149 :355–373, 1984.

[95] I. Wygnanski and H. Fiedler. Some measurements in the self-preserving jet. *J. Fluid Mech.*, 38 :577–612, 1969.

[96] George W.K. *Self-preservation of turbulent flows and its relation to initial conditions and coherent structures.* Arndts, R. (Eds.) Adv. Turbulence, Springer, Berlin, 1989.

[97] H. Tennekes and J. L. Lumley. *A First Course in Turbulence*. Mass MIT Press, Cambridge, 1972.

[98] Yue Zou. *Air jets in ventilation applications*. PhD thesis, KTH, Department of Building Sciences, 2001.

[99] Abdul-Monsif Shinneeb. *Confinement Effects in Shallow Water Jets*. PhD thesis, Department of Mechanical Engineering, University of Saskatchewan, Canada, August 2006.

[100] P. Roux, A. Herbst, G.M. Richardson, and P. Delpech. Full-scale measurement of spray-drift from a vineyard sprayer in a controlled wind-tunnel environment. *Journal of Wind Engineering and Industrial Aerodynamics*, Submitted, 2006.

[101] S. Webb and Ian P. Castro. Axisymmetric jets impinging on porous walls. *Experiments in Fluid*, 40 :951–961, March 2006.

[102] A Lagrangian model for spray behaviour within vine canopies. Da silva, a. and sinfort, c. and tinet, c. and pierrat, d. and huberson, s. *Journal of Aerosol*, 37(5) :658–674, 2006. ISSN 0021-8502.

[103] Y. Gil, C. Sinfort, Y. Brunet, V. Polveche, and B. Bonicelli. Loss of spray above an artificial vineyard during air-assisted spraying. *Atmospheric Environment*, Submitted, 2006.

[104] PISC. Spray drift management : Principles, strategies and supporting information. Primary Industries Standing Committee. Report 82. Technical report, CSIRO Publishing, Australia, 2002.

[105] D.E. Aylor. Modelling spore dispersal in a barley crop. *Agricultural Meteorology*, 26 :215–219, 1982.

[106] P.J. Walklate. A simulation study of pesticide drift from air-assisted orchard sprayer. *Journal of Agricultural Engineering Research*, 51 :263–283, 1992.

[107] C.S. Parkin and P.R. Young. Measurements and computational fluid dynamic simulations of the capture of drops by spray drift samplers. *Aspects of Applied Biology*, 57 :113–120, 2000.

[108] Ghosh S. and Hunt J.C.R. Induced air velocity in droplet-driven sprays. *Proc. R. Soc. Lond.*, A 444 :105–127, 1994.

[109] Y. Gil and C. Sinfort. Emission of pesticides to the air during sprayer application : A bibliographic review. *Atmospheric Environment*, 39 :5183–5193, 2005.

[110] Srivastava Smriti and Indra N. Sinha. Classification of air pollution dispersion models : a critical review. In *Proceedings of the National Seminar on Environmental Engineering with special emphasis on Mining Environment, NSEEME-2004*, volume 19-20, March 2004.

[111] Rodger Grayson and Günter Blöschl. *Spatial Patterns in Catchment hydrology*. Cambridge University Press, 2000.

[112] M.J. Borysiewicz, I. Garanty, and Kozubal A. Air quality modelling. Manhaz Monograph, Models and Techniques for Health and Environmental Hazard Assessment and Management , Institute of Atomic Energy, Poland.

[113] D. Anfossi, E. Ferrero, G. Brusasca, A. Marzorati, and T. Tinarelli. A simple way of computing buoyant plume rise in a lagrangian stochastic dispersion model for airborne dispersion. *Atmos. Environ.*, 27A :1443–1451, 1993.

[114] L. Liu and S. Du. A computationally efficient particle-puff model for concentration variance from steady releases. *Environ. Model. Softw.*, 18 :25–33, 2003.

[115] Atfeh Bilal. *Méthode des lignes de courant appliquée à la modélisation des bassins*. PhD thesis, Université de Provence, 2003.

[116] O. Mohammadi, B. & Pironneau. *Analysis of the k-epsilon turbulence model*. Wiley, 1994.

[117] W.R. Tobler. Three presentations on geographical analysis and modeling. Technical Report 93-1, NCGIS, 1993.

[118] F. Alauzet, P-L. George, P. Frey, and B. Mohammadi. Transient fixed point based unstructured mesh adaptation. *Int. J. Numer. Meth. Fluids*, 43/6 :729–745, 2002.

[119] F. Hecht and B. Mohammadi. Mesh adaptation by metric control for multi-scale phenomena and turbulence. *AIAA paper*, 0859, 1997.

[120] H. Borouchaki, e P-L. Georg, and B. Mohammadi. Delaunay mesh generation governed by metric specifications. *Finite Element in Analysis and Design*, 2 : :85–109, 1997.

[121] J. Simpson. *Gravity currents in the environment and laboratory.* Cambridge University Press, 2nd edition, 1997.

[122] B. Mohammadi and G. Puigt. Wall functions in computational fluid dynamics. *Computers & Fluids*, 40-3 :2101–2124, 2006.

[123] ArcGIS. Geographic information system, `http ://www.esri.com/software/arcgis`, 2006.

[124] J. Cousteix. *Turbulence et couche limite.* Wiley Series in Agrochemicals and Plant Protection, Cepadues publishers, 1989.

[125] Ph. Ciarlet. *The finite element method. for elliptic problems.* North-Holland, 1978.

[126] Charles Chemel. *Transport et mélange en terrain complexe, application à la dynamique atmosphérique dans les vallées encaissées.* PhD thesis, Université Joseph Fourier - Grenoble I, 2005.

[127] Laurent Menut. Introduction à la modélisation en dynamique et chimie de l'atmosphère, polycopié de cours, laboratoire de météorologie dynamique, 2004.

[128] Julie Pullen, Jay P. Boris, Theodore Young, Gopal Patnaik, and John Iselinc. A comparison of contaminant plume statistics from a gaussian puff and urban cfd model for two large cities. *Atmospheric Environment*, 39 :1049–1068, 2005.

[129] Eugene Gutkin and Serge Tabachnikov. Billiards in finsler and minkowski geometries. *Journal of Geometry and Physics*, 40 :277–301, 2002.

[130] Vladimir Kolmogorov and Yuri Boykov. What metrics can be approximated by geocuts, or global optimization of length/area and flux. In *Proceedings of "International Conference on Computer Vision" (ICCV), vol. I*, Beijing, China, 2005.

[131] Waldo Tobler. *Map Transformations of Geographic Space.* PhD thesis, University of Washington, 1961.

[132] Michael John de Smith. *Distance and Path - The development, interpretation and application of distance measurement in mapping and spatial modelling.* PhD thesis, Centre for Advanced Spatial Analysis, University College, London, 2003.

[133] Panos Georgopoulos. Exposure modeling course. RAS, 2004.

[134] David M. Glover, William J. Scott Jenkins, and C. Doney. Modeling, data analysis and numerical techniques for geochemistry (course). RAS, May 2005.

[135] John D. Wilson. Introduction to wind and wind transport near ground. Notes, September 2005.

[136] Torben Mikkelsen and Morten Nielsen. Modelling of pollutant transport in the atmosphere. Atmospheric Physics Division Wind Energy Department Risø National Laboratory Dk-4000 Roskilde, Denmark, Workshop on short-range transport and dispersion modeling for decision making, Otwock-Swierk (PL), Unpublished., 17-18 Nov 2003.

[137] Barsotti S., Neri A., and Scire J. Assessing volcanic ash hazard by using the calpuff system. The 2nd International Conference on Volcanic Ash and Aviation Safety, June 2004.

[138] Quélo Denis. *Simulation numérique et assimilation de données variationnelle pour la dispersion atmosphérique de polluants*. PhD thesis, Ecole Nationale des Ponts et Chaussées, 2004.

[139] Davidson Martins Moreira, Paulo de Vilhena Ferreira Neto, , and Jonas da Costa Carvalho. Analytical solution of the eulerian dispersion equation for non-stationary conditions : development and evaluation. *Environmental Modelling & Software*, 20(1-4) :1159–1165, 2005.

[140] Thomas Lowry and Shu-Guang Li. A finite analytic method for solving the 2-d time-dependent advection-diffusion equation with time-invariant coefficients. *Advances in Water Resources*, 28 :117–133, 2005.

[141] Perkins R., L. Soulhac, P. Mejean, and I. Rios. Modélisation de la dispersion des émissions atmosphériques d'un site industriel. Synthèse de l'étude 0805, RE.CO.R.D., 2005.

[142] Tognet Frédéric, Rouil Laurence, and Lacome Jean-Marc. Modélisation diffusion dans l'atmosphère et identification d'une source de légionelles. Rapport d'étude INERIS - DRC 06 - 76476 MECO - Fto n̊117, INERIS, 2006.

[143] Woodson Clifton Brock. *Thin Layers : Physical and chemical cues contributing to observed corepod aggregations*. PhD thesis, School of Civil and Environmental Engineering, Georgia Institute of Technology, Atlanta, GA, December 2005. Doctor of Philosophy in Civil Engineering.

[144] McMahon Niall. Derivation of boundary-layer equations for two-dimensional flow. School of Computer Applications, Dublin City University, Friday January 24th 2003.

[145] Kreith Frank, Berger S.A., and al. *Fluid Mechanics, The CRC Handbook of Mechanical Engineering*, chapter Fluid Mechanics. Boca Raton : CRC Press LLC, 1999.

[146] Prieve Dennis C. A course in fluid mechanics with vector field theory. Department of Chemical Engineering, Carnegie Mellon University, Pittsburgh, PA 15213, 2000.

[147] Gerard-Varet David. Formal derivation of boudary layers in fluid mechanics. *J. Math. Fluid Mech.*, 7(2) :179 – 200, 2005.

[148] Gheorghe Stan. *Fundamental Characteristics of Turbulent Opposed Impinging Jets*. PhD thesis, University of Waterloo, Ontario, Canada, 2000.

[149] Sudhaker Chhabra, Thomas N. Shipman, and Ajay K. Prasad. The entrainment behavior of a turbulent axisymmetric jet in a viscous host fluid. *Experiments in Fluids*, 38(1) :70–79, 2005.

[150] Lasse Rosendahl. Fluids and combustion engineering master programme. Course of Institute of Energy Technology, Aalborg University, Denmark.

[151] Oleg Zastavniouk. *Shidy of Mixing Phenornena in a Dual Fuel Diesel Engine Air Intake Manifold*. PhD thesis, Department of Mechanical Engineering, University of Alberta, Edmonton, Canada, Fall 1997.

[152] Springer, editor. *Modelling the flow in droplet driven sprays.*, Stockholm, 1991. Advances in Turbulence 3 : Proceedings of the 3rd European Turbulence Conference (ed. A. V. Johansson & P. H. Alfredsson).

[153] B. Panneton, B. Lacasse, and R. Thériault. Penetration of spray in apple trees as a function of airspeed, airflow, and power for tower sprayers. *Canadian Biosystems Engineering*, 47 :2.13–2.20, 2005.

[154] Willem A.H. Asman and Peter Kryger Jensen. Dry deposition and spray drift of pesticides to nearby water bodies. Report Pesticides Research 66, Danish Environmental Protection Agency, Copenhagen, Denmark, 2003.

[155] Hunt J. and Carruthers (CERC) D. Annual report. Technical Report ISBN 0-85951-525-7, UK Atmospheric Dispersion Modelling Liaison Committee., 2002-2003. Annex C : Dispersion from accidental releases in urban areas.

[156] Yvan Gil Pinto and Carole Sinfort. Emission of pesticides to the air during sprayer application : A bibliographic review. *Atmospheric Environment*, 39(28) :5183–5193, 2005.

[157] M. Farooq, R. Balachandar, Wulfsohn D., and Wolf T.M. Agricultural sprays in cross-flow and drift. *Journal of Agricultural Engineering Research*, 78(4) :347–358(12), April 2001.

[158] S. Ghosh and J.C.R. Hunt. Spray jets in a cross-flow. *J. Fluid Mech.*, 365 :109–136, 1998.

[159] Lardoux Yvan. *Etude de la répartition au sol des produits phytosanitaires sous une rampe en mouvement à partir d'une modélisation dynamique - application à la définition de méthodes d'évaluation des pulvérisateurs à jets projetés*. PhD thesis, Ecole Nationale Supérieure Agronomique de Montpellier, 2002.

[160] Mehrdad Darvishvand Taher. *A Virtual Nozzle for Modeling Pesticide Spray Deposition in a Plant Canopy*. PhD thesis, Univ. of Guelph, Canada, 1998.

[161] Istasse Eric. *Contribution à l'étude de la dispersion hydrodynamique et de son couplage à la convection naturelle en milieux poreux modèles fracturés*. PhD thesis, Université libre de Bruxelle, Faculté des sciences appliquées, Chimie et sciences des matériaux, Belgique, 2004.

[162] Spadaro Joseph Vito. *Evaluation des dommages de la pollution de l'air : modélisation, études de sensibilité, et applications*. PhD thesis, l'Ecole des Mines de Paris, 1999.

[163] Michael K.H. Leung, Chun-Ho Liu, Alan H.S. Chanb, Dennis Y.C. Leung, W.C. Yam, S.P. Ng, and Lilian L.P. Vrijmoed. Prediction of transient turbulent dispersion by cfd-statistical hybrid modeling method. *Atmospheric Environment*, 39 :6345–6351, july 2005.

[164] Bijan Mohammadi and Jean-Marc Brun. Reduced-order modelling of dispersion. In *Computational Modeling with Partial Differential Equations in Science and Engineering*. Springer, 2007. to appear.

[165] Julie M. Styles. *A wind tunnel study of the velocity field above a model plant canopy*. PhD thesis, The Australian National University, Camberra, 1997.

[166] Benjamin Ivorra. *Optimisation Globale Semi-Déterministe et Applications Industrielles*. PhD thesis, Université de Montpellier II, 2006.

[167] S. Ulbrich. Optimal control of nonlinear hyperbolic conservation laws with source terms, 2001.

[168] Burkardt John, Du Qiang, Gunzburger Max, and Lee Hyung-Chun. Reduced-order modeling of complex systems. In *Proceedings Biennial Conference on Numerical Analysis (NA03)*, UK, June 24-27 2003. Dundee.

[169] Jörg Härterich. Viscous profiles for traveling waves of scalar balance laws : The uniformly hyperbolic case. *Electronic Journal of differential equations*, 30 :1–22, April 2000. ISSN : 1072-6691, Southwest Texas State University and University of North Texas.

[170] Jörg Härterich and Julia Ehrt. Heteroclinic orbits between rotating waves in hyperbolic balance laws, February 19 1998. Freie Universität Berlin, Mathematisches Institut I, Arnimalle, Germany.

[171] Jörg Härterich. Equilibrium solutions of viscous scalar balance laws with a convex flux. *Nonlinear differ. equ. appl.*, 6 :413–436, 1999.

[172] Yaping Wu and Xiuxia Xing. The stability of travelling fronts for general scalar viscous balance law. *J. Math. Anal. Appl.*, 2 :698–711, 2005.

[173] Alexandre Petroff. Mechanistic study of aerosol dry deposition on vegetated canopies. *Radioprotection*, 40(Suppl. 1) :S443–S450, 2005. EDP Sciences.

[174] Mehrez Samaali. *Evaluation d'un modèle de couche limite atmosphérique 3D dans un cas homogène : application à une parcelle agricole de Soja*. PhD thesis, Université de Provence, Ecole Polytechnique de Marseille, 2002.

,

Table des figures

Liste des tableaux

Résumé - Cette étude présente une plateforme de modèles à complexité réduite pour le transport et la dispersion atmosphérique d'un scalaire passif pour applications environnementales. Une approche multi-échelle est appliquée avec une définition de l'espace de recherche adéquat pour la solution à chaque niveau. Au niveau local, la dérive en champ proche est estimée par la théorie des jets turbulents et détermine le terme source pour le niveau d'ordre supérieur. On utilise notamment les solutions de similitudes pour les panaches dans une métrique non-symétrique pour le transport sur des grandes distances. L'approche ne nécessite pas la solution d'EDP, donc pas de maillage et il est possible accéder à la valeur en un point sans avoir à calculer la solution sur l'ensemble du domaine.

Mots-clés : *Dispersion atmosphérique, Complexité réduite, Optimisation, Dérive, Modèles analytiques, Jets turbulents*

Abstract - A platform of low complexity models for the transport of passive scalars for environmental applications is presented. Multi-level analysis has been used with a reduction in dimension of the solution space at each level. Local spray drift distribution is estimated thanks to the turbulent jet theory and determine the source term. Similitude solutions are used in a non symmetric metric for the transport over long distances. Model parameters identification is based on data assimilation. The approach does not require the solution of any PDE and therefore is mesh free. The model also permits to access the solution in one point without computing the solution over the whole domain.

Key-words : *Atmospheric dispersion, Reduced order modelling, Optimization, Spray Drift, Analytical model, Turbulent Jet*

Jean-Marc Brun

Université Montpellier II
Laboratoire I3M- CNRS UMR 5149
CC 051 - Place Eugène Bataillon
34095 Montpellier Cedex 5 (France)

email : brun@math.univ-montp2.fr / jean-marc.brun@montpellier.cemagref.fr